Discovering the tumour suppressor function of hepatocyte NF-κB1

Julia Concetti

Thesis submitted for the degree of Doctor of Philosophy

Newcastle University

Faculty of Medical Sciences

Institute of Cellular Medicine

March 2020

Declaration

I hereby declare that this thesis has been composed by myself and has not been accepted in application of a degree. All work was performed by myself unless otherwise stated. All sources of information have been acknowledged appropriately by means of a reference.

Julia Concetti

Abstract

Aberrant activation of the NF-κB signalling pathway is associated with the development of many cancers. We have previously demonstrated that global NFKB1 knock-out mice ($Nfkb1^{-/-}$) develop spontaneous low-level chronic inflammation, liver disease and cancer as they age. In addition, when they are given the carcinogen diethylnitrosamine (DEN) to induce liver cancer they develop significantly more tumours and at an earlier stage. $Nfkb1^{-/-}$ mice present with defects in both the immune and the epithelial compartment, therefore it is not possible to dissect the cell-specific role of NFKB1 as a tumour suppressor.

To determine the hepatocyte-specific tumour suppressor role of NFKB1, we have generated a novel hepatocyte-specific NFKB1 knock-out mouse ($Nfkb1^{hep-/-}$). WT or $Nfkb1^{hep-/-}$ mice were subjected to different treatment regimens with either the hepatotoxin CCl_4 or the carcinogen DEN to induce acute inflammation, fibrosis or hepatocellular carcinoma, to assess the role of hepatocyte NFKB1 in the progression from liver inflammation to cancer. In addition, acute CCl_4 injury and chronic DEN injury experiments were conducted in AAV-TBG-CRE mice, whereby adenoviral deletion of hepatocyte NFKB1 was induced.

Here we demonstrate that, while hepatocyte Nfkb1 showed a limited protective role in acute inflammation and fibrosis, mice lacking hepatocyte Nfkb1 displayed a significant increase in tumour number and grade when compared with WT mice in the chronic DEN model. Importantly, they also displayed a higher percentage of PCNA+ proliferative tumours, indicative of a more aggressive tumour phenotype. Immune cell infiltration including monocytes, macrophages and neutrophils was significantly increased in $Nfkb1^{hep-/-}$ mice.

These data provide strong evidence that NFKB1 acts as a hepatocyte-specific tumour suppressor, playing an essential role in the control of inflammation, tumour initiation, progression and proliferation.

Acknowledgements

Firstly, I would like to thank my supervisors, Dr Caroline Wilson, Prof Derek Mann and Prof Jelena Mann for their support and encouragement throughout my project, as well as Dr Simi Ali and Prof Jon Higgins for their guidance throughout my PhD.

I would also like to thank the members of the Newcastle University Fibrosis Research Group both past and present for all of their help and support during my PhD. I would also like to acknowledge the contribution of the undergraduate student Sam Murray to the generation of data for this thesis.

The work completed during this PhD was supported by an MRC funded PhD studentship. I would therefore like to extend my gratitude to the MRC, without whom I would not have been able to undertake the research for my PhD.

Finally, I would like to thank my entire family for their continuous support, especially my parents whose financial and emotional support have made this possible, as well as my friends who have always been there, including my fellow scientific friends who have given me their input and guidance during my PhD.

Table of Contents

Declaration ..... **i**

Abstract ..... **ii**

Acknowledgements ..... **iii**

Table of Contents ..... **iv**

List of Figures ..... **xi**

List of Tables ..... x**vii**

List of Abbreviations ..... x**viii**

Chapter 1. Introduction **1**

1.1 Nuclear Factor Kappa B (NF-κB) **1**

1.1.1 NF-κB transcription factor family members and structures 1

1.1.2 NF-κB activation pathways 2

1.1.3 NF-κB activity modulation 5

1.2 Nuclear Factor Kappa B1 (NF-κB1) **7**

1.2.1 p105 structure and function 8

1.2.2 p50 structure and function 8

1.2.3 p105 and p50 cofactor complexes 9

1.2.4 NF-κB1 in inflammation 11

1.2.5 NF-κB1 in cancer 13

1.3 Liver function, inflammation, disease and fibrosis **20**

1.3.1 Cells of the liver 21

1.3.2 Structure and function of the liver 22

1.3.3 Hepatocyte injury mechanisms and resolution 25

1.3.4 Liver epithelial-immune cell crosstalk 26

1.3.5 Liver disease progression 26

1.3.6 Liver fibrosis 27

1.3.7 NF-κB1 in liver disease and fibrosis 27

1.4 Hepatocellular Carcinoma (HCC) 28
1.4.1 HCC initiation and progression 28
1.4.2 NF-κB1 in HCC 30
1.5 Project Aims 32
Chapter 2. Materials and Methods 33
2.1 Animals 33
2.1.1 Ethics and Husbandry 33
2.1.2 Strains 33
2.1.3 Genotyping 36
2.2 Cell culture 37
2.2.1 Isolation of primary mouse hepatocytes 37
2.2.2 Primary mouse hepatocyte culture 38
2.2.3 Primary mouse hepatocyte treatment 38
2.2.4 Isolation of immune cells 38
2.2.5 Isolation of primary mouse tumour cells 38
2.2.6 Primary mouse tumour cell culture 39
2.2.7 Long term cell storage 39
2.3 In vivo models of liver injury 39
2.3.1 Adeno-associated virus knockout models 39
2.3.2 Acute carbon tetrachloride (CCl_4) injury 40
2.3.3 Acute diethylnitrosamine (DEN) injury 41
2.3.4 Chronic CCl_4 injury 41
2.3.5 Chronic DEN injury 41
2.4 RNA isolation and quantification 42
2.4.1 RNA isolation 42
2.4.2 cDNA synthesis 43
2.4.3 Primer design 43
2.4.4 Quantitative real-time PCR 44

2.5 Protein isolation and analysis 45
2.5.1 Cell lysate preparation 45
2.5.2 Tissue lysate preparation 45
2.5.3 Protein quantification (BCA assay) 46
2.5.4 Western blotting 46
2.6 Immunohistochemistry and histology 48
2.6.1 Paraffin embedded section preparation 48
2.6.2 Haematoxylin and Eosin staining (H&E) 48
2.6.3 Sirius Red staining 49
2.6.4 Immunostaining 49
2.6.5 Image analysis 51
2.7 Enzyme-linked immunosorbent assay (ELISA) 51
2.8 RNA-Sequencing 52
2.9 Statistics 53
Chapter 3. The role of hepatocyte NF-κB1 in acute liver injury 54
3.1 Introduction 54
3.2 Characterisation of the Nfkb1$^{hep-/-}$ mice 54
3.3 The role of hepatocyte NF-κB1 in acute CCl_4 liver injury 60
3.3.1 p50 protein expression after acute CCl_4 liver injury 61
3.3.2 Liver damage serum ALT (alanine transaminase) and AST (aspartate transaminase) enzymes 61
3.3.3 Hepatocyte Nfkb1 knock-out does not alter neutrophil recruitment to the liver 63
3.3.4 Hepatocyte Nfkb1 knock-out does not affect the neutrophil chemokine expression network 64
3.3.5 Hepatocyte Nfkb1 knock-out increases macrophage recruitment to the liver 66
3.3.6 Hepatocyte Nfkb1 knock-out does not affect CCL2 and CCL5 liver chemokine expression 68

3.3.7 Hepatocyte Nfkb1 knock-out does not affect anti-apoptotic gene expression 69

3.3.8 Hepatocyte Nfkb1 knock-out does not affect apoptosis or cell death 71

3.4 The role of hepatocyte Nfkb1 in acute CCl_4 liver injury in an adeno-associated viral Nfkb1 knock-out model 74

3.4.1 Validation of AAV-TBG-Cre Nfkb1 hepatocyte-specific knockout 74

3.4.2 Liver damage serum ALT and AST enzymes 76

3.4.3 Hepatocyte knock-out does not alter neutrophil recruitment to the liver 77

3.4.4 Hepatocyte Nfkb1 knock-out does not affect the neutrophil chemokine expression network 78

3.4.5 Hepatocyte Nfkb1 knock-out increases macrophage recruitment to the liver after 48h, but not 24h, CCl_4 liver injury 80

3.4.6 Hepatocyte Nfkb1 knock-out does not affect CCL2 and CCL5 liver chemokine expression 82

3.4.7 Hepatocyte Nfkb1 knock-out does not affect anti-apoptotic gene expression 83

3.4.8 Hepatocyte Nfkb1 knock-out does not affect apoptosis or cell death 85

3.5 The role of NF-κB1 in acute DEN liver injury 87

3.5.1 Validation of Nfkb1 hepatocyte-specific knockout 88

3.5.2 Liver damage serum ALT and AST enzymes 88

3.5.3 Inflammation 89

3.5.4 Neutrophil recruitment in acute DEN liver injury 90

3.5.5 Neutrophil chemokine expression in acute DEN liver injury 91

3.5.6 Monocyte/macrophage recruitment in acute DEN liver injury 92

3.5.7 Expression of chemokines involved in monocyte recruitment in acute DEN liver injury 93

3.5.8 Anti-apoptotic/oncogene expression in acute DEN liver injury 94

3.5.9 Proliferation in acute DEN liver injury 96

3.5.10 DNA damage in acute DEN liver injury 97

3.7 Chapter Discussion 98

Chapter 4. Global, but not hepatocyte-only, NF-κB1 restricts the liver inflammatory and fibrotic phenotype in a chronic CCl_4 model of liver injury . 100

4.1 Introduction 100

4.2 Liver/body rate ratio in chronic CCl_4 liver injury 101

4.3 p50 expression in $Nfkb1^{fl/fl}$ and $Nfkb1^{hep-/-}$ mice 102

4.4 Liver damage serum ALT and AST enzymes 103

4.5 Lack of global NF-κB1, but not hepatocyte p50, increases liver inflammation 104

4.5.1 Increased liver neutrophil infiltration in global, but not hepatocyte-specific, Nfkb1 knock-out mice 104

4.5.2 Increased chemokine expression in global, but not hepatocyte-specific, Nfkb1 knock-out mice 105

4.5.3 Nfkb1 does not modulate liver monocyte infiltration in a chronic CCl_4 liver injury model 107

4.6 Lack of global NF-κB1, but not hepatocyte NF-κB1, increases liver fibrosis 109

4.6.1 Increased fibrogenic gene expression in global, but not hepatocyte-specific, Nfkb1 knock-out mice 109

4.6.2 Increased collagen deposition and fibrosis score in global, but not hepatocyte-specific, Nfkb1 knock-out mice 110

4.6.3 Nfkb1 does not modulate liver alpha-SMA expression in a chronic CCl_4 liver injury model. 111

4.7 Chapter Discussion 112

Chapter 5. The tumour-suppressive role of hepatocellular NF-κB1 in hepatocellular carcinoma 114

5.1 Introduction 114

5.2 p50 expression in $Nfkb1^{fl/fl}$ and $Nfkb1^{hep-/-}$ mice 115

5.3 Liver damage ALT and AST serum enzymes not affected by hepatocyte Nfkb1 knock-out 115

5.4 Hepatocyte-specific Nfkb1 knock-out increases tumour incidence *in vivo* 116

5.4.1 Hepatocyte Nfkb1 knock-out increases tumour incidence 116

5.4.2 Hepatocyte Nfkb1 knock-out increases hepatocyte proliferation 117

5.4.3 Higher HCC tumour grade in Nfkb1$^{hep-/-}$ mice 118

5.5 Hepatocyte-specific Nfkb1 knock-out increases liver immune cell infiltration 119

5.5.1 Increased immune cell infiltration in hepatocyte Nfkb1 knock-out mice ... 119

5.5.2 Increased neutrophil infiltration in hepatocyte Nfkb1 knock-out mice 120

5.5.3 Neutrophil chemokine S100A9, CXCL1 and CXCL2 expression unaltered in hepatocyte Nfkb1 knock-out mice 121

5.5.4 Increased monocyte and macrophage infiltration in hepatocyte Nfkb1 knock-out mice 122

5.5.5 Monocyte chemoattractant chemokine CCL2 and CCL5 expression unaltered in hepatocyte Nfkb1 knock-out mice 123

5.5.6 Lack of hepatocyte NF-κB1 does not affect T cell liver infiltration or T cell subsets 124

5.5.7 Lack of hepatocyte NF-κB1 does not affect B cell liver infiltration 127

5.6 Hepatocyte NF-κB1 regulation of apoptosis and oncogene expression . 127

5.6.1 Anti-apoptotic genes and oncogenes expression upregulated in the absence of hepatocyte NF-κB1 in liver tumours but not in adjacent liver tissue 128

5.6.2 Hepatocyte NF-κB1 does not modulate anti-apoptotic gene and oncogene expression at the protein level 128

5.6.3 Lack of NF-κB1 does not alter cleaved caspase 3 protein expression 130

5.7 NF-κB subunit expression comparison in Nfkb1 floxed and Nfkb1 hepatocyte knock-out mice 132

5.8 Differential mRNA expression profile in Nfkb1 hepatocyte knock-out mice tumours 132

5.9 The role of hepatocyte NF-κB1 in tumour initiation in an adeno-associated viral Nfkb1 knock-out 151

5.9.1 p50 expression in AAV-TBG-Null and AAV-TBG-Cre mice 151

5.9.2 Liver damage ALT and AST serum enzymes 152

5.9.3 Tumour number and grade 153

5.9.4 Proliferation 154

5.9.5 Immune cell infiltration 155

5.9.6 Neutrophil recruitment to the liver in AAV-TBG-Null and AAV-TBG-Cre mice 156

5.9.7 Neutrophil chemokines 157

5.9.8 Monocytes/macrophages recruitment to the liver in AAV-TBG-Null and AAV-TBG-Cre mice 158

5.9.9 Monocyte chemoattractant chemokines 159

5.9.10 Tumour and liver anti-apoptotic/oncogene expression in AAV-TBG-Null and AAV-TBG-Cre mice 160

5.10 The role of hepatocyte NF-κB1 in aged 19 month mice 161

5.11 Chapter Discussion 162

Chapter 6. Discussion 165

References 171

List of Figures

Figure 1.1: NF-κB subunit structures and dimeric combinations **2**

Figure 1.2: NF-κB1 activation and regulation of gene expression in cancer **4**

Figure 1.3: NF-κB-activating stimuli and target genes **7**

Figure 1.4: p105 and p50 homodimer complexes **11**

Figure 1.5: Cells of the liver **22**

Figure 1.6: Liver lobule structure **23**

Figure 1.7: Liver microstructure **24**

Figure 1.8: Functions of the liver **25**

Figure 2.1: LoxP recombination of exon 3 in the Nfkb1 gene **34**

Figure 2.2: Nfkb1$^{hep-/-}$ mice generation **35**

Figure 2.3: CCl_4 mechanism of hepatotoxicity **40**

Figure 2.4: Mouse harvest set up **42**

Figure 3.1: Western blot analysis of NF-κB1 p50 expression comparison between control and Nfkb1$^{hep-/-}$ mice **55**

Figure 3.2: Genotyping analysis of mice from Nfkb1$^{fl/fl}$ X Alb-Cre$^{+/-}$ breeding ... **56**

Figure 3.3: Nfkb1 immunohistostain with ab32360 antibody, 1 and 2 day protocols **57**

Figure 3.4: Nfkb1 immunohistostain with D4P4D antibody, 1 and 2 day protocols **58**

Figure 3.5: Nfkb1 immunohistostain with sc-114 antibody, 1 and 2 day protocols **59**

Figure 3.6: Nfkb1 immunohistostain with D7H5M antibody, 1 and 2 day protocols **60**

Figure 3.7: Western blot analysis of Nfkb1 p50 expression in control and Nfkb1$^{hep-/-}$ mice livers following CCl_4 injection **61**

Figure 3.8: Serum ALT and AST enzyme level comparison at 24h and 48h post-CCl_4 injection **62**

Figure 3.9: Ly6G immunostain of mice livers following acute CCl_4 injury **63**

Figure 3.10: Neutrophil chemokine network gene expression in acute CCl_4-injured mice livers **65**

Figure 3.11: TNFα and IL-6 liver gene expression in acute CCl_4 injury **66**

Figure 3.12: F4/80 immunostain of mice livers subjected to acute CCl_4 injury . **67**

Figure 3.13: Monocyte chemoattractant chemokine gene expression in the liver following acute CCl_4 injury **68**

Figure 3.14: Anti-apoptotic gene expression in acute CCl_4 injury **70**

Figure 3.15: XIAP and BAX gene expression in acute CCl_4 injury **71**

Figure 3.16: Cleaved caspase 3 immunostain of livers following acute CCl_4 injury **72**

Figure 3.17: Percentage necrosis area quantified by H&E stain in acute CCl_4 liver injury **73**

Figure 3.18: Western blot analysis of p50 expression following AAV-TBG-Cre injection **75**

Figure 3.19: Western blot analysis of p50 expression in acute CCl_4 injury **76**

Figure 3.20: Serum ALT and AST levels following acute CCl_4 injury **77**

Figure 3.21: Liver Ly6G immunostain in acute CCl_4 injury **78**

Figure 3.22: Neutrophil chemokine liver mRNA expression in acute CCl_4 injury **79**

Figure 3.23: IL-6 and TNFα chemokine expression in the liver in acute CCl_4 injury **80**

Figure 3.24: F4/80 liver immunostain in acute CCl_4 injury **81**

Figure 3.25: Gene expression of monocyte chemoattractant chemokines in the liver in acute CCl_4 injury **83**

Figure 3.26: Anti-apoptotic gene expression in the liver in acute CCl_4 injury ... **84**

Figure 3.27: Gene expression of BAX and XIAP in acute CCl_4 liver injury **85**

Figure 3.28: Cleaved caspase 3 liver immunostain in acute CCl_4 injury **86**

Figure 3.29: Percentage necrosis area quantification from H&E stained liver tissue in acute CCl_4 injury **87**

Figure 3.30: Western blot analysis of p50 expression in Nfkb1fl/fl and Nfkb1$^{hep-/-}$ mice **88**

Figure 3.31: Serum ALT and AST levels in acute DEN liver injury **89**

Figure 3.32: Immune cell infiltration assessed by H&E stain and TNFα gene expression in response to acute DEN liver injury **90**

Figure 3.33: NIMP immunostain of the liver in acute DEN injury **91**

Figure 3.34: Gene expression of neutrophil chemoattractant chemokines in acute DEN liver injury **92**

Figure 3.35: CD68 immunostain of the liver in acute DEN injury **93**

Figure 3.36: Gene expression of monocyte chemoattractant chemokines in acute DEN liver injury **94**

Figure 3.37: Expression of anti-apoptotic genes Gadd45β, Bcl-xL and Bcl-2 in acute DEN liver injury **95**

Figure 3.38: PCNA liver immunostain in acute DEN liver injury **96**

Figure 3.39: γH2AX liver immunostain in acute DEN liver injury **97**

Figure 4.1: Liver/body weight ratio after chronic CCl_4 treatment **102**

Figure 4.2: p50 expression in Nfkb1$^{fl/fl}$ and Nfkb1$^{hep-/-}$ mice **103**

Figure 4.3: Serum ALT and AST levels after CCl_4 treatment **104**

Figure 4.4: Ly6G liver immunostaining after chronic CCl_4 treatment **105**

Figure 4.5: Neutrophil chemoattractant chemokine expression following chronic CCl_4 treatment **106**

Figure 4.6: Inflammatory chemokine expression following chronic CCl_4 treatment **107**

Figure 4.7: CD68 liver immunostain following chronic CCl_4 injury **108**

Figure 4.8: Macrophage polarisation chemokine expression following chronic CCl_4 injury **109**

Figure 4.9: Fibrogenic gene expression following chronic CCl_4 treatment **110**

Figure 4.10: Sirius red stain following chronic CCl_4 treatment **111**

Figure 4.11: α-SMA immunostain following chronic CCl_4 treatment **112**

Figure 5.1: Western blot analysis of p50 expression in Nfkb1$^{fl/fl}$ and Nfkb1$^{hep-/-}$ mice **115**

Figure 5.2: Serum ALT and AST levels in Nfkb1$^{fl/fl}$ and Nfkb1$^{hep-/-}$ mice **116**

Figure 5.3: Liver tumours and liver/body weight ratio in Nfkb1$^{fl/fl}$ and Nfkb1$^{hep-/-}$ mice **117**

Figure 5.4: PCNA immunostain of Nfkb1$^{fl/fl}$ and Nfkb1$^{hep-/-}$ mice livers after 40 weeks DEN **118**

Figure 5.5: Liver tumour grade in Nfkb1$^{fl/fl}$ and Nfkb1$^{hep-/-}$ mice **119**

Figure 5.6: H&E stain and TNFα gene expression of Nfkb1$^{fl/fl}$ and Nfkb1$^{hep-/-}$ liver tissue **120**

Figure 5.7: NIMP liver immunostaining in Nfkb1$^{fl/fl}$ and Nfkb1$^{hep-/-}$ mice **121**

Figure 5.8: Gene expression of neutrophil chemoattractant chemokines S100A9, CXCL1 and CXCL2 in tumour and liver tissue **122**

Figure 5.9: CD68 liver immunostain in Nfkb1$^{fl/fl}$ and Nfkb1$^{hep-/-}$ mice **123**

Figure 5.10: Tumour and liver gene expression of CCL2 and CCL5 in Nfkb1$^{fl/fl}$ and Nfkb1$^{hep-/-}$ mice **124**

Figure 5.11: CD3 liver immunostain in Nfkb1$^{fl/fl}$ and Nfkb1$^{hep-/-}$ mice **125**

Figure 5.12: CD4 liver immunostaining in Nfkb1$^{fl/fl}$ and Nfkb1$^{hep-/-}$ mice **126**

Figure 5.13: CD8 liver immunostaining in Nfkb1$^{fl/fl}$ and Nfkb1$^{hep-/-}$ mice **126**

Figure 5.14: FOXP3 liver immunostaining in Nfkb1$^{fl/fl}$ and Nfkb1$^{hep-/-}$ mice **126**

Figure 5.15: B220 liver immunostain in Nfkb1$^{fl/fl}$ and Nfkb1$^{hep-/-}$ mice **127**

Figure 5.16: Tumour and liver gene expression of Gadd45β, Bcl-xL and Bcl-2 ..... **128**

Figure 5.17: Liver and tumour expression of apoptotic signalling proteins ... **129**

Figure 5.18: Tumour and liver expression of ERK and JNK signalling proteins **130**

Figure 5.19: Cleaved caspase 3 liver immunostain in Nfkb1$^{fl/fl}$ and Nfkb1$^{hep-/-}$ mice **131**

Figure 5.20: γH2AX liver immunostain in Nfkb1$^{fl/fl}$ and Nfkb1$^{hep-/-}$ mice **131**

Figure 5.21: NF-κB subunit protein expression in Nfkb1$^{fl/fl}$ and Nfkb1$^{hep-/-}$ mice **132**

Figure 5.22: PCA plot comparing Nfkb1$^{-/-}$, Nfkb1$^{hep-/-}$ and Nfkb1$^{fl/fl}$ samples **133**

Figure 5.23: Sample distance heatmap comparing Nfkb1$^{-/-}$, Nfkb1$^{hep-/-}$ and Nfkb1$^{fl/fl}$ samples **134**

Figure 5.24: Volcano plot comparing Nfkb1$^{-/-}$ and Nfkb1$^{fl/fl}$ samples **135**

Figure 5.25: Volcano plot comparing Nfkb1$^{hep-/-}$ and Nfkb1$^{fl/fl}$ samples **136**

Figure 5.26: Volcano plot comparing Nfkb1$^{-/-}$ and Nfkb1$^{hep-/-}$ samples **137**

Figure 5.27: Gene ontology and pathway analysis plot comparing Nfkb1$^{-/-}$ and Nfkb1$^{fl/fl}$ samples **138**

Figure 5.28: Gene ontology and pathway analysis plot comparing Nfkb1$^{-/-}$ and Nfkb1$^{fl/fl}$ samples **139**

Figure 5.29: KEGG analysis plot comparing Nfkb1$^{-/-}$ and Nfkb1$^{fl/fl}$ samples **140**

Figure 5.30: KEGG analysis plot comparing Nfkb1$^{-/-}$ and Nfkb1$^{fl/fl}$ samples **141**

Figure 5.31: Gene ontology and pathway analysis plot comparing Nfkb1$^{hep-/-}$ and Nfkb1$^{fl/fl}$ samples **142**

Figure 5.32: Gene ontology and pathway analysis plot comparing Nfkb1$^{hep-/-}$ and Nfkb1$^{fl/fl}$ samples **143**

Figure 5.33: KEGG pathway analysis plot comparing Nfkb1$^{hep-/-}$ and Nfkb1$^{fl/fl}$ samples **144**

Figure 5.34: KEGG pathway analysis plot comparing Nfkb1$^{hep-/-}$ and Nfkb1$^{fl/fl}$ samples **145**

Figure 5.35: Gene ontology and pathway analysis plot comparing Nfkb1$^{-/-}$ and Nfkb1$^{hep-/-}$ samples **146**

Figure 5.36: Gene ontology and pathway analysis plot comparing Nfkb1$^{-/-}$ and Nfkb1$^{hep-/-}$ samples **147**

Figure 5.37: KEGG pathway analysis plot comparing Nfkb1$^{-/-}$ and Nfkb1$^{hep-/-}$ samples **148**

Figure 5.38: KEGG pathway analysis plot comparing Nfkb1$^{-/-}$ and Nfkb1$^{hep-/-}$ samples **149**

Figure 5.39: p50 expression in Nfkb1$^{fl/fl}$ and Nfkb1$^{hep-/-}$ livers and tumours **152**

Figure 5.40: Serum ALT and AST levels in AAV-TBG-Null and AAV-TBG-Cre mice **152**

Figure 5.41: HCC liver tumour number and grade in AAV-TBG-Null and AAV-TBG-Cre mice **154**

Figure 5.42: PCNA liver immunostain in AAV-TBG-Null and AAV-TBG-Cre mice **155**

Figure 5.43: Tumour and liver TNFα gene expression in AAV-TBG-Null and AAV-TBG-Cre mice **156**

Figure 5.44: NIMP liver immunostain in AAV-TBG-Null and AAV-TBG-Cre mice **157**

Figure 5.45: Tumour and liver gene expression of neutrophil chemoattractant chemokines **158**

Figure 5.46: CD68 liver immunostain from AAV-TBG-Null and AAV-TBG-Cre mice **159**

Figure 5.47: Tumour and liver gene expression of monocyte chemoattractant chemokines in AAV-TBG-Null and AAV-TBG-Cre mice **160**

Figure 5.48: Tumour and liver apoptotic signalling gene and oncogene expression in AAV-TBG-Null and AAV-TBG-Cre mice **161**

Figure 5.49: Liver steatosis in Nfkb1$^{hep-/-}$ 19 month old aged mice **162**

List of Tables

Table 2.1: Genotyping PCR cycle **36**

Table 2.2: Genotyping primers **37**

Table 2.3: qPCR mouse primer sequences **44**

Table 2.4: qPCR cycle **45**

Table 2.5: Western blot antibodies **48**

Table 2.6: Immunostaining antibodies **51**

Table 5.1: Differentially expressed genes in Nfkb1$^{hep-/-}$ tumours compared to Nfkb1$^{fl/fl}$ liver tumours in DEN-induced HCC **150**

Table 6.1: Summary table of data from all liver injury models **170**

List of Abbreviations

°C	degrees celcius
AAV	adeno-associated virus
Ab	antibody
ALCL	anaplastic large-cell lymphoma
ALT	Alanine Transaminase
ANOVA	analysis of variance
aSMA	alpha smooth muscle actin
AST	Aspartate Aminotransferase
BAG-1	BCL-2 associated athanogene
Bcl-2	B-cell lymphoma 2
Bcl-3	B-cell lymphoma 3
BCR	B cell receptor
BMM	bone marrow derived macrophages
bp	base pair
C57Bl	C57 Black
CCL	CC chemokine ligand
CCl_4	carbon tetrachloride
CCR	CC chemokine receptor
C/EBP	CCAAT enhancer-binding protein
c-FLIP	cellular FLICE-like inhibitory protein
CLD	chronic liver disease
CXCL	CXC chemokine ligand
CXCR	CXC chemokine receptor
DAB	3,3'-diaminobenzidine
DAMP	damage associated molecular patterns
DC	dendritic cell
DDR	DNA damage response
DMEM	Dulbecco's Minimum Eagle Media
DMSO	dimethyl sulfoide
DNA	deoxyribonucleic acid
dNTP	deoxyribonucleoside triphosphate

dsDNA	double stranded
EBV	Epstein–Barr virus
ECL	enhanced chemiluminescence
ECM	extracellular matrix
EDTA	Ethylenediaminetetraacetic acid
EGFR	epidermal growth factor receptor
EMSA	electrophoresis mobility shift assay
EMT	epithelial-mesenchymal transition
ERK	extracellular regulated kinase
FCS	fetal calf serum
g	gram
GFP	green fluorescent protein
H&E	Haemotoxylin and Eosin
HBSS	Hanks Balance Salt Solution
HCA	hepatocellular adenoma
HCC	hepatocellular carcinoma
HCl	hydrochloric acid
HDAC1	histone deacetylase 1
HGF	hepatocyte growth factor
HPF	high powered field
HPV16	human papilloma virus 16
HRP	horseradish peroxidase
HSC	hepatic stellate cell
IFN	interferon
IGF	insulin growth factor
IgG	immunoglobulin
IHC	immunohistochemistry
IκB	inhibitor of κB
IKK	IkB kinase
IL	interleukin
IP	intraperitoneal injection
JAK-STAT	Janus kinase-Signal transducer and activator of transcription
kbp	kilobase pair
kg	kilogram

KPC1	Kip1 ubiquitination-promoting complex 1
LPS	lipopolysaccharide
M	molar
M1 or CAM	classically activated macrophage
M2 or AAM	alternatively activated macrophage
MEK	mitogen-activated protein kinase kinase
mg	milligram
ug	microgram
miRNA	micro RNA
ml	millileter
ul	microliter
mm	millimetre
mM	millimolar
um	micrometre
uM	micromolar
MMP	matrix metalloproteinase
mRNA	messenger RNA
Ms	mouse
NBD	NEMO binding domain
NEMO	NF-κB essential modulator
NF-κB1	nuclear factor kappaB 1
NF-κB	nuclear factor kappaB
nm	nanometre
NO	nitric oxide
NOS2	nitric oxide synthase 2
NSCLC	non-small-cell lung carcinoma
NTD	N-terminal domain
PAMP	pathogen-associated molecular patterns
PBS	phosphate buffer saline
PCR	polymerase chain reaction
PDGF	platelet derived growth factor
PD-L1	programmed death-ligand 1
PPR	pathogen pattern receptor
PTEN	phosphatase and tensin homolog

PTM	post translational modification
qPCR	quantitative PCR
Rb	rabbit
RHD	REL homology domain
RLTD	relative level of transcriptional difference
RNA	ribonucleic acid
ROI	region of interest
ROS	reactive oxygen species
RTK	receptor tyrosine kinase
s.e.m.	standard error of the mean
SASP	Senescence-associated secretory phenotype
SDS	Sodium dodecyl sulfate
ssDNA	single stranded
STAT	signal transducer and activator of transcription
TAD	transactivation domain
TAM	tumour-associated macrophage
TBG	Thyroxine-binding globulin
TBS	tris-buffered saline
TBS-T	TBS-Tween 20
TEMED	Tetramethylethylenediamine
TGF	transforming growth factor
Th	T helper lymphocyte
TIM-3	T-cell immunoglobulin and mucin-domain containing-3
TIMP	tissue inhibitor of metalloproteinase
TLR	toll-like receptor
TNF	tumour necrosis factor
Tpl-2	tumour progression locus 2
U	units
V	volts
v:v	volume per volume
VEGF	vascular endothelial growth factor
WT	Wild type
x g	centrifugal force

Chapter 1. Introduction

1.1 Nuclear Factor Kappa B (NF-κB)

The NF-κB (Nuclear Factor kappa-light-chain-enhancer of activated B cells) family of transcription factors, discovered in 1986, plays a fundamental role in living organisms by regulating a number of key cellular pathways involved in immune responses, inflammation and cancer (Hoesel & Schmid, 2013).

1.1.1 NF-κB transcription factor family members and structures

The NF-κB family of transcription factors consists of five members, including RelA (also known as p65), RelB, c-Rel, NF-κB1 and NF-κB2. NF-κB1 and NF-κB2 are synthesized as precursors (p105 and p100) then proteolytically cleaved to p50 and p52 respectively. The NF-κB proteins, which form homo- and hetero- dimers, all possess a Rel homology domain (RHD) which contains a nuclear localisation sequence and is essential for dimerization, DNA binding and interaction with the IκB inhibitory proteins. In addition, RelA, RelB and c-Rel have a transcriptional activation domain (TAD), enabling them to activate transcription when bound to genes. This domain is absent in NF-κB1 and NF-κB2, and thus prevents them from activating transcription in the absence of co-activating factors. RelB additionally has a leucine zipper (LZ) domain, a leucine-rich N-terminal extension, which is important for transactivation (alterations in the LZ structure lead to a decrease in RelB transcriptional capacity) (Dobrzanski et al., 1993). NF-κB1 p105 and p50, and NF-κB2 p100 and p52 have a glycine rich region (GRR) domain which is important for proteasomal processing (Collins et al., 2016). p105 and p100 also have an Ankyrin repeat domain (ANK), enabling them to act as inhibitors of NF-κB dimers (Savinova et al., 2009).

The following NF-κB dimers are therefore transcription-activating: p50:p65, p50:c-Rel, p50:RelB, p52:p65, p52:c-Rel, p52:RelB, p65:p65, p65:c-Rel, and c-Rel:c-Rel. The dimers with no TAD domain, p50:p50, p50:p52 and p52:p52 are unable to activate transcription alone and generally act as repressors of gene transcription, competing with activatory dimers to bind DNA (Hoesel & Schmid, 2013; Lawrence, 2009). When in complex with activatory cofactors however, these dimers can activate transcription. p65:RelB, c-Rel:RelB and RelB:RelB dimers are thought to have limited DNA binding

capacity. p65 and p50 form the most commonly seen heterodimer in the NF-κB family, activated in the canonical NF-κB pathway (Lawrence, 2009; Hoesel & Schmid, 2013).

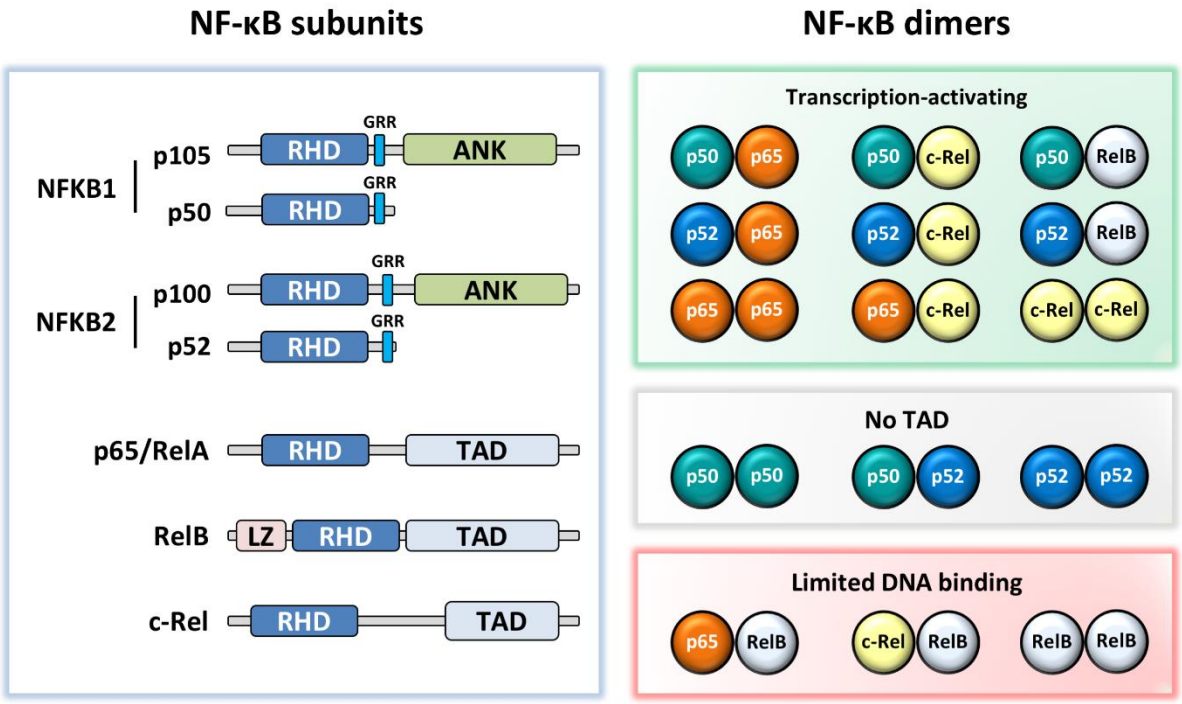

Figure 1.1 NF-κB subunit structures and dimeric combinations (Concetti & Wilson, 2018)**.** Figure shows the different NF-κB subunits and their structure, as well as the different NF-κB dimer possibilities and their function.

1.1.2 NF-κB activation pathways

In response to stimuli, such as pro-inflammatory cytokines or genotoxic stress, the NF-κB pathway is activated, initiated by the activation of the IKK-complex. This complex consists of two catalytic subunits, IKKα and IKKβ, as well as a regulatory subunit, NEMO (NF-κB essential modifier), also known as IKKγ. IKKα and IKKβ phosphorylate IκB proteins, which leads to their proteasomal degradation, thus allowing for NF-κB protein activation and translocation to the nucleus (Hayden & Ghosh, 2004). In the canonical NF-κB pathway (the classical NF-κB pathway), IKKβ is the predominant IκB kinase, whereas IKKα is mainly implicated in the alternative pathway, where it leads to processing of p100 to p52 by the 26S proteasome. NEMO represents a key player in the activation of the IKK complex, whereby it undergoes Lys63-linked ubiquitylation through the interaction with upstream signalling molecules, allowing it to recruit kinases

which will in turn activate IKKβ by phosphorylating their activation loops (Perkins, 2007). Stimulation of the IL-1R or TLR receptor leads to their dimerization and recruitment of the Myddosome complex, consisting of MyD88, IRAK4 and IRAK1 (or IRAK2). IRAK1 is phosphorylated by IRAK4 then associates with ubiquitin E3 ligase TRAF6, subsequently activating it. TRAF6 and the ubiquitin E2 complex, comprising Ubc13 and Uev1A, catalyze the synthesis of K63-linked polyubiquitin chains which are conjugated to other proteins or unanchored. Unanchored K63 polyubiquitin chains bind the TAB2 subunit of the TAK1 kinase complex, promoting autophosphorylation of TAK1, and thus resulting in its activation. The polyubiquitin chains also bind NEMO to recruit the IKK complex, which facilitates the phosphorylation of IKKβ by TAK1. IKK is then activated to phosphorylate IκBα.

Once IκB is phosphorylated at serines 32 and 36, this is recognised by SCFBeta-TrCP (Skp1-cullin1-F-box protein, beta-transducin repeat-containing proteins), a ubiquitin ligase complex which ubiquitinates it, marking IκB for proteasomal degradation. This subsequently allows the rapid translocation of NF-κB dimers to the nucleus, where they will bind to κB sites in promoter and regulatory regions of NF-κB target genes and activate transcription (Figure 1.2) (Orian et al., 2000).

Upon activation and translocation to the nucleus, NF-κB also activates the transcription of IκBα, generating a negative feedback loop in order to limit the NF-κB-mediated response, whereby IκBα dissociates NF-κB-DNA complexes, shuttling NF-κB back to the cytoplasm. Additionally, ubiquitination of NF-κB subunits also leads to the degradation of NF-κB and termination of transcription (Collins et al., 2016).

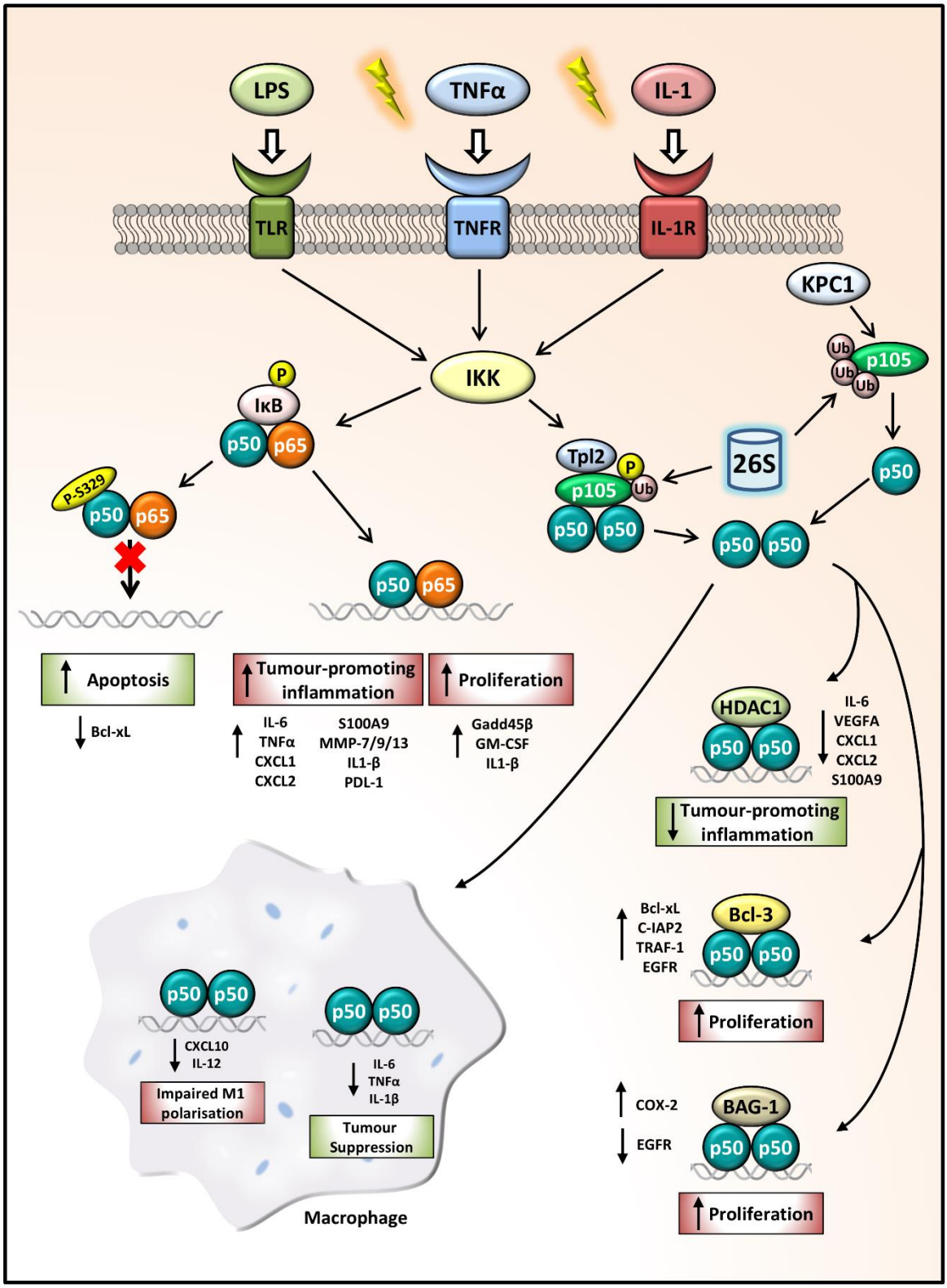

Figure 1.2 NF-κB1 activation and regulation of gene expression in cancer (Concetti & Wilson, 2018). NF-κB1 p105/p50 regulation of gene expression in cancer. Following inflammatory stimulation, IKK functions as the key activator of the NFKB1 signalling pathway. Phosphorylation and ubiquitination of IκB releases p50:p65 dimers which can drive the transcription of tumour-promoting inflammatory genes and anti-apoptotic and proliferative

genes. p50 phosphorylation at the S329 site impairs p50:p65 dimer binding to DNA, decreasing Bcl-xL expression leading to increased apoptosis, hindering cancer progression. p105 phosphorylation and ubiquitination leads to its processing by the 26S proteasome, releasing p50 homodimers. The p50:p50:HDAC1 complex represses tumour-promoting inflammatory gene expression thus acting as a tumour-suppressor complex, while p50 homodimers in complex with Bcl-3 or BAG-1 can drive proliferation. In macrophages, aberrant p50 homodimer repression of CXCL10 and IL-12 leads to impaired M1 polarisation. Whilst p50:p50 repression of pro-inflammatory and proliferative mediators can also promote tumour suppression.

1.1.3 NF-κB activity modulation

NF-κB is known to play a central role in the regulation of inflammation, immunity, cell proliferation and apoptosis, and increasing evidence suggests a crucial role for NF-κB in the development of cancer. A variety of different stimuli are able to trigger the activation of the NF-κB pathway, which culminates in positive or negative regulation of gene transcription (Oeckinghaus et al., 2011). Cytokines, notably TNFα (Tumour necrosis factor α) and IL-1 (interleukin 1), and pathogen-associated molecular patterns (PAMPs) including LPS (lipopolysaccharide), found in the outer membrane of Gram-negative bacteria, represent three main activators of the NF-κB signalling cascade (Lawrence, 2009). These bind cell-surface receptors, including TNFRs, IL-1Rs and TLRs (Toll-like receptors), resulting in the translocation of NF-κB dimers to the nucleus, driving the transcription of genes involved in orchestrating the immune response. TLRs are specifically involved in recognising PAMPs, and thus represent key players in pathogen recognition and defence mechanisms (Mogensen, 2009). Downstream of the pathway, dimers bind to their target genes, activating the transcription of inflammatory genes coding for cytokines and chemokines such as TNFα, IL1-β, IL-8 and RANTES; this in turn further enhances the NF-κB signalling pathway through additional binding to chemokine and cytokine receptors, creating a positive feedback loop (Bonizzi & Karin, 2004).

NF-κB's role in the regulation of immune responses extends from the innate to the adaptive immune system. It is responsible for triggering the first line of defence through mediating transcription of pro-inflammatory genes. These not only include cytokines and chemokines, but also genes encoding adhesion molecules, allowing for the extravasation of immune cells, as well as matrix metalloproteinases which mediate

chemotaxis (Eck et al., 1993; Vincenti et al., 1998). Cells of the innate immune system, including macrophages, neutrophils and DCs (dendritic cells), migrate to the site of infection in response to the detection of foreign particles. This is followed by APCs (antigen-presenting cells), notably DCs, interacting with T cells in the initiation of the adaptive immune response.

The successful activation of T cells requires the upregulation of costimulatory molecule expression on the surface of APCs (CD80 and CD86), a process dependent on NF-κB (Hoebe et al., 2003). Subsequently, antigen recognition by TCRs (T cell receptors) and BCRs (B cell receptors) also leads to the activation of NF-κB in order to upregulate cytokines that support proliferation and differentiation, as well as anti-apoptotic factors (Gerondakis & Siebenlist, 2010).

It is known that NF-κB plays a central role in hematopoeisis, the formation of blood cells, derived from the lymphoid, myeloid and granulocytic lineages. These include B cells and T cells (lymphoid lineage), monocytes, macrophages and dendritic cells (myeloid lineage), as well as basophils, neutrophils and eosinophils (granulocytes). Most immune cells undergo rapid turnover and therefore require a tight regulation of proliferation and apoptosis. NF-κB is a key player in this, ensuring rapid expansion of immune cells during immune responses, as well as targeted cell death in the resolution of the immune response (Hayden et al., 2006). The role of NF-κB is therefore contrasted in that it can exhibit pro-survival and anti-apoptotic properties, in addition to its ability to mediate apoptosis in different conditions.

With increasing research linking inflammation and dysregulated immune responses to cancer, evidence has suggested that the NF-κB pathway is strongly involved in carcinogenesis (Okamoto et al., 2007; Brücher & Jamall, 2019). It is now widely accepted that chronic inflammation and infection represent major risk factors for certain cancers. An example includes chronic HBV (hepatitis B virus) and HCV (hepatitis C virus) infections which significantly increase the risk of developing HCC (hepatocellular carcinoma). Similarly, Helicobacter pylori infections have been associated with gastric cancers (Karin, 2006). NF-κB has also been implicated in several inflammation-linked cancers, including colitis-associated cancer and MALT (mucosal-associated lymphoid tissue) lymphoma. These are characterized by elevated expression of NF-κB, whereby NF-κB is persistently activated, leading to the suppression of apoptosis and to uncontrolled proliferation (Viennois et al., 2013; Ruland et al., 2001). Chronic infection and inflammation lead to the NF-κB-dependent transcription of genes coding for

inflammatory cytokines, cell cycle modulators, growth factors and survival signals, and angiogenic factors which contribute to tumorigenesis. The expression of these factors culminates in the activation of other signalling pathways, further enhancing tumour promotion (Karin, 2006).

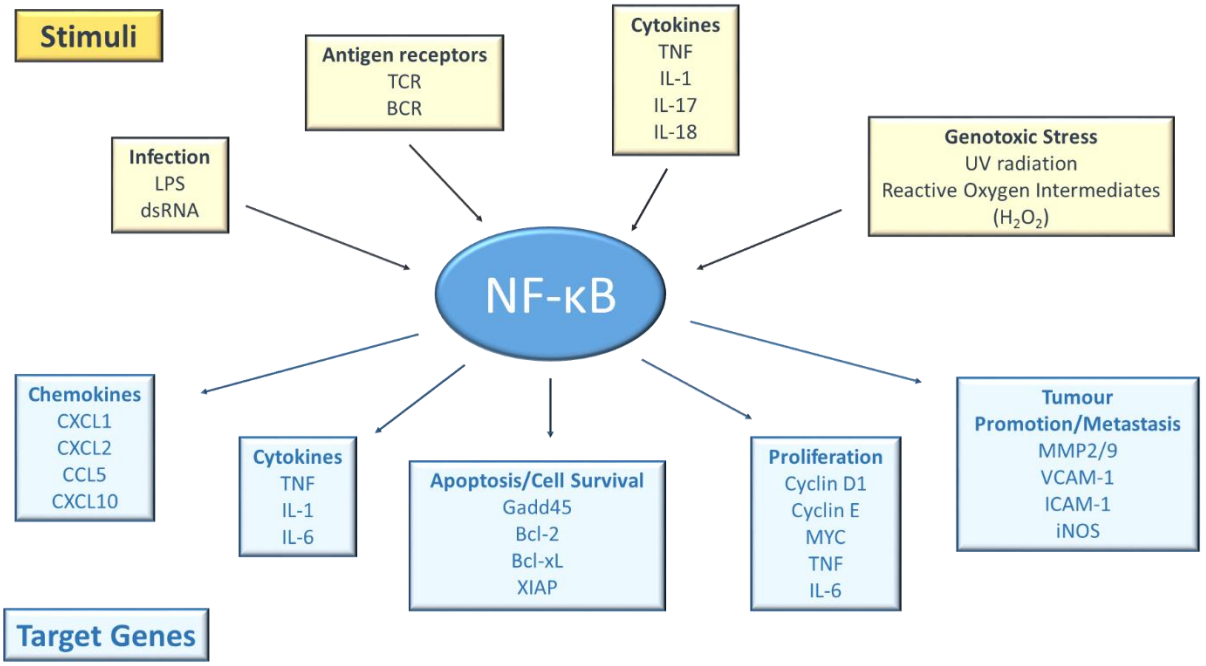

Figure 1.3 NF-κB-activating stimuli and target genes. Diagram shows the different NF-κB stimuli including infection, antigen receptors, cytokines and genotoxic stress, and some of the different NF-κB target genes including chemokines, cytokines, apoptosis/cell survival genes, proliferation genes and genes involved in tumour promotion and metastasis.

1.2 Nuclear Factor Kappa B1 (NF-κB1)

NF-κB1 comprises p105 and p50. The p50 subunit of NF-κB results from the proteolytic cleavage of its precursor, p105. Studies have established different means of p105 processing to p50, including co-translational proteasomal degradation of p105 (Lin et al., 1998), and signal-induced degradation of p105 by phosphorylation and ubiquitination (Fujimoto et al., 1995). In the latter case, upon stimuli, p105 is phosphorylated in its C-terminal domain containing an ankyrin repeat, followed by degradation in a ubiquitin-proteasome dependent manner. The degradation of the inhibitory C-terminal region subsequently leads to p50 activation. This mechanism is similar to that of IκBs, which undergo the same degradation pathway, releasing the

inhibition of NF-κB dimers. A recent study identified KPC1 (KIP1 ubiquitination-promoting complex) as the ubiquitin ligase that ubiquitinates p105 following binding to the ankyrin repeat domain. Interestingly, overexpression of KPC1 led to the inhibition of tumour growth; this was suggested to be caused by the increased production of p50, and the subsequent downregulation of p65, thus leading to an increase in p50:p50 complexes and a decrease in tumorigenic p50:p65 complexes (Kravtsova-Ivantsiv et al., 2015a).

1.2.1 p105 structure and function

p105 has a dual function. It acts as a precursor for p50, undergoing processing and thus regulating the availability of p50 for NF-κB dimer formation. Upon stimuli, p105 is phosphorylated in its C-terminal domain containing an ankyrin repeat (ANK), similar to that of the IκB inhibitory proteins, followed by partial degradation in an ubiquitin-proteasome dependent manner. The degradation of the inhibitory C-terminal region subsequently leads to p50 activation (Perkins, 2007). p105 also inhibits preformed NF-κB dimers, acting in an IκB manner via its ANK domain. In mice where p105 serine residues 927 and 932 are mutated to alanine, there is impaired p105 processing and as a result p50:p65 release and activity is inhibited (Sriskantharajah et al., 2009; Jacque et al., 2014). Aside from its direct role in the control of NF-κB activation, p105 also plays an additional role in stabilising Tpl2 kinase (tumour progression locus 2). p105 inhibits Tpl2-mediated activation of the MEK/ERK (mitogen-activated protein kinase kinase/extracellular regulated kinase) pathway and this inhibition is abrogated following IKK-induced proteolysis of p105 (Beinke et al., 2004; Concetti & Wilson, 2018).

1.2.2 p50 structure and function

The function of the p50 subunit of NF-κB differs depending on its dimerization partner. When dimerised with p65, the p50:p65 complex activates the transcription of NF-κB target genes. However, when p50 is dimerized with another p50 subunit, these dimers are unable to activate transcription due to the lack of a TAD, and thus act as transcriptional repressors when bound to DNA, preventing activatory NF-κB dimers from binding. Although p50 homodimers are unable to activate transcription alone, they

are able to turn genes on when complexed with activatory cofactors; in contrast inhibitory cofactors enhance the repressive function of p50 homodimers (Lawrence, 2009).

1.2.3 p105 and p50 cofactor complexes

p105 proteins are known to interact with several factors to modulate apoptosis and cell cycle. Of these, Tpl2 (tumour progression locus 2) and ABIN2 (A20-binding inhibitor of NFKB2) have been shown to be stabilised and inhibited by p105, leading to the repression of MEK/ERK pathway signal transduction, with p105 acting as a competitive inhibitor of Tpl2 substrates (Babu et al., 2006; Beinke et al., 2003). p105 has also been shown to interact with c-FLIP (Cellular FLICE (FADD-like IL-1β-converting enzyme)-inhibitory protein), ZUD (also known as DD-containing protein Unc5CL) and LYL1 (lymphoblastic leukaemia associated haematopoiesis regulator 1)(Zhang et al., 2004; Ferrier et al., 1999; Li et al., 2003).

p50 homodimers repress inflammation by competing with activating NF-κB dimers and preventing them from binding to κB sites on the promoters of target genes, further strengthened by the recruitment of co-repressors. Histone deacetylases (HDAC) repress gene transcription by removing acetyl groups from histones, often leading to chromatin condensation and transcriptional repression. The p50:p50:HDAC1 complex is able to repress multiple inflammatory genes, including GM-CSF, CCL2, CXCL-10, and MMP-13 (Elsharkawy et al., 2010). We have recently identified the site of p50:HDAC1 interaction and shown that mutagenesis of this binding site on p50 prevents HDAC1 binding with p50 homodimers. As a result of this loss of p50:HDAC1 interaction, we observed increased expression of the inflammatory genes CXCL1, CXCL2, and IL-6 both basally and in response to stimulus (Cartwright et al., 2018).

The IκB family protein B cell lymphoma 3 (Bcl-3) plays a dual role in p50 transcriptional regulation. As a co-activator it can bind p50 via ankyrin repeats and help drive gene transcription when complexed with p50 homodimers, and is also able to recruit other transcriptional regulators including STAT1, AP-1, c-Jun, c-fos (Chang & Vancurova, 2014). However, Bcl-3 can also stabilize the p50 homodimer by masking ubiquitination sites and preventing removal from gene promoters. Therefore, Bcl-3 can also function as a co-repressor of gene transcription by preventing transcriptionally active NF-κB dimers from binding to these gene promoters and driving transcription (Collins et al.,

2014). Indeed, following LPS (lipopolysaccharide) stimulation of macrophages, p50:p50:Bcl-3 complexes negatively regulate TNFα (tumour necrosis factor), IL-1α, and IL-1β expression, while activating anti-inflammatory IL-10 gene transcription (Collins et al., 2014). In this context Bcl-3 enhances p50 homodimer-dependent TNF repression, as p50 is also able to repress TNF in the absence of Bcl-3, though to a lesser extent (Wessells et al., 2004a). However, it is highly unlikely that these complexes are as simple as this; it is far more realistic to view these known protein interactions as parts of the jigsaw when in reality they are likely to form large multimeric complexes consisting of numerous co-factors. In support of this, both HDAC1 and Bcl-3 have also been found in nuclear complexes together in LPS stimulated cells (Wessells et al., 2004a).

Other factors known to interact with and modulate p50 homodimer activity include IκBζ and C/EBP (CCAAT enhancer binding protein) which has been shown to displace HDAC1 and HDAC3 bound to p50 homodimers, abrogating anti-apoptotic gene repression and contributing to aberrant p50 activity in acute myeloid leukemia (Paz-Priel et al., 2011; Yamamoto et al., 2004). Also, the PARP (Poly (ADP-ribose) polymerase) regulation of the co-activator p300 is necessary for p50 transcriptional activation in primary lung fibroblasts following TNF and LPS stimulation (Hassa et al., 2003). EHMT1 can also be recruited by p50 homodimers and catalyses repressive methylation (H3K9) in antiviral immunity genes regulated by IFN-1 (interferon type 1) (Ea et al., 2012). The various p105 and p50 complexes are illustrated in Figure 1.4.

The dual ability of p50 to both activate and repress gene transcription instigates a complex relationship between this NF-κB subunit and cancer, with much controversy as to its role played in carcinogenesis. Given the complex and diverse nature of cancer as a disease, it is not surprising that the function of NF-κB1 can differ substantially in a cell, organ, and cancer specific manner. I will discuss how NF-κB1 is implicated in carcinogenesis, acting both as a pro- and anti-tumorigenic transcription factor.

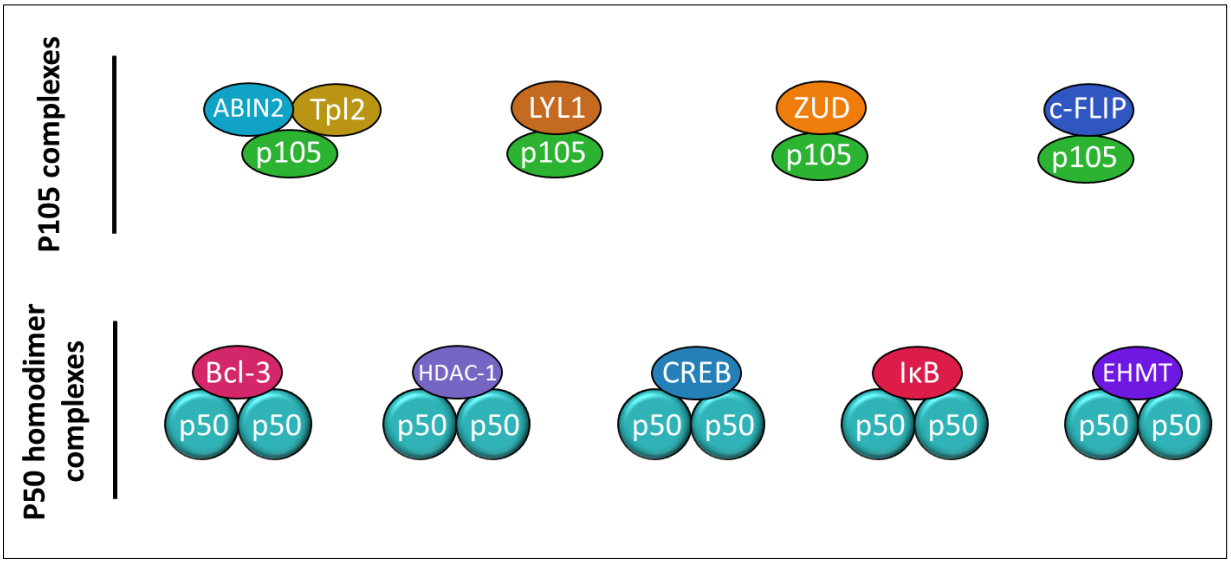

Figure 1.4 p105 and p50 homodimer complexes. p105 has been shown to interact with ABIN2, Tpl2, LYL1, ZUD and c-FLIP, while p50 homodimers have been shown to interact with Bcl-3, HDAC-1, CREB, IκB and EHMT.

1.2.4 NF-κB1 in inflammation

Studies in Nfkb1$^{-/-}$ mice have shown that, in the absence of p105/p50, multifocal defects in immune responses can be observed. Mice lacking this subunit exhibit impaired B lymphocyte proliferation and responses to infection. However, they do not display any developmental abnormalities (Sha et al., 1995a). In contrast, RelA knock-out mice are embryonic lethal, as a result of foetal hepatocyte apoptosis (Doi et al., 1999a). Nfkb1$^{-/-}$ mice have also been shown to experience accelerated ageing, driven by underlying chronic inflammation (Bernal et al., 2014; Jurk et al., 2014). Additionally, the absence of p105 also affects the Tpl2–MAPK–ERK (Tumour progression locus-2-mitogen-activated protein kinase- extracellular signal-regulated kinase) pathway, whereby Tpl2 and ABIN-2 (A20-binding inhibitor of NF-κB 2) expression is dramatically decreased (Lee et al., 2015). Tpl2 is thought to induce TNFα expression in inflammatory responses.

Due to the absence of transactivation domains, p50 homodimers are unable to activate gene transcription alone. In order to drive transcription, they must recruit co-activating factors. p50 homodimers are, however, mostly recognised as repressors of transcription. This has led to the belief that p50 plays a crucial role as an anti-inflammatory transcription factor and in the resolution of inflammation, by dampening the expression of pro-inflammatory genes (Lawrence, 2009). A study conducted by S.

Kang et al. showed that p50:p50 complexes repress IL-2 (interleukin-2) expression in CD4+ T lymphocytes. This was supported by the observations that p50 overexpression led to repressed IL-2 expression, and increased expression of IL-2 correlated with a decrease in p50 homodimers (Kang et al., 1992). Additionally, it was also shown by J. Bohuslav et al. that increased p50 expression leads to a downregulation of TNF production following LPS stimulation (Bohuslav et al., 1998). Conversely, p50 has been shown to promote the expression of IL-10, an anti-inflammatory cytokine, with the help of the co-activator CREB (cAMP response element-binding protein), a known activator of transcription (Cao et al., 2006). The same group showed that p50 homodimers negatively regulate TNF and IL-12, thus suggesting a contrasted role for these dimers in the modulation of cytokine production. Combined together this evidence strongly supports the role of p50 as an anti-inflammatory transcription factor.

Furthermore, it was shown that p50 is able to limit the inflammatory injury during pneumonia (Mizgerd et al., 2003). J. P. Mizgerd et al. showed that Nfkb1$^{-/-}$ mice displayed an increase in the expression of NF-κB-regulated cytokines including KC, MIP-2, TNFα, IL-6 and IL1-β. They subsequently postulated that p50 homodimers are essential to limit later inflammatory gene expression in the context of E.coli pneumonia. This further supports a role for p50 in the resolution of inflammatory responses. Additionally, another study found that following carbon tetrachloride injection (repeated intraperitoneal hepatotoxin injection throughout 12 weeks), which leads to hepatic injury, Nfkb1$^{-/-}$ mice displayed more inflammation and fibrosis compared to wild type mice. TNFα expression was increased in the absence of p50, which our group showed to be the result of the inability of p50 to repress TNFα in a HDAC (histone deacetylase)-dependent manner (Elsharkawy et al., 2010).

The mechanisms by which p50 homodimers bring about repression of transcription still remain incompletely understood; however several studies have supported a role for the recruitment of transcriptional co-repressors, including HDAC1. This enzyme deacetylates histones, causing these to bind DNA more tightly and thus leading to chromatin condensation. This is in contrast to HATs (histone acetylases), which lead to the decondensation of chromatin, making gene promoters more readily accessible for transcription activators to bind (Choudhary et al., 2009). It has been shown that the p50:p50:HDAC1 complex represses the transcription of multiple pro-inflammatory genes (Elsharkawy et al., 2010). Here, HDAC1 was shown to be recruited to several promoters of genes repressed by p50, including GM-CSF, CCL2 and CXCL10. The

same study also showed that HDAC1 mediates the repression of MMP-13 (matrix metallopeptidase 13) through the interaction with p50 homodimers. S. A. Williams et al. also found that p50 recruitment of HDAC1 led to transcriptional repression, promoting HIV virus latency (Williams et al., 2006). Additionally, work from our lab showed through chromatin immunoprecipitation assays that p50 and HDAC1 are both recruited to the promoters of the CXCL1, CXCL2 and S100A9 genes, which represent neutrophil chemokines (Wilson et al., 2015). In contrast, HDAC1 was absent in these regions in Nfkb1$^{-/-}$ mice.

Conversely, Bcl-3 (B-cell lymphoma 3 encoded protein) can act as a transcriptional co-activator as well as being able to repress transcription, depending on the context. A study looking at the role of p50 and Bcl-3 in LPS (lipopolysaccharide)-induced inflammatory responses in macrophages found that p50-Bcl-3 complexes negatively regulate TNFα, IL-1α and IL-1β, while activating anti-inflammatory IL-10 gene transcription (Wessells et al., 2004b). They proposed that Bcl-3 can enhance p50-dependent TNFα repression, since p50 is able to repress TNFα in the absence of Bcl-3 as well. Their results also suggested that HDAC1 was involved in the Bcl-3-mediated repression of TNFα, as HDAC1 and Bcl-3 were found to be in nuclear complexes together in LPS-stimulated cells (demonstrated by co-immunoprecipitation assays). p50 homodimers in complex with HDAC1 and Bcl3 were found to gradually replace NF-κB-activating dimers in response to LPS stimulation in macrophages, so as to attenuate NF-κB target genes (Wessells et al., 2004b). Furthermore, another group demonstrated that p50 homodimers and Bcl-3 repress gene transcription in tolerant CD4+ T cells, including transcription of the cytokine IL-2 (Grundström et al., 2004). This further supports the idea that p50 plays a major role in the resolution of inflammatory responses. Additionally, N. Watanabe et al. showed that Bcl-3 activates p50 homodimers and mediates their translocation to the nucleus, where they are able to modulate transcription (Watanabe et al., 2003).

1.2.5 NF-κB1 in cancer

Current evidence strongly suggests that aberrant activation of the NF-κB signalling pathway is associated with carcinogenesis. A number of key cellular processes are governed by the effectors of this pathway, including immune responses and apoptosis, both crucial in the development of cancer. Therefore, it is not surprising that

dysregulated and chronic NF-κB signalling can have a profound impact on cellular homeostasis.

p50 homodimers are primarily considered to repress gene transcription, dampen inflammatory responses, and abrogate anti-apoptotic signalling (Elsharkawy et al., 2010; Wilson et al., 2015; Schmitt et al., 2011). Chronic inflammation and the evasion of apoptosis are hallmarks of cancer (Hanahan & Weinberg, 2011), hence it is no surprise that there is an abundance of emerging evidence supporting a role for p50 homodimers as tumour-suppressors. KPC1 (KIP1 ubiquitination promoting complex 1) was recently identified as the ubiquitin ligase that mediates the processing of p105 to p50 (Kravtsova-Ivantsiv et al., 2015b). Kravtsova-Ivantsiv and colleagues showed that KPC1 overexpression in a mouse xenograft tumour model derived from either the glioblastoma cell line (U87-MG cells) or the human breast cancer cell line (MDA-MB 231 cells) inhibits tumour growth via increased p50 generation. This was further supported by p50 overexpression that also reduced the growth of both tumours. Interestingly, p65 expression was significantly decreased in KPC1 and p50 overexpressing tumours, and an increase in the formation of p50 homodimers over p50-p65 heterodimers was confirmed by EMSA. The increase in p50 homodimer formation resulted in downregulated genes including HMGI-C, lin-28 homolog A, IL-6, IL-6R and VEGFA and an upregulation of tumour suppressor genes including PTEN (Phosphatase and tensin homolog). Moreover, in support of this, in a human context both p50 and KPC1 expression was significantly decreased in human head, neck, and glioblastoma tumours compared to normal tissue, and p50 expression decreased in breast cancer tumours (Kravtsova-Ivantsiv et al., 2015b). Together their findings strongly suggest that KPC1, and hence p50, inhibit the growth of various tumours, likely via inhibition of p50:p65-mediated pro-tumorigenic gene transcription.

One of the main infection-driven gastric cancers is caused by Helicobacter pylori. Helicobacter Pylori produces a number of virulence factors able to activate the NF-κB pathway, which in turn lead to the recruitment of inflammatory cells and the production of inflammatory mediators that help drive tumorigenesis (Sokolova & Naumann, 2017). In conjunction with liver cancer studies the complexity of NF-κB activation in gastric tumorigenesis has also been highlighted using IKK cell-specific knockouts. $IKK^{-/-}$ in the gastric epithelial cell compartment leads to accelerated development of dysplasia, whereas knockout in only myeloid cells inhibited progression to gastric atrophy and dysplasia (Shibata et al., 2010). However, also in correlation with liver cancer

development, mice lacking Nfkb1 develop spontaneous invasive GC. Here the Nfkb1$^{-/-}$ mice display characteristics of gastric cancer in humans including T cell and NK cell infiltration, increased pro-inflammatory gene expression including IL-1b, IL-6, TNFa and osteopontin, and the metalloproteinases MMP-7, MMP-9 and MMP-13. Mechanistically, this is explained by aberrant JAK-STAT (Janus kinase-Signal transducer and activator of transcription) signalling via increased pro-inflammatory mediators, STAT1 expression and increased expression of the immune checkpoint inhibitor PD-L1 (Abstract, 2018). Importantly, in this model Nfkb1 expression was required in both the epithelial and immune cell compartments in order to prevent GC. The findings of this study are consistent with human GC patient data linking NFKB1 gene polymorphisms, including rs28362491, with reduced p105/p50 expression and GC development (Hua et al., 2014; Arisawa et al., 2013). In contrast, both NFKB1 and p65 have been shown at higher levels in GC cell lines and primary human GC tumours when compared to normal gastric epithelial cells which correlated with poor survival in patients (Huang et al., 2016). Mechanistically, it was revealed that the NFKB1 targeting miRNA miR-508-3p was downregulated in GC cells, suggesting a tumour-suppressive function for this miRNA (Huang et al., 2016). This reiterates the potentiality that p50:p65 dimers are pro-tumorigenic drivers as opposed to p50 homodimers in this context.

Aside from the suppressive effects of p50 homodimers, p105 itself can also exert a tumour-suppressive function. A recent study highlighted a role for p105 as a tumour suppressor via stabilisation of Tpl2. In a urethane-induced lung cancer mouse model which re-enacts human lung cancers associated with tobacco smoking, both Nfkb1$^{-/-}$ and Tpl2$^{-/-}$ mice showed a significant increase in lung tumour size and number when compared to wild type mice. Following the observation that Tpl2 expression was also decreased in a NFKB1$^{-/-}$ human lung cancer cell line, Fan Sun and colleagues (Sun et al., 2016) demonstrated that re-expressing p105, and not p50, restored Tpl2 levels in these cells, resulting in reduced tumour growth. Contrastingly, Tpl2 knockdown increased lung tumour cell growth. This study highlights the importance of p105 stabilisation of Tpl2 in suppressing lung carcinogenesis (Sun et al., 2016). Analysis of human non-small-cell lung carcinoma (NSCLC) tumours graded from stage 1 to 3A revealed that p105 stromal and epithelial tumour cell expression was a positive prognostic indicator of disease-specific survival (Al-Saad et al., 2008). However, it has also recently been shown that co-expression of p65 and phosphorylated p105 is

associated with poor prognosis in NSCLC, whereas expression of p65 or phosphorylated p105 alone was not associated with this (Lin et al., 2018). Again, this strongly suggests that it is p50:p65 dimer activity and not p50 homodimer activity that is detrimental in NSCLC.

mRNA expression analysis has revealed that NFKB1 is downregulated in multiple human haematological malignancies, including T and B-cell lymphoma and acute myeloid leukemia, while p65 expression is upregulated. DNA alkylation damage leads to increased lymphomas in Nfkb1$^{-/-}$ mice when compared with wild type mice. Mice heterozygous for Nfkb1 exhibit an intermediary phenotype whilst maintaining p50 function, indicating the haploinsufficient nature of Nfkb1 as a tumour suppressor (Voce et al., 2015). Interestingly, p50 phosphorylation by CHK1 (checkpoint kinase 1) at serine 329 ensures the elimination of replication-associated DNA-damaged cells and is necessary for genome maintenance. Phosphorylation of p50 at this site during the S phase of the cell cycle inhibits its activity and DNA binding, downregulating the expression of the anti-apoptotic protein Bcl-xL sensitizing cells to DNA strand breaks. Transfection of Nfkb1$^{-/-}$ MEFs (mouse embryonic fibroblasts) with S329A mutant p50 prevents p50 phosphorylation and inhibition, and blocks the observed decrease in Bcl-xL expression during S phase (Crawley et al., 2015). Similarly, it has also been shown that S329 p50 phosphorylation is involved in promoting apoptosis in cells that have undergone O6-methylguanine (O6-MeG) DNA lesions, by preventing the expression of anti-apoptotic genes (Schmitt et al., 2011). Therefore, p50 may play a protective role in preventing the survival of DNA-damaged cells that have the potential to become cancerous. In support of this, it was shown by EMSA that in adult T-cell leukemia (ATL) patients, NF-κB-DNA complexes consist of both p50:p65 heterodimers and p50 homodimers, whereas in healthy patients they are predominantly p50 homodimers. Moreover, only p50:p65 dimers, and not p50 homodimers, were able to activate the transcription of IL-2Ra in ATL patients, demonstrating that constitutive activation of p50:p65 is a major driver of ATL (Mori et al., 1999). These studies highlight that aberrant p50:p65, rather than p50:p50 signalling could be implicated in haematological malignancies where DNA-damaged cells have evaded apoptosis.

In contrast to p50:p50 homodimers, an increase in DNA bound p50:p65 heterodimers leads to increased expression of NF-κB regulated genes including pro-inflammatory (IL-1β, TNFα, CXCL1), anti-apoptotic (Bcl-xL, Bcl-2, Gadd45β) and proliferative (IL-6,

GM-CSF) to name a few. Therefore, it is not surprising that NF-κB1 acts as a tumour promoter in this context. In addition, there are also a number of cancers including lymphomas and colorectal cancer where recruitment of co-activators will actually promote the expression of a similar array of tumour-promoting genes.

The aforementioned Bcl-3 complexed with p50 homodimers is associated with tumorigenesis in several malignancies (Mathas et al., 2005). Notably, classical Hodgkin/Reed-Sternberg (HRS), anaplastic large cell lymphoma (ALCL) and T cell lymphomas, exhibit constitutive p50 homodimer activity associated with Bcl-3, verified by EMSA and IP shift. Additionally, increased p50 and Bcl-3 expression in HRS and ALCL cell lines are mainly in the nuclear fractions verified by co-immunoprecipitation and is associated with increased expression of the anti-apoptotic genes Bcl-xL, c-IAP2, and TRAF-1 in the HRS cell lines (Mathas et al., 2005).

In accordance with this, several other studies confirm that increased tumour expression of p50 (and not p65) correlates with an increased expression of Bcl-3. For instance, mouse skin papillomas and squamous cell carcinomas (SCC) display increased p50 and p52 expression compared to normal epithelial tissue from the middle stages of cancer development, while p65 levels remained unchanged. This correlates with increased Bcl-3 expression in late stage skin papillomas and SCC, suggesting a role for the p50:p50:Bcl-3 complex in tumour promotion (Budunova et al., 1999). Other examples of co-expression in malignant tissue include HPV16 (human papilloma virus 16) positive oral cancers, nasopharyngeal carcinoma and breast cancer (Cogswell et al., 2000; Thornburg et al., 2003; Mishra et al., 2006). Together these findings suggest that p50 homodimers in complex with Bcl-3 may play an important role in carcinogenesis, likely via the upregulation of NF-κB target genes. Importantly, to verify where p50:p50:Bcl3 complexes truly function as tumour promoters in-depth molecular analysis such as EMSA, nuclear localisation, IP and analysis of other NF-κB subunits should be included.

Studies involving breast and gynaecological cancers suggest an association with increased NFKB1 expression and nuclear localisation. Increased p50 DNA binding and to a lesser extent p65 binding has been observed in a subset of high-risk estrogen receptor positive breast cancers (Zhou et al., 2005). Also, knock-down of NFKB1 in the inflammatory breast cancer cell line (SUM-149) suggests that NFKB1 expression

positively regulates Rho C expression and cell motility, which may contribute to the metastatic phenotype of inflammatory breast cancer (Brenner et al., 2008). Overexpression of p105 along with p100 in cervical carcinoma-derived keratinocytes expressing the HPV16 oncoproteins E7 or E6, show localisation is predominantly cytoplasmic when E7 is expressed, and nuclear in the case of E6; therefore, these viral oncoproteins may actually dictate the subcellular localisation of p105 and p100 and hence activity of p105 and p100 (Havard et al., 2005). Contrasting results exist in cervical cancer describing both increased nuclear p50 and p65 correlating with poor tumour grade and larger tumour size, and increased expression of predominantly p50 homodimers with no observed increase in p65 (Prusty et al., 2005; Li et al., 2009). Whereas in ovarian cancer it is both p50 and p65 that are increased when compared to borderline and benign tumours, indicating the involvement of p50:p65 heterodimers rather than p50 homodimers (I et al., 2014).

However, caution must be applied when thinking about mechanism and the cell-specific implications of NF-κB. Whilst there are many studies focused on subunit expression in tumours, specifically that of p50 and p65, as suggested earlier, epithelial versus immune cell NF-κB activation could have very different outputs. For instance, p50 and not p65 is overexpressed in tumour-associated macrophages from human ovarian cancer. As a result, p50:p50 homodimers repress the activation signals required for M1 polarisation leading to defective IL-12 production. When $Nfkb1^{-/-}$ mice are implanted with murine fibrosarcoma there is no observed defect in M1 cytokine production and tumour growth is significantly reduced. The $Nfkb1^{-/-}$ mice also show enhanced CXCL-10 chemokine expression and hence CD4+ and CD8+ T cell infiltration that help combat tumour growth in this model (Saccani et al., 2006). Thus, highlighting the importance of dissecting cell-specific roles of NF-κB1 if we are to attempt to manipulate its function as a potential future therapy for inflammation and cancer.

Similar to the previously mentioned study (Saccani et al., 2006), it has also been recently described that p50 homodimers impair macrophage M1 polarisation, driving the development of colorectal cancer (Porta et al., 2018). In this study, $Nfkb1^{-/-}$ mice displayed fewer colorectal tumours and increased expression of IL-12 and CXCL-10, supporting the idea that p50 homodimers repress these genes in macrophages, orchestrating their pro-tumorigenic phenotype (Porta et al., 2018). BAG-1 (Bcl-2

associated athanogene) is an anti-apoptotic protein highly expressed in pre-malignant and colon cancer tissue. The interaction between BAG-1 and p50 homodimers has been demonstrated in both colorectal epithelial cells and in the colorectal carcinoma cell line HCT116 with knockdown of either protein leading to cell death. This complex is present at both the EGFR and the COX2 gene (PTGS2) promoters. Furthermore, the complex is able to differentially regulate gene expression by suppressing transcription of EGFR and promoting COX-2 transcription, both known to promote colon cancer (Southern et al., 2012).

Increased p50 signalling is also implicated in pancreatic carcinogenesis. Annexin A2 (ANXA2), is a calcium-dependent phospholipid binding protein involved in the progression and metastasis of a number of tumours and is shown to interact and translocate to the nucleus in a complex with p50 (Jung et al., 2015). Increased NF-κB activity is observed in both resting and TNF stimulated pancreatic cancer cells (Mia-Paca2). Furthermore, TNF treatment of HeLa cells expressing ANXA2 leads to the induction of several NF-κB target genes linked to anti-apoptotic signalling and drug resistance in cancer, including GM-CSF, IL-1β, IL-6 and Gadd45β. This suggests a link between increased ANXA2 expression and p50 interaction leading to increased anti-apoptotic gene expression and drug resistance in pancreatic cancer cells (Jung et al., 2015). However, in a mouse pancreatic tumour model, increased tumour growth was observed when pancreatic cancer cells were co-injected with $p50^{-/-}$ compared to wild type PSC (pancreatic stellate cells), suggesting a potential role for PSC p50 in pancreatic prevention (Giri et al., 2016). Thus, NF-κB1 plays very contrasting roles in the development of colon and pancreatic cancers, and further research is needed to elucidate its cellular and context-dependent function.

In an E-TCL1 mouse model of chronic lymphocytic leukemia, the incidence of leukemia is significantly lower in mice lacking Nfkb1, with CD19/CD5+ B cell numbers decreased despite no difference in overall survival. $Nfkb1^{+/-}$ TCL1 mice still show a significant reduction in leukemia incidence, demonstrating that even a partial reduction in Nfkb1 can impede disease development (Chen et al., 2017). It is known that intrinsic B cell defects are characteristic of mice deficient in Nfkb1, including proliferative defects and impairment in antibody class-switching (Sha et al., 1995b). Therefore, NF-κB1 could be directly linked to B cell proliferation in chronic lymphocytic leukemia, characterised

by an abnormally increased level of B cells in the lymph nodes, bone marrow, and blood (Kipps et al., 2017).

Diffuse large B-cell lymphoma (DLBCL) has two distinct molecular subtypes: germinal centre B cell like (GCB) and activated B cell like (ABC). ShRNA silencing of either p105 or p100 in two lymphoma cell lines identified a set of distinctly regulated genes that were later confirmed in primary DLBCL samples. Pathway analysis identified patterns of predominantly p105 signalling associated with the GCB lymphoma subtype, whereas p100 was associated with ABC potentially as a consequence of mutations in upstream activators of either the canonical or non-canonical pathway respectively (Guo et al., 2017). Moreover, in a study conducted on 465 patients, p50 activation in ABC DLBCL was associated with poorer survival, despite significant correlations between p50 nuclear expression and downregulation of Bcl-2, p53, phospho-AKT, CXCR4 and Myc. The poor outcome in p50 positive patients was attributed to immune dysregulation including immune suppression by TIM-3 and TNF upregulation. A similar correlation was found in GCB DLBCL patients with wild-type TP53, however p50 expression in GBC DLBCL patients with TP53 mutants was associated with a significantly improved outcome, as well as reduced expression of Bcl-2, Myc and p53 (Cai et al., 2017).

The role of p50 therefore differs substantially depending on its dimerization partner and the co-factors involved, as well as the cell type and cancer type, whereby gene expression can either be repressed or activated, hindering or driving tumorigenesis (summarised in Figure 1.4) (Concetti & Wilson, 2018).

1.3 Liver function, inflammation, disease and fibrosis

The liver is an essential organ in the body with diverse functions owed to the numerous cell types it harbours. Dysregulation of these functions or aberrant cell activity can lead to pathogenesis of the liver in different ways.

1.3.1 Cells of the liver

As the largest and one of the most complex organs of the body, the liver harbours many different cell types, the majority of which are hepatocytes. These represent the main functional liver cell and account for 60-80% of all liver cells (Stanger, 2015) (Figure 1.5). Hepatocyte functions include lipid, amino acid and carbohydrate metabolism, as well as protein synthesis and xenobiotic detoxification (Zhou et al., 2016).

Non-hepatocyte liver cells, which make up 20-40% of the liver, comprise endothelial cells, kupffer cells, lymphocytes, cholangiocytes and stellate cells (Bouwens et al., 1992). Endothelial cells act as barriers between hepatocytes and the blood, regulating the exchange of material between them. Kupffer cells are liver-resident macrophages, whose main function is the regulation of the liver's inflammatory response, by responding to stresses including infection and toxins, performing phagocytosis, processing and presentation of antigens, and through the release of pro-inflammatory cytokines. Liver lymphocytes include T cells, NK (natural killer cells) and B cells, which are important in the liver's immune defence mechanism. Cholangiocytes, also known as biliary epithelial cells, transport bile from the liver to the gall bladder and duodenum. Hepatic stellate cells, located in the space of Disse, are quiescent in normal conditions and function as storage cells for vitamin A, and excrete extracellular matrix. When activated, by injury and pro-inflammatory signals, these differentiate into fibrogenic myofibroblasts, characterised by an increased expression of a-SMA (a-smooth muscle actin) and cytokines, and increased production of extracellular matrix (Kmiec, 2001; Bouwens et al., 1992).

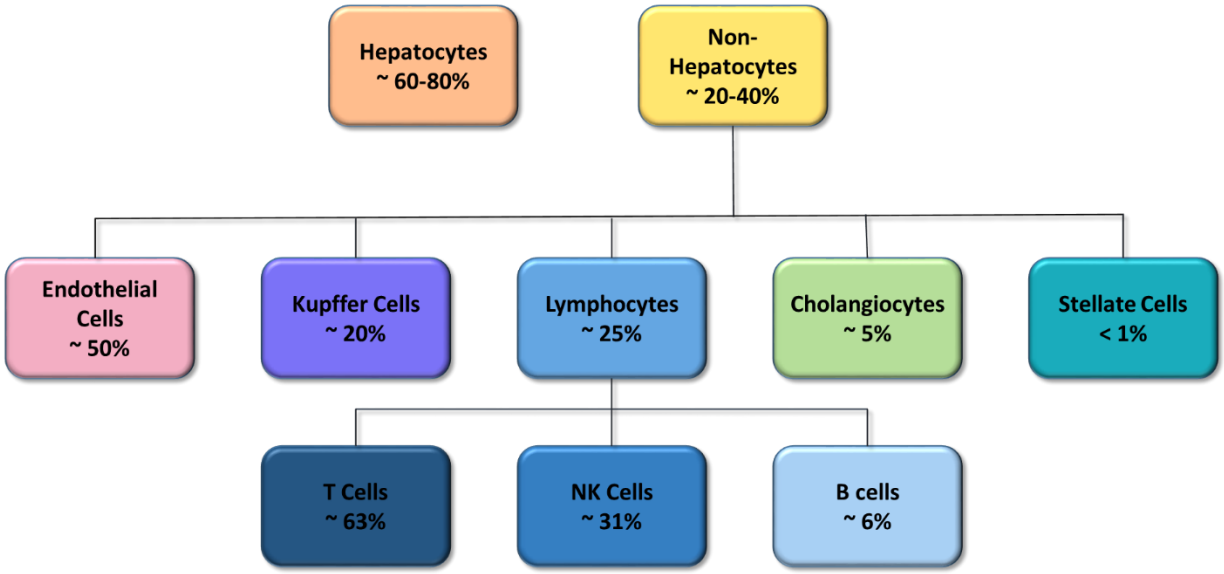

Figure 1.5 Cells of the liver. Diagram showing the proportion of different cells comprising the liver, with the majority being hepatocytes (60-80%) and non-hepatocyte cells accounting for 20-40%.

1.3.2 Structure and function of the liver

The liver structure can be defined as microscopic lobule structural units, which take the form of a polygonal shape and comprise portal triads, consisting of a hepatic artery, a portal vein and a bile duct. This system highlights the blood flow from the peripheral portal vein and hepatic artery to the central vein, and bile duct flow from the central vein to the bile duct (Krishna, 2013; Corless, 1983) (Figure 1.6).

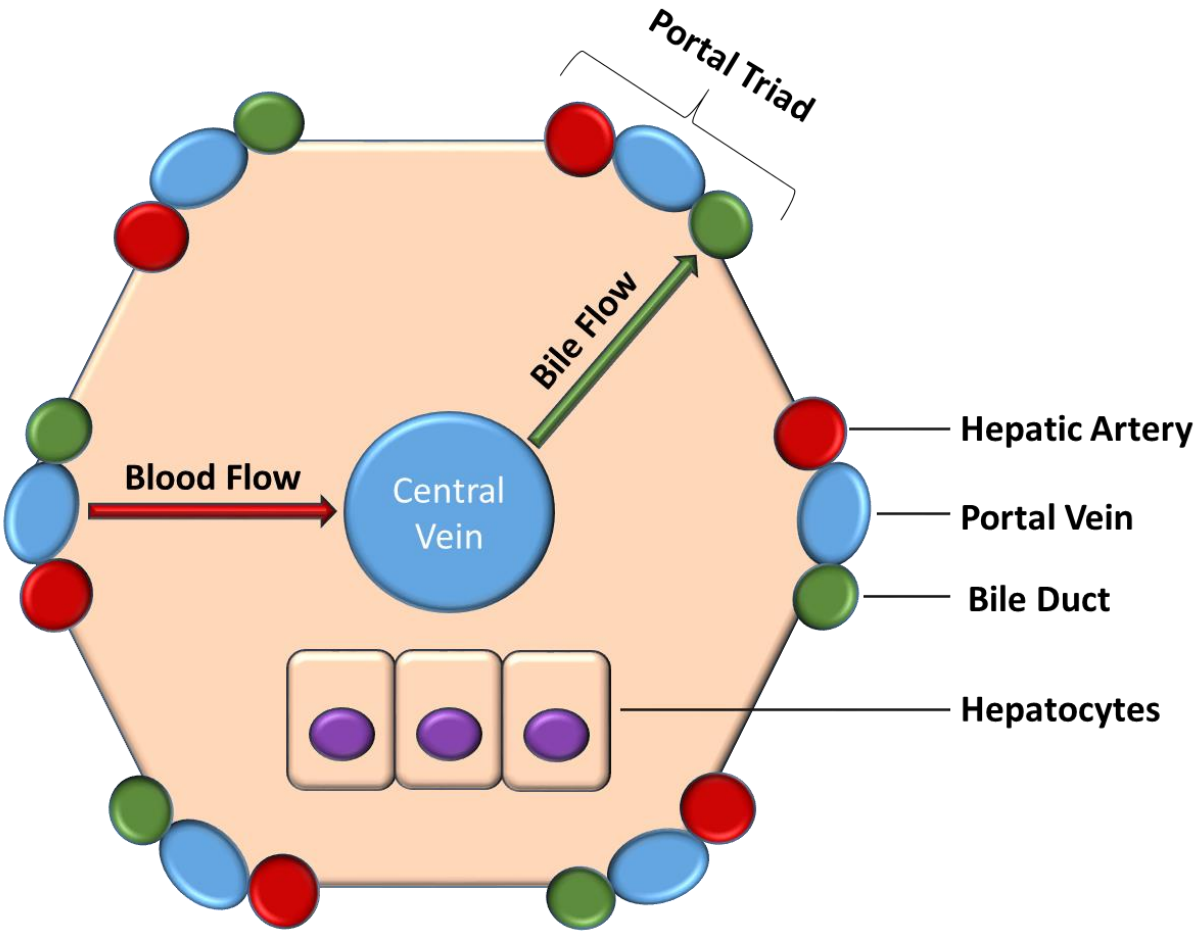

Figure 1.6 Liver lobule structure. Diagram shows liver lobule structure with blood flow from the hepatic artery and portal vein to the central vein and bile flow from the central vein to the bile duct.

The microstructure of the liver can also be represented longitudinally, with the exchange of material between the blood and hepatocytes occurring in the sinusoid (Vekemans & Braet, 2005) (Figure 1.7).

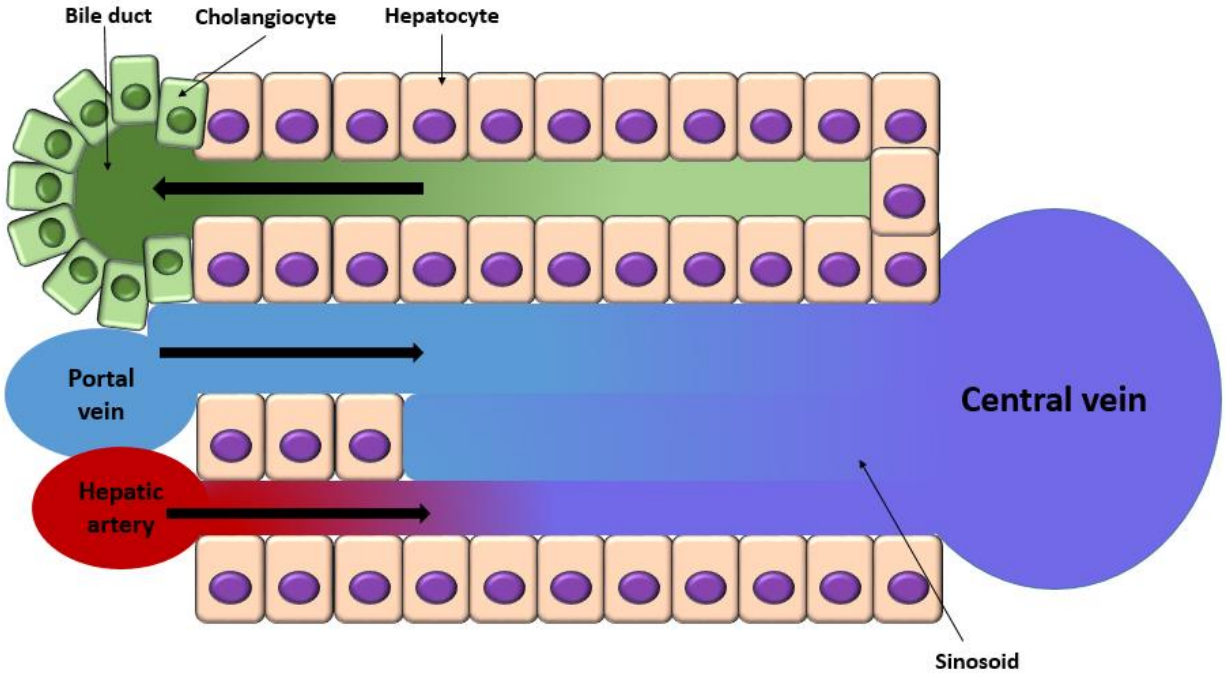

Figure 1.7 Liver microstructure. Diagram showing the blood flow from the portal vein and hepatic artery to the central vein through the sinusoid, where exchange of materials take place between the blood and hepatocytes, and the bile flow from the central vein to the bile duct.

The liver carries out many essential functions, including nutrient metabolism (carbohydrates, proteins and lipids), as mentioned previously (Zhou et al., 2016). It also plays an important role in the storage of iron, copper, vitamins A, D and B12, as well as the excretion of a number of different materials including bile salts, bilirubin, drugs, phospholipids and cholesterol (Bonkovsky, 1991). Additionally, the liver is a major site for the synthesis of proteins including albumin, coagulation factors, complement factors and protease inhibitors (de Feo & Lucidi, 2002). The liver also carries out important immune defence functions, notably through the action of kupffer cells (Gao, 2016; Concetti & Wilson, 2018) (Figure 1.8).

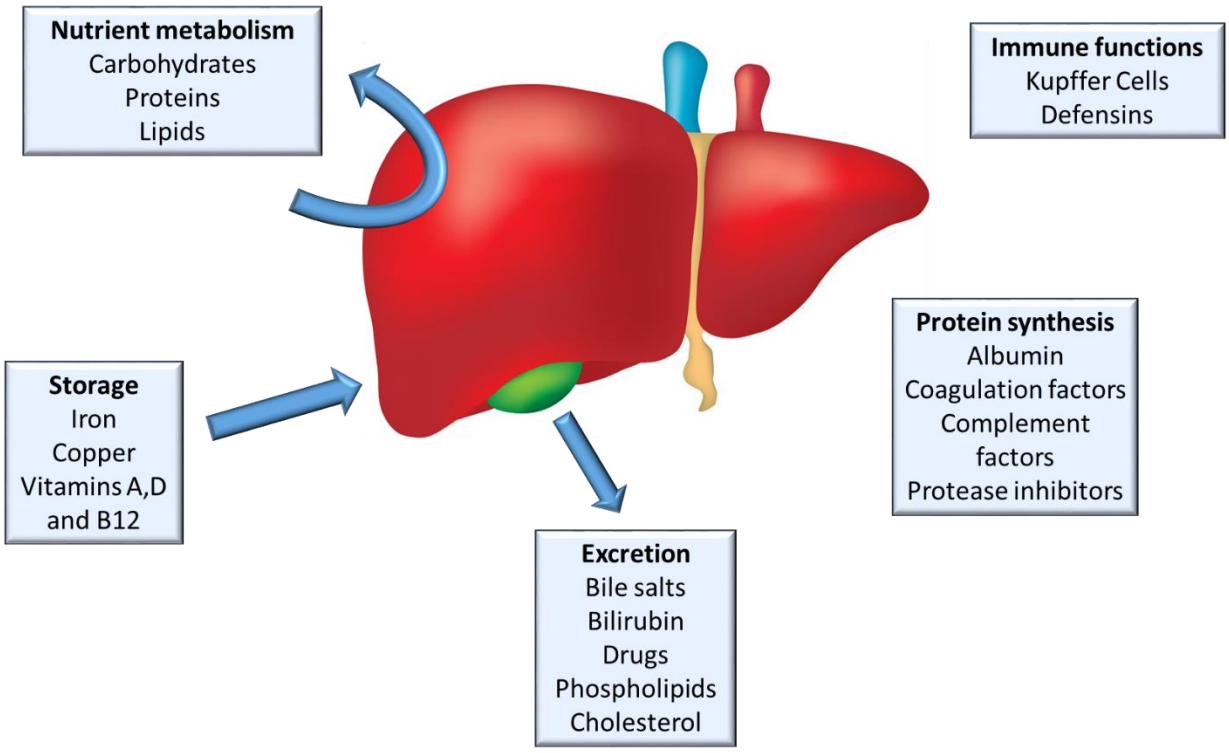

Figure 1.8 Functions of the liver. Diagram shows the different functions carried out by the liver including nutrient metabolism, storage, excretion, protein synthesis and immune functions.

1.3.3 Hepatocyte injury mechanisms and resolution

Liver injury can arise from various different causes. These include drug and alcohol toxicity, pathogen infection (notably viral hepatitis), aberrant immune function, and inadequate diet quality and quantity (de Boer et al., 2017; Sijamhodžić et al., 2019; Canbay et al., 2011).

In response to liver injury, the liver employs various defence and injury resolution mechanisms. Hepatocyte apoptosis (programmed cell death) represents an essential part of this process (Cao et al., 2016; Guicciardi & Gores, 2005). Injured hepatocytes undergo apoptosis which is characterised by cytoplasmic shrinkage, nuclear fragmentation, chromatin condensation and cellular rounding up, following caspase activation. These caspase proteases cleave at aspartate residues. This process allows for the elimination of injured cells that could cause further damage in their microenvironment, exhibit abnormal functions and potentially undergo mutations which could render them cancerous, in an orderly manner (Guicciardi & Gores, 2005; Cao et al., 2016). In certain conditions, hepatocyte cell necrosis (unprogrammed cell death)

can also occur, which is characterised by swelling, and rupture of the plasma membrane (Guicciardi et al., 2013). Mitochondria play an important role in hepatocyte cell death, with their outer membrane polarisation leading to the activation of signalling cascades leading to cell death. A number of anti-apoptotic and apoptotic factors are also involved in this, including BAX and Bcl-2 family proteins (Tsujimoto, 1998).

The immune cells present in the liver also play a crucial role in injury resolution mechanisms. The different immune cells of the liver exhibit distinct functions, and their interaction with hepatocytes generates an epithelial-immune cell crosstalk which plays an important role in determining the overall response.

1.3.4 Liver epithelial-immune cell crosstalk

By secreting innate immunity proteins, including cytokines and chemokines, hepatocytes are able to signal to and activate surrounding immune cells in their environment (Zhou et al., 2016). While certain hepatocyte-secreted factors are able to provide direct defence, such as bactericidal proteins and iron-sequestering proteins that block iron uptake from bacteria, others activate the innate immune system, such as fibrinogen (a coagulation factor) and pro-inflammatory mediators including IL-6 and TNF-α. The upregulation of these pro-inflammatory factors is in part mediated by the activation of NF-κB in response to liver injury (Ambrosino et al., 2003).

1.3.5 Liver disease progression

While the liver hosts a range of mechanisms to combat injury, these can sometimes prove insufficient and the injury can prevail when it is persistent. Additionally, aberrant immune responses can also be a driver of chronic liver inflammation leading to liver disease (Meli et al., 2014). Liver disease can take different forms which largely depends on the injury. Poor diet can lead to NAFLD (non-alcoholic fatty disease) which can sometimes develop into NASH (non-alcoholic steatohepatitis) (Benedict & Zhang, 2017), while alcohol consumption can also lead to liver disease (Bruha et al., 2012). Regardless of the chronic liver injury though, liver disease is characterised by excessive inflammation which culminates in similar disease scenarios (Robinson et al., 2016). Chronic liver inflammation can lead to the development of fibrosis initially, characterised by scarring of the liver tissue through excessive production of

extracellular matrix. This can progress onto cirrhosis, a more severe fibrotic phenotype with loss of liver architecture and function. This later stage liver disease can then turn into liver cancer, of which hepatocellular carcinoma is the most common, although some HCC livers have no underlying late stage liver disease.

1.3.6 Liver fibrosis

Liver fibrosis occurs in response to chronic liver injury. As a means of repairing itself, the liver undergoes wound healing through the deposition of collagen and other extracellular matrix components (Bataller & Brenner, 2005; Brenner, 2009). However, repeated injury can lead to excessive wound healing and therefore excessive extracellular matrix production, leading to scarring of the liver tissue. Hepatic stellate cells play a major role in this process. While normally quiescent and responsible for vitamin A storage, these cells can become activated and differentiate into myofibroblasts which secrete collagen upon liver injury. Remodelling of fibrotic tissue can occur through MMP (matrix metalloproteinase) digestion of extracellular matrix, which can in turn be modulated by TIMPs (tissue inhibitors of matrix metalloproteinases), notably TIMP-1. This dynamic process ensures the regression of fibrosis is possible, however once an advanced stage of fibrosis has been reached this becomes more challenging for the liver to overcome.

Additionally, chronic inflammation mediated by an excessive response from immune cells in the liver leads to the release of pro-inflammatory and fibrogenic factors which further drive fibrogenesis. These include TNFα (tumour necrosis factor α) and TGF-β (tumour growth factor β) (Yang et al., 2015). Fibrosis can eventually progress onto end-stage cirrhosis, and a proportion of patients with cirrhosis will then go on to develop liver cancer (O'Rourke et al., 2018a). The triggers for fibrosis and liver cancer development remain incompletely understood, though many factors have been linked to liver disease. Of these, NF-κB plays an essential role, acting as a central immune regulator and modulating the expression of pro-inflammatory and fibrogenic genes.

1.3.7 NF-κB1 in liver disease and fibrosis

NF-κB is known to play a key role in immune responses and regulating inflammatory responses. While canonical NF-κB signalling drives the expression of pro-inflammatory

factors, NF-κB1 is generally thought to repress these genes when in its p50 homodimer form, and therefore p50 homodimers are thought to play a protective role in fibrosis and liver disease progression. Previous work has shown that in a chronic CCl_4 model of induced fibrosis, $Nfkb1^{-/-}$ mice exhibited worse inflammatory and fibrotic phenotypes (Oakley, Meso, et al., 2005). This was notably characterised by increased neutrophil infiltration in the liver and the upregulation of pro-inflammatory cytokines, including TNFα. Furthermore, $Nfkb1^{-/-}$ mice exhibited increased α-SMA gene and protein expression, and increased Sirius red stain compared to WT mice.

1.4 Hepatocellular Carcinoma (HCC)

Hepatocellular carcinoma (HCC) is currently the second leading cause of cancer-related deaths worldwide, and the sixth most prevalent cancer (McGlynn et al., 2015; Ghouri et al., 2017). Despite this, to date treatments have remained limited, with options often restricted to surgical resection and/or conventional chemotherapy and radiotherapy. The only molecular-targeted therapy proven to have a beneficial effect is sorafenib, which is given in some cases of advanced HCC, however this tyrosine kinase leads to a number of side effects and has demonstrated limited efficacy. With increasing incidence of HCC yet poor long-term prognosis, the need for more research towards developing therapeutics is becoming greater.

1.4.1 HCC initiation and progression

Most patients who develop HCC often have an underlying chronic liver disease. Hepatitis viral infection with HBV or HBC is one of the most frequent causes of HCC (Xie, 2017). Another major contributing factor is the progression from non-alcoholic fatty liver disease (NAFLD) to non-alcoholic steatohepatitis (NASH), characterized by inflammation and lipid accumulation in the liver (Anstee et al., 2019). Some patients also present with fibrosis and cirrhosis, the latter being at the highest risk of developing HCC (Ramakrishna et al., 2013). Fibrosis represents the hardening and/or scarring of tissue, with the excessive deposition of collagen and other extracellular matrix components. Cirrhosis represents an advanced stage of liver tissue scarring. Overall, only a minority of patients with liver disease will progress to HCC; the mechanisms behind this progression are still incompletely understood, though it is thought that

multiple ‘pathogenic hits’ are needed. Some of the key risk factors include obesity, insulin resistance and a sedentary lifestyle.

Additionally, several mutations associated with hepatocarcinogenesis have been identified. Recent studies have shed the light on the mutational landscape of HCC thanks to recent advances in genomic technologies. TERT (Telomerase reverse transcriptase), TP53 (Tumour protein 53), CTNNB1 (Catenin beta 1), ARID1A and ARID2 (both belonging to the AT-rich interaction domain family) are among the most frequently mutated genes in HCC, in descending order of frequency, with TERT mutations classified as the most potent drivers of HCC (mutated in 47.1% of cases). ARID1A and ARID2 are involved in chromatin remodelling, and hence highlight the importance of epigenetic aberrations in carcinogenesis (Lee, 2015). These findings provide important insights into potential therapeutic targets that could be exploited to generate personalised medicines in order to treat liver cancer.

An increasing role for epigenetics is being recognised in disease progression, and epigenetic dysregulation plays a major role in the development of hepatocellular carcinoma. These include alterations in DNA methylation, histone modifications, as well as changes in microRNA expression. More specifically to HCC, global hypomethylation has been documented, caused by altered expression of DMNTs (DNA methyltransferases) or reduced availability of SAM (S-adenosyl-L-methionine), the universal methyl donor. Aberrant expression of histone modifying enzymes and dysregulation of histone modifications have also been established as emblematic characteristics of HCC. Among these histone deacetylase enzymes including HDAC1 have been implicated in hepatocarcinogenesis (Pogribny & Rusyn, 2014).

Given that over 90% of HCC develops on the background of chronic inflammation (Hayato & Shin, 2012), it is important to deepen the understanding of the mechanisms linking inflammation and hepatocarcinogenesis, which has led to the success of immunotherapies. NF-κB, a well-established master regulator of inflammation and apoptosis, has been proposed to mediate a central link between liver injury, fibrosis and hepatocellular carcinoma (Luedde & Schwabe, 2011a). The role of NF-κB in liver disease has been underlined in mouse models of NF-κB subunit specific knock-outs leading to spontaneous liver injury, fibrosis and HCC. Among these, Nfkb1 global knockouts exhibit increased inflammation, early onset ageing and higher incidence of liver cancer (Wilson et al., 2015). The role of NF-κB is compartmentalised in the different cells in the liver, where it influences survival in hepatocytes, inflammation in

Kupffer cells (liver-resident macrophages), as well as inflammation, survival and activation in hepatic stellate cells (HSCs). The complex and diverse functions of NF-κB render this transcription factor a key player in chronic liver disease.

1.4.2 NF-κB1 in HCC

A study by H. Yokoo et al. highlighted the implication of p50 in hepatocellular carcinoma. Following histological analysis of HCC patient samples, they found that increased p50 expression was correlated with higher recurrence of HCC. They subsequently suggested that p50 expression could potentially be used as a prognostic marker for HCC recurrence following surgery. These suggestive findings however provided insufficient evidence to establish p50 staining as a prognosis marker and metastatic potential in HCC (Yokoo et al., 2011). A more recent study conducted by our group demonstrated that NF-κB1 functions as a suppressor of neutrophil-driven carcinoma (Wilson et al., 2015). Here, it was shown that p50 homodimers in complex with the HDAC1 co-repressor exert a tumour suppressor function. C. Wilson et al. demonstrated that p50:p50:HDAC1 complexes are recruited to the promoters of neutrophil chemokines S100A9, CXCL1 and CXCL2, where they repress the hepatic expression of these genes, thus reducing inflammation. They also found that disrupting p50 homodimer assembly by mutation of Ser342 (which they established as a key residue for p50 homodimer assembly) increased the susceptibility to HCC. More research into the tumour suppressive and anti-inflammatory function of p50 is required in order to elucidate the mechanisms by which it protects against liver disease progression and HCC.

The role of NF-κB in liver cancer has been extensively studied and its first role in liver homeostasis highlighted in p65 deficient mice which suffer embryonic lethality due to TNF-induced hepatocyte death during development (Doi et al., 1999b). Contrasting and cell-specific effects of IKK deletion in liver epithelial versus myeloid cells highlight the complexity of its role at different stages of HCC development. Knockdown of IKK in hepatocytes leads to increased liver cancer, whereas knockdown in myeloid cells results in significantly decreased hepatocarcinogenesis (Maeda et al., 2005). These studies of course merely highlight the implications of inhibiting the entire canonical NF-κB pathway which researchers are beginning to appreciate is far more complex and requires further refinement if we are to manipulate it in a more specific and productive

way, including a more in-depth understanding of the epigenetic regulation and post-translational modifications of the individual subunits.

We have previously provided evidence that NF-κB1, acting through p50 homodimers, is a suppressor of neutrophil-driven hepatocellular carcinoma (HCC).We previously demonstrated using a model of diethylnitrosamine (DEN)-induced HCC that Nfkb1$^{-/-}$ mice exhibited accelerated HCC and significantly increased tumour numbers compared to wild type mice. This was mediated in part by p50 homodimers complexed with HDAC1 repressing the hepatic expression of the neutrophil chemokines S100A9, CXCL1, and CXCL2. Treatment with a neutrophil-depleting antibody (anti-Ly6G) reduced tumour growth considerably in Nfkb1$^{-/-}$ mice. Furthermore, we identified that the phosphorylation of Ser342 is critical for p50 homodimer assembly, and that Nfkb1$^{-/-}$ mice with a serine to alanine mutation at position 342(S342A) display increased neutrophil numbers, neutrophil chemokine expression, and increased tumour burden in the DEN HCC mouse model. Combined this data confirmed that p50 homodimers in complex with HDAC1 play an important role in preventing liver inflammation and tumorigenesis by repressing neutrophil recruitment and as a result, neutrophil tumour-promoting effects. Interestingly, in a non-experimentally-induced context, aged 20 month old Nfkb1$^{-/-}$ mice also develop spontaneous chronic liver disease and liver cancer characterised by dysplastic nodules, increased tumour incidence, features of steatohepatitis and fibrosis (Wilson et al., 2015).

In HCC patients where ~90% of cancers develop on a background of aberrant liver inflammation, we have also confirmed that an increase in neutrophil to lymphocyte ratio is associated with a poorer prognosis and worsened survival outcome (Margetts et al., 2018). Furthermore, mRNA, miRNA, and methylation profiling of 337 HCC patients identified NF-κB1 and the MAPK (mitogen-activated protein kinase) pathway as important players in HCC progression. Here, NFKB1 inhibition was mediated via the miRNA let-7a at all stages of HCC, resulting in aberrant target gene regulation including Gadd45b and dysregulated cell proliferation and apoptosis. In addition, NFKB1 was differentially methylated in stage II and III HCC, but not stage IV (Li et al., 2016). The miRNA silencing of NFKB1 and its differential methylation could therefore be a potential mediator of HCC development; however, further research is needed in order to elucidate the specific role of p50 in different stages of HCC including liver inflammation and disease, and cancer initiation and progression. Whilst contrasting studies exist including correlating p50 expression with early recurrence of HCC and

Akt phosphorylation, p65 expression was not assessed here (Yokoo et al., 2011). Increased p50 and Bcl-3 co-expression in tumours compared to adjacent tissue has also been described. However, these studies simply describe p50 expression levels and fail to address functionality and mechanism.

1.5 Project Aims

This project aims to elucidate the role that hepatocyte NF-κB1 plays in damaged hepatocytes in educating the immune system and inflammation in the context of acute liver injury, as well as the role of NF-κB1 in controlling hepatocyte damage and progression to cancer in chronic liver injury.

For this, acute CCl_4 and DEN liver injury models were carried out to assess the role of NF-κB1 in acute liver injury. A chronic CCl_4 fibrosis model was also carried out to assess the role of hepatocyte NF-κB1 in fibrogenesis. Lastly, a 40-week DEN-induced HCC model was carried out to assess the role of NF-κB1 in liver carcinogenesis.

The overall aim is to determine the importance of hepatocyte NF-κB1 in regulating gene expression to modulate liver disease progression. Understanding the process bridging acute liver injury through chronic injury and cancer development is crucial to understand the causes underlying liver carcinogenesis.

NF-κB1 being a central regulator of inflammatory processes and cell survival, and p50 homodimers being known to repress gene transcription, it was hypothesized that hepatocyte NF-κB1 would play a protective role in liver disease, and that mice lacking hepatocyte NF-κB1 would exhibit a worse phenotype in response to liver injury, particularly increased HCC development.

Chapter 2. Materials and Methods

2.1 Animals

2.1.1 Ethics and husbandry

All animal work was carried out in accordance to Home Office regulations and experiments were performed under a UK Home Office license (PPL - P1FF204BF). Protocols were designed for each study and approved by a Senior Animal Technician/Named Animal Care and Welfare Officer before the start of the study. Animals were housed in the Comparative Biology Centre (CBC) at Newcastle University and were kept in an air-conditioned environment on a 12-hour light/dark cycle with a humidity of 50% ± 10% and a temperature of 23°C ± 1°C. Mice were kept in saw-dust filled and filter topped, individually ventilated cages and kept no more than 6 to a cage. Food and water were provided ad-libitum and bedding was changed twice weekly.

2.1.2 Strains

All experiments were performed on male C57BL/6 mice. Mice used include Nfkb1 floxed mice ($Nfkb1^{fl/fl}$), hepatocyte-specific Nfkb1 knockout mice ($Nfkb1^{hep-/-}$), Nfkb1 global knockout mice ($Nfkb1^{-/-}$), albumin-cre recombinase heterozygous mice (Alb-$cre^{+/-}$), and albumin-cre recombinase homozygous mice (Alb-$cre^{+/+}$). $Nfkb1^{fl/fl}$ mice were used as a control for all experiments. These mice have 2 LoxP recombination sites that flank exon 3 of the Nfkb1 gene, and are comparable to wild type mice as they have no gene expression alterations. $Nfkb1^{hep-/-}$ mice were generated using an albumin promoter-cre recombinase system, by crossing $Nfkb1^{fl/fl}$ mice with Alb-cre mice in 3 different mating steps. The first step consists of crossing a homozygous cre transgene mouse with a homozygous floxed mouse. This generates mice which are heterozygous for both the cre and Nfkb1 floxed gene. The second mating step consists of crossing a heterozygous cre and floxed mouse with a homozygous floxed mouse. This generates 3 different offspring genotypes: cre heterozygous floxed homozygous, floxed homozygous, and cre and floxed heterozygous. The final mating step consists of crossing a heterozygous cre homozygous floxed mouse with a homozygous floxed mouse. All mice generated from this mating are homozygous floxed and approximately 50% will contain the cre transgene. The mice expressing cre will be $Nfkb1^{hep-/-}$.

The cre recombinase enzyme introduces Nfkb1 exon 3 gene deletions in these mice by splicing the DNA sequence flanked by LoxP sites. The DNA strands are cut by cre recombinase and rejoined by DNA ligase. $Nfkb1^{hep-/-}$ mice thus lack exon 3 of Nfkb1, preventing Nfkb1 protein expression. In $Alb\text{-}cre^{+/-}$ and $Nfkb1^{hep-/-}$ mice, the expression of cre recombinase is driven by an albumin promoter, which is hepatocyte and cholangiocyte specific; Nfkb1 is therefore only knocked out in these cell types (liver epithelial cells).

Additionally, a viral-induced $Nfkb1^{hep-/-}$ mouse model was generated by injecting AAV8-TBG-Cre (Adeno-associated virus 8-thyroid hormone-binding globulin-Cre) intravenously in $Nfkb1^{fl/fl}$ mice, whereby the TBG-Cre system specifically targets hepatocytes. Full knock-out of Nfkb1 was observed 2 weeks after AAV8-TBG-Cre injection. In experiments where AAV8-TBG-Cre was used to knock out Nfkb1 in $NFKB1^{fl/fl}$ mice, AAV8-Null control virus was injected in a control group of $Nfkb1^{fl/fl}$ mice to account for any virus-mediated effects. AAV8-TBG-Cre and AAV8-Null virus was obtained from Pennysylvania University.

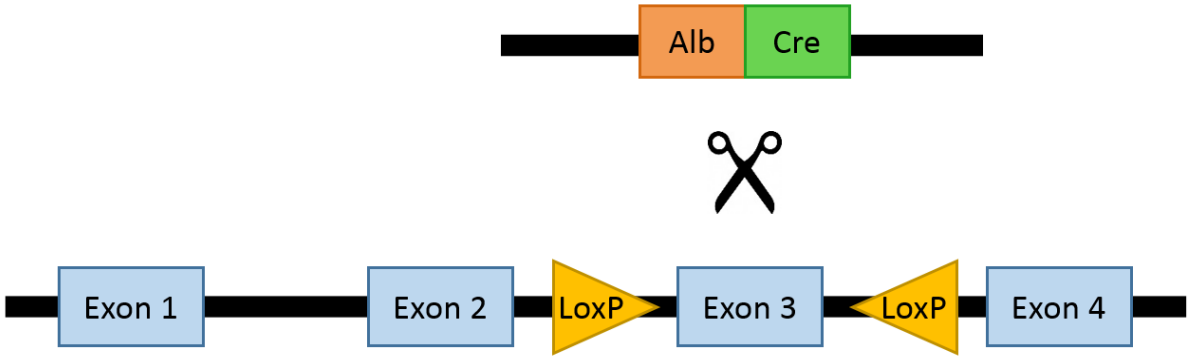

Figure 2.1 LoxP recombination of exon 3 in the Nfkb1 gene. Schematic diagram showing the Albumin-driven Cre-recombinase-mediated recombination of the Nfkb1 gene at the LoxP sites which flank exon 3 of the gene.

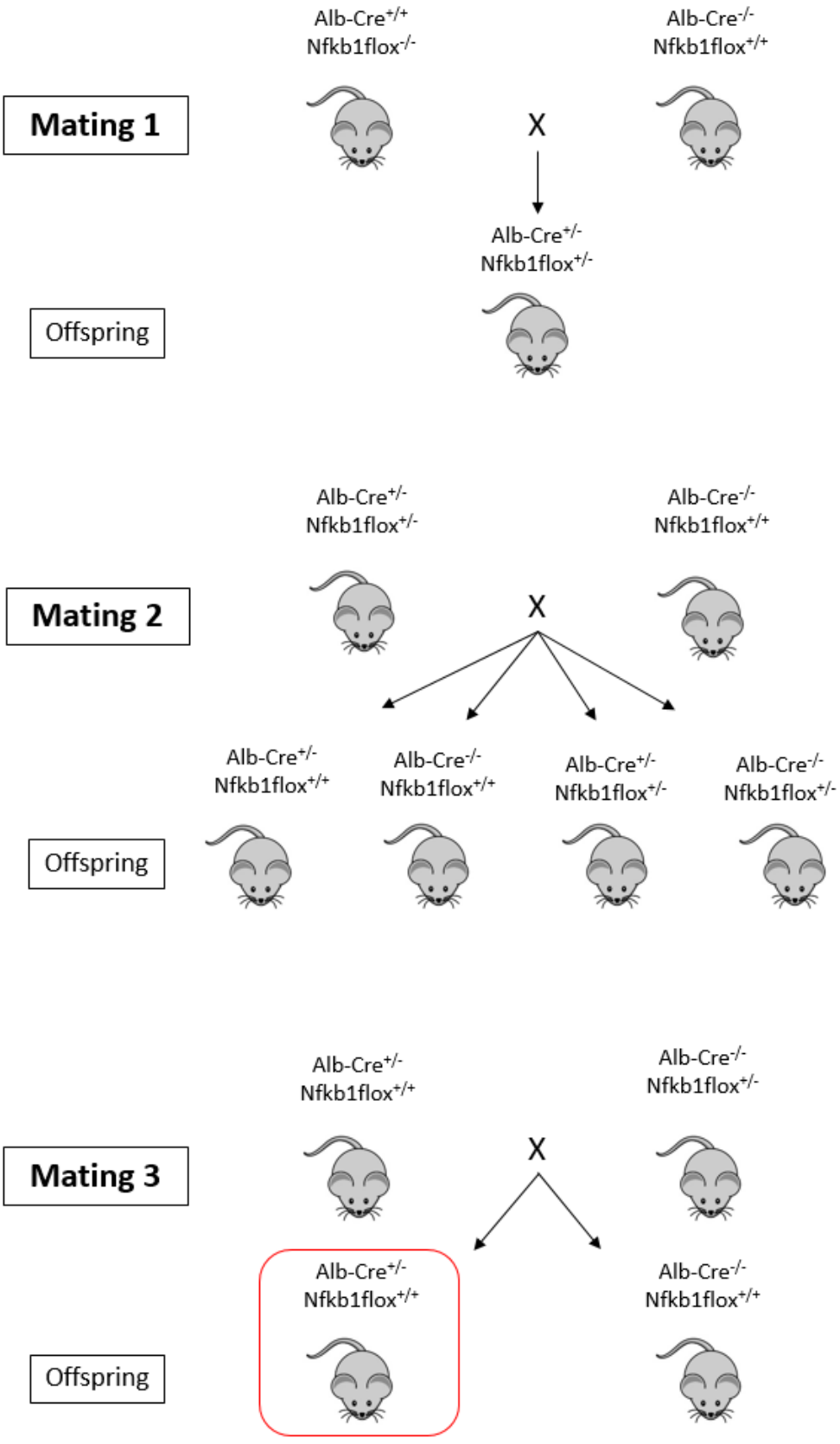

Figure 2.2 Nfkb1$^{hep-/-}$ mice generation. Schematic diagram of Nfkb1$^{fl/fl}$ and Alb-Cre mice matings to generate Nfkb1$^{hep-/-}$ mice.

2.1.3 Genotyping

All DNA isolation from mouse ear punches was performed using the REDExtract-N-Amp Tissue PCR (Polymerase chain reaction) Kit (Sigma Aldrich, UK). Ear punches were incubated in 100µL of extraction solution and 25µL of tissue preparation solution at 95°C for 4 minutes, after which 100µL of neutraliser solution was added to the samples and mixed by vortexing. The solution containing the genomic DNA was stored at -30°C until required. All PCR reactions were carried out with the same reagents, with different forward and reverse primers. PCR reactions consisted of 4µL of genomic DNA, 10µL REDExtract-N-Amp PCR Reaction Mix, 0.2µL of each 10µM primer, and were made up to a final volume of 16µL with nuclease-free water. PCR reactions were carried out as follows: initial 5 minute incubation at 95°C followed by 32 PCR cycles of 30s denaturation step at 95°C, 45s annealing step at 55°C, followed by a 1 minute elongation step at 72°C. The PCR reaction was terminated by incubating at 4°C after a final elongation reaction of 10 minutes at 72°C. PCR products were then separated by electrophoresis at 100V for 30 minutes through a 2% w/v agarose gel containing ethidium bromide and visualised under UV light.

Step	Temperature	Time	
Initial denaturing	95°C	5mins	
Denaturing	95°C	30s	32 cycles
Annealing	55°C	45s	
Elongation	72°C	1min	
Final Elongation	72°C	10min	
Hold	4°C	∞	

Table 2.1 Genotyping PCR cycle

Primer	Sequence
Alb-cre WT FW	TGCAAACATCACATGCACAC
Alb- cre Common RV	TTGGCCCCTTACCATAACTG
Alb-cre Mutant FW	GAAGCAGAAGCTTAGGAAGATGG
Generic Cre Forward	CGTACTGACGGTGGGAGAAT
Generic Cre Reverse	CCCGGCAAAACAGGTAGTTA
Nfkb1-5arm-WTF	CTAAGACCTCCAGCCAGCAA
Nfkb1-Crit-WTR	CATCTTCGGAGCCAAGAGAG
5mut-R1	GAACTTCGGAATAGGAACTTCG

Table 2.2 Genotyping primers

2.2 Cell culture

2.2.1 Isolation of primary mouse hepatocytes

Hepatocytes were isolated from Nfkb1$^{fl/fl}$, Nfkb1$^{hep-/-}$ and Nfkb1$^{-/-}$ mice livers using a collagenase perfusion method. Mice were first culled by ketamine and xylazine anaesthesia overdose, their abdomen opened and the inferior vena cava cannulated. The diaphragm was then opened to clamp the superior vena cava. The liver was perfused with 50ml Krebs-ringer bicarbonate buffer (Sigma) with EDTA followed by 50ml Krebs-ringer bicarbonate buffer with calcium chloride and 1mg/ml collagenase (collagenase from clostridium histolyticum, Sigma), using the portal vein as an outlet. The liver was dissected out, removing the bile duct, and the hepatocytes isolated by tearing and agitating the perfused liver in Krebs-ringer buffer, then filtering it through a 100µm cell strainer. The cells were then centrifuged at 500 rpm for 10 minutes, the supernatant was either kept for non-parenchymal liver cell isolation (500 x g 5 minutes centrifugation) or removed, and the cells were washed 3 times in PBS (Dulbecco's phosphate buffer saline, Sigma) with 3 minute 500 rpm centrifugation steps. After the last wash, the cell pellet was resuspended in 10ml of 10% Williams E medium (Gibco) containing 10% fetal bovine serum (FBS), 2mM glutamine, 100U/ml penicillin and 100µg/ml streptomycin. A percoll gradient was then carried out to get rid of non-viable cells. For this, 40% percoll (40ml percoll (GE Healthcare), 54ml water, 6ml 10% PBS) was added drop by drop to the falcon tube (tilted sideways) containing the cells in Williams E medium, followed by a centrifugation step at 200 x g for 7 minutes. The

supernatant was then removed and the pellet (containing viable hepatocytes) resuspended in Williams E medium. Hepatocytes were either cultured or stored at -80C for protein extraction. For hepatocyte culture, as an additional verification, cell viability was determined by trypan blue stain, then counted with a haemocytometer and plated in collagen (collagen I, Rat Tail, Gibco)-coated 6-well plates at a density of 1 million cells per well with Williams E medium. The medium was replaced with fresh medium after 24 hours.

2.2.2 Primary mouse hepatocyte culture

Primary mouse hepatocytes were cultured in Williams E medium as described in the previous section. Cells were maintained at 37C and 5% CO_2 and treated the day following isolation.

2.2.3 Primary mouse hepatocyte treatment

$Nfkb1^{fl/fl}$ and $Nfkb1^{hep-/-}$ mice were treated with either 250μM H_2O_2 for 1h or DEN (diethylnitrosamine, Sigma) for 6h or 24h to induce genotoxic injury. $Nfkb1^{fl/fl}$ mice were treated with 10ng/ml or 20ng/ml TNFα for either 2h, 6h or 24h to optimise the best conditions to assess inflammatory gene expression. Treatment of 20ng/ml TNFα for 24h was subsequently carried out in $Nfkb1^{hep-/-}$ and $Nfkb1^{-/-}$ mice. The cells were then washed and collected with a cell scraper for RNA in RLT buffer containing betamercaptoethanol (Sigma).

2.2.4 Isolation of immune cells

Mice primary immune cells were isolated from femur and tibia bone marrow. The skin was removed by nicking and tearing, and the tissue removed from the femur and tibia. The bones were then flushed with a 25G needle in HBSS- (Corning) and the immune cells recovered by centrifugation for 5 minutes at 500 x g. The pellet containing the immune cells was washed twice with PBS and stored at -80°C for protein extraction.

2.2.5 Isolation of primary mouse tumour cells

Primary mouse tumour cells were isolated from mice at the time of harvest for the 40 week DEN study. Tumours were excised from the liver and the tissues minced with a sterile scalpel in a petri dish in a sterile hood until disaggregated. The disaggregated tissue was then washed 3 times with HBSS+ (LONZA) without EDTA, containing 2mM glutamine, 100U/ml penicillin and 100μg/ml streptomycin. The HBSS+ was removed and 10ml of 1mg/ml collagenase in HBSS+ was added to the petri dish, and incubated

at 37°C for 20 minutes. After 10 minutes of incubation the collagenase suspension was pipetted up and down to mix. The suspension was then filtered through a 100µm cell strainer to separate the dispersed cells and tissue fragments from the larger pieces. The suspension was then washed 3 times by centrifugation in HBSS at 1200 rpm for 5 minutes. The pellet was resuspended in DMEM High Glucose medium (Biosera) comprising 10% FBS, 2mM glutamine, 100U/ml penicillin and 100µg/ml streptomycin. Cells were seeded in a 6 well plate at a density of 1 million cells per well and the medium changed the next day.

2.2.6 Primary mouse tumour cell culture

When adherent cells reached 75-95% confluence, they were passaged with Accutase (Corning) and transferred to T25 flasks. For passaging, the cell medium was removed, the cells washed twice with PBS and incubated with Accutase at 37°C and 5% CO2 for 5-10 minutes to detach cells. When confluent in T25 flasks, cells were passaged and transferred to T75 flasks. The medium was changed and cells passaged as necessary.

2.2.7 Long term cell storage

Primary mouse tumour cells were frozen down and stored long term in liquid nitrogen (-200°C). The cells were detached as described in 2.2.6 and pelleted by centrifugation at 1000 x g for 5 minutes. Cells were resuspended in freezing medium comprising 10% DMSO in FBS. The cell suspension was then aliquoted in sterile cryovials (1ml/cryovial). Aliquots were cooled in an isopropanol filled Mr Frosty freezing container (Thermo scientific UK) and chilled at -80°C, where the cells were cooled at a rate of 1°C per hour. The next day the cells were transferred to liquid nitrogen for long term storage.

2.3 In vivo models of liver injury

2.3.1 Adeno-associated virus knockout models

Where the AAV8-TBG-CRE viral knockout model of hepatocyte Nfkb1 was used, mice were injected with a single intravenous tail vein injection of 1×10^{11} virus 2 weeks prior to acute liver injury (CCl_4 and DEN). Where the AAV8-TBG-CRE viral knockout model of hepatocyte Nfkb1 was used in the 40 week DEN model of HCC, mice were injected with virus at 32 weeks (8 weeks prior to harvest). In all experiments where virus was

used, AAV8-TBG-CRE virus was injected in Nfkb1$^{fl/fl}$ mice to induce the knockout of Nfkb1 (full knockout observed 2 weeks post-injection), and AAV8-Null control virus was injected to a control group of Nfkb1$^{fl/fl}$ mice.

2.3.2 Acute carbon tetrachloride (CCl_4) injury

Mice received a single intraperitoneal (IP) injection of CCl_4 (carbon tetrachloride) at roughly 8 weeks of age, at a dose of 2ml/kg of body weight (1:1 v/v in olive oil) to induce liver injury. Mice were harvested at either 24h or 48h post-injection. 5-7 mice were used per group. CCl_4 is a strong hepatotoxin widely used in research to produce liver injury. It is metabolised in the liver by cytochrome p450 CYP enzymes into CCl_3 radicals, which react with lipids, proteins and nucleic acids. This leads to lipid peroxidation, ROS (reactive oxygen species) formation, lowered membrane permeability, mutations and generalized hepatic damage characterized by inflammation.

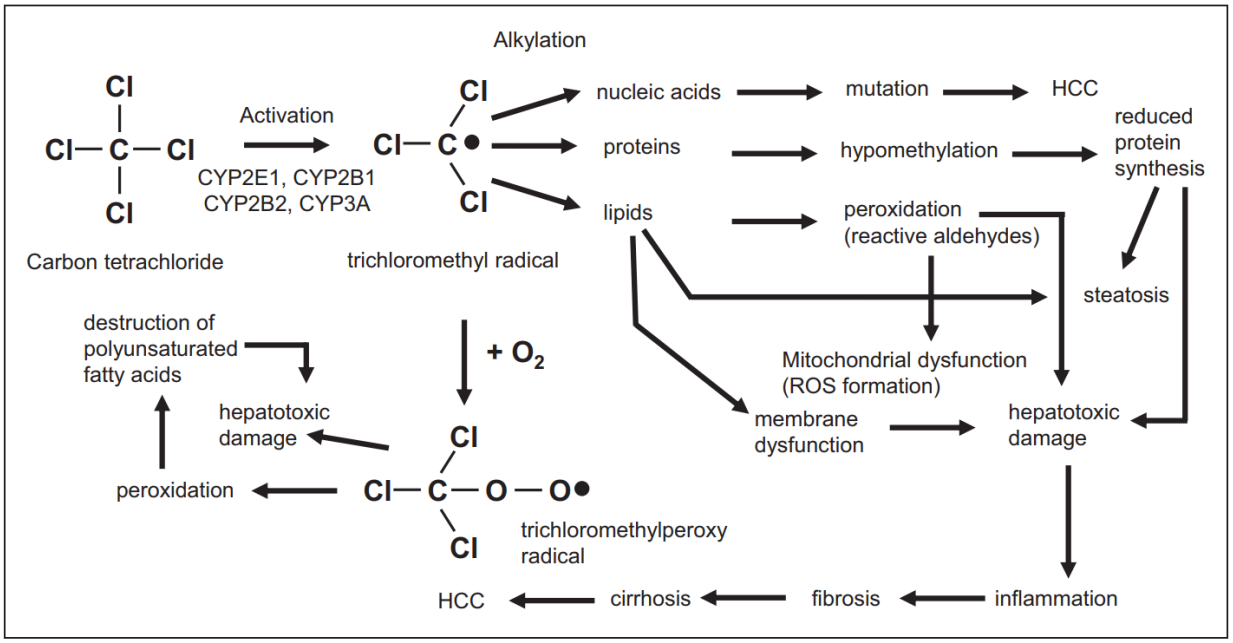

Figure 2.3 CCl_4 mechanism of hepatotoxicity. (D. Scholten et al., 2015). Diagram showing the biochemical steps of CCl_4 liver metabolism leading to hepatotoxicity.

2.3.3 Acute diethylnitrosamine (DEN) injury

Mice received a single IP injection of DEN at roughly 8 weeks of age, at a dose of 4µl/g of body weight of 25mg/ml DEN. Mice were harvested either 24h or 48h post-injection. 5-7 mice were used per group. DEN is a hepatotoxin and carcinogen metabolised by cytochrome p450 CYP2E1 in the liver and leads to the production of reactive metabolites which results in DNA alkylation and the formation of DNA lesions, including N7-methylguanine and O6-methylguanine. This gives rise to DNA mutations, from guanine to thymine transversions and base mispairing. A single IP injection of DEN in 8 week old mice causes generalized hepatic damage and inflammation, notably ROS production and NF-κB activation, but does not suffice to promote tumorigenesis.

2.3.4 Chronic CCl_4 injury

Mice received biweekly IP injections of CCl_4 at a dose of 2ml/kg of body weight (1:3 v/v in olive oil) for 6 weeks to induce fibrosis. Control mice received biweekly IP injections of olive oil at a dose of 1ml/kg of body weight for 6 weeks. Mice were humanely culled by anaesthesia 24h after the last CCl_4 injection. 4-6 mice were used per group. Chronic administration of CCl_4 is a widely used liver injury model in research to induce fibrosis.

2.3.5 Chronic DEN injury

14 day old mice received a single IP injection of 30mg/kg DEN in 0.9% saline to induce HCC (hepatocellular carcinoma). Mice were harvested at 40 weeks post DEN injection. 11-12 mice were used per group. This model of DEN IP injection in 14 day old mice is commonly used in research to study HCC. At this age, the liver cells are still undergoing rapid proliferation, therefore the DNA lesions caused by DEN metabolites lead to a significant number of mutations which ultimately lead to liver carcinogenesis. The majority of liver tumours that result from this model harbour Ha-ras or B-raf gene mutations. The pathophysiological alterations in this model have high similarity with what is observed in HCC in humans.

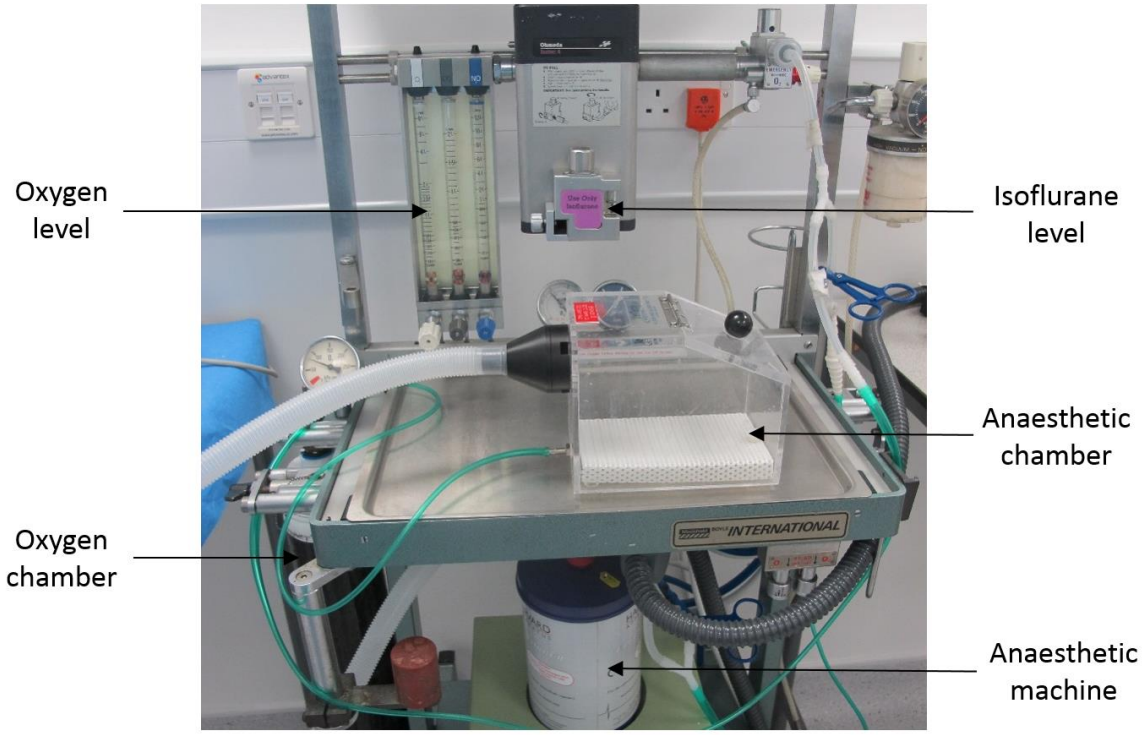

Figure 2.4 Mouse harvest set up. Diagram showing the set up with the anaesthetic machine used for mouse harvest.

2.4 RNA isolation and quantification

2.4.1 RNA isolation

Total RNA (ribonucleic acid) was isolated from tissue samples and cells using the RNeasy Kit (Qiagen). Tissues and cells were homogenised with a pestle and lysed in 350µl of RLT lysis buffer containing β-mercaptoethanol (1:100). The lysate was transferred to a Qiashredder column and centrifuged at 13 000 rpm for 2 minutes for homogenisation. The flow-through was then transferred to a new tube and an equal volume of 70% ethanol (350µl) was added and mixed repeatedly by pipetting. The sample was then transferred to an RNeasy spin column, centrifuged for 30s at 8000 rpm, and the flow-through discarded. The column was then washed with 700µl of RW1 buffer followed by with 500µl of RPE buffer, each time spun for 30s at 8000 rpm and the flow-through discarded. A final wash step was carried out with a 500µl RPE wash with a 2 minute spin at 8000 rpm and the flow-through discarded. The column was then spun at 13000 rpm to dry the membrane. The columns were subsequently placed in fresh collection tubes and the RNA eluted with 30µl of nuclease-free water. The RNA

was then quantified using a nanodrop 2000 spectrophotometer by measuring absorbance at 260nm and 280nm. Both concentration and purity were calculated, with absorbance A260/A280 ratios between 1.8 and 2 indicating acceptable purity.

2.4.2 cDNA synthesis

Promega kit reagents were used for cDNA synthesis. 1µg of RNA template was diluted in nuclease-free water to make a total volume of 8µl. The diluted RNA was first incubated at 37°C for 30 minutes with 1µl of DNase buffer and 1µl of DNase to digest any potential remaining genomic DNA carried over from the RNA isolation. DNase activity was then stopped with 1µL of DNase stop solution (0.5M EGTA), then 0.5µl of random hexamers (primers) and 2µl of nuclease-free water was added to the sample and incubated for 5 minutes at 70°C. The samples were then placed on ice for 5 minutes and the reverse transcriptase mixture comprising 0.5µl RNAsin (25 units), 1µl MMLV-RT (200 units), 1µl 10mM dNTPs oligonucleotides and 4µl 5 x MMLV-RT buffer (250mM Tris-HCl, 375mM KCl, 15mM MgCl2 AND 50mM DTT) was added. The reaction was then incubated at 42°C for 60 minutes and the cDNA diluted to 10ng/ml in nuclease-free water and stored at -30°C.

2.4.3 Primer design

All primers were designed using cDNA sequences from Ensembl. The Primer3 primer design software was used to analyse the cDNA sequences and generate primers between 18-22 base pairs in length capable of amplifying and yielding products approximately 200bp long, with a guanine and cytosine content between 40-60% and a melting temperature Tm close to 60°C. Oligonucleotide primer pairs were ordered from Sigma and reconstituted to 100µM in 1 x Tris-EDTA buffer, and the optimum annealing temperature was determined for each pair of primers. Primers were stored at -30°C.

Gene	Forward Sequence	Reverse Sequence
GAPDH	GCACAGTCAAGGCCGAGAAT	GCCTTCTCCATGGTGGTGAA
S100A9	CACCCTGAGCAAGAAGGAAT	TGTCATTTATGAGGGCTTCATTT
CXCL1	CTGGGATTCACCTCAAGAACATC	CAGGGTCAAGGCAAGCCTC
CXCL2	CCAACCACCAGGCTACAGG	GCGTCACACTCAAGCTCTG
CXCL10	GGATGGCTGTCCTAGCTCTG	ATAACCCCTTGGGAAGATGG

CCL2	CCAATGAGTAGGCTGGAGAG	TTCAAAGGTGCTGAAGACCT
CCL5	TGCTGCTTTGCCTACCTCTCC	TGGCACACTTGGCGGTTCC
IL-6	GAGGATACCACTCCCAACAGA	AAGTGCATCATCGTTGTTCATA
TNFA	GACCAGGCTGTCGCTACATCA	CGTAGGCGATTACAGTCACGG
BCL-2	CACACACACACATTCAGGCA	GGCAATTCCTGGTTCGGTTT
BCL-XL	CCCAGAGACTGACAGCCTGA	TGTAGGGTGAGGGGAGAGG
GADD45B	CTCCTGGTCACGAACTGTCA	TTGCCTCTGCTCTCTTCACA
XIAP	ACCCTGCCATGTGTAGTGAA	ACGATCACAGGGTTCCCAAT
ASMA	TCAGCGCCTCCAGTTCT	AAAAAAAACCACGTAACAA
TIMP1	GCAACTCGGACCTGGTCATAA	CGGCCCGTGATGATGAGAAACT
COL1A1	TTCACCTACAGCACGCTTGTG	GATGACTGTCTTGCCCCAAGTT
TGF-B	CTCCCGTGGCTTCTAGTGC	GCCTTAGTTTGGACAGGATCTG
MMP-13	CTTCTTCTTGTTGAGCTGGACTC	CTGTGGAGGTCACTGTAGACT
ARG1	GGAAAGCCAATGAAGAGCTG	GCTTCCAACTGCCAGACTGT
ARG2	TCCTCCACGGGCAAATTCC	GCTGGACCATATTCCACTCCTA

Table 2.3 qPCR mouse primer sequences

2.4.4 Quantitative real-time PCR

Quantitative real-time PCR was performed using a 7500 Fast System. A master mix containing 6.5µl SYBR Green Master Mix (Sigma-Aldrich), 1µl of each 2.5µM primer, made up to a total volume of 11µl with nuclease free water. 2µl of cDNA was then added to each well and the plate was sealed with an optical film (Applied Biosystems). The plates were centrifuged at 1000 rpm for 30s before being placed in the PCR machine. The reaction consisted of 40 cycles of denaturing for 15s at 95°C, annealing at 55-60°C (depending on the primer) for 30s and elongation at 72°C for 30s. A melt curve was obtained with a cycle of 95°C for 10s, 60°C for 60s and 95°C for 30s, to check primer specificity. All results were normalised to a house-keeping gene control (GAPDH), and the data displayed as relative levels of transcriptional difference (RTLD), relative to a control sample arbitrarily given a value of 100%. Relative transcriptional differences were calculated using the (1/2A)_100 calculation.

Step	Temperature	Time	
Initial denaturing	95°C	10s	
Denaturing	95°C	10s	40 cycles
Annealing	55-60°C	30s	
Elongation	72°C	30s	
Melt curve	95°C	15s	
	60°C	1min	
	95°C	30s	

Table 2.4 qPCR cycle

2.5 Protein isolation and analysis

2.5.1 Cell lysate preparation

Cells were washed twice with PBS then scraped in ice cold PBS and transferred to a microcentrifuge tube. Samples were centrifuged at 1200 rpm for 5mins, the supernatant removed, and the pellet resuspended in 300µl RIPA (radio immune-precipitation assay) lysis buffer containing 50mM Tris-HCl pH8, 1% Triton x-100, 0.5% sodium deoxycholate, 0.1% SDS, 150mM NaCl, 10µl/ml phosphatase inhibitors and 4µl/ml protease inhibitors. Cells were lysed with a pestle and transferred to a Qiashredder column and centrifuged at 13 000 rpm for 2 minutes for homogenisation. The flow-through was transferred to a new tube and centrifuged at 10 000 rpm for 10 minutes at 4°C to remove cellular debris. The supernatant was transferred to a new tube, taking care not to disturb the pellet. Samples were then either stored at -80°C or protein quantified by BCA assay.

2.5.2 Tissue lysate preparation

Tissue was snap frozen in liquid nitrogen and stored at -80°C until required. 700µl of RIPA lysis buffer was added to each sample and tissues were homogenised with a pestle then transferred to a Qiashredder column and centrifuged at 13 000 rpm for 2 minutes. The flow-through was transferred to a new tube and centrifuged at 10 000

rpm for 10 minutes at 4°C to remove cellular debris. The supernatant was transferred to a new tube, taking care not to disturb the pellet. Samples were then either stored at -80°C or protein quantified by BCA assay.

2.5.3 Protein quantification (Bio-Rad assay)

Protein concentration of samples was determined by Bio-Rad assay (BD biosciences). 2µl of protein sample was added to 18µl of distilled water, with the blank sample consisting of 2µl of RIPA lysis buffer and 18µl of distilled water. 100µl of AS mixture (98% buffer A and 2% buffer S) was added to each sample, followed by 800µl of buffer B. The samples were incubated in the dark at room temperature for 20 minutes then the absorbance measured at 750nm on the spectrophotometer. Protein concentration was calculated with the following formula: (absorbance/0.0157)/2. The concentration was obtained in µg/ul.

2.5.4 Western blotting

40µg of protein sample was diluted in distilled water to a final volume of 20µl. 5µl of 5 x SDS (sodium dodecylsulfate)-loading dye containing 10% SDS, 50% glycerol, 0.25M Tris pH 6.8, betamercaptoethanol (160µl/ml) and bromophenol blue was added to each sample and samples were incubated at 95°C for 5 minutes for protein denaturation. Samples were then loaded on a gel consisting of a 10% SDS-polyacrylamide resolving gel and a 4% stacking gel, and run for approximately 2 hours at 100V. The gels were then transferred to a nitrocellulose membrane at 100V for 1.5 hours, sandwiched between filter paper and scouring pads in a transfer cassette and placed in a tank containing ice cold transfer buffer and an ice pack. Membranes were then washed in TBS-T (Tris-buffered saline containing 200mM NaCl, 20mM Tris and 0.01% v/v Tween 20 at pH 7.4) and stained with Ponceau Red (Ponceau S Solution, Sigma) to verify accurate sample loading. Membranes were washed again in TBS-T to remove the Ponceau Red, then blocked in 5% w/v skimmed milk powder in TBS-T for 1 hour at room temperature to prevent non-specific binding. Membranes were then incubated with a primary antibody diluted in TBS-T at 4°C overnight. The next day the primary antibody was removed, the membrane washed 3 times for 5 minutes in TBS-T and a HRP (horseradish peroxidase)-conjugated secondary antibody added for a 1 hour incubation at room temperature. Membranes were then washed again 3 times for 5 minute sin TBS-T and developed using the Pierce ECL substrate (Thermo Scientific) for chemiluminescent detection. Membranes were incubated for 1 minute at room

temperature in a solution containing equal amounts of reagent 1 and 2. Excess substrate was then removed and membranes placed in a film cassette. X-ray films were exposed to the membranes in a dark room and developed using an automated developer (RP X-OMAT, Kodak, Hertfordshire, UK).

Antigen	Primary Antibody	Secondary Antibody
Nfkb1 p105/p50	Rb mAb to NFkB p105/p50 HRP (ab195854)	/
p65	Rb pAb to NFkB p65 (ab2615-100)	Anti-rabbit IgG HRP-linked Ab (#7073, CST)
c-REL	Rb pAb to c-Rel (sc-71, Santa Cruz Biotechnology)	Anti-rabbit IgG HRP-linked Ab (#7073, CST)
p52	Mouse mAb to NFkB p52 (sc-7386, Santa Cruz Biotechnology)	Anti-mouse IgG peroxidase Ab (A4416, Sigma)
BCL-2	Rb mAb to Bcl-2 (#2870, CST)	Anti-rabbit IgG HRP-linked Ab (#7073, CST)
BCL-XL	Rb mAb to Bcl-xL (#2052A, R&D systems)	Anti-rabbit IgG HRP-linked Ab (#7073, CST)
GADD45β	Rb pAb to GADD45β (orb215494, biorbyt)	Anti-rabbit IgG HRP-linked Ab (#7073, CST)
ERK	Rb Ab to p44/42 MAPK (Erk1/2) (#9102, CST)	Anti-rabbit IgG HRP-linked Ab (#7073, CST)
p-ERK	Rb Ab to p-p44/42 MAPK (T202/Y204) (#9101. CST)	Anti-rabbit IgG HRP-linked Ab (#7073, CST)
JNK	Rb Ab to SAPK/JNK (#9252, CST)	Anti-rabbit IgG HRP-linked Ab (#7073, CST)
p-JNK	Mouse mAb to p-SAPK/JNK (T183/Y185) (#9255, CST)	Anti-mouse IgG peroxidase Ab (A4416, Sigma)
Caspase 3	Rb mAb to cleaved caspase-3 (D175) (5A1E) (#9664, CST)	Anti-rabbit IgG HRP-linked Ab (#7073, CST)

γH2AX	Rb mAb to γH2AX (CST #9718)	Anti-rabbit IgG HRP-linked Ab (#7073, CST)
Cyclin D1	Rb mAb to cyclin D1 (#2978, CST)	Anti-rabbit IgG HRP-linked Ab (#7073, CST)
GAPDH	Rb pAb to GAPDH (ab22555)	Anti-rabbit IgG HRP-linked Ab (#7073, CST)
β-Actin	Mouse mAb to β-actin (A5441, Sigma)	Anti-mouse IgG peroxidase Ab (A4416, Sigma)

Table 2.5 Western blot antibodies

2.6 Immunohistochemistry and histology

2.6.1 Paraffin embedded section preparation

Tissue samples were fixed in 10% formalin for 24 hours then transferred to 70% ethanol until processed. Samples were processed and embedded by the BioBank laboratory and cut by microtome onto Superfrost Plus slides (Fisher) with a thickness of 6um.

2.6.2 Haematoxylin and Eosin staining (H&E)

H&E staining was carried out to examine tissue histology. Paraffin-embedded formalin-fixed sections were dewaxed in clearene for 2 x 5 minutes, then rehydrated in 100% ethanol for 5 minutes followed by 70% ethanol for 5 minutes. Sections were then washed in tap water and placed in Mayer's haemotoxylin for 1.5 minutes, then washed in running tap water to remove any unbound stain. Sections were then placed in Scott's water for 1 minute to blue to Haemotoxylin stain, then washed again in running tap water and placed in Eosin for 1.5 minutes. Sections were washed in running tap water to remove any residual unbound eosin followed by dehydration through graded ethanols (10s in 50%, 10s in 70%, 2 minutes in 100% and 2 minutes again in 100%), before being transferred to clearene for 2 x 5 minutes. The sections were then mounted in pertex.

2.6.3 Sirius Red staining

Paraffin-embedded formalin-fixed sections were dewaxed and rehydrated as described above then washed in distilled water. Sections were incubated in 0.2% phosphomolybidic acid for 5 minutes, then washed in distilled water and stained with 0.1% Sirius Red F3B in saturated picric acid for 2 hours. Sections were then washed twice in 0.01M HCl and dehydrated in graded ethanols and transferred to clearene as described above, followed by mounting in pertex.

2.6.4 Immunostaining

Formalin-fixed paraffin-embedded tissue sections were dewaxed and rehydrated as described above. Sections were incubated in a 0.6% hydrogen peroxide methanol solution for 15 minutes to block endogenous peroxidase activity. Antigen retrieval was dependent on the antibody used (Table 2.6). Endogenous avidin and biotin was then blocked using the Avidin/Biotin Blocking Kit (Vector Laboratories), with a 3 x 5 minutes PBS wash after incubation with each reagent for 20 minutes. 20% swine serum in PBS was then added for 20-60 minutes to block non-specific binding, followed by the primary antibody incubated at 4°C overnight. The next day slides were returned to room temperature and left for 30 minutes, then washed 3 x 5 minutes in PBS. Appropriate biotinylated secondary antibody was added for 1-2 hours. Slides were then washed 3 x 5 minutes in PBS and incubated with Vectastain Elite ABC Reagent for 1 hour. Staining was visualised using the DAB peroxidase substrate kit and counterstained in Mayer's Haemotoxylin, followed by dehydration through graded ethanols (5 minutes in 50%, 70%, 100% and 100%), then incubated in clearene for 10 minutes before mounting in pertex.

Antigen	Antigen Retrieval	Primary Antibody	Secondary Antibody
CD68	Citrate (Vectorshield) Micowave 15 mins	Rb pAb to CD68 (OABB00472) 1:200 dilution	Swine anti-rabbit biotin conjugated 1:200 dilution
Ly6G	Citrate (Vectorshield)	Rat mAb to Ly6G (clone 1A8, InVivoPlus)	Goat anti-rat biotin conjugated

	Microwave 15 mins + 0.2% trypsin 37°C 30 mins	1:700 dilution	1:200 dilution
NIMP	Citrate (Vectorshield) Microwave 15 mins + 0.2% trypsin 37°C 30 mins	Rat mAb to NIMP-R14 (Ab2557) 1:200 dilution	Goat anti-rat biotin conjugated 1:200 dilution
CD3	1mM EDTA pH8 Microwave 15 mins	Rat anti-human CD3 (MCA1477) 1:200 dilution	Goat anti-rat biotin conjugated 1:200 dilution
CD4	Citrate (Vectorshield) Microwave 15 mins	Rat anti-mouse eBioscience (14-9766-82) 1:100 dilution	Goat anti-rat biotin conjugated 1:200 dilution
CD8	1mM EDTA pH8 Microwave 15 mins	Rat anti-mouse eBioscience (14-0808-82) 1:100 dilution	Goat anti-rat biotin conjugated 1:200 dilution
CD45R	Citrate (Vectorshield) Microwave 15 mins	Rat mAb to CD45R (Ab64100) 1:200 dilution	Goat anti-rat biotin conjugated 1:200 dilution
FOXP3	1mM EDTA pH8 Microwave 15 mins	Rat anti-mouse eBioscience (14-5773-82) 1:100 dilution	Goat anti-rat biotin conjugated 1:200 dilution
CASPASE 3	Citrate (Vectorshield)	Rb mAb to cleaved caspase-3 (Asp175,	Swine anti-rabbit biotin conjugated

	Microwave 15 mins	5A1E, #9664 CST) 1:200 dilution	1:200 dilution
PCNA	Citrate (Vectorshield) Microwave 15 mins	Rb pAb to PCNA (Ab18197) 1:6000 dilution	Swine anti-rabbit biotin conjugated 1:200 dilution
γH2AX	1mM EDTA pH8 Microwave 15 mins	Rb mAb to γH2AX (CST #9718) 1:100 dilution	Swine anti-rabbit biotin conjugated 1:200 dilution
αSMA	Citrate (Vectorshield) Microwave 15 mins	Ms mAb to αSMA-FITC conjugated (F3777) 1:1000 dilution	anti-FITC biotin conjugated 1:300 dilution

Table 2.6 Immunostaining antibodies

2.6.5 Image analysis

A Nikon Eclipse microscope and NIS-Elements BR analysis software was used for brightfield image analysis. 15 fields per slide/mouse (5 fields per liver lobe: large lobe, bilobulated lobe and triangular lobe) were used for image analysis. Densitometry was performed for Sirius Red and alpha-SMA stains, by applying a predefined threshold to images acquired at x10 magnification. A percentage of positively stained area was subsequently calculated from this. Cell counts were performed on x20 images using the ImageJ software cell counter tool.

2.7 Enzyme-linked immunosorbent assay (ELISA)

An R&D systems kit was used to quantify the amount of mouse MCP-1 protein present within the liver tissue harvested from the acute CCl4 study. High-binding 96 well plates (Greiner) were coated with assay appropriate concentrations of capture antibody diluted in PBS and incubated overnight at room temperature. The next day the capture antibody was removed and the plate washed 3 times with wash buffer containing

0.05% PBS-Tween 20. The plate was then blocked with blocking buffer (1% BSA in PBS) for 1 hour at room temperature. The blocking buffer was then aspirated and the plate washed three times, followed by the addition of standards and optimum dilutions of samples and incubation for 2 hours at room temperature. The plate was then washed 3 times and detection antibody added to the plate and incubated for 2 hours at room temperature. The plate was then washed 3 times and HRP-streptavidin antibody added for 30 minutes at room temperature, followed by another 3 washes. 25µl of a 1:1 ratio of Substrate Reagent A (stabilised hydrogen peroxide) and Reagent B (stabilized TMB) substrate was added to each well for 20 minutes at room temperature in the dark. The reaction was quenched with 25µl stop solution 2N H_2SO_4 (ABT Trinitorm) and the OD was measured spectrophotometrically at 450nm using a SpectraMax Plate reader. The background level of MCP-1 expression in control samples was determined and subtracted from conditioned samples and samples were quantified using the Softmax Pro Software.

2.8 RNA-Sequencing

mRNA sequencing was carried out in 5 DEN-induced HCC tumour samples from each of $Nfkb1^{fl/fl}$, $Nfkb1^{hep-/-}$ and $Nfkb1^{-/-}$ mice (a total of 15 samples). Only samples with a purity A260/A280 ratio of approximately 2 to exclude the presence of protein or other contaminants, and a RIN (RNA Integrity Number) value above 7 were used. Samples were sequenced at >25 M 75 bp single reads. Salmon was used to directly quantify RNA-Seq reads against a reference transcriptome (from GenCode: gencodegenes.org). This quantification data was then read into R using tximeta and analysed for differential expression using DESeq2 which applies a Negative Binomial model to determine differentially expressed genes. Cut-offs of 2-fold change in either direction, and a p-value (adjusted for multiple tests by the Benjamini-Hochberg FDR correction) of 0.05 were applied. The expression ratios between conditions are expressed by DESeq2 in log2 space – therefore a 2-fold change is a log2(fold change) of > 1 or < -1. The genes which passed these thresholds were then submitted for GO and KEGG analysis using Fisher's Exact Test to determine over-represented functional terms amongst the DEGs when compared to the 'background' of all the genes expressed in the experiment. Again, an adjusted p-value (BH correction, as before) was used to determine statistically significant over-representation.

2.9 Statistics

Statistical analysis was performed using the GraphPad Prism software. Data are reported as means +/- the SEM (standard error of the mean). For comparison between 2 groups, a Student's 2-tailed t-test was used to determine statistical significance, which was considered when $p<0.05$. For comparison between more than 2 groups, a one-way or two-way ANOVA was carried out, followed by a Tukey post-hoc text for multiple comparisons, with values of $p<0.05$ accepted as statistically significant.

Chapter 3. The role of hepatocyte NF-κB1 in acute liver injury

3.1 Introduction

The NF-κB transcription factor family plays a central role in the resolution of acute liver injury and inflammation, with a key role in innate immune response activation and in the regulation of cell survival and proliferation (Karin, 2009). Upon liver injury, activation of the NF-κB pathway leads to the translocation of NF-κB dimers into the nucleus, where they activate the transcription of genes involved in the resolution of liver injury including cytokines, chemokines and apoptotic regulatory genes. While this response represents a means of overcoming cell injury, over-activation of the NF-κB pathway can have detrimental effects. NF-κB1 p50, unable to activate transcription alone due to the lack of a transactivation domain, is generally thought to repress gene transcription in its homodimer form, dampening inflammatory and anti-apoptotic signalling (Cartwright et al., 2016).

Several different models of acute liver injury in mice exist and are commonly used in research. Of these, the CCl_4 and DEN-induced hepatotoxicity models represent useful tools for understanding the role of genetic alterations in liver injury mechanisms. These acute models are particularly used for the study of inflammation, ROS damage and apoptosis (Tolba, Kraus, Liedtke, Schwarz, Weiskirchen, et al., 2015a; Uehara et al., 2014).

The primary aim of this study was to assess whether the knockout of Nfkb1 in hepatocytes leads to a worse phenotype in mice when subjected to hepatotoxin IP injections. NF-κB1 p50 homodimers being known for their anti-inflammatory function, it was hypothesized that knocking out p50 in hepatocytes, and thus eliminating p50 homodimers, would lead to a worse outcome compared to control mice with normal p50 homodimer expression.

3.2 Characterisation of the $Nfkb1^{hep-/-}$ mice

To validate the hepatocyte-specific knockout of Nfkb1 in $Nfkb1^{hep-/-}$ mice, hepatocytes and non-parenchymal liver cells were isolated from $Nfkb1^{fl/fl}$ control and $Nfkb1^{hep-/-}$ mice, and western blot analysis was performed to look at p50 expression. p50 was abundantly expressed in $Nfkb1^{fl/fl}$ mice hepatocytes while showing no expression in

Nfkb1$^{hep-/-}$ mice hepatocytes, whereas p50 expression levels were similar in non-parenchymal cells across both genotypes, demonstrating the hepatocyte-specific knockout by Alb-Cre recombinase (Figure 3.1a). p50 western blot analysis was also performed on spleen tissue and isolated bone marrow cells from these mice, to ensure similar p50 expression between control and Nfkb1$^{hep-/-}$ mice in immune cells, where p50 is known to play an important role and be expressed in high levels. Similar p50 expression was observed between both genotypes, additionally confirming the hepatocyte-specific knockout of Nfkb1 p50 in Nfkb1$^{hep-/-}$ mice (Figure 3.1b). To further confirm this, p50 expression was assessed in several different organs in control and Nfkb1$^{hep-/-}$ mice. As expected, p50 expression levels were comparable between both groups (Figure 3.1c).

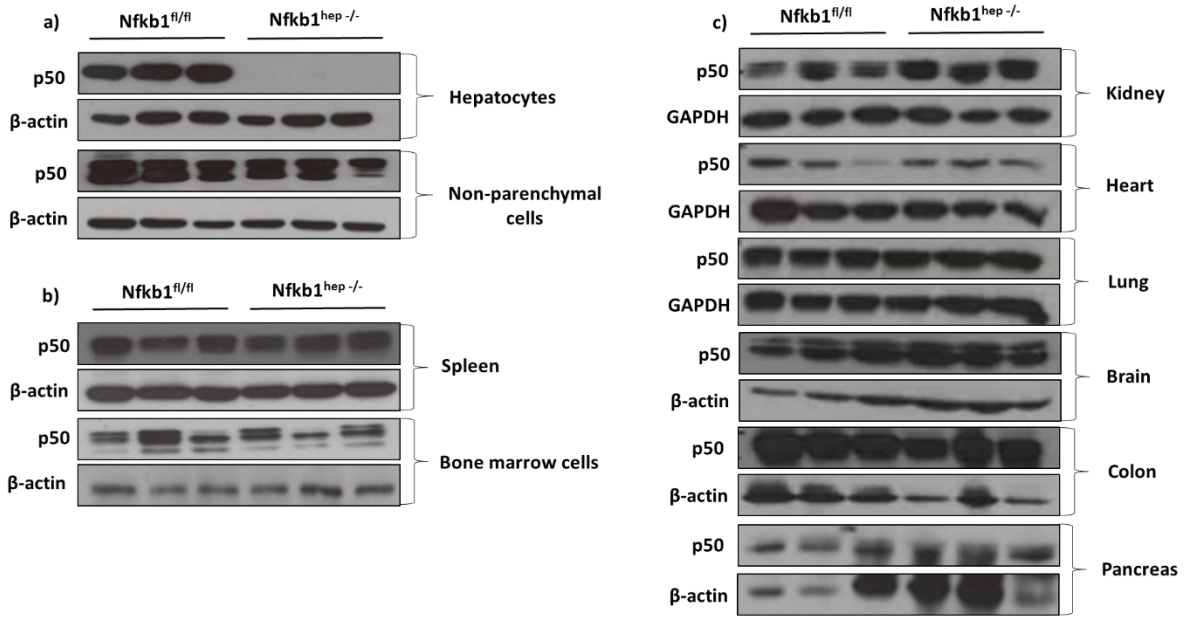

Figure 3.1 Western blot analysis of NF-κB1 p50 expression comparison between control and Nfkb1$^{hep-/-}$ mice. Western blots show p50 expression in Nfkb1$^{fl/fl}$ and Nfkb1$^{hep-/-}$ mice in hepatocytes and non-parenchymal liver cells (a), in spleen and bone marrow cells (b), and in kidney, heart, lung, brain, colon and pancreas tissue (c).

To determine the genotype of mice resulting from Nfkb1$^{fl/fl}$ X Alb-Cre$^{+/-}$ breeding, DNA was extracted from mice small ear punches and PCR performed with the relevant

primers (see methods section) followed by agarose gel electrophoresis to determine the presence or absence of cre expression (cre is expressed in Nfkb1$^{hep-/-}$ mice), and the presence of LoxP sites on both alleles (representative of Nfkb1$^{fl/fl}$ mice). For cre expression genotyping, the presence of a band means cre is expressed and therefore the mouse is Nfkb1$^{hep-/-}$. When no band is present, cre is not expressed and the mouse is Nfkb1$^{fl/fl}$.

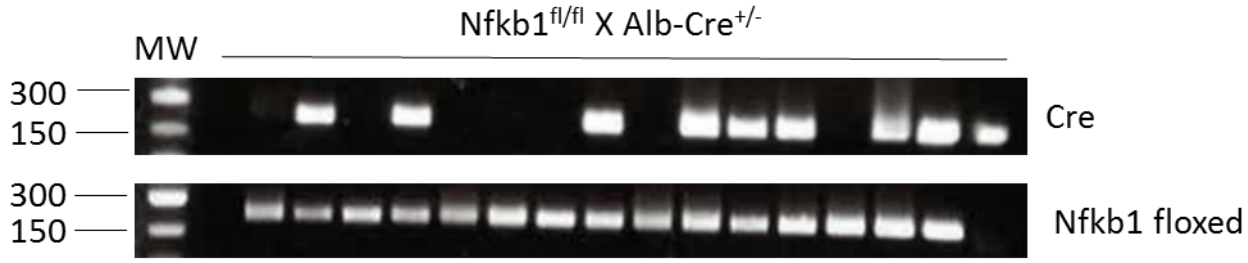

Figure 3.2 Genotyping analysis of mice from Nfkb1$^{fl/fl}$ X Alb-Cre$^{+/-}$ breeding. Gel images from PCR products show the presence or absence of cre expression (top) and homozygous Nfkb1 floxed genes (single band).

To further confirm Nfkb1 knockout specificity, Nfkb1 immunohistochemistry was performed on WT and Nfkb1$^{-/-}$ formalin-fixed paraffin-embedded mouse liver tissue, with different anti-Nfkb1 antibodies, with 1 day and 2 day protocols, however none appeared to be successful (Figure 3.3, 3.4, 3.5, and 3.6).

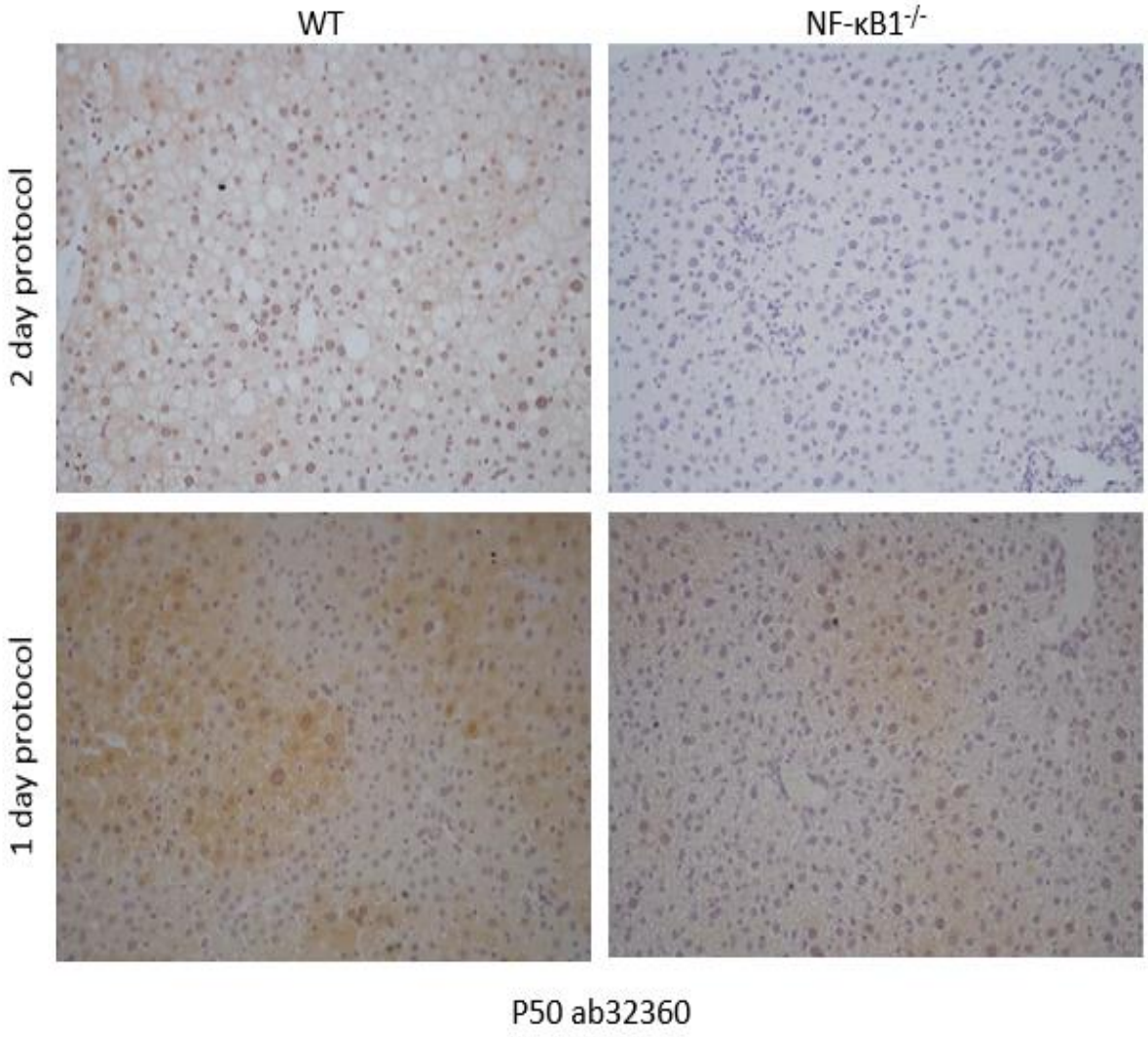

Figure 3.3 NF-κB1 immunohistostain with ab32360 antibody, 1 and 2 day protocols. Images show X20 NF-κB1 1-day and 2-day immunostaining with ab32360 anti-NF-κB1 antibody in WT and Nfkb1$^{-/-}$ formalin-fixed paraffin-embedded mice liver tissue.

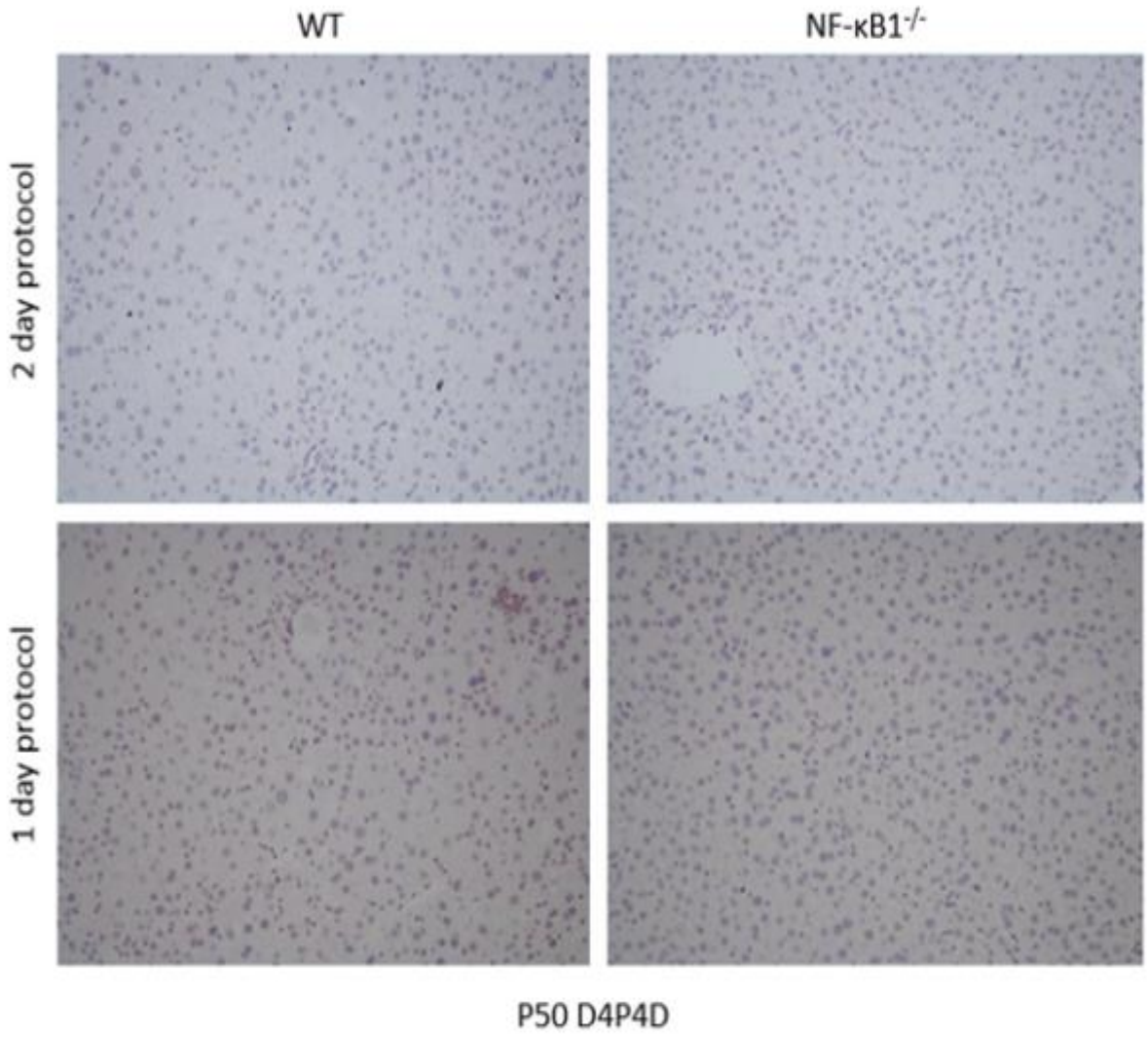

Figure 3.4 NF-κB1 immunohistostain with D4P4D antibody, 1 and 2 day protocols. Images show X20 NF-κB1 1-day and 2-day immunostaining with D4P4D anti-NF-κB1 antibody in WT and Nfkb1$^{-/-}$ formalin-fixed paraffin-embedded mice liver tissue.

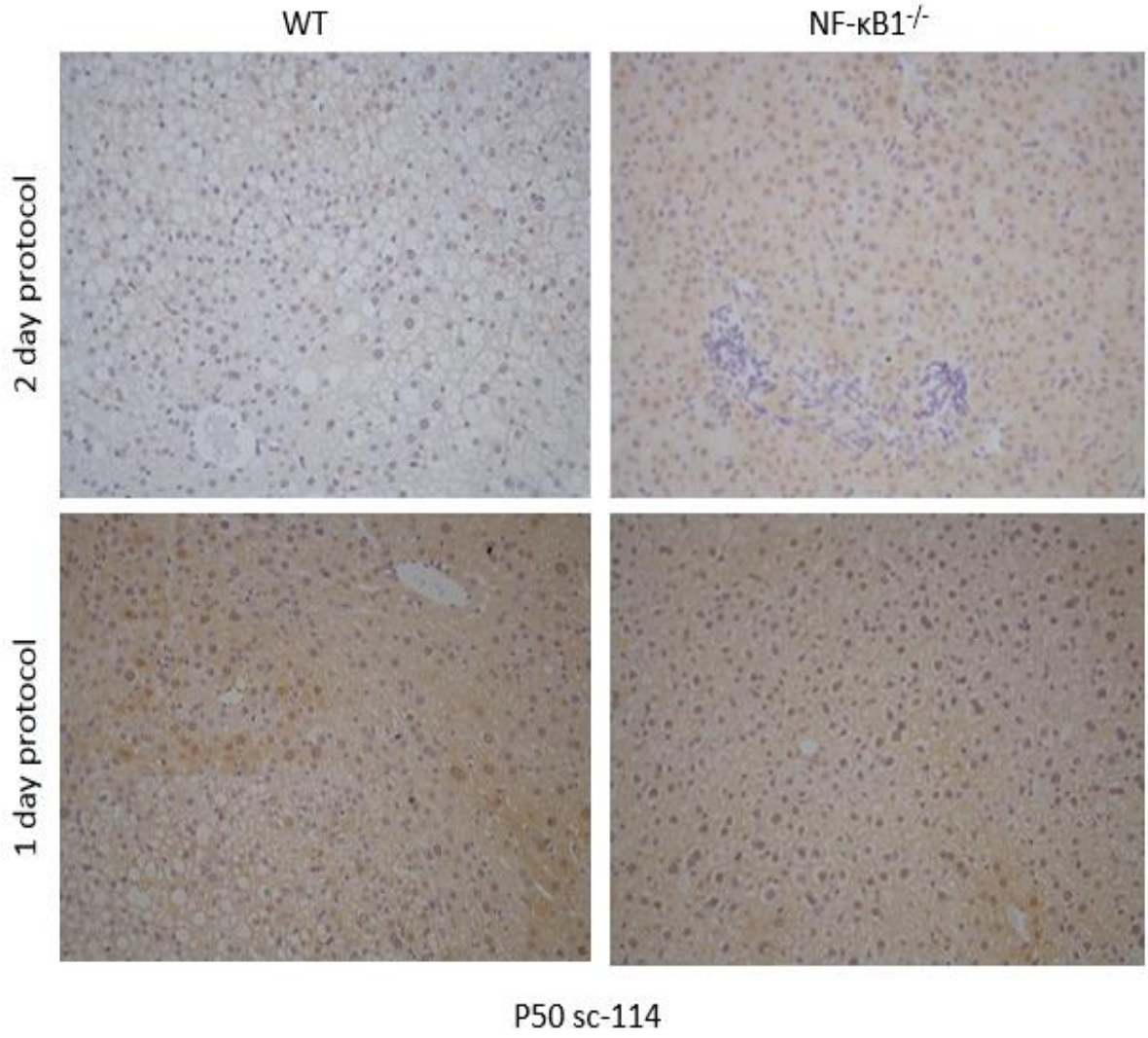

Figure 3.5 NF-κB1 immunohistostain with sc-114 antibody, 1 and 2 day protocols. Images show X20 NF-κB1 1-day and 2-day immunostaining with sc-114 anti-NF-κB1 antibody in WT and Nfkb1$^{-/-}$ formalin-fixed paraffin-embedded mice liver tissue.

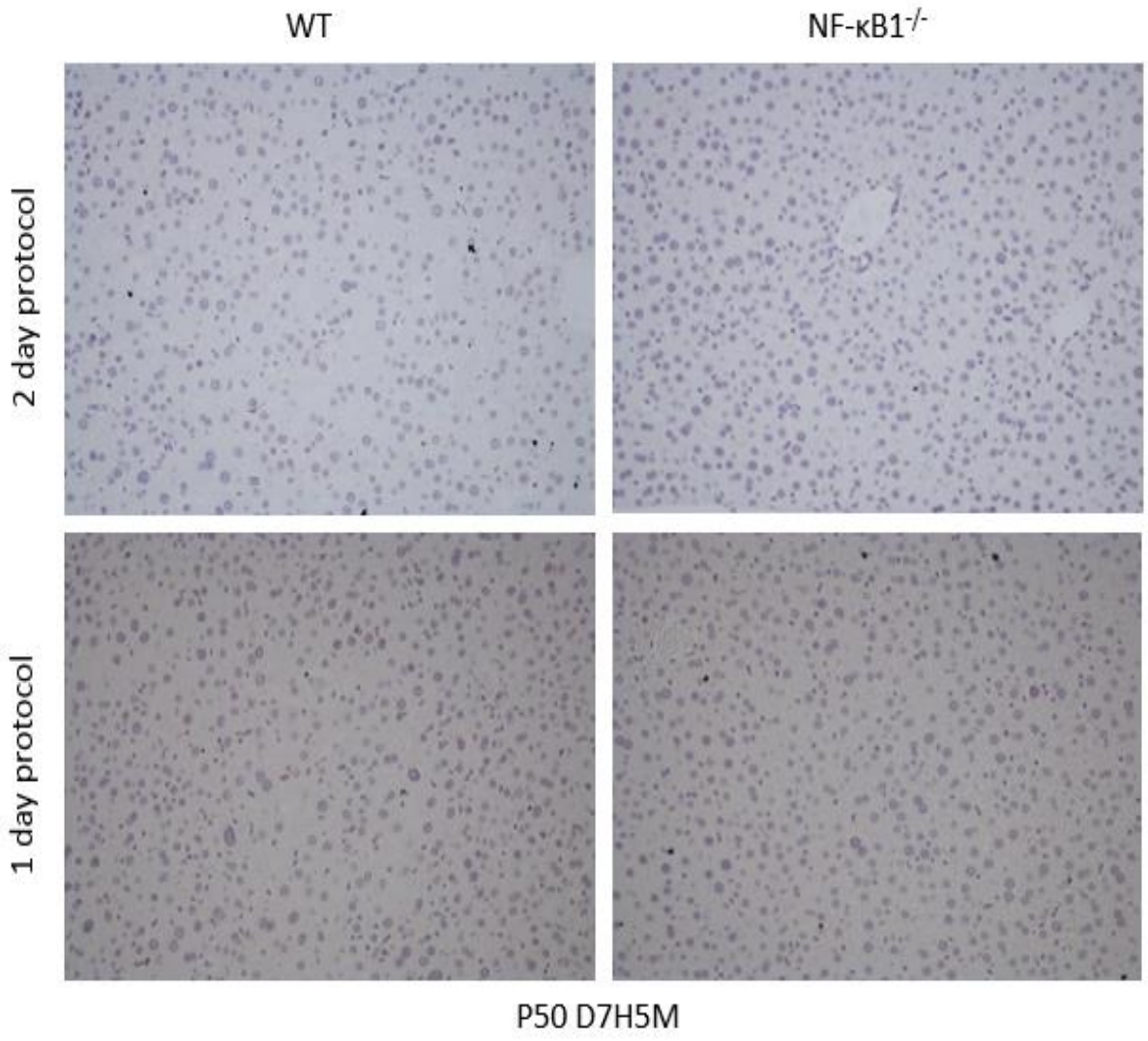

Figure 3.6 NF-κB1 immunohistostain with D7H5M antibody, 1 and 2 day protocols. Images show X20 NF-κB1 1-day and 2-day immunostaining with D7H5M anti- NF-κB1 antibody in WT and Nfkb1$^{-/-}$ formalin-fixed paraffin-embedded mice liver tissue.

3.3 The role of hepatocyte NF-κB1 in acute CCl_4 liver injury

Acute treatment with the hepatotoxin CCl_4 is known to cause inflammation and cell death in mice livers (Scholten et al., n.d.). An acute CCl_4 experiment was carried out at two time-points, with mice livers harvested after 24h and after 48h following a single CCl_4 intraperitoneal (IP) injection, to assess the role of NF-κB1 in acute liver inflammation. 24h following the liver injury represents the peak of inflammation and increased apoptosis is usually observed after 48h (Tzirogiannis et al., 2003; Horiguchi et al., 2010). Three different groups of mice were used in this study: Nfkb1$^{fl/fl}$ and Alb-Cre$^{+/-}$ control mice, and Nfkb1$^{hep-/-}$ mice, with Nfkb1$^{fl/fl}$ representing wild type littermate

controls for Nfkb1$^{hep-/-}$ mice, and Alb-Cre$^{+/-}$ mice representing a control group accounting for any Cre enzyme expression specific effects (Nfkb1$^{hep-/-}$ mice express Cre recombinase). Cre recombinase expression has been shown to increase inflammation and cell death in certain conditions (Xiao et al., 2012). 6 mice were used per group and per time-point.

3.3.1 p50 protein expression after acute CCl_4 liver injury

CCl_4 was injected IP in 8 week old Nfkb1$^{fl/fl}$ and Nfkb1$^{hep-/-}$ mice and their livers were harvested 24h or 48h post-injection. 6 mice from each genotype were used per time-point. Western blot analysis was performed to assess p105 and p50 expression in these livers, to ensure the correct knockout of Nfkb1 in Nfkb1$^{hep-/-}$ mice. Figure 3.7 shows significantly lower expression levels of p105 and p50 in Nfkb1$^{hep-/-}$ mice livers, indicating successful Cre recombination. The low levels of p105/p50 expression in Nfkb1$^{hep-/-}$ mice can be attributed to non-parenchymal liver cells, accounting for around 25% of the liver (Seo & Jeong, 2016), since western blot analysis was performed on whole liver tissue lysate samples.

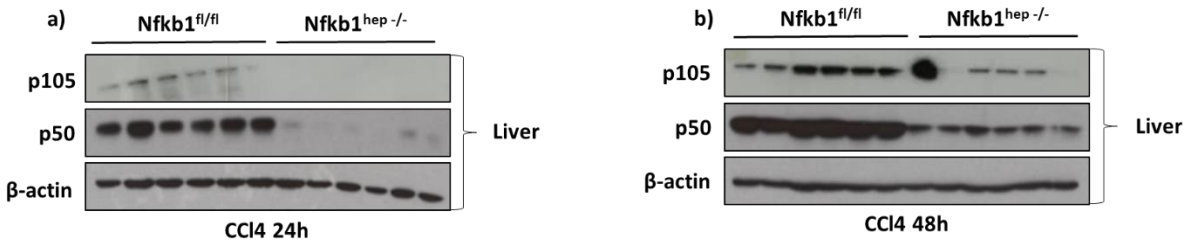

Figure 3.7 Western blot analysis of NF-κB1 p50 expression in control and Nfkb1$^{hep-/-}$ mice livers following CCl_4 injection. Western blots show p105 and p50 expression in Nfkb1$^{fl/fl}$ and Nfkb1$^{hep-/-}$ mice in livers harvested 24h post-CCl_4 injection (a), and 48h post-CCl_4 injection (b)

3.3.2 Hepatocyte Nfkb1 knock-out does not alter liver damage serum ALT (alanine transaminase) and AST (aspartate transaminase) enzyme levels following acute CCl_4 liver injury

Serum levels of ALT and AST were measured to assess liver damage. These transaminase enzymes are commonly used as biomarkers of liver damage, with higher levels indicating increased liver damage (Giannini et al., 2005). No significant difference in serum ALT or AST levels was observed at either the 24h or the 48h time point across the three groups, though there appeared to be a slight decrease in ALT (p=0.1) and AST (p=0.188) in $Nfkb1^{hep-/-}$ mice compared to $Nfkb1^{fl/fl}$ mice 24h following CCl_4 injection (Figure 3.8). This demonstrates similar liver injury levels caused by the CCl_4 hepatotoxin, indicating that hepatocyte Nfkb1 knockout does not affect the initial liver damage caused by CCl_4.

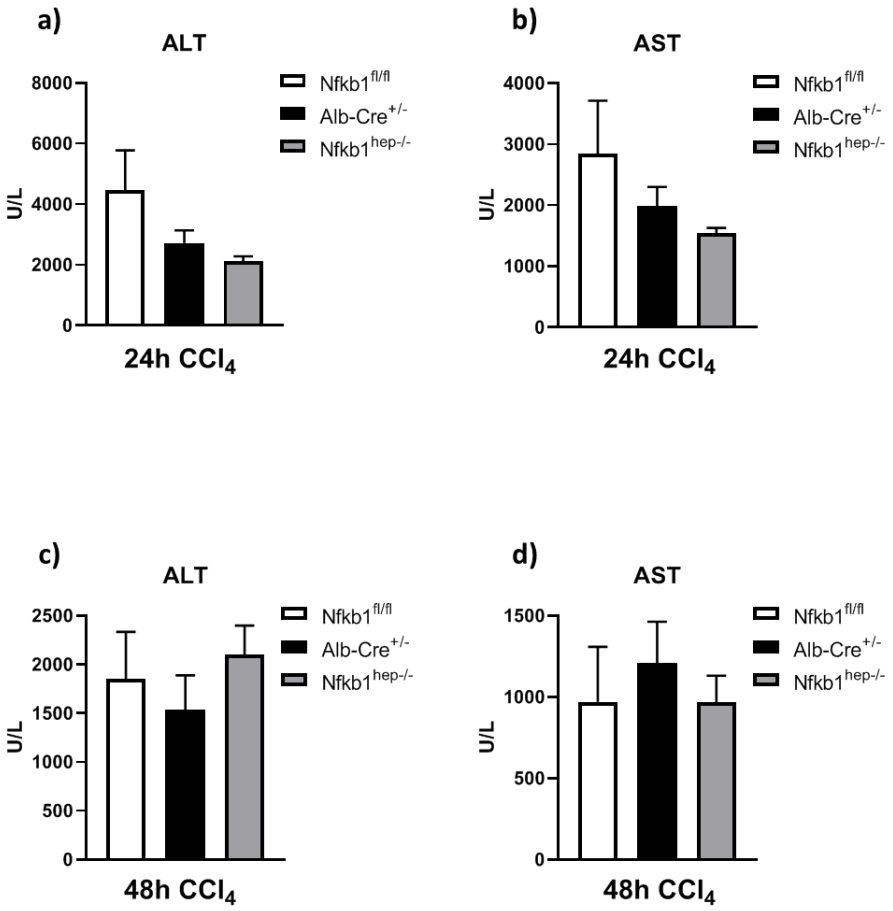

Figure 3.8 Serum ALT and AST enzyme level comparison at 24h and 48h post-CCl_4 injection. Graphs show serum levels of ALT 24h post-CCl_4 injection (a), AST 24h post-CCl_4 injection (b), ALT 48h post-CCl_4 injection (c), and AST 48h post-CCl_4 injection. Data are mean ± SEM of n=6 $Nfkb1^{fl/fl}$, n=6 Alb-$Cre^{+/-}$ and n=6 $Nfkb1^{hep-/-}$ mice livers. Statistical significance was determined using a one-way ANOVA followed by a post-hoc Tukey test. P values below 0.05 were considered statistically significant, with *P<0.05, **P<0.01 and ***P<0.001.

3.3.3 Hepatocyte Nfkb1 knock-out does not alter neutrophil recruitment to the liver

Previous work has shown important involvement of NF-κB1 p50 in dampening neutrophil recruitment to the liver in the context of liver injury and inflammation. Increased neutrophil chemoattractant chemokine expression was observed in global Nfkb1 knockout mice and hepatocytes, however the direct effect of hepatocyte Nfkb1 knockout remains unknown (Wilson et al., 2015). It was therefore hypothesized that Nfkb1$^{hep-/-}$ mice would display increased neutrophil liver infiltration compared to control mice. Ly6G immunohistochemistry staining, which is specific for neutrophils, was carried out in formalin-fixed paraffin-embedded liver tissue from the CCl_4-injured mice. However, no significant difference in Ly6G positive staining was observed between the three groups, indicating that hepatocyte p50 does not contribute to neutrophil recruitment in the liver following CCl_4 injury (Figure 3.9).

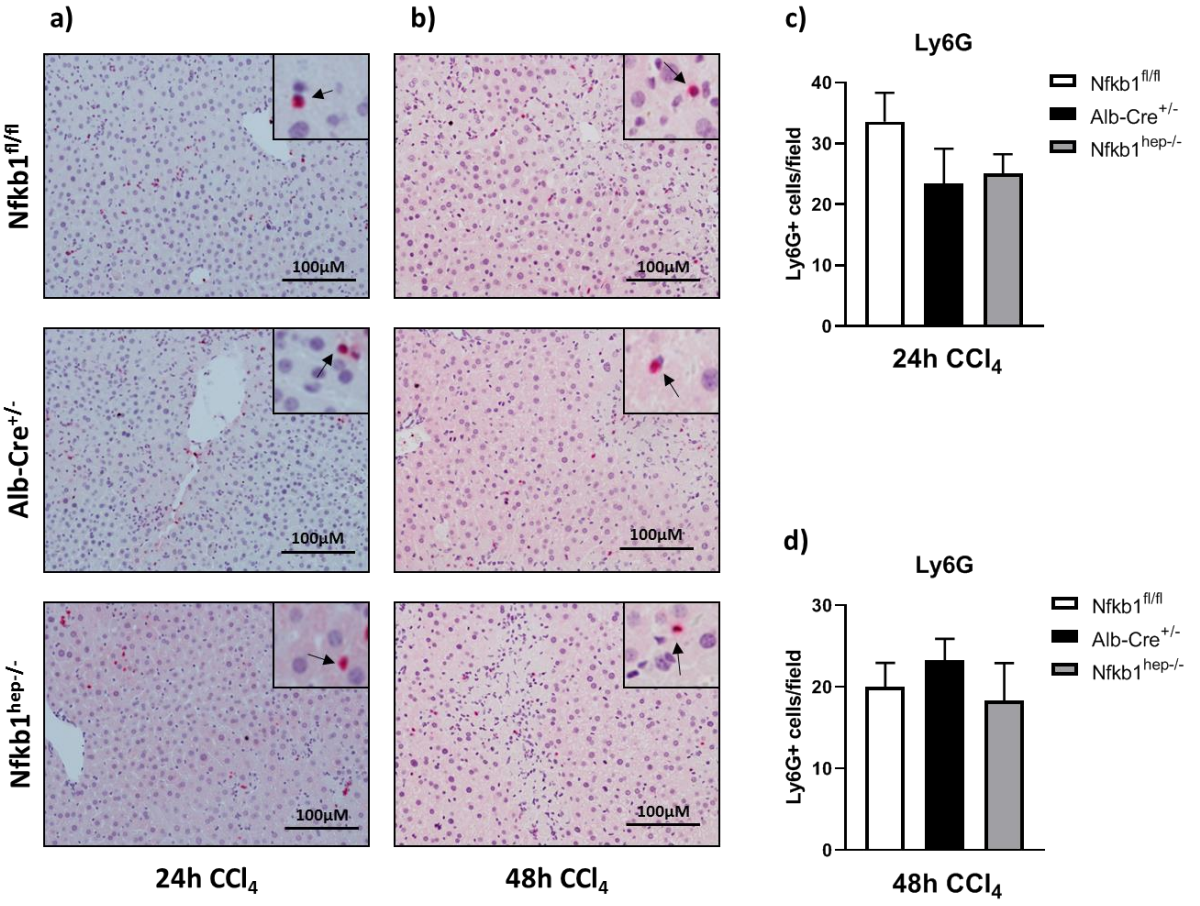

Figure 3.9 Ly6G immunostain of mice livers following acute CCl_4 injury. Images show X20 Ly6G immunostaining in Nfkb1$^{fl/fl}$, Alb-Cre$^{+/-}$ and Nfkb1$^{hep-/-}$ formalin-fixed paraffin-

embedded liver tissue 24h following CCl_4 injection (a), and 48h following CCl_4 injection (b). Graphs show Ly6G+ cells per field at 24h (c) and at 48h (d). Data are mean ± SEM of n=6 $Nfkb1^{fl/fl}$, n=6 Alb-$Cre^{+/-}$ and n=6 $Nfkb1^{hep-/-}$ mice livers. Statistical significance was determined using a one-way ANOVA followed by a post-hoc Tukey test. P values below 0.05 were considered statistically significant, with *P<0.05, **P<0.01 and ***P<0.001.

3.3.4 Hepatocyte Nfkb1 knock-out does not affect the neutrophil chemokine expression network

The gene expression levels of neutrophil chemokines S100A9, CXCL1 and CXCL2, known to be controlled by p50, were also assessed by RT-qPCR, as they were found to be significantly upregulated in global Nfkb1 knockout mice (Wilson et al., 2015). CXCL1 mRNA expression was significantly decreased in $Nfkb1^{hep-/-}$ mice compared to Alb-$Cre^{+/-}$ mice at the 48h time-point (p=0.005), however it was comparable to CXCL1 expression in $Nfkb1^{fl/fl}$ mice at this time-point (Figure 3.10). No significant difference was observed in the expression of S100A9, CXCL1 (p=0.292 $Nfkb1^{fl/fl}$ vs $Nfkb1^{hep-/-}$, and p=0.211 Alb-$Cre^{+/-}$ vs $Nfkb1^{hep-/-}$), CXCL2 between the three groups 24h post-CCl_4 injection, and no significant difference was observed in the expression of S100A9 (p=0.063 Alb-$Cre^{+/-}$ vs $Nfkb1^{hep-/-}$) and CXCL2 (p=0.067 Alb-$Cre^{+/-}$ vs $Nfkb1^{hep-/-}$) between the three groups 48h post-CCl_4 injection.

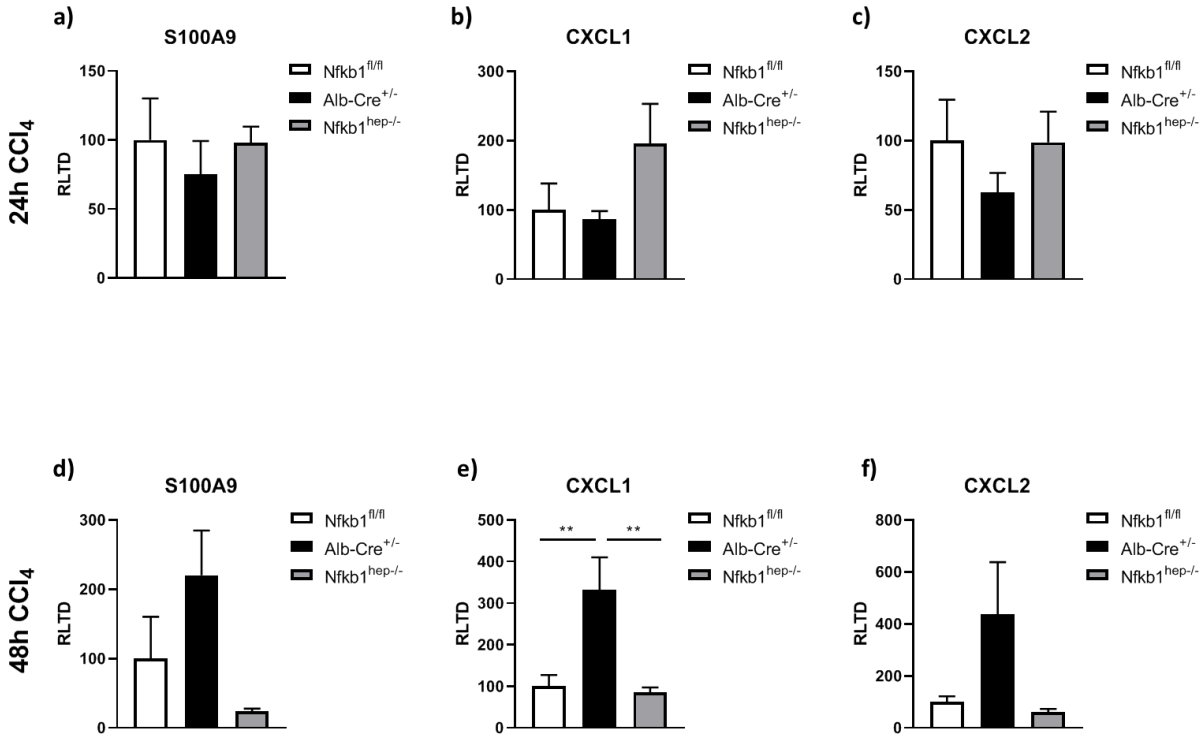

Figure 3.10 Neutrophil chemokine network gene expression in acute CCl_4-injured mice livers. Graphs show liver mRNA expression obtained by RT-qPCR analysis 24h after CCl_4 injection of S100A9 (a), CXCL1 (b), and CXCL2 (c), and 48h after CCl_4 injection of S100A9 (d), CXCL1 (e), and CXCL2 (f). Data are mean ± SEM of n=6 $Nfkb1^{fl/fl}$, n=6 Alb-$Cre^{+/-}$ and n=6 $Nfkb1^{hep-/-}$ mice livers. Statistical significance was determined using a one-way ANOVA followed by a post-hoc Tukey test. P values below 0.05 were considered statistically significant, with *P<0.05, **P<0.01 and ***P<0.001.

Additionally, given the implication of NF-κB1 p50 in inflammation (Cartwright et al., 2016), the gene expression of the chemokines TNFα and IL-6 was also assessed by RT-qPCR, however no significant difference was observed between the three groups at either time-point. TNFα and IL-6 expression appeared to be slightly increased in Alb-$Cre^{+/-}$ mice livers compared to the other two groups 48h post-CCl_4 injection, but this did not reach significance.

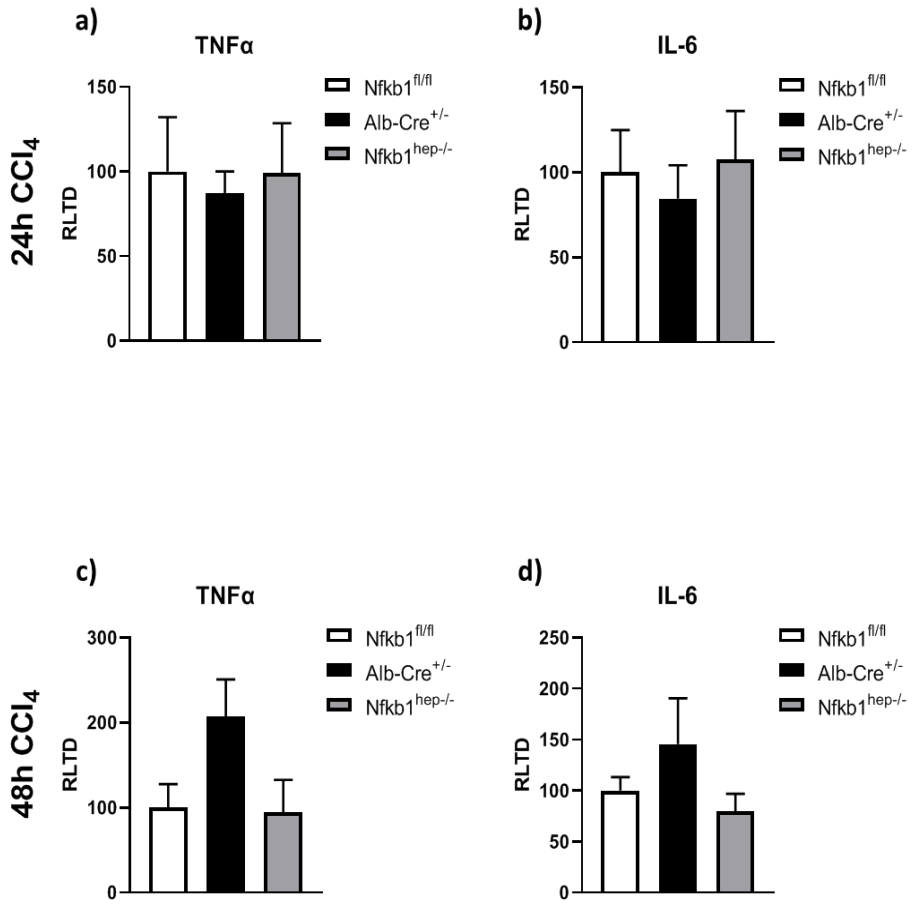

Figure 3.11 TNFα and IL-6 liver gene expression in acute CCl_4 injury. Graphs show liver mRNA expression obtained by RT-qPCR analysis 24h after CCl_4 injection of TNFα (a) and IL-6 (b), and 48h after CCl_4 injection of TNFα (c) and IL-6 (d). Data are mean ± SEM of n=6 $Nfkb1^{fl/fl}$, n=6 $Alb\text{-}Cre^{+/-}$ and n=6 $Nfkb1^{hep-/-}$ mice livers. Statistical significance was determined using a one-way ANOVA followed by a post-hoc Tukey test. P values below 0.05 were considered statistically significant, with *P<0.05, **P<0.01 and ***P<0.001.

3.3.5 Hepatocyte NF-κB1 knock-out increases macrophage recruitment to the liver

With NF-κB1 p50 known to be a regulator of innate immune responses (Wilson et al., 2015), macrophage recruitment to the liver was assessed by F4/80 immunohistochemistry, a marker for liver macrophages, in formalin-fixed paraffin-embedded tissues. A significant increase in F4/80 positive cells was observed in $Nfkb1^{hep-/-}$ mice compared to both control groups 24h post-CCl_4 injection (p=0.0062 $Nfkb1^{fl/fl}$ vs $Nfkb1^{hep-/-}$ and p=0.0045 $Alb\text{-}Cre^{+/-}$ vs $Nfkb1^{hep-/-}$), indicating a significant increase in macrophage liver infiltration in the absence of NF-κB1 p50 (Figure 3.12).

No significant difference in F4/80 positive cells was observed across the three groups at the 48h time-point.

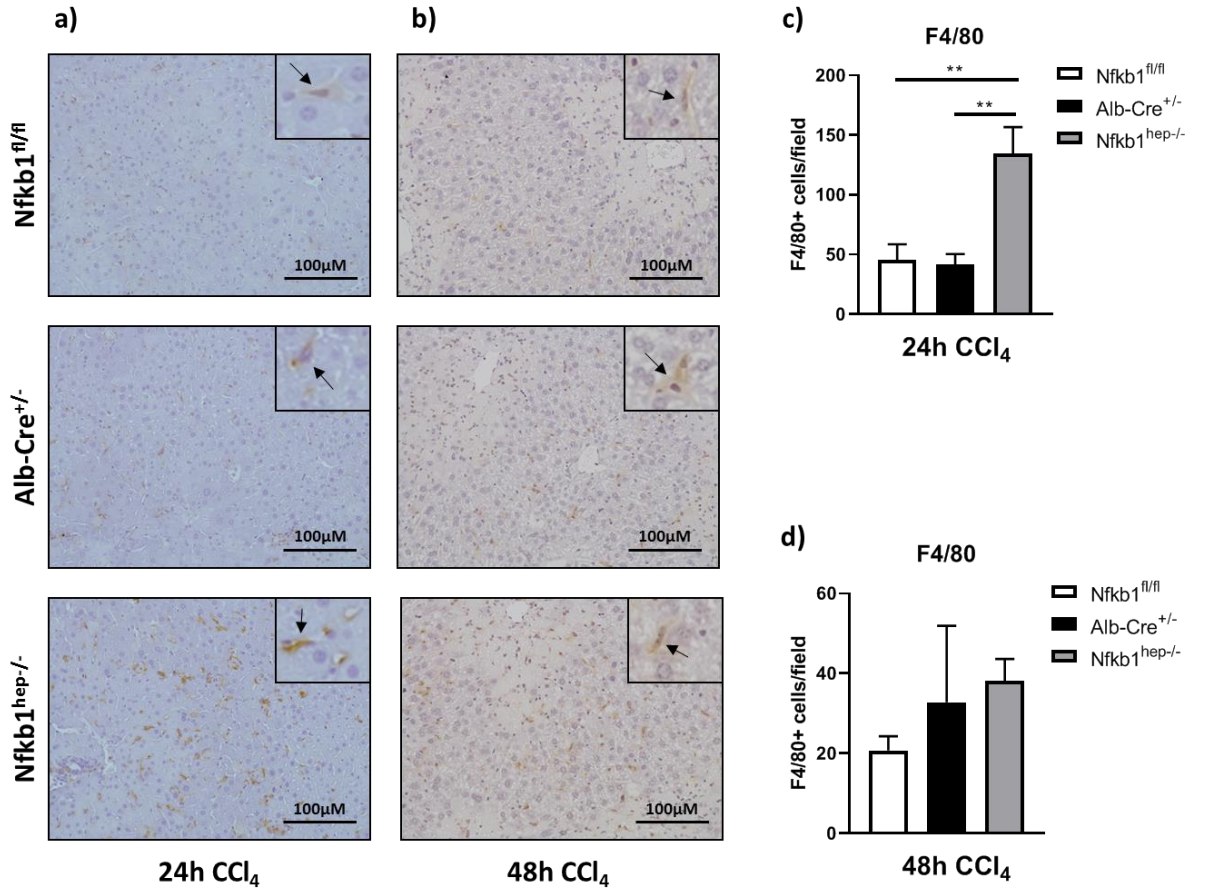

Figure 3.12 F4/80 immunostain of mice livers subjected to acute CCl_4 injury. Images show X20 F4/80 immunostaining in Nfkb1$^{fl/fl}$, Alb-Cre$^{+/-}$ and Nfkb1$^{hep-/-}$ formalin-fixed paraffin-embedded liver tissue 24h following CCl_4 injection (a), and 48h following CCl_4 injection (b). Graphs show F4/80+ cells per field at 24h (c) and at 48h (d). Data are mean ± SEM of n=6 Nfkb1$^{fl/fl}$, n=6 Alb-Cre$^{+/-}$ and n=6 Nfkb1$^{hep-/-}$ mice livers. Statistical significance was determined using a one-way ANOVA followed by a post-hoc Tukey test. P values below 0.05 were considered statistically significant, with *P<0.05, **P<0.01 and ***P<0.001.

3.3.6 Hepatocyte Nfkb1 knock-out does not affect CCL2 and CCL5 liver chemokine expression

It was subsequently hypothesized that the observed increase in macrophages in Nfkb1$^{hep-/-}$ mice livers was due to an increase in the expression of monocyte chemoattractant chemokines, thereby recruiting monocytes to the liver, which then differentiate into macrophages. CCL2 and CCL5 are both known potent monocyte chemoattractants (Bartfai et al., 2020; Keepers et al., 2007; Deshmane et al., 2009), and therefore the gene expression of these two chemokines was assessed by RT-qPCR. Surprisingly, no significant difference in CCL2 or CCL5 expression was observed between the three groups at the 24h and the 48h time-point, and CCL5 expression appeared slightly decreased in Nfkb1$^{hep-/-}$ mice compared to the control groups (Figure 3.13). This suggests other chemokines must be responsible for the observed increase in macrophage infiltration in the livers of Nfkb1$^{hep-/-}$ mice after 24h, such as CCL7, or liver-resident macrophages, kupffer cells, are being activated.

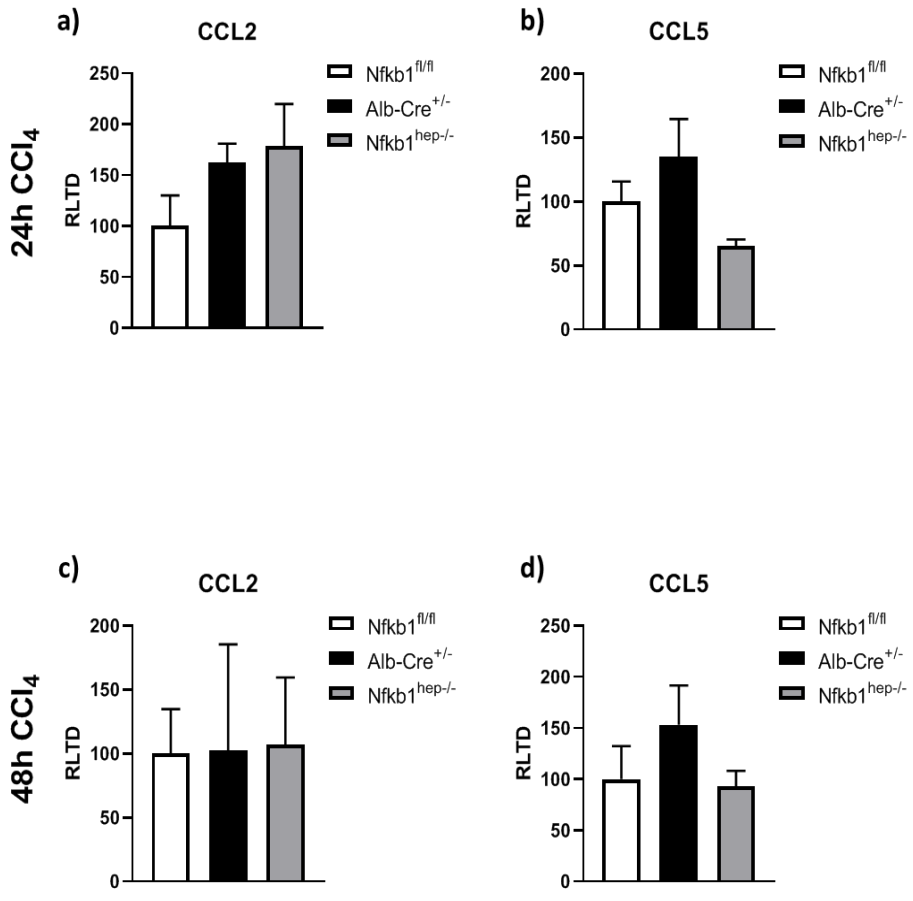

Figure 3.13 Monocyte chemoattractant chemokine gene expression in the liver following acute CCl_4 injury. Graphs show liver mRNA expression obtained by RT-qPCR analysis 24h after CCl_4 injection of CCL2 (a) and CCL5 (b), and 48h after CCl_4 injection of CCL2 (c) and CCL5 (d). Data are mean ± SEM of n=6 $Nfkb1^{fl/fl}$, n=6 $Alb\text{-}Cre^{+/-}$ and n=6 $Nfkb1^{hep-/-}$ mice livers. Statistical significance was determined using a one-way ANOVA followed by a post-hoc Tukey test. P values below 0.05 were considered statistically significant, with *P<0.05, **P<0.01 and ***P<0.001.

3.3.7 Hepatocyte Nfkb1 knock-out does not affect anti-apoptotic gene expression

Another major effect caused by acute CCl_4 hepatotoxicity is apoptosis and cell death (Keepers et al., 2007). The gene expression of apoptotic genes Gadd45β, Bcl-xL and Bcl-2 was therefore assessed by RT-qPCR in the livers of CCl_4 injured mice, to assess the role of NF-κB1 in this process. A significant decrease in Gadd45β expression was observed in $Nfkb1^{hep-/-}$ mice compared to $Alb\text{-}Cre^{+/-}$ mice (p=0.031), but not compared to $Nfkb1^{fl/fl}$ mice, 24h post-CCl_4 injection (Figure 3.14). Bcl-xL was significantly upregulated in $Alb\text{-}Cre^{+/-}$ mice compared to $Nfkb1^{fl/fl}$ (p=0.0054) and $Nfkb1^{hep-/-}$ mice (0.006) at the 48h time-point. Bcl-xL expression in $Nfkb1^{hep-/-}$ mice is therefore decreased compared to the $Alb\text{-}Cre^{+/-}$ control mice but comparable to $Nfkb1^{fl/fl}$ mice, 48h following CCl_4 injection. This suggests that lack of hepatocyte Nfkb1 p50 decreases Bcl-xL- and Gadd45β-mediated anti-apoptotic signalling, thereby increasing apoptosis, when the comparison is made with $Alb\text{-}Cre^{+/-}$ mice, however if comparison is made with $Nfkb1^{fl/fl}$ mice, it can be concluded that lack of NF-κB1 p50 does not affect Bcl-xL- and Gadd45β-mediated anti-apoptotic signalling in acute CCl_4 injury. Additionally, Gadd45β gene expression seemed to be slightly increased in $Alb\text{-}Cre^{+/-}$ mice compared to the two other groups, and Bcl-2 expression seemed to be slightly decreased compared to the other groups at the 48h time-point.

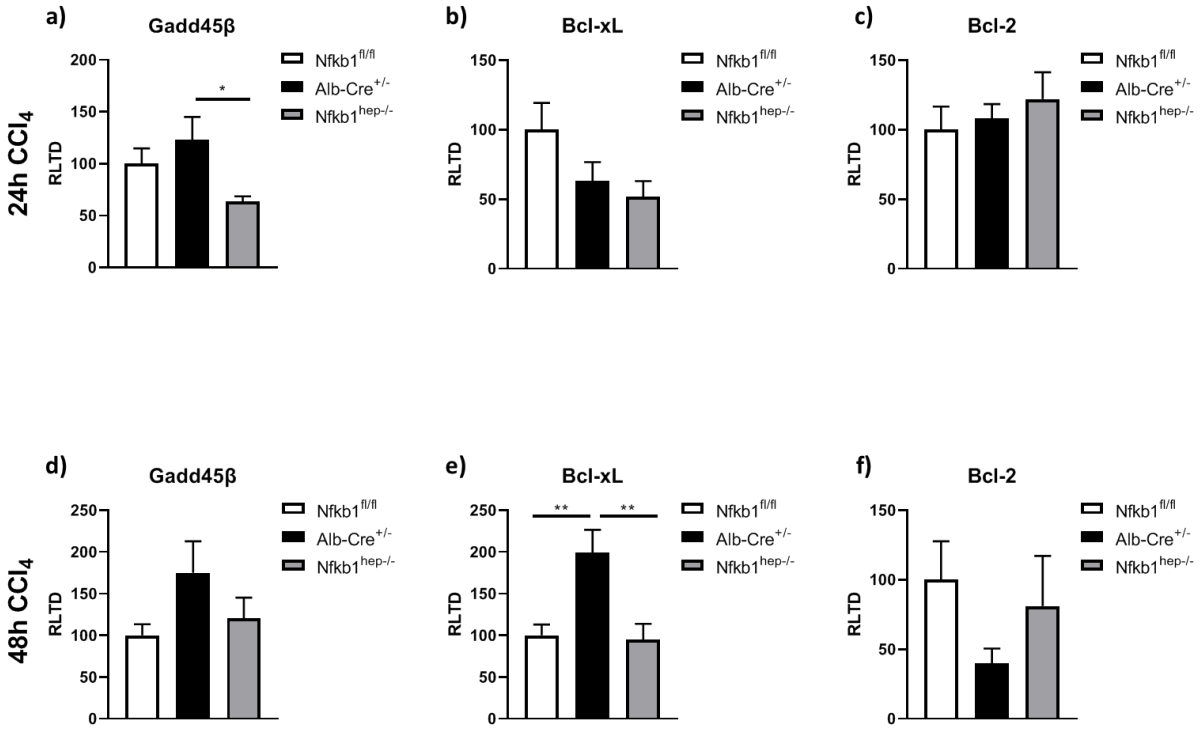

Figure 3.14 Anti-apoptotic gene expression in acute CCl_4 injury. Graphs show liver mRNA expression obtained by RT-qPCR analysis 24h after CCl_4 injection of Gadd45β (a), Bcl-xL (b), and Bcl-2 (c), and 48h after CCl_4 injection of Gadd45β (d), Bcl-xL (e), and Bcl-2 (f). Data are mean ± SEM of n=6 $Nfkb1^{fl/fl}$, n=6 $Alb\text{-}Cre^{+/-}$ and n=6 $Nfkb1^{hep-/-}$ mice livers. Statistical significance was determined using a one-way ANOVA followed by a post-hoc Tukey test. P values below 0.05 were considered statistically significant, with *P<0.05, **P<0.01 and ***P<0.001.

The expression of apoptotic signalling genes XIAP (anti-apoptotic) and BAX (pro-apoptotic) was also assessed by RT-qPCR. XIAP expression was significantly decreased in $Alb\text{-}Cre^{+/-}$ mice compared to $Nfkb1^{fl/fl}$ mice after 24h CCl_4 (p=0.021), and $Nfkb1^{hep-/-}$ mice were comparable to $Alb\text{-}Cre^{+/-}$ mice, but no significant difference in XIAP expression was observed in $Nfkb1^{hep-/-}$ mice compared to the control groups at the 24h and 48h time-point (Figure 3.15). No significant difference in BAX expression levels was observed across all three groups at either time-point.

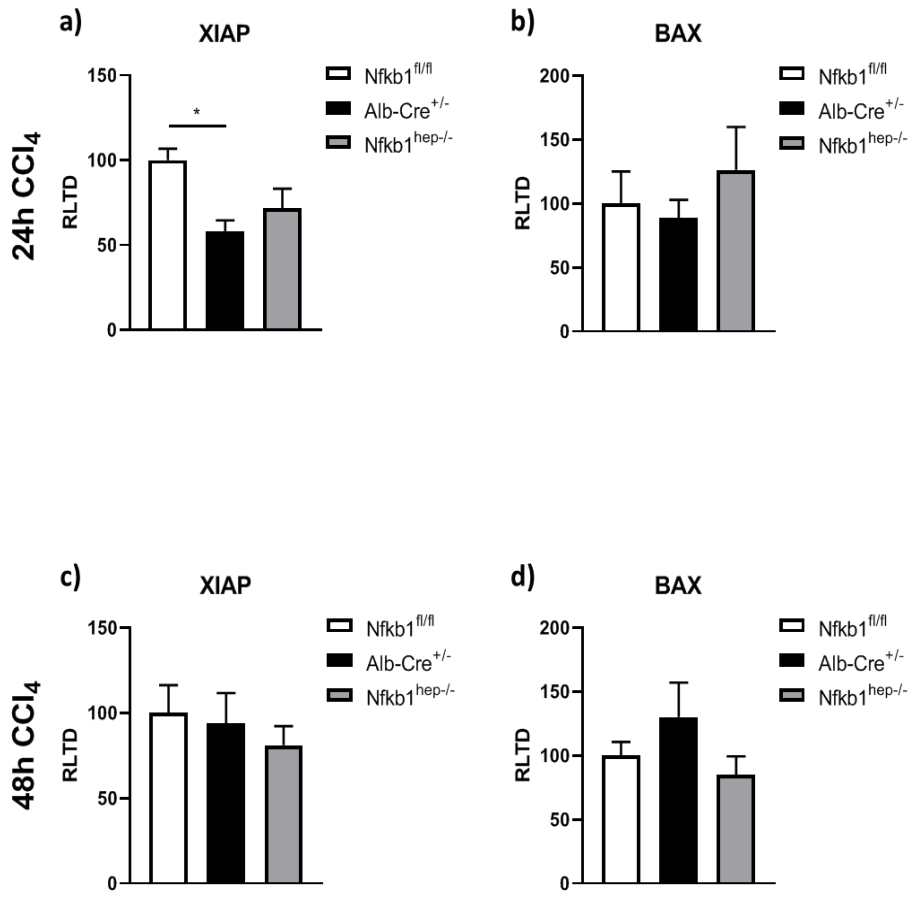

Figure 3.15 XIAP and BAX gene expression in acute CCl_4 injury. Graphs show liver mRNA expression obtained by RT-qPCR analysis 24h after CCl_4 injection of XIAP (a) and BAX (b), and 48h after CCl_4 injection of XIAP (c) and BAX (d). Data are mean ± SEM of n=6 $Nfkb1^{fl/fl}$, n=6 $Alb\text{-}Cre^{+/-}$ and n=6 $Nfkb1^{hep-/-}$ mice livers. Statistical significance was determined using a one-way ANOVA followed by a post-hoc Tukey test. P values below 0.05 were considered statistically significant, with *P<0.05, **P<0.01 and ***P<0.001.

3.3.8 Hepatocyte Nfkb1 knock-out does not affect apoptosis or cell death

While overall no major difference in apoptotic signalling gene expression was observed between $Nfkb1^{hep-/-}$ mice and both control groups, mRNA expression does not always translate to equivalent protein expression, and not all apoptotic signalling genes were covered in this study, therefore apoptosis and cell death was assessed at the phenotypic level. Cleaved caspase 3 immunohistochemistry, which shows activation of the apoptosis pathway (Crowley & Waterhouse, 2016; McIlwain et al., 2013; Porter & Jänicke, 1999), was carried out on formalin-fixed paraffin-embedded liver tissues to assess the role of NF-κB1 p50 in apoptosis, and percentage necrosis area was

quantified using H&E staining. Unsurprisingly, no significant difference in cleaved caspase 3 positive hepatocytes was observed between the three groups 24h post-CCl_4 injection (Figure 3.16). Interestingly, after 48h, cleaved caspase 3 hepatocyte staining was significantly increased compared to Alb-$Cre^{+/-}$ mice (p=0.0495), but not compared to $Nfkb1^{fl/fl}$ mice. This shows that apoptosis may be increased in $Nfkb1^{hep-/-}$ mice if comparison is made with Alb-$Cre^{+/-}$ mice, but if comparison is made with $Nfkb1^{fl/fl}$ mice then it can be concluded that lack of hepatocyte NF-κB1 p50 does not alter apoptotic signalling in acute CCl_4 liver injury.

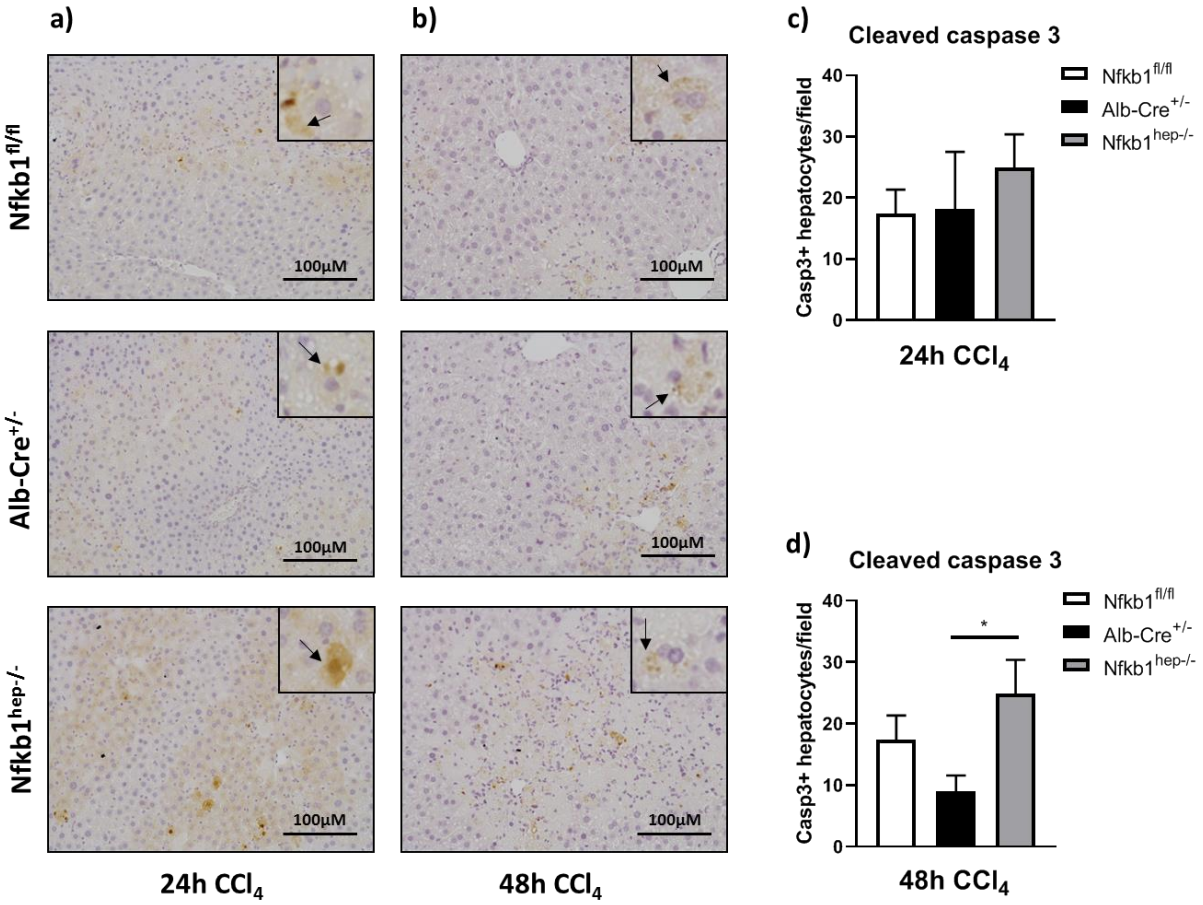

Figure 3.16 Cleaved caspase 3 immunostain of livers following acute CCl_4 injury. Images show X20 cleaved caspase 3 immunostaining in $Nfkb1^{fl/fl}$, Alb-$Cre^{+/-}$ and $Nfkb1^{hep-/-}$ formalin-fixed paraffin-embedded liver tissue 24h following CCl_4 injection (a), and 48h following CCl_4 injection (b). Graphs show cleaved caspase 3 + cells per field at 24h (c) and at 48h (d). Data are mean ± SEM of n=6 $Nfkb1^{fl/fl}$, n=6 Alb-$Cre^{+/-}$ and n=6 $Nfkb1^{hep-/-}$ mice livers. Statistical significance was determined using a one-way ANOVA followed by a post-hoc Tukey test. P values below 0.05 were considered statistically significant, with *P<0.05, **P<0.01 and ***P<0.001.

Necrosis being another form of cell death in response to liver injury, it was hypothesized that NF-κB1 p50 could play a role in this cellular process. Unlike apoptosis, which is a highly regulated process, necrosis is characterised by uncontrolled cell death (Fink & Cookson, 2005; Syntichaki & Tavernarakis, 2002). Percentage necrosis area was quantified from H&E stains of formalin-fixed paraffin-embedded liver tissues. Bands of lighter pink cells represent necrotic cells while the darker cells are normal and healthy (Elmore et al., 2016). No significant difference was observed between the three groups at either time-point, however necrosis seemed to be slightly decreased in Nfkb1$^{hep-/-}$ mice compared to both control mice after 24h, and slightly increased compared to Alb-Cre$^{+/-}$ mice after 48h (Figure 3.17).

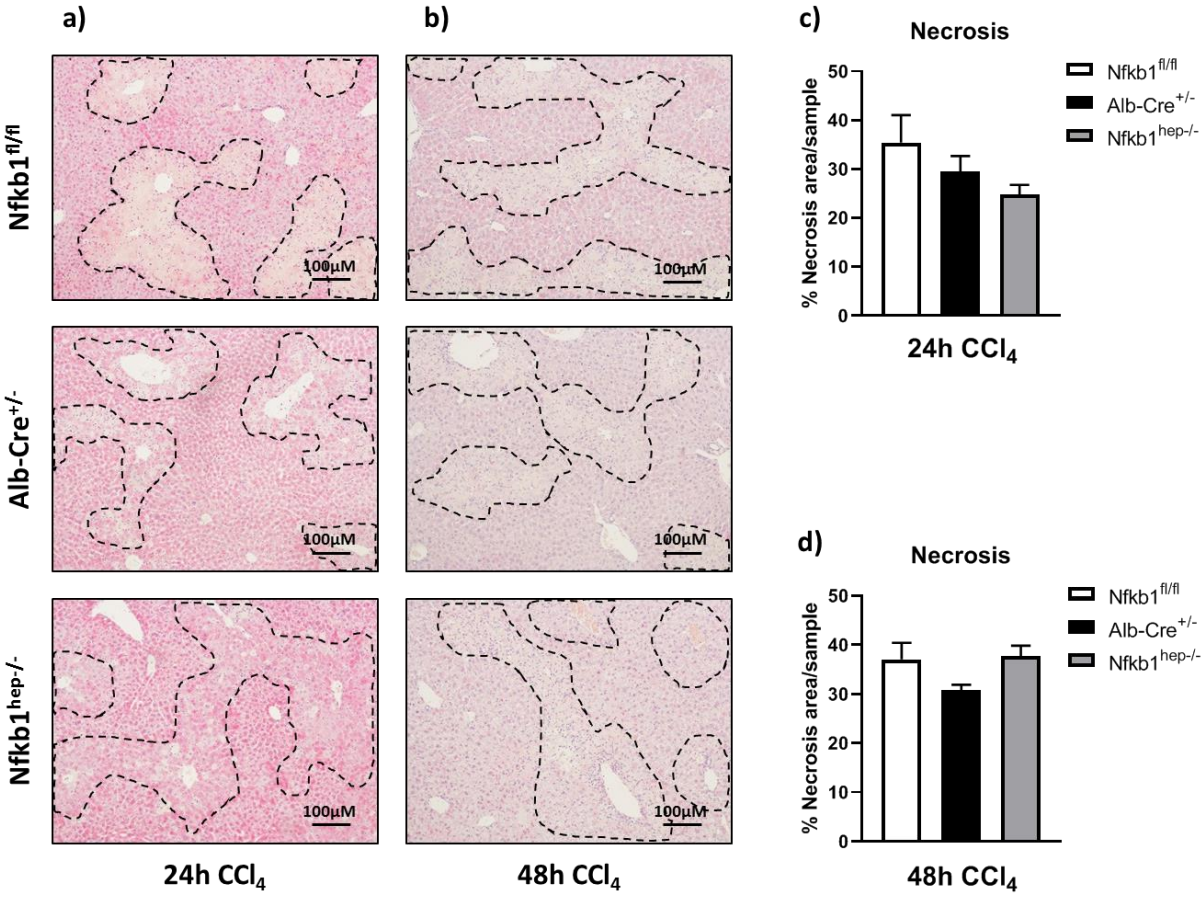

Figure 3.17 Percentage necrosis area quantified by H&E stain in acute CCl_4 liver injury. Images show H&E staining in Nfkb1$^{fl/fl}$, Alb-Cre$^{+/-}$ and Nfkb1$^{hep-/-}$ formalin-fixed paraffin-embedded liver tissue 24h following CCl_4 injection (a), and 48h following CCl_4 injection (b). Graphs show percentage necrosis area at 24h (c) and at 48h (d). Data are mean ± SEM of

n=6 $Nfkb1^{fl/fl}$, n=6 $Alb\text{-}Cre^{+/-}$ and n=6 $Nfkb1^{hep-/-}$ mice livers. Statistical significance was determined using a one-way ANOVA followed by a post-hoc Tukey test. P values below 0.05 were considered statistically significant, with *P<0.05, **P<0.01 and ***P<0.001.

3.4 The role of hepatocyte NF-κB1 in acute CCl_4 liver injury in an adeno-associated viral Nfkb1 knock-out model

While the albumin-cre recombinase system represents a useful tool to study the effects of hepatocyte-specific Nfkb1 knockout, cholangiocytes can also express albumin (Tanimizu et al., n.d.), therefore these cells may also lack Nfkb1 in this model. The AAV-TBG-Cre system, whereby transfection with the AAV-TBG-Cre virus leads to the Cre recombinase knock-out of Nfkb1, driven by the TBG promoter, is completely hepatocyte specific (TBG is not expressed in cholangiocytes, whereas albumin can be). This therefore allows for a more specific study of the role NF-κB1 plays in hepatocytes (Yan et al., 2012a; Carrillo-Carrasco et al., 2010; Yan et al., 2012b).

Initially, AAV-TBG-Cre virus was injected intravenously (IV) in $Nfkb1^{fl/fl}$ mice, and mice were harvested at different time-points to establish the optimum time to knock out hepatocyte Nfkb1 and carry out CCl_4 injury following virus injection. After establishing the time required to effectively knock-out Nfkb1 in hepatocytes, a similar acute CCl_4 injury study as the previous one mentioned was conducted, with liver harvest after 24h and 48h following CCl_4 IP injection. AAV-TBG-Null virus was injected in $Nfkb1^{fl/fl}$ mice as control.

The aim of this study was to assess the role of hepatocyte NF-κB1 in acute liver injury resolution, with a focus on inflammation and cell death. The results from this study can also be compared to those from the previous acute CCl_4 study, in order to validate the previously observed results and consolidate conclusions on the role hepatocyte p50 plays.

3.4.1 Validation of AAV-TBG-Cre Nfkb1 hepatocyte-specific knockout

$Nfkb1^{fl/fl}$ mice were injected IV with AAV-TBG-Cre virus, and livers and spleens were harvested at 3, 6, 10, 13 and 16 days to assess p50 expression. Additionally, hepatocyte isolation, along with non-parenchymal cell, bone marrow cell, kidney and spleen isolation, was carried out two weeks and 1 month post-AAV-TBG-Cre injection.

Western blot analysis showed a gradual decrease in p50 expression from 3 days to 16 days post-injection (Figure 3.18). Hepatocytes isolated from AAV-TBG-Cre injected mice showed no expression of p50 after 2 weeks and after 1 month, while WT hepatocytes as well as non-parenchymal cells, bone marrow cells, kidney and spleen showed abundant p50 expression at these time-points, demonstrating the AAV-TBG-Cre hepatocyte-specific knockout of p50. Full hepatocyte knock-out of p50 was therefore observed two weeks from virus injection, thus CCl_4 was injected two weeks after AAV-TBG-Cre injection for this study.

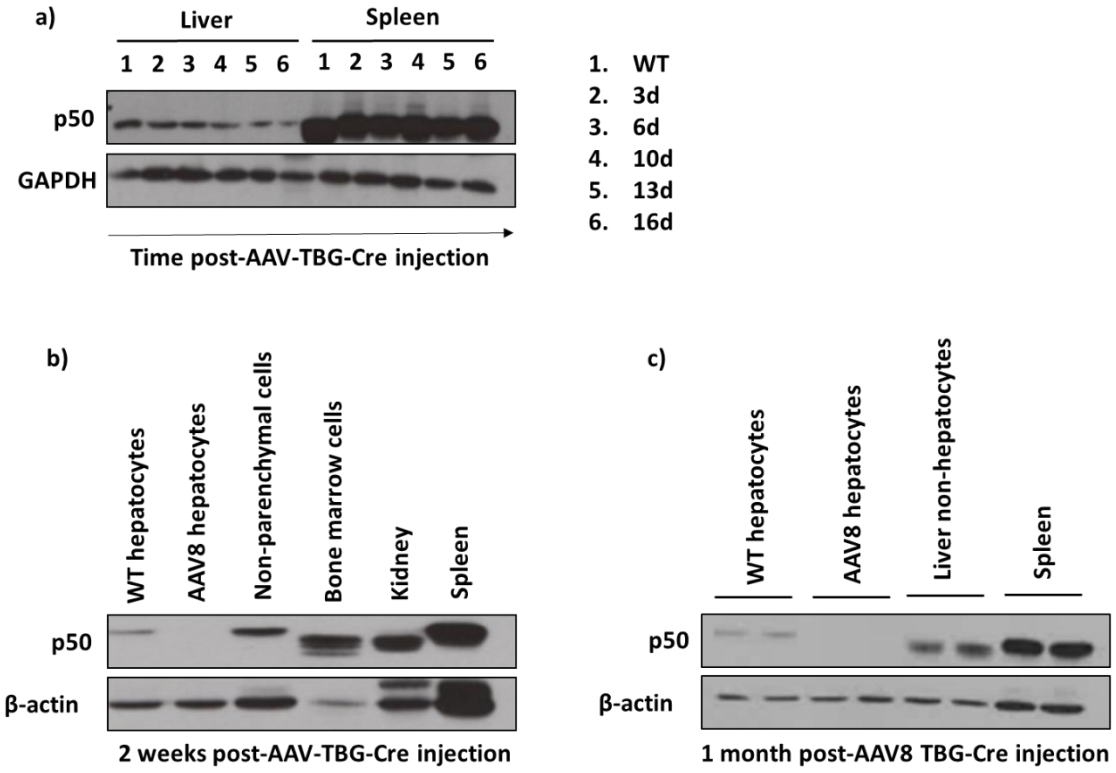

Figure 3.18 Western blot analysis of p50 expression following AAV-TBG-Cre injection. a) Western blot showing p50 expression in the liver and spleen in WT mice and AAV-TBG-Cre-IV injected Nfkb1$^{fl/fl}$ mice between 3 and 16 days post-AAV-TBG-Cre injection. b) Western blot showing p50 expression in WT hepatocytes, hepatocytes isolated from AAV-TBG-Cre-injected mice, non-parenchymal liver cells, bone marrow cells, kidney and spleen 2 weeks post-AAV-TBG-Cre injection in Nfkb1$^{fl/fl}$ mice. c) Western blot showing p50 expression in WT hepatocytes, hepatocytes isolated from AAV-TBG-Cre-injected mice, non-parenchymal liver cells and spleen 1 month post-AAV-TBG-Cre injection in Nfkb1$^{fl/fl}$ mice.

Western blot analysis was performed on livers from CCl_4-injured mice to assess p50 expression. AAV-TBG-Null-injected mice display notably higher p50 expression compared to AAV-TBG-Cre-injected mice at both the 24h and 48h time-point, indicating successful hepatocyte Nfkb1 p50 knockout. The observed p50 expression in AAV-TBG-Cre-injected mice livers can be attributed to non-parenchymal liver cells, including immune cells.

Figure 3.19 Western blot analysis of p50 expression in acute CCl_4 injury. Western blots show liver p50 expression in $Nfkb1^{fl/fl}$ mice injected with AAV-TBG-Null or AAV-TBG-Cre virus 24h post-CCl_4 injection (a), and 48 post-CCl_4 injection (b).

3.4.2 Hepatocyte Nfkb1 knock-out limits serum AST, but not ALT, liver damage enzyme levels 24h post-CCl_4 injection

Liver damage was assessed by measuring the serum levels of ALT and AST. ALT levels appeared slightly reduced in AAV-TBG-Cre mice 24h post-CCl_4 injection, though this did not reach significance. However, AST levels were significantly reduced in AAV-TBG-Cre mice at this time-point ($p=0.0322$). No difference was observed in ALT or AST at the 48h time-point. This suggests the initial damage caused by CCl_4 may be lower in AAV-TBG-Cre mice compared to control mice, though by 48h there is no difference in liver damage.

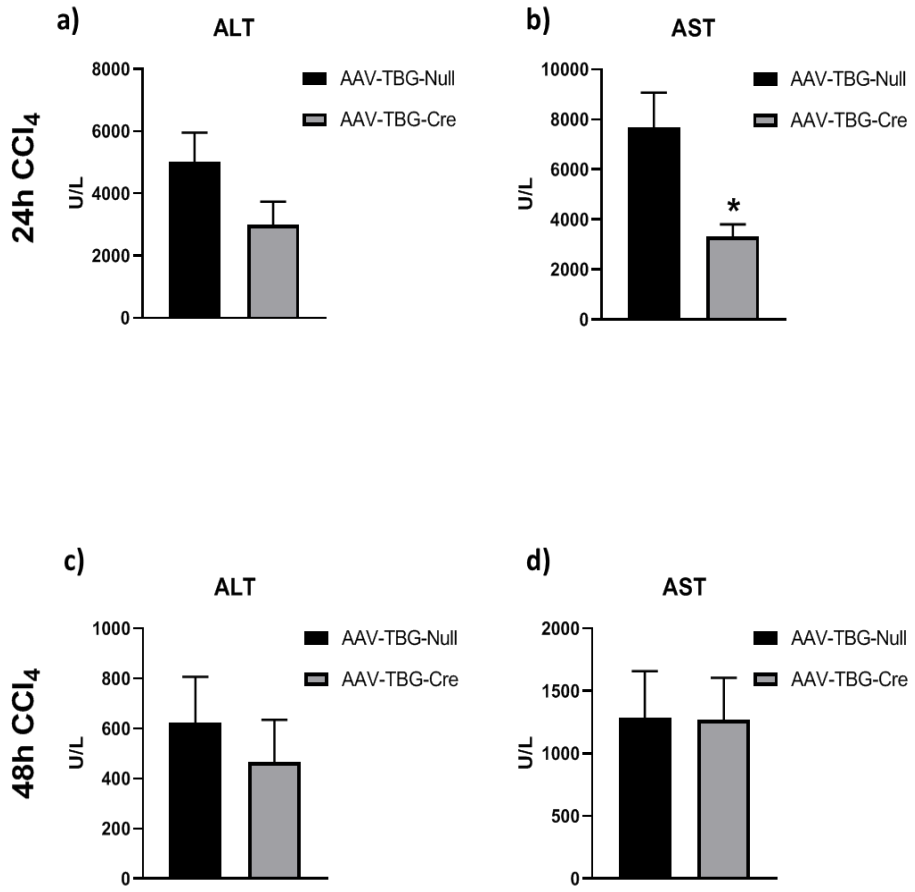

Figure 3.20 Serum ALT and AST levels following acute CCl_4 injury. Graphs show serum levels of ALT 24h post-CCl_4 injection (a), AST 24h post-CCl_4 injection (b), ALT 48h post-CCl_4 injection (c), and AST 48h post-CCl_4 injection. Data are mean ± SEM of n=6 AAV-TBG-Null and n=6 AAV-TBG-Cre mice livers. Statistical significance was determined using a Student's two-tailed t-test. P values below 0.05 were considered statistically significant, with *P<0.05, **P<0.01 and ***P<0.001.

3.4.3 Hepatocyte knock-out does not alter neutrophil recruitment to the liver

Similarly to the previous acute CCl_4 study, neutrophil recruitment to the liver was assessed by Ly6G immunohistochemistry in formalin-fixed paraffin-embedded liver tissues. As previously observed, there was no significant difference in neutrophil recruitment to the liver between AAV-TBG-Cre and AAV-TBG-Null mice, though there appeared to be a slight increase in Ly6G+ staining in AAV-TBG-Cre mice (p=0.1109 at 24h and p=0.0616 at 48h) (Figure 3.21).

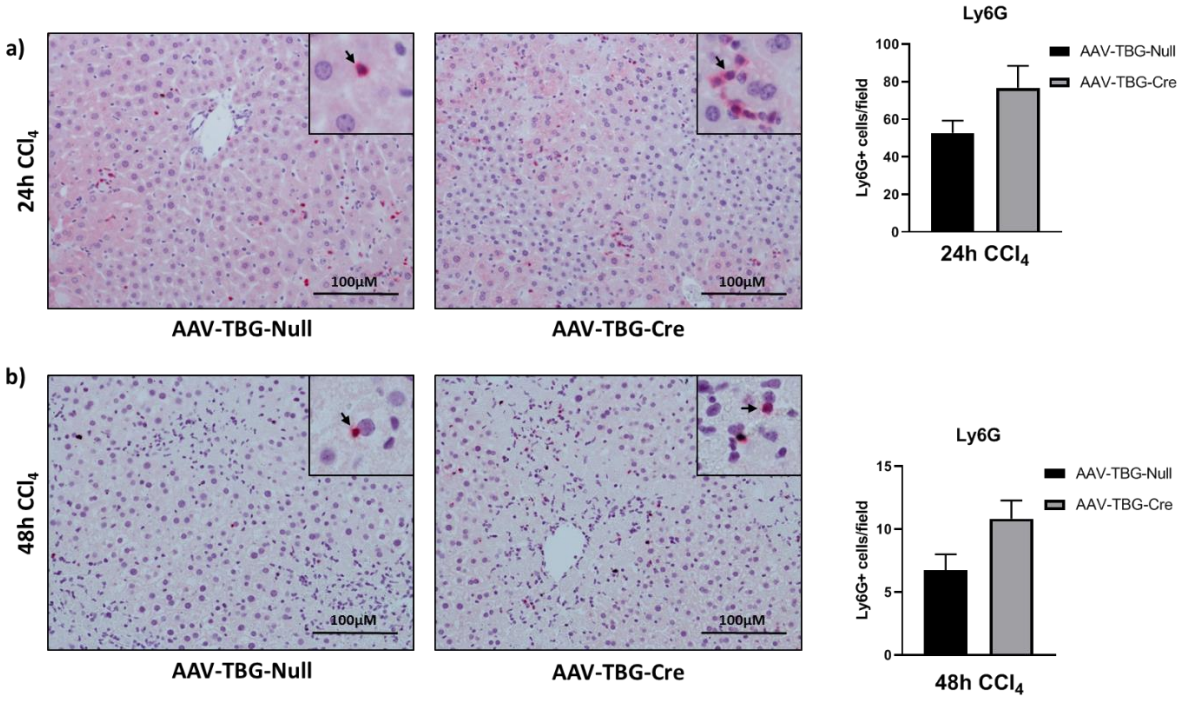

Figure 3.21 Liver Ly6G immunostain in acute CCl_4 injury. Images show X20 Ly6G immunostaining in AAV-TBG-Null and AAV-TBG-Cre formalin-fixed paraffin-embedded liver tissue 24h following CCl_4 injection (a), and 48h following CCl_4 injection (b). Graphs show Ly6G+ cells per field at 24h (a) and at 48h (b). Data are mean ± SEM of n=6 AAV-TBG-Null and n=6 AAV-TBG-Cre mice livers. Statistical significance was determined using a Student's two-tailed t-test. P values below 0.05 were considered statistically significant, with *P<0.05, **P<0.01 and ***P<0.001.

3.4.4 Hepatocyte Nfkb1 knock-out does not affect the neutrophil chemokine expression network

The mRNA expression of neutrophil chemoattractant chemokines S100A9, CXCL1 and CXCL2 was assessed by RT-qPCR. No significant difference was observed between AAV-TBG-Cre and AAV-TBG-Null mice after 24h and after 48h following CCl_4 injection (Figure 3.22). Neutrophil chemokine expression was however evidently increased in AAV-TBG-Cre and AAV-TBG-Null mice compared to WT uninjured mice, indicating that CCl_4 injury is inducing an increase in the expression of these chemokines. The low n number of WT uninjured mice (3) may explain why this difference did not reach significance.

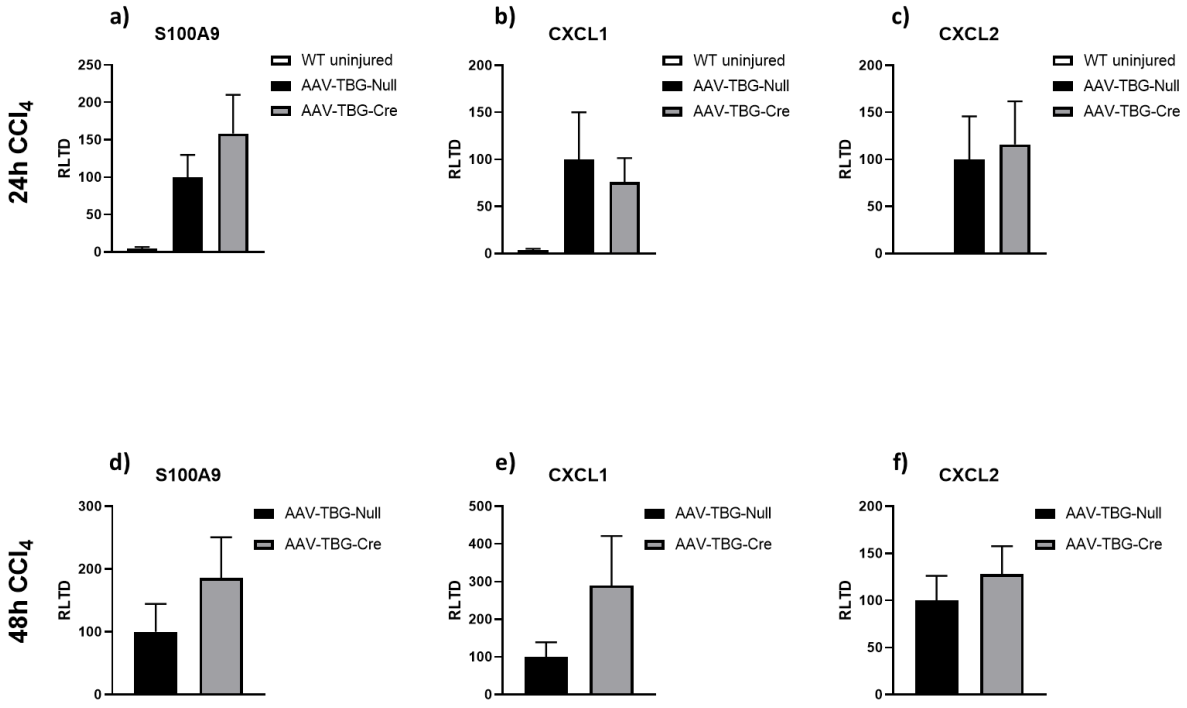

Figure 3.22 Neutrophil chemokine liver mRNA expression in acute CCl_4 injury. Graphs show liver mRNA expression obtained by RT-qPCR analysis 24h after CCl_4 injection of S100A9 (a), CXCL1 (b), and CXCL2 (c), and 48h after CCl_4 injection of S100A9 (d), CXCL1 (e), and CXCL2 (f). Data are mean ± SEM of n=6 AAV-TBG-Null and n=6 AAV-TBG-Cre mice livers. Statistical significance was determined using a one-way ANOVA followed by a post-hoc Tukey test (a,b,c) or a Student's two-tailed t-test (d,e,f). P values below 0.05 were considered statistically significant, with *P<0.05, **P<0.01 and ***P<0.001.

To further assess whether Nfkb1 knockout has an effect on inflammation caused by acute CCl_4 liver injury, the gene expression of the chemokines IL-6 and TNFα was measured by RT-qPCR. No significant difference was observed between AAV-TBG-Cre and AAV-TBG-Null mice at the 24h and 48h time-points, and a notable increase was observed in these mice compared to WT uninjured mice 24h following CCl_4 injection, indicating that IL-6 and TNFα expression is upregulated in response to acute CCl_4 liver injury (Figure 3.23).

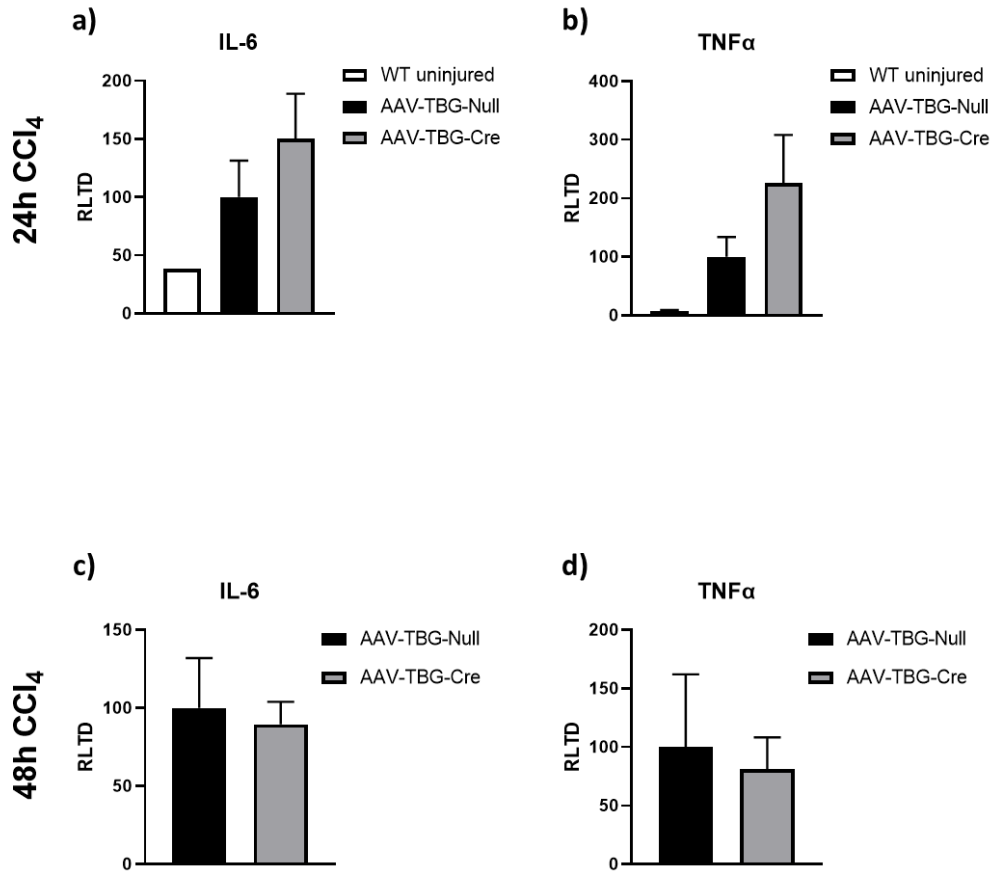

Figure 3.23 IL-6 and TNFα chemokine expression in the liver in acute CCl_4 injury. Graphs show liver mRNA expression obtained by RT-qPCR analysis 24h after CCl_4 injection of TNFα (a) and IL-6 (b), and 48h after CCl_4 injection of TNFα (c) and IL-6 (d). Data are mean ± SEM of n=6 AAV-TBG-Null and n=6 AAV-TBG-Cre mice livers. Statistical significance was determined using either a one-way ANOVA followed by a post-hoc Tukey test (a,b), or a Student's two-tailed t-test. P values below 0.05 were considered statistically significant, with *P<0.05, **P<0.01 and ***P<0.001.

3.4.5 Hepatocyte Nfkb1 knock-out increases macrophage recruitment to the liver after 48h, but not 24h, CCl_4 liver injury

To further examine the role of hepatocyte NF-κB1 in acute CCl_4 liver injury, F4/80 immunohistochemistry was carried out on formalin-fixed paraffin-embedded liver tissues to compare macrophage recruitment to the liver. No significant difference in F4/80+ cells was observed at 24h, however the number of F4/80+ cells was significantly increased in AAV-TBG-Cre mice at 48h (p=0.0181) (Figure 3.24). This shows that in the presence of hepatocyte NF-κB1 p50, macrophage recruitment to the

liver is limited, likely due to the repression of monocyte chemoattractant chemokines by p50 homodimers; however when hepatocytes lack NF-κB1 p50, this repression is abrogated, leading to an increase in the expression of monocyte chemoattractant chemokines, resulting in an increase in macrophages.

Interestingly, the previous acute CCl_4 study showed a significant increase in F4/80+ staining in $Nfkb1^{hep-/-}$ mice compared to control mice at 24h, but not at 48h, whereas here the difference is observed at the 48h later time-point. The AAV virus may be affecting immune responses by delaying them, or earlier hepatocyte Nfkb1 knock out in $Nfkb1^{hep-/-}$ mice may alter compensatory mechanisms affecting immune responses, but both studies should be repeated to better understand the underlying mechanism for this.

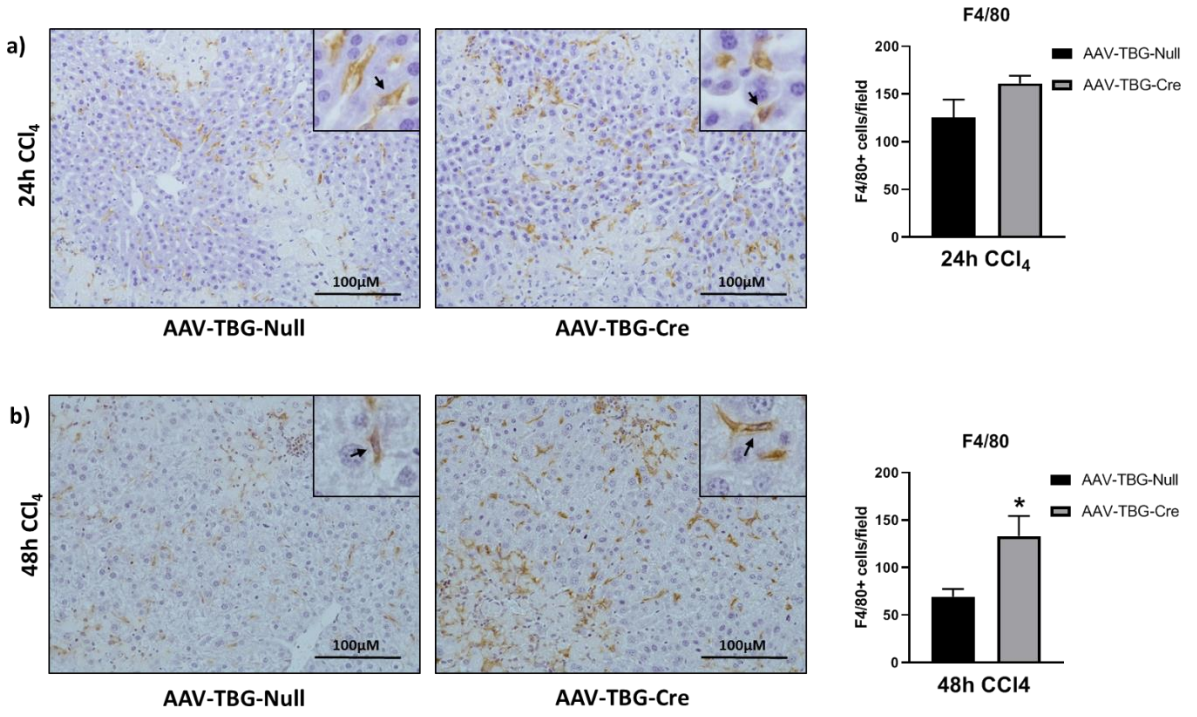

Figure 3.24 F4/80 liver immunostain in acute CCl_4 injury. Images show X20 F4/80 immunostaining in AAV-TBG-Null and AAV-TBG-Cre formalin-fixed paraffin-embedded liver tissue 24h following CCl_4 injection (a), and 48h following CCl_4 injection (b). Graphs show F4/80+ cells per field at 24h (a) and at 48h (b). Data are mean ± SEM of n=6 AAV-TBG-Null and n=6 AAV-TBG-Cre mice livers. Statistical significance was determined using a Student's two-tailed t-test. P values below 0.05 were considered statistically significant, with *P<0.05, **P<0.01 and ***P<0.001.

3.4.6 Hepatocyte Nfkb1 knock-out does not affect CCL2 and CCL5 liver chemokine expression

To further investigate the increase in macrophage recruitment, the liver gene expression of monocyte chemoattractant chemokines CCL2 and CCL5 was assessed by RT-qPCR. No significant difference was observed between AAV-TBG-Cre and AAV-TBG-Null mice at 24h or 48h, although CCL2 appeared increased in AAV-TBG-Cre mice compared to control mice at the 48h time-point (0=0.0522) (Figure 3.25). However, no similar observation was made on CCL2 expression at this time-point in the previous acute CCl_4 study. CCL2 expression was significantly increased in AAV-TBG-Null (p=0.0005) and AAV-TBG-Cre mice (p=0.004) compared to WT uninjured mice at the 24h timepoint. Overall this shows that other monocyte chemoattractant chemokines must be responsible for the observed increase in macrophages when Nfkb1 p50 is knocked out in hepatocytes. Assessment of the expression of further monocyte chemoattractant chemokines is necessary to elucidate this. However, it is important to remember that protein expression trends don't always follow gene expression trends, therefore CCL2 and/or CCL5 may be increased at the protein level in the absence of NF-κB1 p50, despite no apparent significant difference in gene expression.

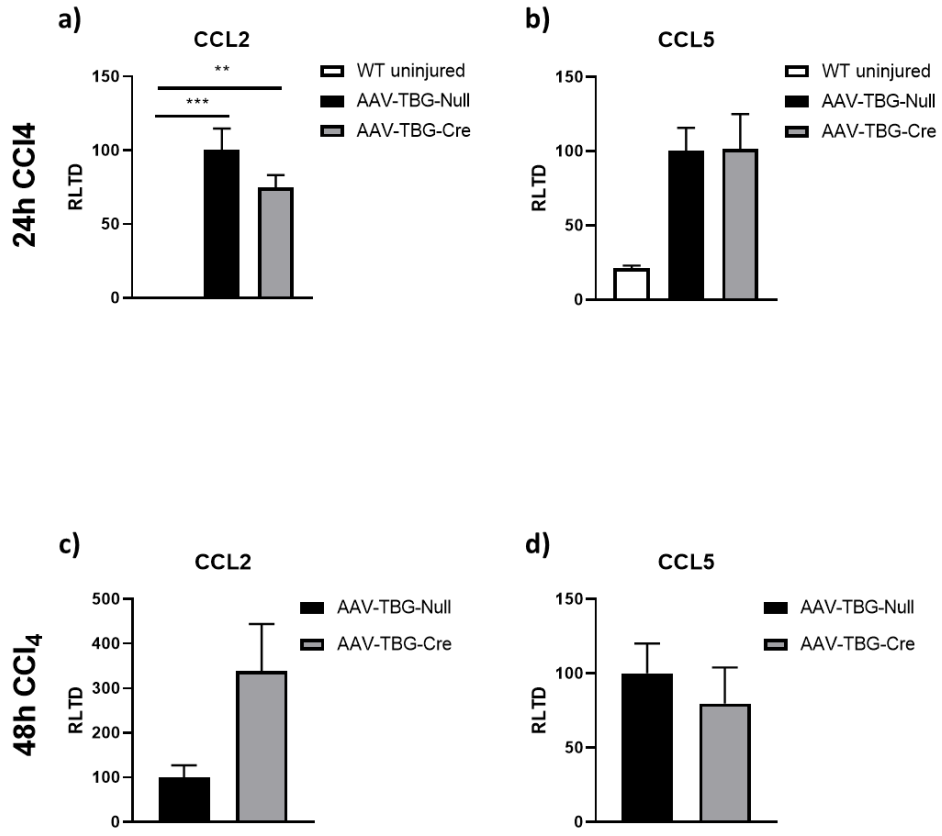

Figure 3.25 Gene expression of monocyte chemoattractant chemokines in the liver in acute CCl_4 injury. Graphs show liver mRNA expression obtained by RT-qPCR analysis 24h after CCl_4 injection of CCL2 (a) and CCL5 (b), and 48h after CCl_4 injection of CCL2 (c) and CCL5 (d). Data are mean ± SEM of n=6 AAV-TBG-Null and n=6 AAV-TBG-Cre mice livers. Statistical significance was determined using either a one-way ANOVA followed by a post-hoc Tukey test (a,b), or a Student's two-tailed t-test. P values below 0.05 were considered statistically significant, with *P<0.05, **P<0.01 and ***P<0.001.

3.4.7 Hepatocyte Nfkb1 knock-out does not affect anti-apoptotic gene expression

Similarly to the previous acute CCl_4 study, the role of NF-κB1 p50 in apoptosis was assessed. The mRNA expression of anti-apoptotic genes Gadd45β, Bcl-xL and Bcl-2 was determined by RT-qPCR. No significant difference was observed between AAV-TBG-Cre and AAV-TBG-Null mice (Figure 3.26). Gadd45β (p=0.013) and Bcl-2 (p=0.0058) gene expression was significantly increased in AAV-TBG-Cre mice compared to WT uninjured mice after 24h, and Bcl-xL was significantly increased in

AAV-TBG-Null mice compared to WT uninjured mice after 24h (p=0.0074). This shows that acute CCl_4 injury leads to the upregulation of anti-apoptotic genes Gadd45β, Bcl-xL and Bcl-2.

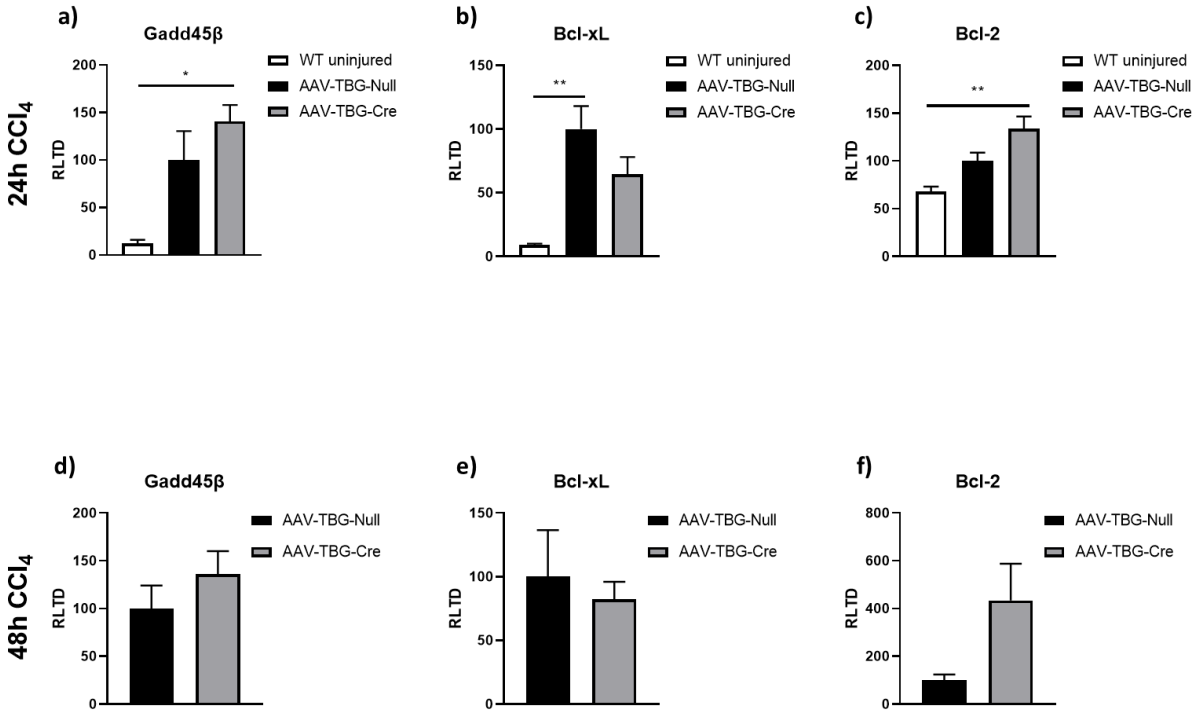

Figure 3.26 Anti-apoptotic gene expression in the liver in acute CCl_4 injury. Graphs show liver mRNA expression obtained by RT-qPCR analysis 24h after CCl_4 injection of Gadd45β (a), Bcl-xL (b), and Bcl-2 (c), and 48h after CCl_4 injection of Gadd45β (d), Bcl-xL (e), and Bcl-2 (f). Data are mean ± SEM of n=6 AAV-TBG-Null and n=6 AAV-TBG-Cre mice livers. Statistical significance was determined using a one-way ANOVA followed by a post-hoc Tukey test (a,b,c) or a Student's two-tailed t-test (d,e,f). P values below 0.05 were considered statistically significant, with *P<0.05, **P<0.01 and ***P<0.001.

Additionally, the gene expression of BAX (pro-apoptotic) and XIAP (anti-apoptotic) was determined. No significant difference was found between AAV-TBG-Cre and AAV-TBG-Null mice after 24h and 48h (Figure 3.27). BAX was significantly increased in AAV-TBG-Cre (p=0.0046) and AAV-TBG-Null mice (p=0.0182) compared to WT uninjured mice after 24h, indicating that the expression of this gene is upregulated in response to acute CCl_4 injury. However, the expression of XIAP remained unchanged

between WT uninjured mice and virus-injected mice, indicating that XIAP is unaffected by acute CCl_4 injury.

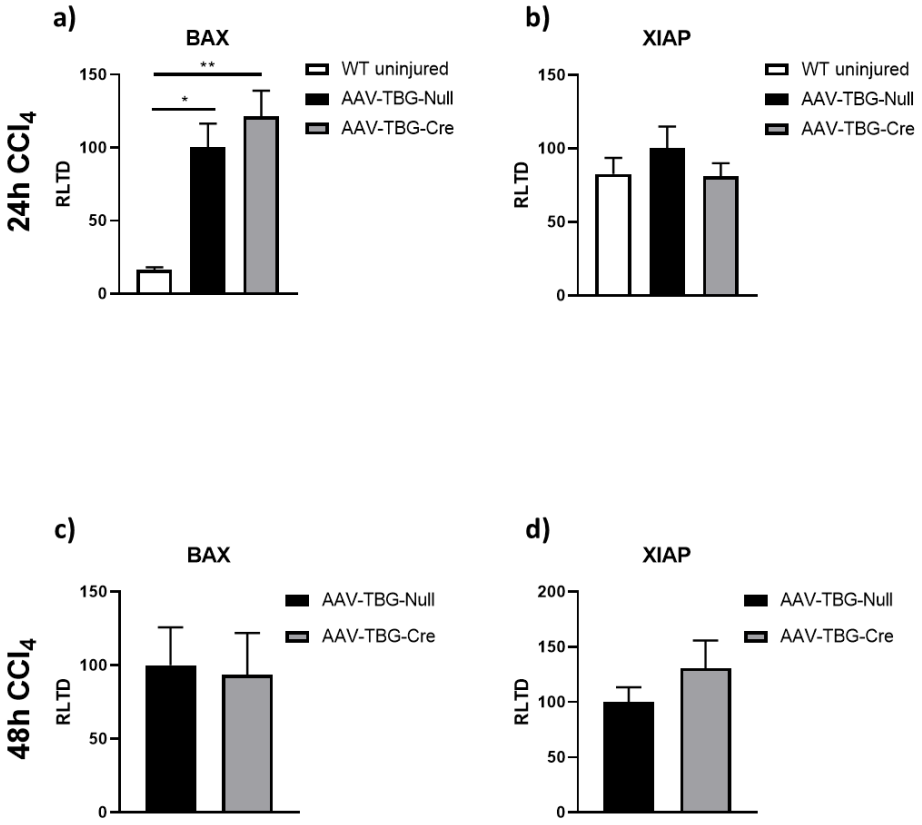

Figure 3.27 Gene expression of BAX and XIAP in acute CCl_4 liver injury. Graphs show liver mRNA expression obtained by RT-qPCR analysis 24h after CCl_4 injection of BAX (a) and XIAP (b), and 48h after CCl_4 injection of BAX (c) and XIAP (d). Data are mean ± SEM of n=6 AAV-TBG-Null and n=6 AAV-TBG-Cre mice livers. Statistical significance was determined using either a one-way ANOVA followed by a post-hoc Tukey test (a,b), or a Student's two-tailed t-test. P values below 0.05 were considered statistically significant, with *P<0.05, **P<0.01 and ***P<0.001.

3.4.8 Hepatocyte Nfkb1 knock-out does not affect apoptosis or cell death

To further investigate whether NF-κB1 p50 plays a role in apoptotic signalling in response to acute CCl_4 injury, cleaved caspase 3 immunohistochemistry was carried out on formalin-fixed paraffin-embedded liver tissues. However, no significant difference in casp3+ hepatocytes was observed between AAV-TBG-Cre and AAV-

TBG-Null mice. This is comparable to what was observed in the previous acute CCl_4 study.

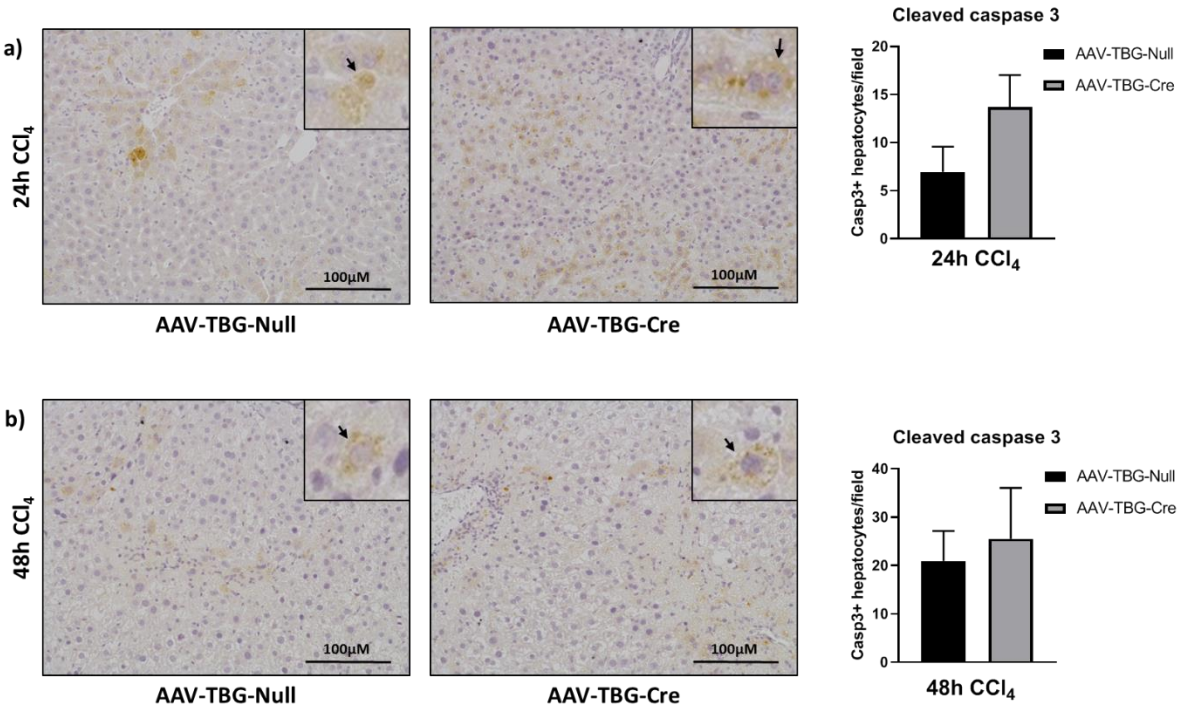

Figure 3.28 Cleaved caspase 3 liver immunostain in acute CCl_4 injury. Images show X20 Cleaved caspase 3 immunostaining in AAV-TBG-Null and AAV-TBG-Cre formalin-fixed paraffin-embedded liver tissue 24h following CCl_4 injection (a), and 48h following CCl_4 injection (b). Graphs show cleaved caspase 3 + cells per field at 24h (a) and at 48h (b). Data are mean ± SEM of n=6 AAV-TBG-Null and n=6 AAV-TBG-Cre mice livers. Statistical significance was determined using a Student's two-tailed t-test. P values below 0.05 were considered statistically significant, with *P<0.05, **P<0.01 and ***P<0.001.

Percentage necrosis area was also determined using H&E stained formalin-fixed paraffin-embedded liver tissue. No significant difference was observed between AAV-TBG-Cre and AAV-TBG-Null mice (Figure 3.29). These results suggest that hepatocyte NF-κB1 p50 is not fundamentally implicated in cell death modulation, including apoptosis and necrosis, in the context of acute CCl_4 liver injury.

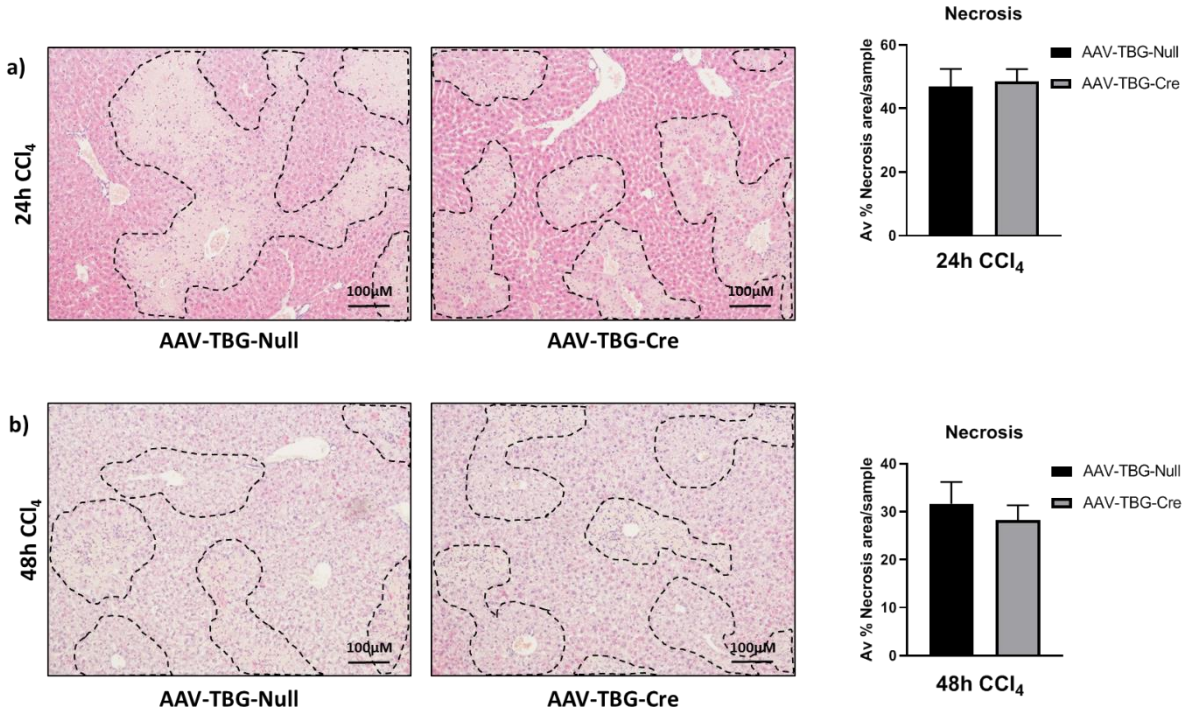

Figure 3.29 Percentage necrosis area quantification from H&E stained liver tissue in acute CCl_4 injury. Images show X10 H&E staining in AAV-TBG-Null and AAV-TBG-Cre formalin-fixed paraffin-embedded liver tissue 24h following CCl_4 injection (a), and 48h following CCl_4 injection (b). Graphs show average percentage necrosis area at 24h (a) and at 48h (b). Data are mean ± SEM of n=6 AAV-TBG-Null and n=6 AAV-TBG-Cre mice livers. Statistical significance was determined using a Student's two-tailed t-test. P values below 0.05 were considered statistically significant, with *P<0.05, **P<0.01 and ***P<0.001.

3.5 The role of NF-κB1 in acute DEN liver injury

DEN (diethylnitrosamine) is a well-established carcinogen known to cause hepatotoxicity, notably though the generation of reactive metabolites (Tolba, Kraus, Liedtke, Schwarz, & Weiskirchen, 2015). To explore the role of NF-κB1 p50 in the pathogenic alterations underlying the formation of liver cancer, an acute DEN experiment was carried out, whereby mice were injected IP with one single dose of DEN, and their livers harvested 24h and 48h post-injection. 6 $Nfkb1^{fl/fl}$ and 6 $Nfkb1^{hep-/-}$ mice used per time-point for this study. Due to $Nfkb1^{fl/fl}$ and Alb-$Cre^{+/-}$ mice showing results that were not comparable in the acute CCl_4 study, $Nfkb1^{fl/fl}$ was chosen as control for subsequent experiments. $Nfkb1^{fl/fl}$ mice and $Nfkb1^{hep-/-}$ being litter mates and

with an N background (Alb-Cre$^{+/-}$ mice had a J background, which means they differed in their genetic background).

3.5.1 Validation of Nfkb1 hepatocyte-specific knockout

Western blot analysis was performed on liver tissue protein lysate to ensure correct knock-out of Nfkb1 p50 in Nfkb1$^{hep-/-}$ mice. Results show abundant p50 expression in Nfkb1$^{fl/fl}$ mice while Nfkb1$^{hep-/-}$ mice display significantly lower p50 liver expression, confirming correct Cre recombination and Nfkb1 p50 knock-out.

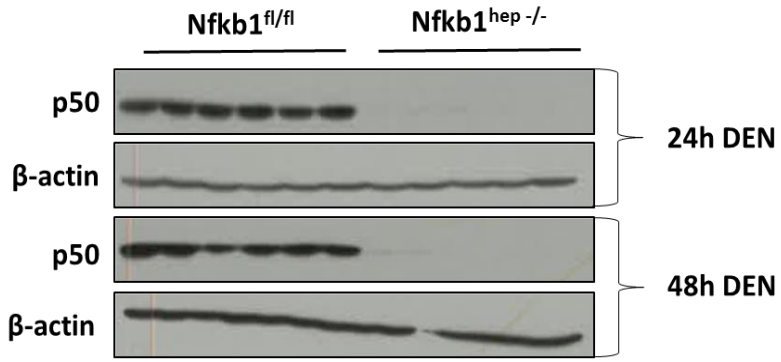

Figure 3.30 Western blot analysis of p50 expression in Nfkb1$^{fl/fl}$ and Nfkb1$^{hep-/-}$ mice. Western blots show p50 expression in Nfkb1$^{fl/fl}$ and Nfkb1$^{hep-/-}$ mice livers 24h and 48h following DEN injection. β-actin expression was used as loading control.

3.5.2 Hepatocyte Nfkb1 knock-out limits serum AST, but not ALT, liver damage enzyme levels 48h post-DEN injection

Liver damage was assessed by measuring serum ALT and AST levels. AST was significantly reduced in Nfkb1$^{hep-/-}$ mice compared to Nfkb1$^{fl/fl}$ control mice 48h following acute DEN injury ($p=0.0392$) (Figure 3.31). No significant difference in ALT levels was found at this time-point, and no significant difference in ALT or AST levels was observed 24h after DEN injury. This implies that the damage experienced by Nfkb1$^{hep-/-}$ livers is inferior to the damage experienced by Nfkb1$^{fl/fl}$ livers after 48h. In acute CCl_4 liver injury, lower AST levels were observed 24h post-injury, but not 48h post-injury, indicating that the damage incurred by acute DEN is delayed compared to that incurred by acute CCl_4 injury.

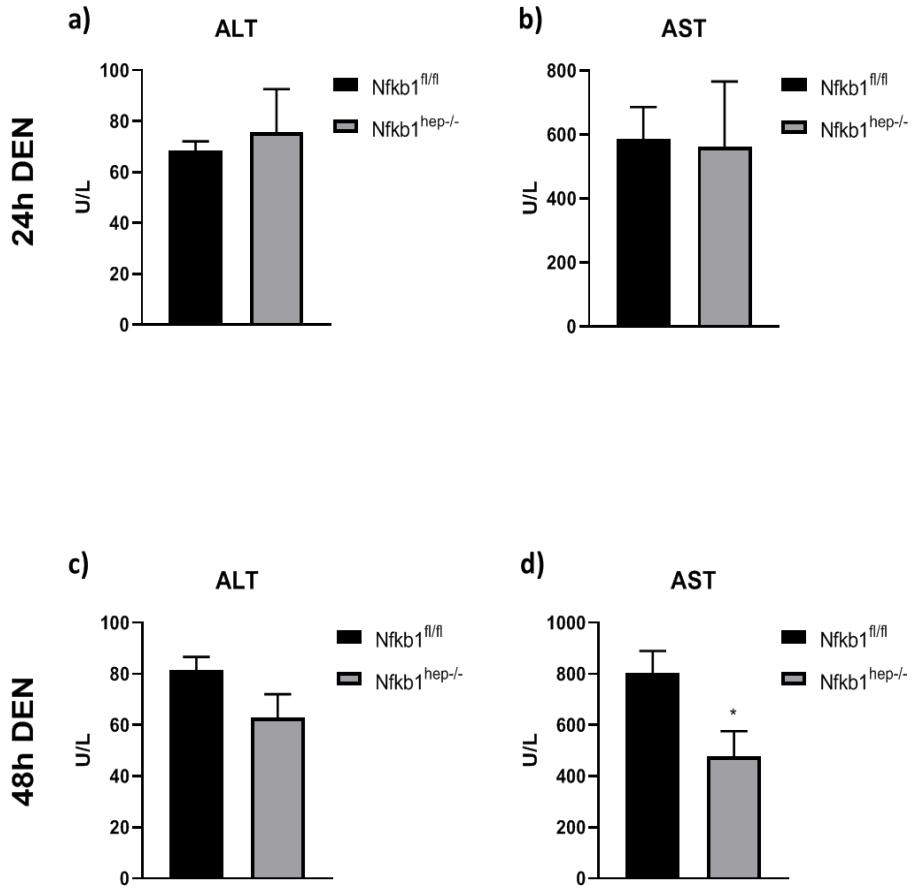

Figure 3.31 Serum ALT and AST levels in acute DEN liver injury. Graphs show serum levels of ALT 24h post-DEN injection (a), AST 24h post-DEN injection (b), ALT 48h post-DEN injection (c), and AST 48h post-DEN injection. Data are mean ± SEM of n=6 Nfkb1$^{fl/fl}$ and n=6 Nfkb1$^{hep-/-}$ mice livers. Statistical significance was determined using a Student's two-tailed t-test. P values below 0.05 were considered statistically significant, with *P<0.05, **P<0.01 and ***P<0.001.

3.5.3. Hepatocyte Nfkb1 in acute DEN-induced Inflammation

In response to hepatotoxin exposure and subsequent liver injury, the triggered inflammatory process is fundamental to the resolution of the liver injury. Immune cell infiltration in the liver was assessed by H&E stain of formalin-fixed paraffin-embedded liver tissue. No visible difference in immune cell infiltration, particularly around the blood vessels, was observed between Nfkb1$^{fl/fl}$ and Nfkb1$^{hep-/-}$ mice after 24h and after 48h following DEN injection. Additionally TNFα gene expression was assessed by RT-qPCR. No significant difference in the expression of this inflammatory chemokine was found between Nfkb1$^{fl/fl}$ and Nfkb1$^{hep-/-}$ mice. These results suggest that lack of NF-κB1

p50 does not affect the inflammatory process and immune cell recruitment following acute DEN liver injury.

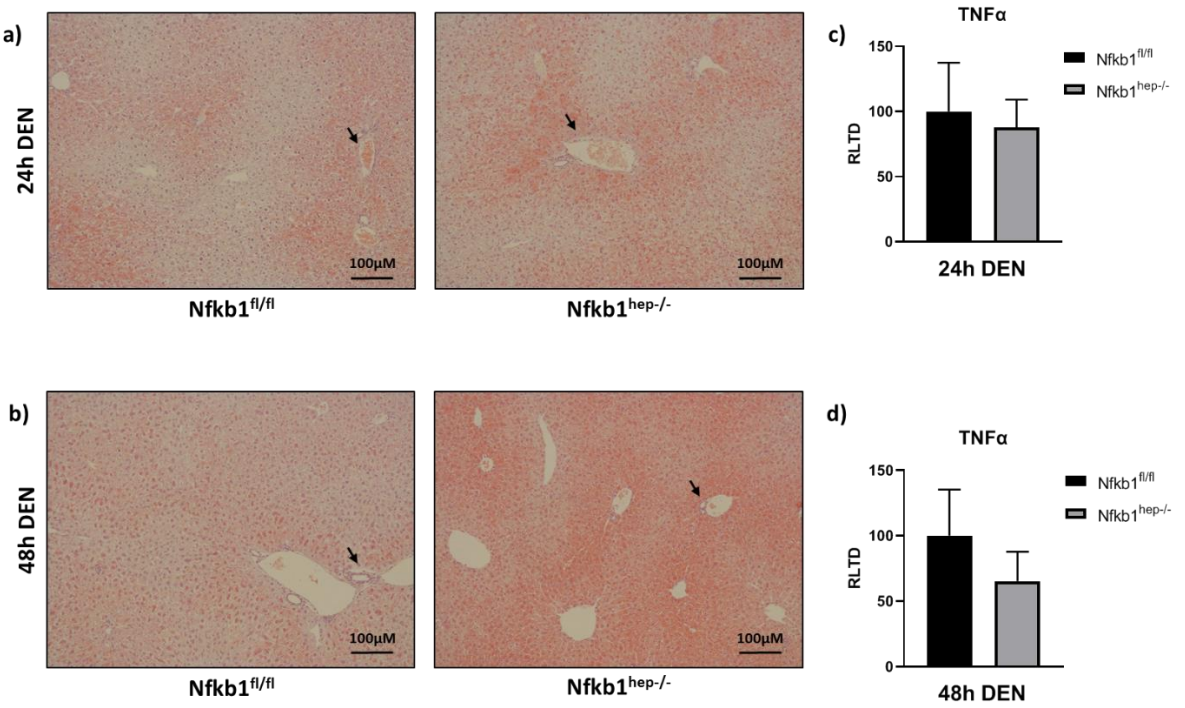

Figure 3.32 Immune cell infiltration assessed by H&E stain and TNFα gene expression in response to acute DEN liver injury. Images show X10 H&E staining and immune cell infiltration in Nfkb1$^{fl/fl}$ and Nfkb1$^{hep-/-}$ formalin-fixed paraffin-embedded liver tissue 24h following DEN injection (a), and 48h following DEN injection (b). Graphs show mRNA expression of TNFα after 24h (c) and after 48h (d). Data are mean ± SEM of n=6 Nfkb1$^{fl/fl}$ and n=6 Nfkb1$^{hep-/-}$ mice livers. Statistical significance was determined using a Student's two-tailed t-test. P values below 0.05 were considered statistically significant, with *P<0.05, **P<0.01 and ***P<0.001.

3.5.4 Hepatocyte Nfkb1 knock-out does not alter neutrophil recruitment in acute DEN liver injury

DEN is known to cause an increase in neutrophil liver infiltration as part of the inflammatory response (Tolba, Kraus, Liedtke, Schwarz, & Weiskirchen, 2015). Neutrophil recruitment to the liver was therefore assessed by NIMP immunohistochemistry on formalin-fixed paraffin-embedded liver tissue (NIMP stain was carried out as part of Sam Murray's undergraduate project under my supervision).

NIMP predominantly stains for neutrophils, but can also stain monocytes. It is specific for Ly-6G and Ly-6C which are components of the myeloid differentiation antigen Gr-1 (Wang et al., 2012). No significant difference in NIMP+ staining was observed between Nfkb1$^{fl/fl}$ and Nfkb1$^{hep-/-}$ mice 24h and 48h post-DEN injection (Figure 3.33). This suggests hepatocyte NF-κB1 p50 is not implicated in the recruitment of neutrophils to the liver in response to acute DEN injury.

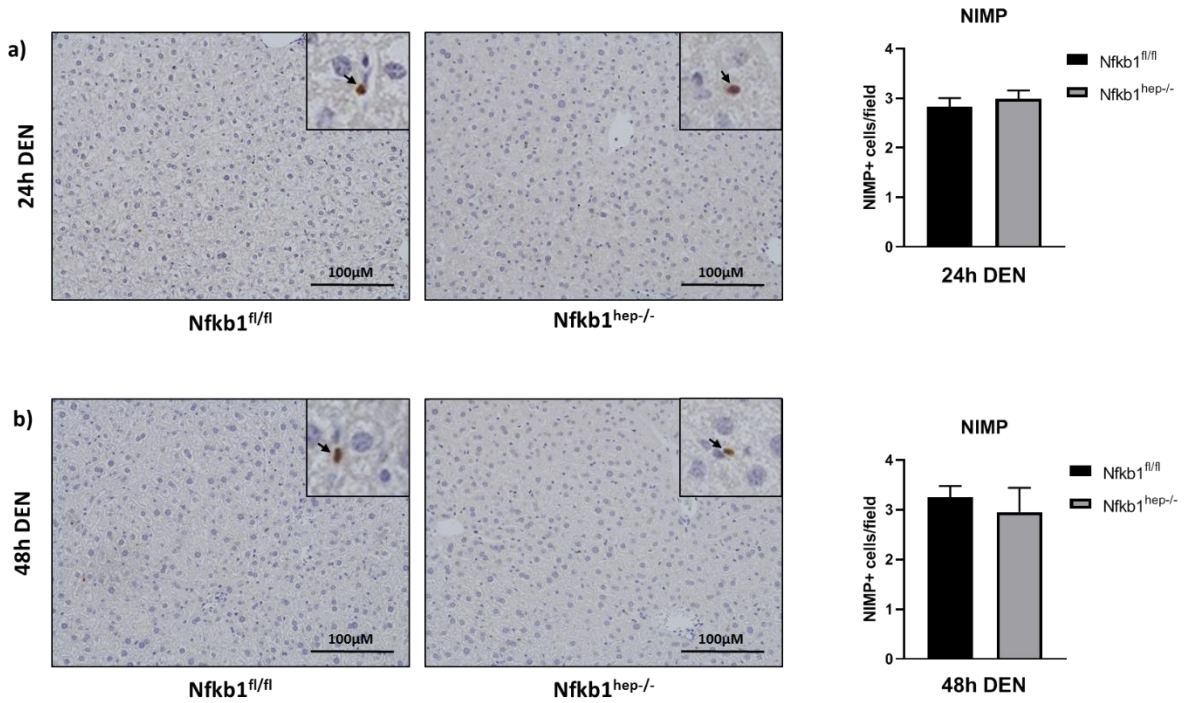

Figure 3.33 NIMP immunostain of the liver in acute DEN injury. Images show X20 NIMP immunostaining in Nfkb1$^{fl/fl}$ and Nfkb1$^{hep-/-}$ formalin-fixed paraffin-embedded liver tissue 24h following DEN injection (a), and 48h following DEN injection (b). Graphs show NIMP+ cells per field at 24h (c) and at 48h (d). Data are mean ± SEM of n=6 Nfkb1$^{fl/fl}$ and n=6 Nfkb1$^{hep-/-}$ mice livers. Statistical significance was determined using a Student's two-tailed t-test. P values below 0.05 were considered statistically significant, with *P<0.05, **P<0.01 and ***P<0.001.

3.5.5 Hepatocyte Nfkb1 knock-out does not alter neutrophil chemokine expression in acute DEN liver injury

Additionally, gene expression of neutrophil chemoattractant chemokines CXCL1, CXCL2 and S100A9 was determined by RT-qPCR. No significant difference between Nfkb1$^{fl/fl}$ and Nfkb1$^{hep-/-}$ mice was observed in either chemokine expression at either

time-point (Figure 3.34). This confirms that hepatocyte NF-κB1 p50 is not involved in neutrophil recruitment in response to acute liver injury.

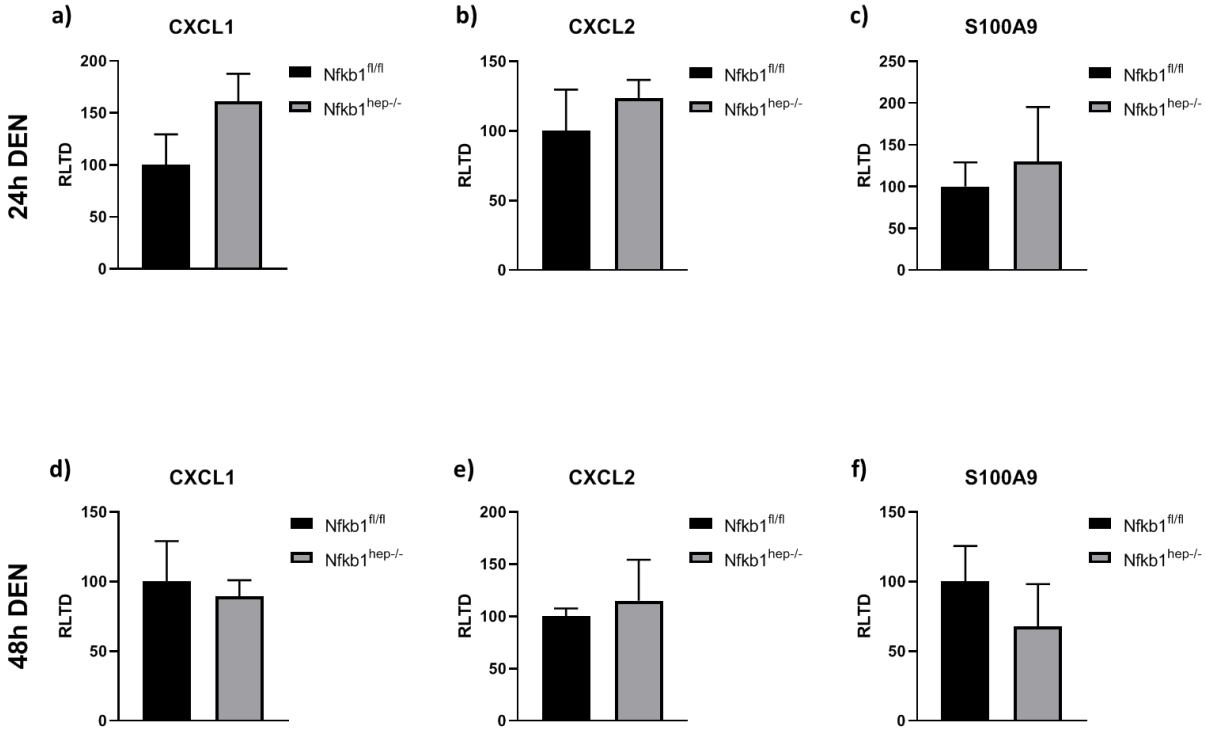

Figure 3.34 Gene expression of neutrophil chemoattractant chemokines in acute DEN liver injury. Graphs show liver mRNA expression obtained by RT-qPCR analysis 24h after DEN injection of S100A9 (a), CXCL1 (b), and CXCL2 (c), and 48h after DEN injection of S100A9 (d), CXCL1 (e), and CXCL2 (f). Data are mean ± SEM of n=6 $Nfkb1^{fl/fl}$ and n=6 $Nfkb1^{hep-/-}$ mice livers. Statistical significance was determined using a Student's two-tailed t-test. P values below 0.05 were considered statistically significant, with *P<0.05, **P<0.01 and ***P<0.001.

3.5.6 Hepatocyte Nfkb1 knock-out does not alter monocyte/macrophage recruitment in acute DEN liver injury

To further assess the involvement of hepatocyte NF-κB1 p50 in the inflammatory response in acute DEN liver injury, monocyte/macrophage recruitment to the liver and the presence of resident kupffer cells were assessed by CD68 immunohistochemistry in formalin-fixed paraffin-embedded tissues (CD68 stain was carried out as part of Sam Murray's undergraduate project under my supervision). Interestingly no difference in CD68+ staining was observed between $Nkb1^{fl/fl}$ and $Nfkb1^{hep-/-}$ mice after 24h and after

48h, indicating that hepatocyte Nfkb1 p50 is not implicated in monocyte and macrophage recruitment to the liver in response to acute DEN injury (Figure 3.35). This differs from the findings in the acute CCl_4 liver injury model, where macrophage numbers were significantly increased in $Nfkb1^{hep-/-}$ mice. It is important to note that CD68 stains for both monocytes and macrophages, whereas F4/80 (used in the acute CCl_4 model), only stains macrophages, which may explain the difference observed between the two models. There may be more macrophages in $Nfkb1^{hep-/-}$ mice, but not more monocytes, or more monocytes may be differentiating into macrophages in $Nfkb1^{hep-/-}$ mice, or the macrophages may have different characteristics to those from $Nfkb1^{fl/fl}$ mice.

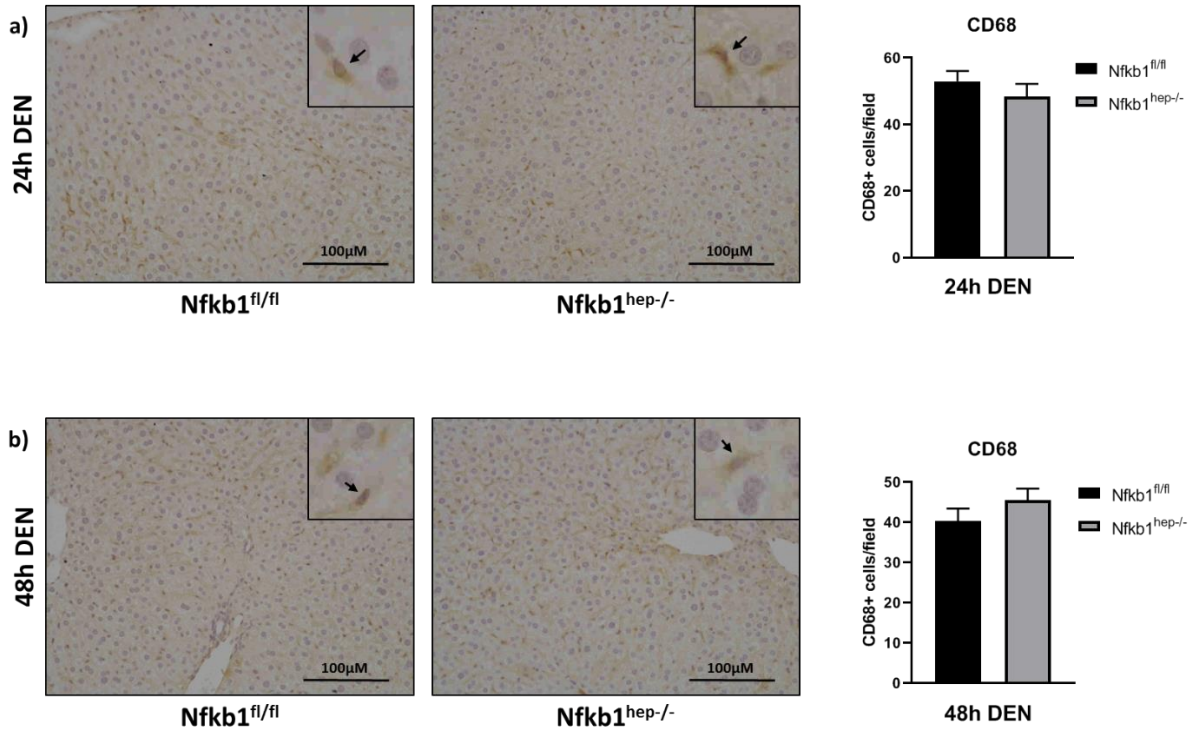

Figure 3.35 CD68 immunostain of the liver in acute DEN injury. Images show X20 CD68 immunostaining in $Nfkb1^{fl/fl}$ and $Nfkb1^{hep-/-}$ formalin-fixed paraffin-embedded liver tissue 24h following DEN injection (a), and 48h following DEN injection (b). Graphs show CD68+ cells per field at 24h (c) and at 48h (d). Data are mean ± SEM of n=6 $Nfkb1^{fl/fl}$ and n=6 $Nfkb1^{hep-/-}$ mice livers. Statistical significance was determined using a Student's two-tailed t-test. P values below 0.05 were considered statistically significant, with *P<0.05, **P<0.01 and ***P<0.001.

3.5.7 Hepatocyte Nfkb1 knock-out does not alter expression of chemokines involved in monocyte recruitment in acute DEN liver injury

To further assess monocyte recruitment to the liver in response to acute DEN injury, the gene expression of monocyte chemoattractant chemokines CCL2 and CCL5 was determined by RT-qPCR. No significant difference in CCL2 or CCL5 expression was found between Nfkb1$^{fl/fl}$ and Nfkb1$^{hep-/-}$ mice 24h and 48h post-DEN injection (Figure 3.36). This suggests that lack of hepatocyte NF-κB1 p50 does not affect monocyte recruitment to the liver in response to acute DEN liver injury.

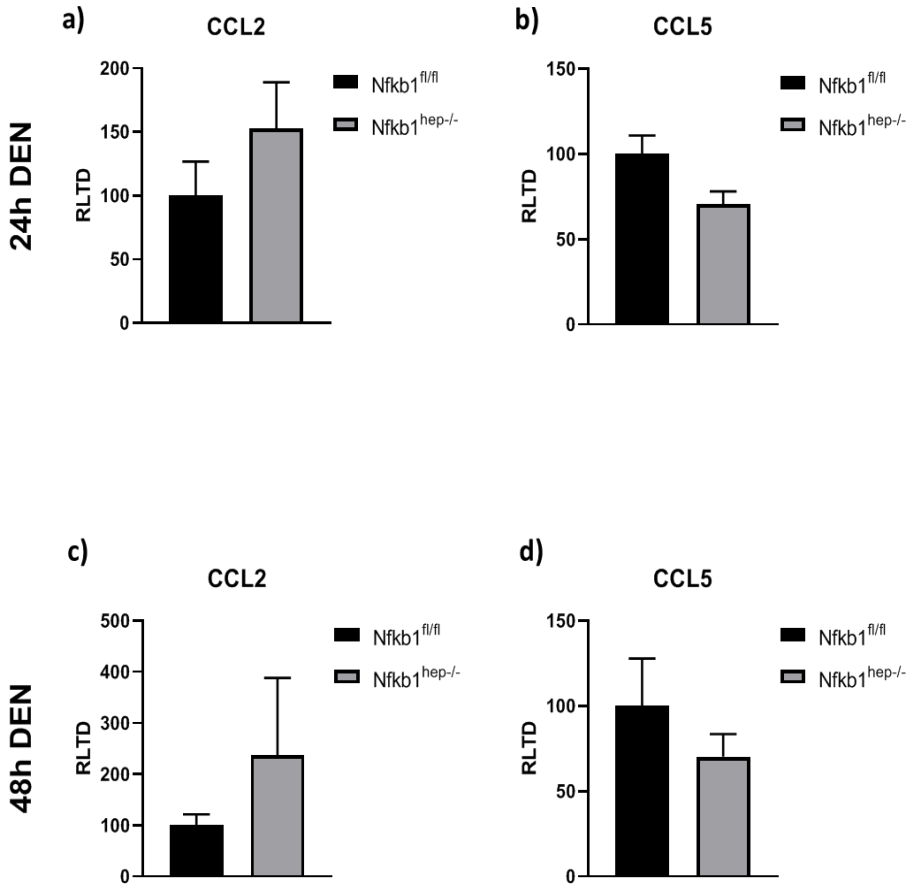

Figure 3.36 Gene expression of monocyte chemoattractant chemokines in acute DEN liver injury. Graphs show liver mRNA expression obtained by RT-qPCR analysis 24h after DEN injection of CCL2 (a) and CCL5 (b), and 48h after DEN injection of CCL2 (c) and CCL5 (d). Data are mean ± SEM of n=6 Nfkb1$^{fl/fl}$ and n=6 Nfkb1$^{hep-/-}$ mice livers. Statistical significance was determined using either a Student's two-tailed t-test. P values below 0.05 were considered statistically significant, with *P<0.05, **P<0.01 and ***P<0.001.

3.5.8 Hepatocyte Nfkb1 knock-out does not alter anti-apoptotic/oncogene expression in acute DEN liver injury

Acute liver injury caused by DEN leads to cell death, notably apoptosis, as an injury resolution response (Tolba, Kraus, Liedtke, Schwarz, & Weiskirchen, 2015). The gene expression of anti-apoptotic genes Gadd45β, Bcl-xL and Bcl-2 was therefore assessed by RT-qPCR to investigate the role of hepatocyte NF-κB1 p50 in apoptotic signalling in response to DEN-induced acute liver damage. No significant difference between $Nfkb1^{fl/fl}$ and $Nfkb1^{hep-/-}$ was found in the expression of these anti-apoptotic genes 24h and 48h after DEN injection (Figure 3.37). These results show that hepatocyte p50 likely doesn't play a role in apoptotic signalling in the context of acute DEN liver injury, although further experiments investigating protein expression for example would be necessary to confirm this.

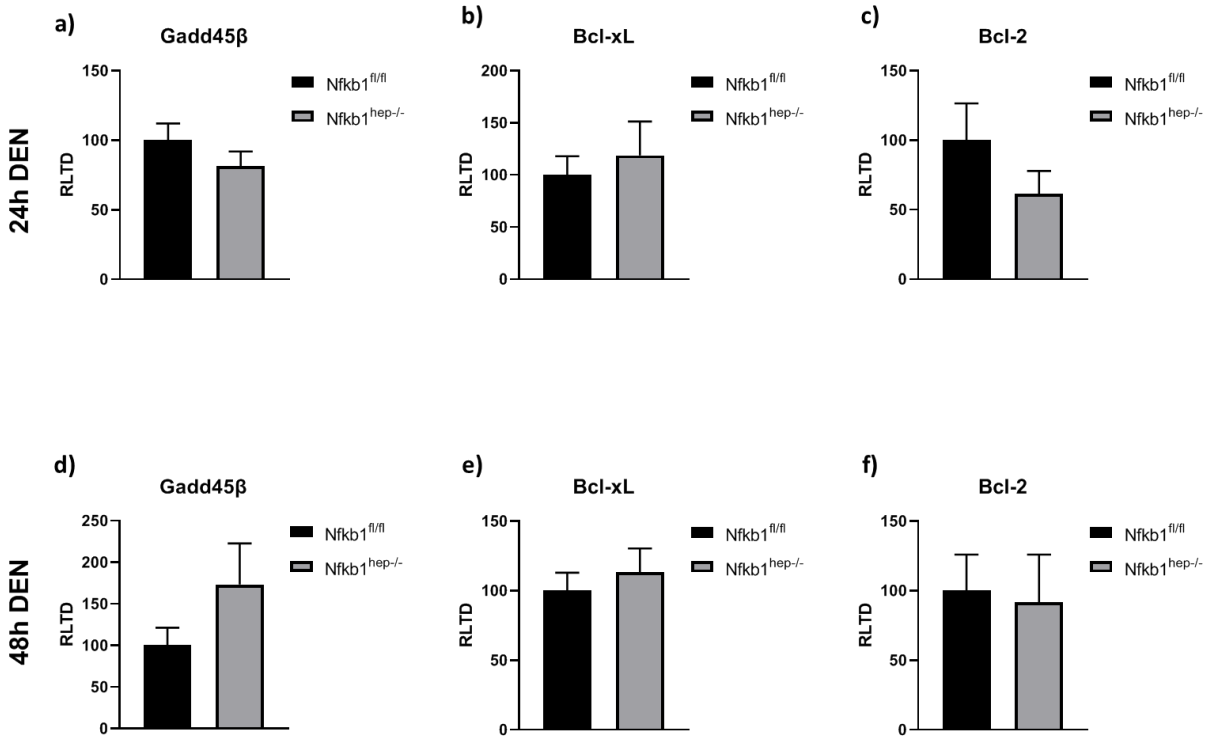

Figure 3.37 Expression of anti-apoptotic genes Gadd45β, Bcl-xL and Bcl-2 in acute DEN liver injury. Graphs show liver mRNA expression obtained by RT-qPCR analysis 24h after DEN injection of Gadd45β (a), Bcl-xL (b), and Bcl-2 (c), and 48h after DEN injection of Gadd45β (d), Bcl-xL (e), and Bcl-2 (f). Data are mean ± SEM of n=6 $Nfkb1^{fl/fl}$ and n=6 $Nfkb1^{hep-/-}$ mice livers. Statistical significance was determined using a Student's two-tailed t-test. P values below 0.05 were considered statistically significant, with *P<0.05, **P<0.01 and ***P<0.001.

3.5.9 Hepatocyte Nfkb1 knock-out does not alter proliferation in acute DEN liver injury

As part of the liver regeneration process following acute injury, proliferation represents an essential process in liver injury resolution. Uncontrolled proliferation however can have detrimental effects and promote carcinogenesis (Feitelson et al., 2015). Proliferation was therefore assessed by PCNA immunohistochemistry in formalin-fixed paraffin-embedded liver tissue, to evaluate the role of hepatocyte NF-κB1 p50 in proliferation following acute DEN liver injury (PCNA stain was carried out as part of Sam Murray's undergraduate project under my supervision). No significant difference in PCNA+ hepatocytes was observed between Nfkb1$^{fl/fl}$ and Nfkb1$^{hep-/-}$ mice after 24h and after 48h (Figure 3.38). This indicated that hepatocyte NF-κB1 p50 does not modulate proliferation in acute DEN liver injury.

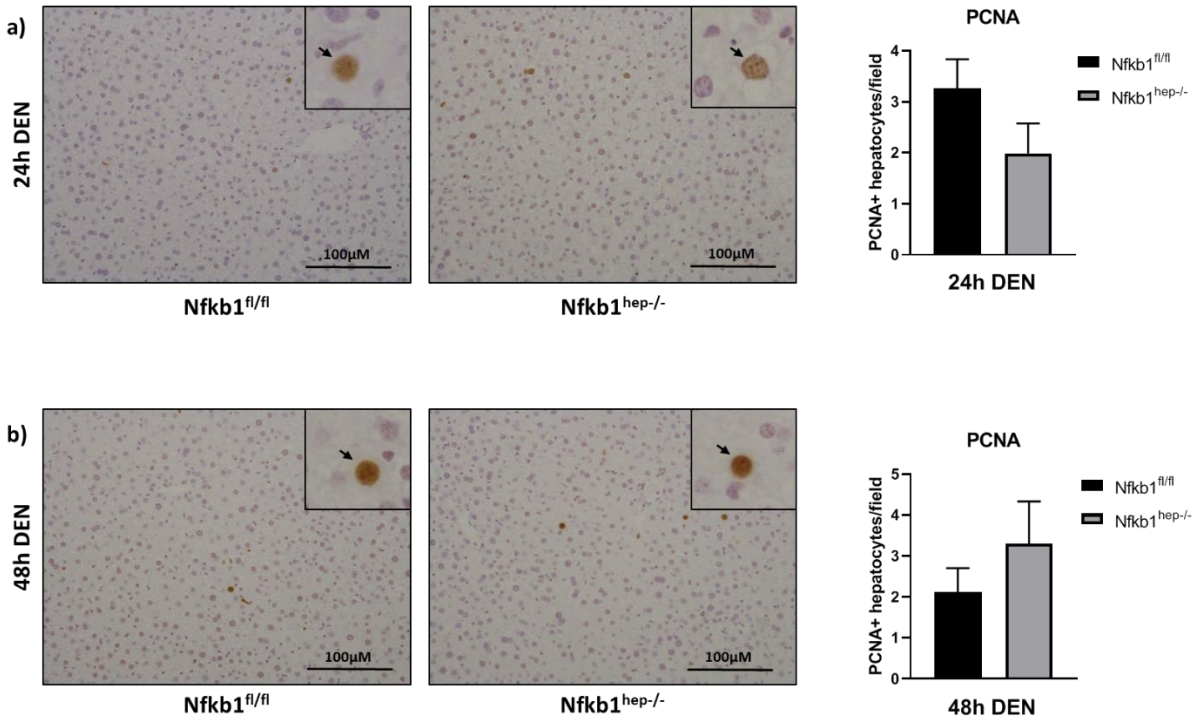

Figure 3.38 PCNA liver immunostain in acute DEN liver injury. Images show X20 PCNA immunostaining in Nfkb1$^{fl/fl}$ and Nfkb1$^{hep-/-}$ formalin-fixed paraffin-embedded liver tissue 24h following DEN injection (a), and 48h following DEN injection (b). Graphs show PCNA+ hepatocytes per field at 24h (c) and at 48h (d). Data are mean ± SEM of n=6 Nfkb1$^{fl/fl}$ and n=6 Nfkb1$^{hep-/-}$ mice livers. Statistical significance was determined using a Student's two-tailed t-test. P values below 0.05 were considered statistically significant, with *P<0.05, **P<0.01 and ***P<0.001.

3.5.10 Hepatocyte Nfkb1 knock-out does not alter DNA damage in acute DEN liver injury

Acute DEN liver injury is also known to cause DNA damage (Tolba, Kraus, Liedtke, Schwarz, & Weiskirchen, 2015), therefore the role of NF-κB1 p50 in DNA damage modulation in acute DEN liver injury was assessed by γH2AX immunohistochemistry on formalin-fixed paraffin-embedded liver tissue (γH2AX stain was carried out as part of Sam Murray's undergraduate project under my supervision). No significant difference was observed in γH2AX+ stain between $Nfkb1^{fl/fl}$ and $Nfkb1^{hep-/-}$ mice after 24h and after 48h. This suggests hepatocyte NF-κB1 p50 does not modulate DNA damage in acute DEN liver injury.

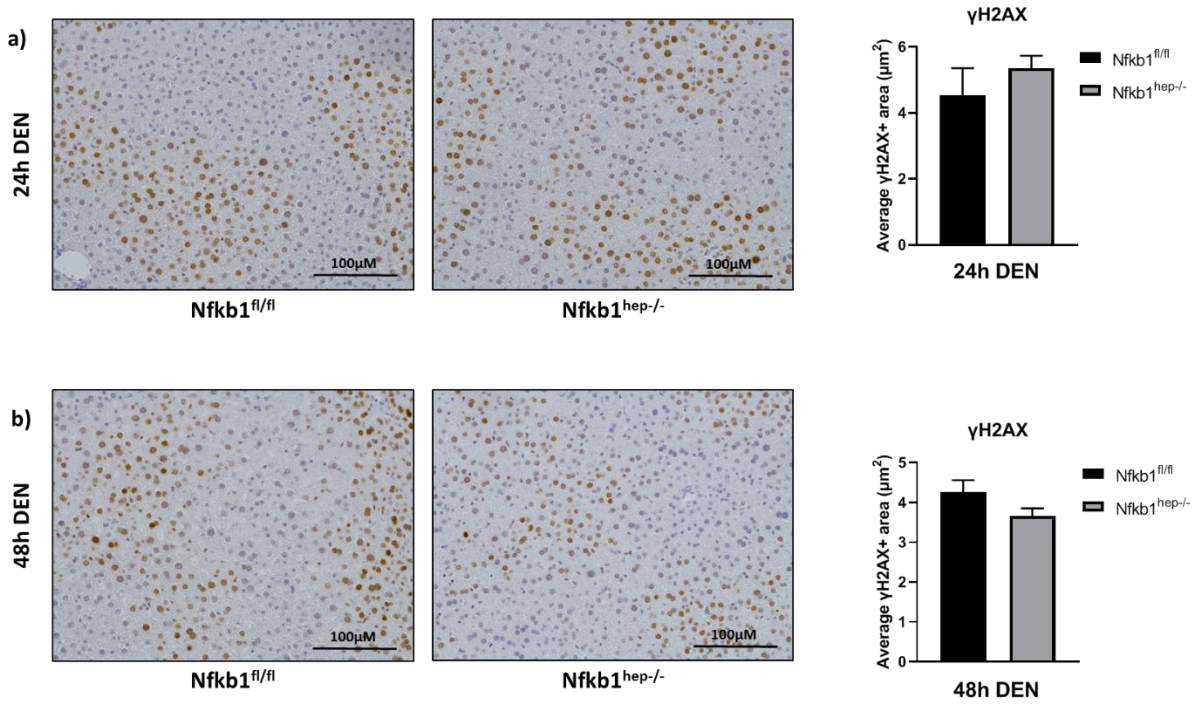

Figure 3.39 γH2AX liver immunostain in acute DEN liver injury. Images show X20 γH2AX immunostaining in $Nfkb1^{fl/fl}$ and $Nfkb1^{hep-/-}$ formalin-fixed paraffin-embedded liver tissue 24h following DEN injection (a), and 48h following DEN injection (b). Graphs show γH2AX+ hepatocytes per field at 24h (c) and at 48h (d). Data are mean ± SEM of n=6 $Nfkb1^{fl/fl}$ and n=6 $Nfkb1^{hep-/-}$ mice livers. Statistical significance was determined using a Student's two-tailed t-test. P values below 0.05 were considered statistically significant, with *P<0.05, **P<0.01 and ***P<0.001.

3.7 Chapter Discussion

Acute liver hepatotoxic injury triggers a number of cellular responses including immune responses, cell survival and proliferation signalling processes. NF-κB1 p50 is known to play an anti-inflammatory role by limiting excessive immune responses following liver injury (Cartwright et al., 2016; Wilson et al., 2015; Southern et al., 2012). The aim of these acute liver injury studies was to understand the importance of NF-κB1 p50 in inflammatory responses in acute CCl_4 and acute DEN liver injury.

Results show that in acute CCl_4 liver injury, mice lacking NF-κB1 display increased macrophage numbers. This indicates that NF-κB1 plays an important role in limiting macrophage infiltration in the liver in acute injury. While macrophages are important for the resolution of injury, excessive numbers may be detrimental to the liver due to excessive release of inflammatory chemokines for example (Krenkel & Tacke, 2017). NF-κB1 could be playing an important protective role, limiting the damage caused by the liver inflammatory response. NF-κB1 may likely be acting by repressing gene expression of monocyte chemoattractant chemokines through p50 homodimers (Guan et al., 2005). CCL2 and CCL5 gene expression showed no significant difference in the presence or absence of hepatocyte NF-κB1, therefore other monocyte chemoattractant chemokines are likely being repressed by p50 homodimers, although CCL2 and CCL5 protein expression levels may be increased in the absence of hepatocyte NF-κB1. Another possible explanation for the observation of increased macrophages in the absence of NF-κB1 could be that more monocytes are being differentiated into macrophages, suggesting that p50 homodimers may limit monocyte differentiation into macrophages by limiting the expression of monocyte differentiation chemokines such as CXCL12 and CCL18. It would also be interesting to explore macrophage polarisation, to see whether NF-κB1 modulates M1/M2 phenotype. Acute DEN liver injury however did not affect macrophage infiltration in the liver, therefore hepatocyte p50-specific responses defer depending on the initial liver injury.

Interestingly, lack of hepatocyte NF-κB1 did not affect the neutrophil chemokine network expression or neutrophil infiltration in the liver in both the acute CCl_4 and acute DEN models. While previous research has shown that NF-κB1 p50 is an important player in limiting neutrophil recruitment, this was shown in chronic liver injury studies, therefore prolonged injury to the liver may be required for any hepatocyte NF-κB1 p50 effects to be observed (Wilson et al., 2015).

Overall, no clear differences or trends were observed between control mice and Nfkb1$^{hep-/-}$ mice in terms of apoptosis and necrosis. Anti-apoptotic genes were not differentially expressed and cleaved caspase 3 staining showed similar results, except 48h after CCl_4 injection where staining was significantly increased in Nfkb1$^{hep-/-}$ mice compared to Alb-Cre$^{+/-}$ mice, however no significant difference was observed between Nfkb1$^{hep-/-}$ and Nfkb1$^{fl/fl}$ control mice. Additionally, no significant difference in percentage necrosis area was observed between Nfkb1$^{hep-/-}$ mice and the control groups. Thus, it can be concluded from these results that hepatocyte NF-κB1 p50 does not modulate cell death in the context of acute CCl_4 liver injury.

Proliferation and DNA damage was additionally assessed in the acute DEN model, through PCNA and H2AX staining, to investigate the role of hepatocyte NF-κB1 p50 in compensatory proliferation and DNA damage following acute injury. No difference was observed indicating that hepatocyte NF-κB1 p50 does not modulate proliferation or DNA damage in the context of acute DEN liver injury.

Importantly, serum AST levels were significantly decreased in mice lacking hepatocyte NF-κB1 24h after CCl_4 injection in the AAV-TBG-Cre model, and 48h after DEN injection. This suggests that hepatocyte damage was inferior in AAV-TBG-Cre and Nfkb1$^{hep-/-}$ mice following acute CCl_4 and DEN injection. It would be interesting to evaluate the expression of enzymes metabolising CCl_4 and DEN: cytochrome p450 enzymes (Chowdhury et al., 2012; Stoyanovsky & Cederbaum, 1996), to see whether the hepatotoxins are metabolised differently in the absence of hepatocyte NF-κB1.

Altogether, these results demonstrate that lack of hepatocyte NF-κB1 has minimal effect in acute liver injury, with the main observation being an increase in macrophage infiltration in the liver. Other cellular processes could be explored in this model, such as cell cycle protein expression and the infiltration of other immune cell types.

Chapter 4. Global, but not hepatocyte-only, NF-κB1 restricts the liver inflammatory and fibrotic phenotype in a chronic CCl_4 model of liver injury

4.1 Introduction

The NF-κB pathway plays an essential role in inflammatory and fibrotic responses in the liver, regulating cell survival, proliferation and immune cell responses, as well as wound healing and repair (Luedde & Schwabe, 2011b). NF-κB1 has been implicated in the protection against liver fibrosis by dampening and limiting cellular responses through gene repression by p50 homodimers (Oakley, Mann, et al., 2005). Global Nfkb1 knockout in mice has been associated with a more severe inflammatory and fibrotic phenotype, notably characterised by increased neutrophil immune cell infiltration in the liver and increased liver collagen deposition (Oakley, Mann, et al., 2005). This indicates that NF-κB1 exerts a protective function in liver fibrogenesis, likely via p50 homodimer repression of inflammatory and fibrogenic gene transcription. However, to date, NF-κB1 cell-specific roles have not been characterised in the liver. With hepatocytes making up the majority of liver cells (70-80%) (Miyaoka et al., 2012; Manco et al., 2018a, 2018b; Tanaka & Miyajima, 2016), we hypothesized that p50 homodimers may play an important protective role in injured hepatocytes in terms of regulating the responses to inflammatory and fibrogenic stimuli, preventing excessive activation of the NF-κB pathway. We therefore chose to assess the role of hepatocyte NF-κB1 in liver chronic inflammatory and fibrotic responses, employing a chronic CCl_4 model of liver fibrosis in mice.

Chronic liver damage and inflammation is widely associated with increased liver cancer risk (Bishayee, 2014), and therefore understanding the biology behind the different stages of liver damage is essential to understand liver cancer development. Many liver fibrosis cases develop into cirrhosis, characterised by a more severe fibrotic phenotype, which often leads to the development of HCC (Keenan et al., 2019; Alexander et al., 2019; O'Rourke et al., 2018b). However, the links between liver disease and cancer remain incompletely understood. The aim of this study was to characterise the role of hepatocyte NF-κB1 in chronic liver inflammation and fibrosis, with the ultimate aim being to understand how repeated liver damage can progress to liver carcinogenesis.

For this, we used a well-established chronic CCl_4 model of liver fibrosis, where mice were injected with the hepatotoxin CCl_4 biweekly for 6 weeks. CCl_4 is metabolised by cytochrome P450 producing reactive radicals which impair key cellular processes, notably leading to lipid peroxidation and the destruction of polyunsaturated fatty acids, subsequently lowering membrane permeability and leading to generalised hepatic damage characterised by inflammation and fibrosis (D Scholten et al., 2015). Three different groups of mice were compared: $Nfkb1^{fl/fl}$, $Nfkb1^{hep-/-}$ and $Nfkb1^{-/-}$ mice. $Nfkb1^{fl/fl}$ mice were used as a control, and levels of inflammation and fibrosis were compared between hepatocyte-specific Nfkb1 knockout mice and global Nfkb1 knockout mice to assess whether the inflammatory and fibrotic phenotype observed in $Nfkb1^{-/-}$ mice can be attributed to the lack of NF-κB1 in hepatocytes. Mice injected with olive oil only were used as controls.

4.2 Liver/body rate ratio in chronic CCl_4 liver injury

Mice body weight, liver weight and liver/body weight ratios were determined at the time of harvest. $Nfkb1^{-/-}$ mice treated with CCl_4 had significantly reduced body and liver weights, as well as liver/body weight ratio compared to both $Nfkb1^{fl/fl}$ ($p=0.0002$) and $Nfkb1^{hep-/-}$ mice ($p=0.0001$) (Figure 4.1). $Nfkb1^{-/-}$ mice also looked notably thinner at the time of harvest. This indicates that $Nfkb1^{-/-}$ mice develop a poorer phenotype in response to chronic CCl_4 liver damage compared to $Nfkb1^{fl/fl}$ and $Nfkb1^{hep-/-}$ mice.

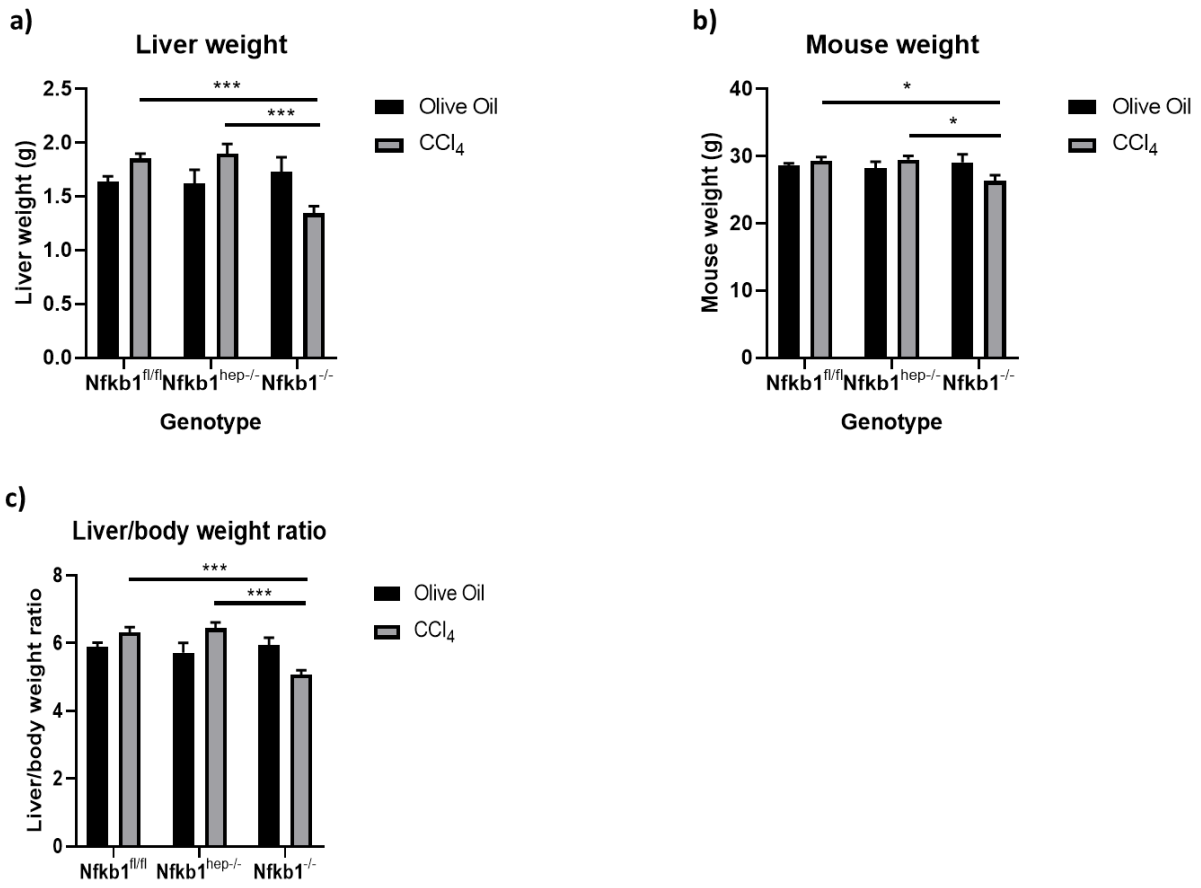

Figure 4.1 Liver/body weight ratio after chronic CCl_4 treatment. Graphs show average liver weights (a), average mouse body weights (b) and liver/body weight ratios of Nfkb1$^{fl/fl}$, Nfkb1$^{hep-/-}$ and Nfkb1$^{-/-}$ mice after olive oil or CCl_4 treatment.

4.3 p50 expression in Nfkb1$^{fl/fl}$ and Nfkb1$^{hep-/-}$ mice

The expression of NF-κB1 p105 and p50 was assessed by western blot analysis in Nfkb1$^{fl/fl}$ and Nfkb1$^{hep-/-}$ mice livers treated with CCl_4. Results show abundant expression of p105 and p50 in Nfkb1$^{fl/fl}$ mice with little to no expression in Nfkb1$^{hep-/-}$ mice.

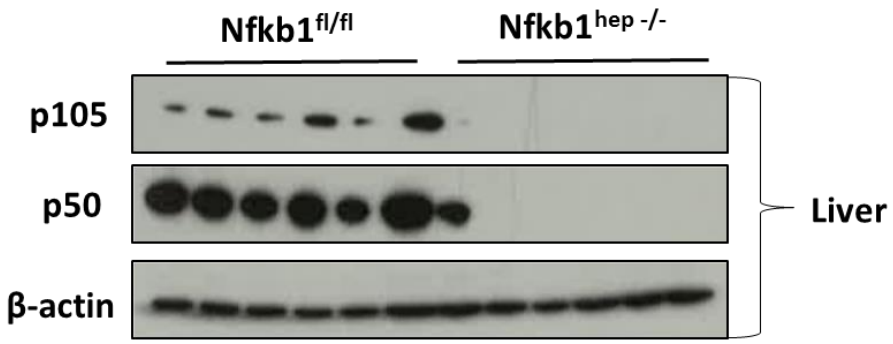

Figure 4.2 p50 expression in Nfkb1$^{fl/fl}$ and Nfkb1$^{hep-/-}$ mice. Western blot showing p105 and p50 expression in Nfkb1$^{fl/fl}$ and Nfkb1$^{hep-/-}$ mice livers treated with CCl_4.

4.4 Global, but not hepatocyte, Nfkb1 knock-out increases liver damage serum ALT and AST enzymes

ALT and AST levels were measured in the serum to assess liver damage. Interestingly, ALT and AST levels were significantly increased in the serum of CCl_4-treated Nfkb1$^{-/-}$ mice ($p=0.005$ for ALT and $p<0.0001$ for AST), but not in CCl_4-treated Nfkb1$^{hep-/-}$ mice, compared to CCl_4-treated Nfkb1$^{fl/fl}$ control mice (Figure 4.3). No significant difference between the three groups was observed when mice were treated with olive oil, confirming the damage caused by chronic CCl_4. ALT levels were also significantly increased in CCl_4-treated Nfkb1$^{-/-}$ mice compared to CCl_4-treated Nfkb1$^{hep-/-}$ mice ($p=0.0087$) and uninjured Nfkb1$^{-/-}$ mice ($p=0.0014$), and AST levels were significantly increased in CCl_4-treated Nfkb1-/- mice compared to CCl_4-treated Nfkb1$^{hep-/-}$ mice (0.0015) and uninjured Nfkb1$^{-/-}$ mice (0.0003). Of note, while there does appear to be a slight increase in serum AST and ALT levels in Nfkb$^{hep-/-}$ mice compared to Nfkb1$^{fl/fl}$ mice, this may be attributed to the outlier observed in Figure 4.2, whereby Nfkb1 hepatocyte knockout could be incomplete, or immune cell infiltration dramatically increased in the liver.

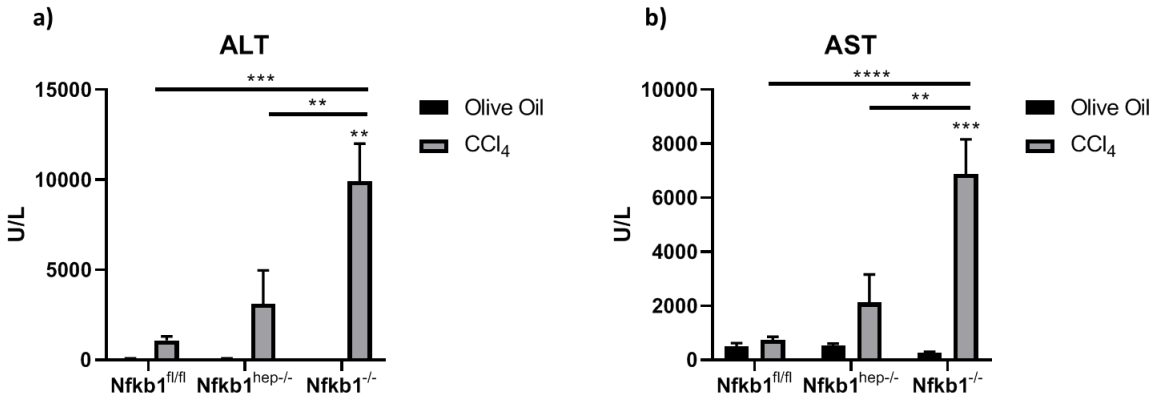

Figure 4.3 Serum ALT and AST levels after CCl_4 treatment. Graphs show serum ALT (a) and AST (b) levels in Nfkb1$^{fl/fl}$, Nfkb1$^{hep-/-}$ and Nfkb1$^{-/-}$ mice treated with either olive oil or CCl_4.

4.5 Lack of global NF-κB1, but not hepatocyte p50, increases liver inflammation

NF-κB1 p50 is known to protect against chronic inflammation. Previous research has shown that global Nfkb1$^{-/-}$ mice exhibit increased immune cell liver infiltration and inflammatory gene expression compared to control mice which express p50 (Margetts et al., 2018). Specifically, Nfkb1$^{-/-}$ mice displayed increased neutrophil infiltration in the liver and increased neutrophil chemokine network expression (CXCL1, CXCL2, S100A9). Immune cell infiltration in the liver and the expression of inflammatory chemokine genes was therefore assessed to evaluate the role of hepatocyte p50 specifically.

4.5.1 Increased liver neutrophil infiltration in global, but not hepatocyte-specific, NF-κB1 knock-out mice

Previous studies have shown that global Nfkb1$^{-/-}$ mice exhibit increased inflammation, particularly characterised by an increase in neutrophil infiltration in the liver (Wilson et al., 2015). We therefore sought to assess whether the knockout of Nfkb1 in hepatocytes specifically would cause a similar effect. Neutrophil infiltration in the liver was assessed by Ly6G immunohistochemistry on formalin-fixed paraffin-embedded mouse liver sections. The number of Ly6G positive cells was significantly increased in Nfkb1$^{-/-}$ mice ($p<0.0001$), but not in Nfkb1$^{hep-/-}$ mice, compared to Nfkb1$^{fl/fl}$ mice (Figure 4.4). Ly6G staining was also significantly increased in CCl_4-treated Nfkb1$^{-/-}$ mice compared to CCl_4-treated Nfkb1$^{hep-/-}$ mice ($p<0.0001$) and uninjured Nfkb1$^{-/-}$ mice

(p<0.0001). Olive oil treated mice showed little neutrophil infiltration in the liver, demonstrating the CCl_4-mediated inflammation.

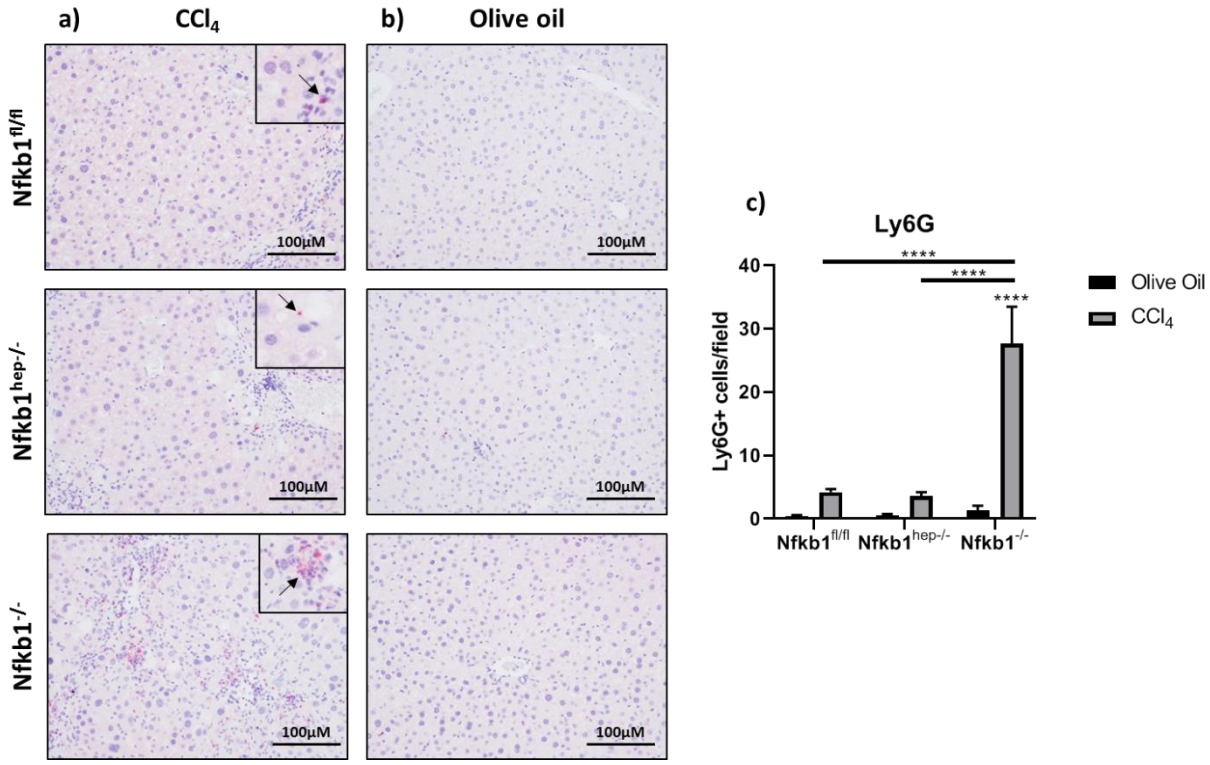

Figure 4.4 Ly6G liver immunostaining after chronic CCl_4 treatment. Images show X20 Ly6G immunostaining in the liver in $Nfkb1^{fl/fl}$, $Nfkb1^{hep-/-}$ and $Nfkb1^{-/-}$ mice treated with either CCl_4 (a) or olive oil (b). Graph shows average Ly6G positive cell count per field in $Nfkb1^{fl/fl}$, $Nfkb1^{hep-/-}$ and $Nfkb1^{-/-}$ mice treated with either olive oil or CCl_4 (c).

4.5.2 Increased chemokine expression in global, but not hepatocyte-specific, Nfkb1 knock-out mice

The expression of several chemokines in the liver was assessed by RT-qPCR in order to further characterise liver inflammation and the recruitment of immune cells to the liver. The increase in neutrophil recruitment to the liver was reflected in the significant upregulation of neutrophil chemokines S100A9 and CXCL1 in $Nfkb1^{-/-}$ mice compared to $Nfkb1^{fl/fl}$ ($p=0.0013$ for S100A9 and $p=0.0013$ for CXCL2) and $Nfkb1^{hep-/-}$ mice ($p=0.0120$ for S100A9 and $p=0.0027$ for CXCL2), with no significant difference in $Nfkb1^{hep-/-}$ mice compared to control mice (Figure 4.5). S100A9 and CXCL2 were also significantly upregulated in $Nfkb1^{-/-}$ mice treated with CCl_4 compared to $Nfkb1^{-/-}$ mice treated with olive oil ($p=0.0089$ for S100A9 and $p=0.0103$ for CXCL2). Other inflammatory chemokines including TNFα ($p=0.0041$), CCL2 ($p=0.0012$) and CXCL10

(p<0.0001) were also significantly upregulated in Nfkb1$^{-/-}$ mice, but not in Nfkb1$^{hep-/-}$ mice compared to Nfkb1$^{fl/fl}$ mice (Figure 4.6), suggesting that NF-κB1 does not function as an inflammatory suppressor in hepatocytes in the context of chronic CCl_4 injury. These chemokines were also significantly expressed in Nfkb1$^{-/-}$ mice treated with CCl_4 compared to Nfkb1$^{-/-}$ mice treated with olive oil.

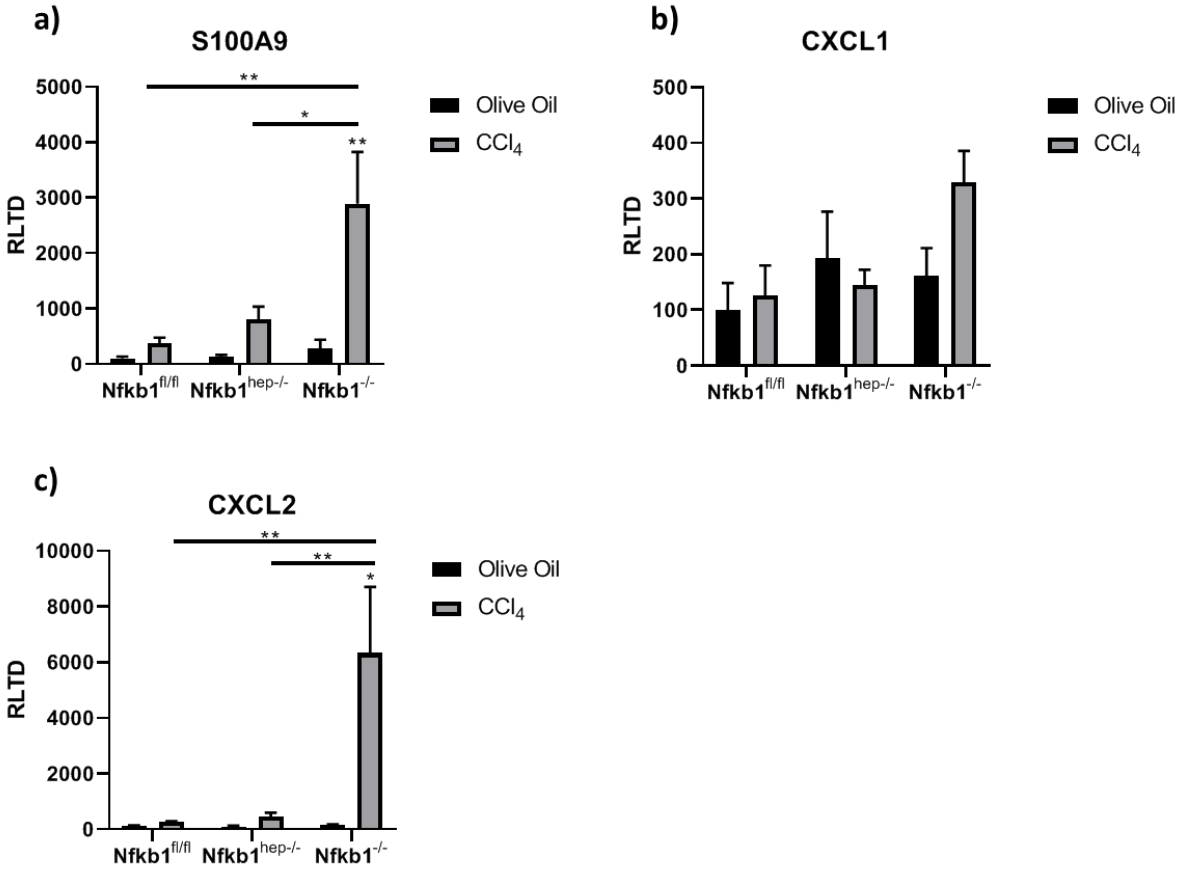

Figure 4.5 Neutrophil chemoattractant chemokine expression following chronic CCl_4 treatment. Graphs show gene expression of neutrophil chemoattractant chemokines S100A9 (a), CXCL1 (b) and CXCL2 (c) in Nfkb1$^{fl/fl}$, Nfkb1$^{hep-/-}$ and Nfkb1$^{-/-}$ mice treated with either olive oil or CCl_4.

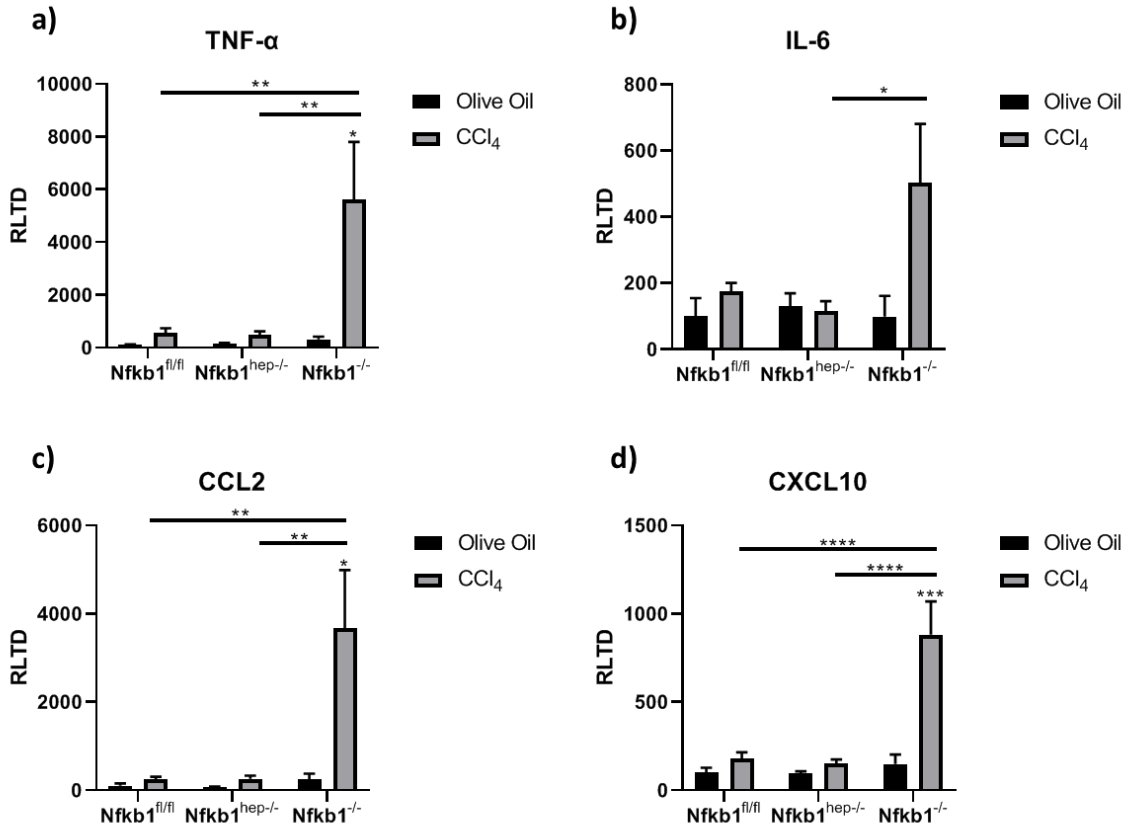

Figure 4.6 Inflammatory chemokine expression following chronic CCl_4 treatment. Graphs show gene expression of inflammatory chemokines TNFα (a), IL-6 (b), CCL2 (c) and CXCL10 (d) in $Nfkb1^{fl/fl}$, $Nfkb1^{hep-/-}$ and $Nfkb1^{-/-}$ mice treated with either olive oil or CCl_4.

4.5.3 NF-κB1 does not modulate liver monocyte infiltration in a chronic CCl_4 liver injury model

Interestingly, despite a marked increase in immune cell infiltration in the liver, particularly of neutrophils, in $Nfkb1^{-/-}$ mice, no significant difference in liver monocyte/macrophage infiltration was observed in either $Nfkb1^{-/-}$ mice or $Nfkb1^{hep-/-}$ mice, assessed by CD68 immunohistochemistry (Figure 4.7). NF-κB1 therefore plays an important role in neutrophil recruitment to the liver in CCl_4-induced inflammation and fibrosis, acting in non-hepatocyte cells, but does not modulate monocyte and macrophage recruitment to the liver in this model of liver injury.

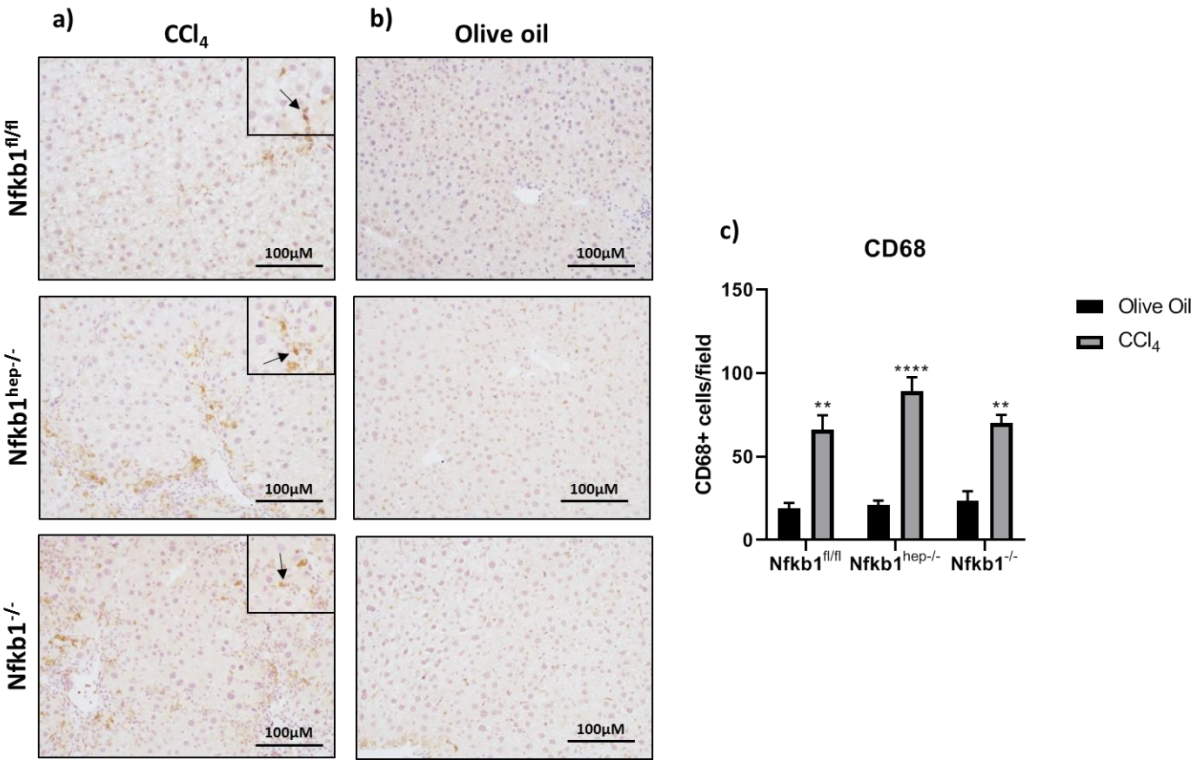

Figure 4.7 CD68 liver immunostain following chronic CCl_4 injury. Images show X20 CD68 immunostaining in the liver in Nfkb1$^{fl/fl}$, Nfkb1$^{hep-/-}$ and Nfkb1$^{-/-}$ mice treated with either CCl_4 (a) or olive oil (b). Graph shows average CD68 positive cell count per field in Nfkb1$^{fl/fl}$, Nfkb1$^{hep-/-}$ and Nfkb1$^{-/-}$ mice treated with either olive oil or CCl_4 (c).

Though no difference was found in macrophage numbers between the three groups, the gene expression levels of pro-inflammatory M1 marker Arg2 and anti-inflammatory M2 marker Arg1 were assessed by RT-qPCR. Arg2 expression was significantly increased in Nfkb1$^{-/-}$ mice treated with CCl_4 compared to Nfkb1$^{fl/fl}$ (p=0.0088) and Nfkb1$^{hep-/-}$ (p=0.0021) mice treated with CCl_4, suggesting that the macrophages in Nfkb1$^{-/-}$ mice have a more pro-inflammatory phenotype (Figure 4.8). In contrast, no significant difference was found in Arg1 expression between the three groups. These results suggest that NF-κB1 p50 may modulate macrophage polarisation, but not via hepatocytes. Additionally, Arg2 expression was significantly increased in Nfkb1$^{-/-}$ mice treated with CCl_4 compared to Nfkb1$^{-/-}$ mice treated with olive oil, which shows the CCl_4-specific mediated inflammation.

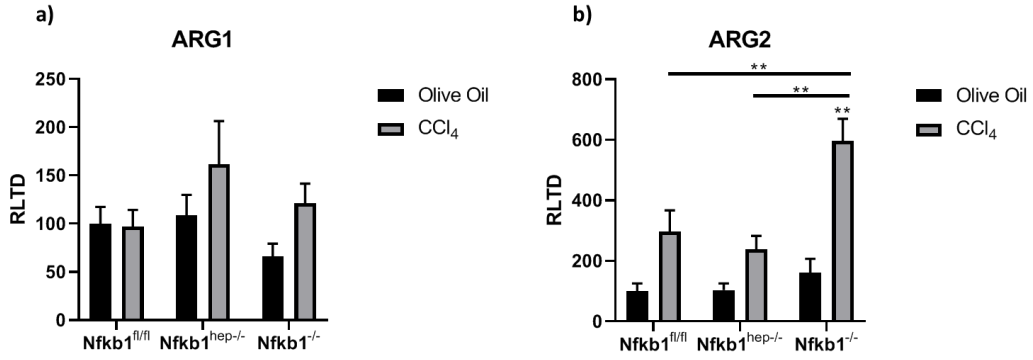

Figure 4.8 Macrophage polarisation chemokine expression following chronic CCl_4 injury. Graphs show gene expression of ARG1 (a) and ARG2 (b) in $Nfkb1^{fl/fl}$, $Nfkb1^{hep-/-}$ and $Nfkb1^{-/-}$ mice treated with either olive oil or CCl_4.

4.6 Lack of global NF-κB1, but not hepatocyte NF-κB1, increases liver fibrosis

As well as assessing the role of hepatocyte NF-κB1 p50 in inflammation following chronic CCl_4 treatment, another important aim of this study was to assess the role of hepatocyte NF-κB1 p50 in fibrosis. For this, fibrotic gene expression was assessed in the liver, and collagen deposition as well as myofibroblast activation was also assessed.

4.6.1 Increased fibrogenic gene expression in global, but not hepatocyte-specific, Nfkb1 knock-out mice

To assess whether hepatocyte NF-κB1 was important in modulating fibrotic responses and the liver fibrotic phenotype, fibrotic gene expression was assessed by RT-qPCR. Surprisingly, no significant difference was observed in α-SMA and COL1A1 expression in neither $Nfkb1^{-/-}$ mice nor $Nfkb1^{hep-/-}$ mice compared to $Nfkb1^{fl/fl}$ control mice (Figure 4.9). While a previous similar study showed an increase in α-SMA and COL1A1 fibrogenic gene expression, it was conducted over 12 weeks (biweekly CCl_4 injections for 12 weeks), suggesting that the 6 week CCl_4 model is insufficient to mirror this response. However, fibrogenic genes TIMP1 ($p=0.0006$) and TGF-β ($p=0.0051$) were significantly increased in $Nfkb1^{-/-}$ mice, but not in $Nfkb1^{hep-/-}$ mice, compared to $Nfkb1^{fl/fl}$ mice. Additionally, TIMP1 ($p=0.0014$) and TGF-β expression ($p=0.01$) was significantly increased in CCl_4-treated $Nfkb1^{-/-}$ mice compared to $Nfkb1^{hep-/-}$ mice. This shows that while NF-κB1 functions as an important regulator of fibrogenic gene expression, this is

not due to its activity in hepatocytes but rather in other cells of the liver, such as innate immune cells including neutrophils and macrophages, or hepatic stellate cells.

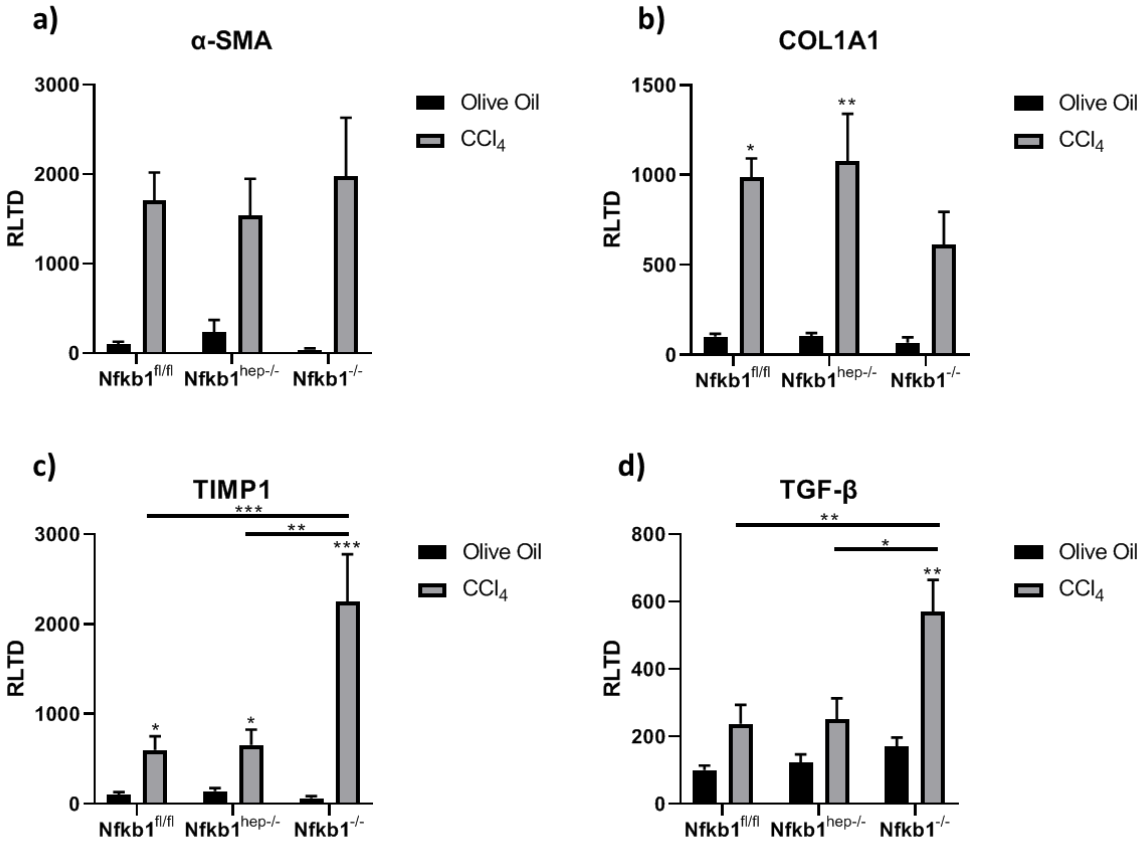

Figure 4.9 Fibrogenic gene expression following chronic CCl_4 treatment. Graphs show gene expression of fibrotic genes α-SMA (a), COL1A1 (b), TIMP1 (c) and TGF-β (d) in $Nfkb1^{fl/fl}$, $Nfkb1^{hep-/-}$ and $Nfkb1^{-/-}$ mice treated with either olive oil or CCl_4.

4.6.2 Increased collagen deposition and fibrosis score in global, but not hepatocyte-specific, Nfkb1 knock-out mice

Collagen deposition, which is characteristic of fibrosis (Wynn, 2008), was assessed by Sirius red stain. Percentage positive Sirius red staining was measured by thresholding. A significant increase in collagen deposition was observed in $Nfkb1^{-/-}$ mice compared to $Nfkb1^{hep-/-}$ mice (p=0.0241), but not compared to $Nfkb1^{fl/fl}$ control mice (Figure 4.10). Additionally, the fibrosis score of $Nfkb1^{-/-}$ mice livers was higher compared to $Nfkb1^{hep-/-}$ mice (p=0.0405). No difference was observed in collagen deposition or fibrosis score between $Nfkb1^{fl/fl}$ mice and $Nfkb1^{hep-/-}$ mice. This shows that hepatocyte NF-κB1 does

not modulate collagen deposition in liver fibrosis, and therefore that NF-κB1 exerts an important role in the regulation of collagen deposition and fibrosis in other liver cells.

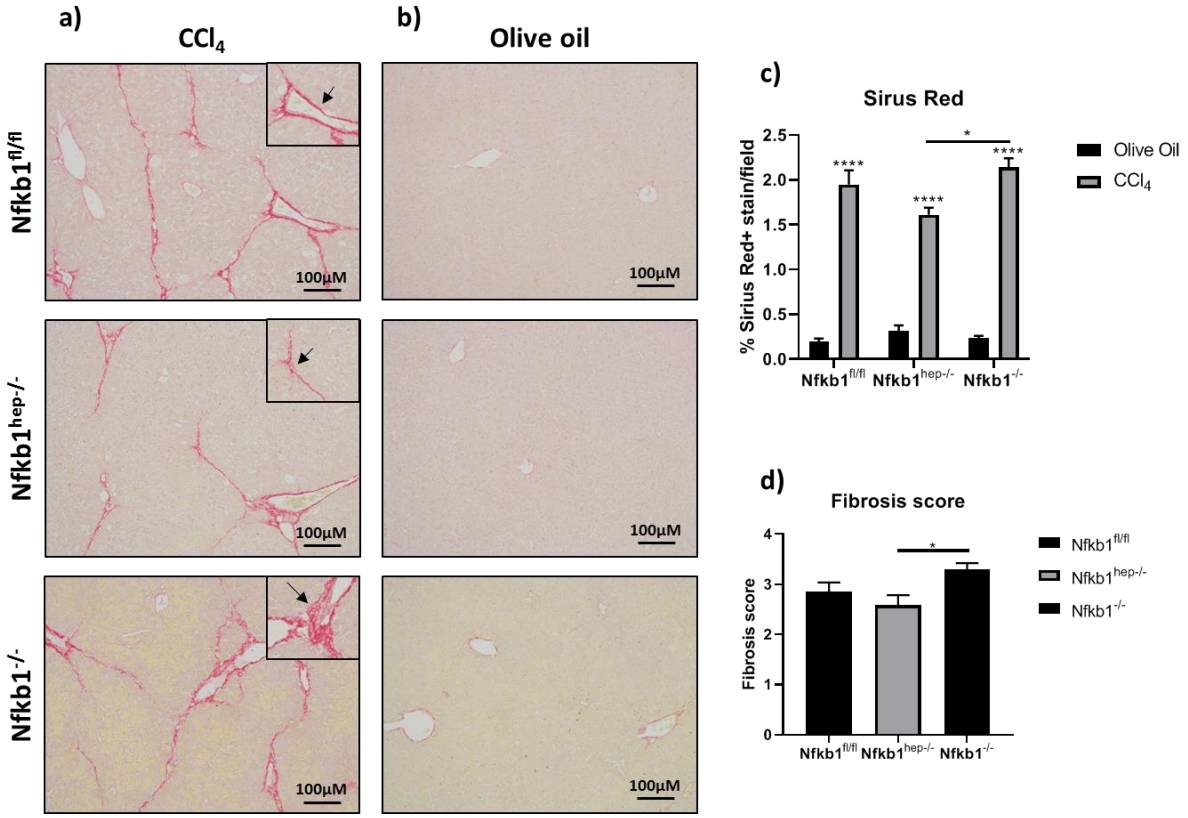

Figure 4.10 Sirius red stain following chronic CCl_4 treatment. Images show X10 sirius red staining of liver tissue from $Nfkb1^{fl/fl}$, $Nfkb1^{hep-/-}$ and $Nfkb1^{-/-}$ mice treated with either CCl_4 (a) or olive oil (b). Graphs show average percentage sirius red staining per field (c) and fibrosis score in $Nfkb1^{fl/fl}$, $Nfkb1^{hep-/-}$ and $Nfkb1^{-/-}$ mice (d).

4.6.3 NF-κB1 does not modulate liver alpha-SMA expression in a chronic CCl_4 liver injury model

α-SMA immunohistochemistry was carried out to assess myofibroblast activation, characteristic of liver fibrosis (Nagaraju et al., 2019; Hinz et al., 2007). In accordance with the α-SMA RT-qPCR results, no significant difference was observed in a-SMA expression between all three groups (Figure 4.11). However previous research showed increased α-SMA expression in $Nfkb1^{-/-}$ mice livers in a 12 week chronic CCl_4 fibrosis model (Oakley, Mann, et al., 2005). Longer exposure to CCl_4 would have likely led to an increase in α-SMA expression in $Nfkb1^{-/-}$ mice compared to $Nfkb1^{hep-/-}$ mice and $Nfkb1^{fl/fl}$ mice. α-SMA expression was significantly increased in $Nfkb1^{fl/fl}$, $Nfkb1^{hep-}$

$^{/-}$ and Nfkb1$^{-/-}$ mice treated with CCl_4 compared to Nfkb1$^{fl/fl}$, Nfkb1$^{hep-/-}$ and Nfkb1$^{-/-}$ mice treated with olive oil respectively, demonstrating CCl_4-induced fibrosis in this model.

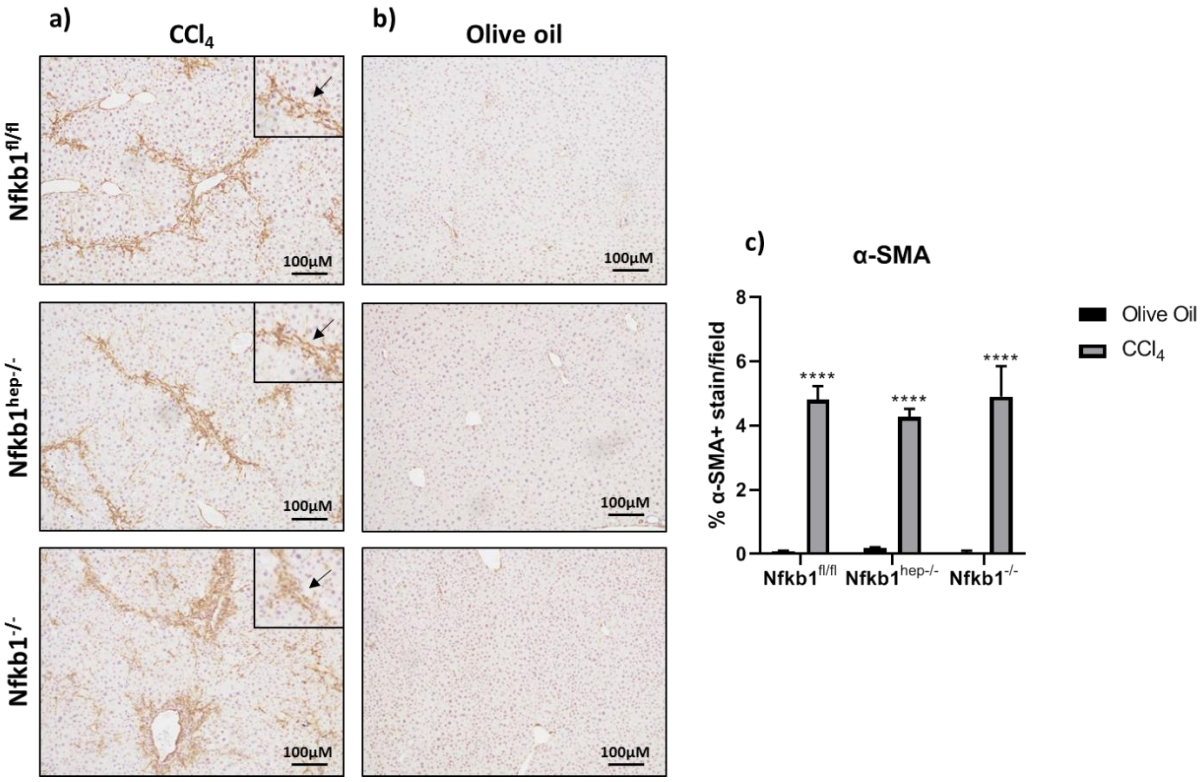

Figure 4.11 α-SMA immunostain following chronic CCl_4 treatment. Images show X10 α-SMA immunostaining of liver tissues in Nfkb1$^{fl/fl}$, Nfkb1$^{hep-/-}$ and Nfkb1$^{-/-}$ mice treated with either CCl_4 (a) or olive oil (b). Graph shows average percentage α-SMA staining per field in Nfkb1$^{fl/fl}$, Nfkb1$^{hep-/-}$ and Nfkb1$^{-/-}$ mice treated with either olive oil or CCl_4 (c).

4.7 Chapter Discussion

The above results show that loss of global NF-κB1 p50 negatively impacts the liver inflammatory and fibrotic phenotype in a chronic CCl_4 liver fibrosis model, whereas hepatocyte NF-κB1 p50 does not modulate inflammation and fibrosis in this liver injury model. This coincides with what has previously been observed in a 12-week chronic CCl_4 fibrosis model, where Nfkb1$^{-/-}$ mice livers also exhibited increased neutrophil infiltration, neutrophil chemoattractant chemokine expression, fibrogenic gene expression and collagen deposition, as observed here in this 6-week CCl_4 model (Oakley, Mann, et al., 2005).

Interestingly, this phenotype was not replicated in Nfkb1$^{hep-/-}$ mice, indicating that hepatocyte NF-κB1 p50 does not modulate inflammation and fibrosis following chronic CCl_4 injury. This is surprising as hepatocytes represent the majority of liver cells (around 75%). Therefore, NF-κB1 p50 must be modulating inflammation and fibrosis in response to chronic CCl_4 treatment in other cell types in the liver. These could be immune cells (e.g. neutrophils or macrophages) or hepatic stellate cells. Further studies could explore the role of NF-κB1 p50 in different cell types, using cell-specific knock-out mice (e.g. PDGF-Cre for hepatic stellate cells or LyZM-Cre for myeloid-derived immune cells) in order to understand where NF-κB1 p50 is acting to limit the inflammatory and fibrotic phenotype.

Chapter 5. The tumour-suppressive role of hepatocellular NF-κB1 in hepatocellular carcinoma

5.1 Introduction

Liver inflammation and fibrosis represent underlying factors for the development of liver cancer (O'Rourke et al., 2018c). Hepatocellular carcinoma (HCC) often develops on the background of chronic liver disease (Shiani et al., 2017). NF-κB1 p50 is a central regulator of inflammation and immune responses (Liu et al., 2017; Li & Verma, 2002), and has been implicated in HCC as a tumour suppressor. Previous research has shown that global Nfkb1$^{-/-}$ mice develop significantly more tumours compared to control WT mice in a DEN-induced HCC cancer model (Wilson et al., 2015). This was accompanied by a significant increase in inflammation, notably increased neutrophil infiltration in the liver and increased neutrophil chemoattractant chemokine expression in Nfkb1$^{-/-}$ mice. Additionally, it was shown in WT mice that p50 homodimers were bound to the promoters of the neutrophil chemokine network genes, repressing the expression of these chemokines and thus acting as a tumour-suppressor (Wilson et al., 2015).

DEN-induced HCC is a commonly used mouse model to study gene-specific effects on HCC development (Tolba, Kraus, Liedtke, Schwarz, Weiskirchen, et al., 2015b; Tang et al., 2017; Heindryckx et al., 2009). In this model, mice are injected with a single dose of the carcinogen DEN at 14 days old, when hepatocytes are still proliferating, and by 40 weeks they develop visible macroscopic tumours. By incorporating into proliferating hepatocytes, DEN leads to the formation of DNA adducts which increases mutations, leading to cancer (Tolba, Kraus, Liedtke, Schwarz, & Weiskirchen, 2015).

Here, the DEN-induced HCC model was carried out in Nfkb1$^{fl/fl}$ and Nfkb1$^{hep-/-}$ mice to assess the role of hepatocyte NF-κB1 p50 in liver carcinogenesis. Additionally, DEN-induced HCC was carried out in AAV-TBG-Null and AAV-TBG-Cre mice, where hepatocyte NF-κB1 was knocked out at 32 weeks following AAV-TBG-Cre virus injection in Nfkb1$^{fl/fl}$ mice. Control Nfkb1$^{fl/fl}$ mice were injected with AAV-TBG-Null virus, which does not knock out Nfkb1. The purpose of this viral Nfkb1 knock-out model was to assess the role of Nfkb1 p50 in tumour progression, knocking out Nfkb1 in

hepatocytes when tumours have started to form, whereas the previous model aimed to assess the role of NF-κB1 in tumour initiation.

It was hypothesized that Nfkb1$^{hep-/-}$ and AAV-TBG-Cre mice would have more tumours at 40 weeks, and display a worse cancer phenotype than WT control mice. Increased inflammation, notably neutrophil infiltration in the liver and neutrophil chemoattractant chemokine expression, was also expected in Nfkb1$^{hep-/-}$ and AAV-TBG-Cre mice, as observed in Nfkb1$^{-/-}$ mice.

5.2 p50 expression in Nfkb1$^{fl/fl}$ and Nfkb1$^{hep-/-}$ mice

NF-κB1 p50 expression was assessed by western blot analysis in Nfkb1$^{fl/fl}$ and Nfkb1$^{hep-/-}$ mice livers harvested at 40 weeks post-DEN injection (Figure 5.1). While Nfkb1$^{fl/fl}$ mice livers showed abundant p50 protein expression, Nfkb1$^{hep-/-}$ mice livers showed notably less p50 expression, confirming the hepatocyte specific knock-out of Nfkb1 p50 in these mice. Where p50 is expressed in Nfkb1$^{hep-/-}$ mice, this can be attributed to p50 expression in other cells of the liver, of which immune cells.

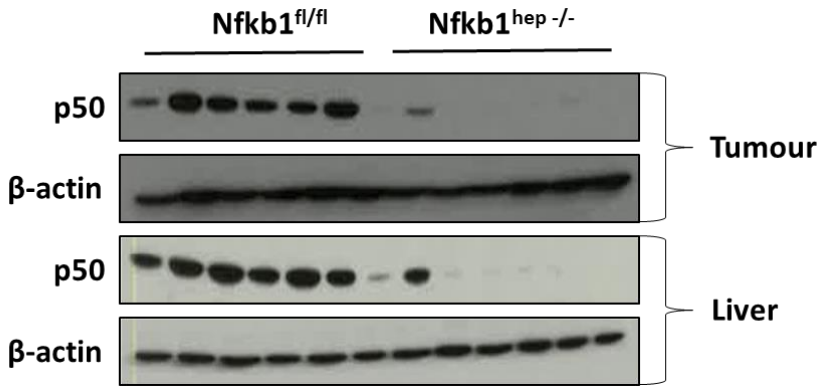

Figure 5.1 Western blot analysis of p50 expression in Nfkb1$^{fl/fl}$ and Nfkb1$^{hep-/-}$ mice. Western blots show p50 expression in the tumours and livers of Nfkb1$^{fl/fl}$ and Nfkb1$^{hep-/-}$ mice 40 weeks after DEN injection.

5.3 Liver damage ALT and AST serum enzymes not affected by hepatocyte Nfkb1 knock-out

Serum ALT and AST levels were measured from Nfkb1$^{fl/fl}$ and Nfkb1$^{hep-/-}$ mice after 40 weeks DEN to assess liver damage. No significant difference in ALT or AST levels

were found between the two groups, indicating that Nfkb1$^{fl/fl}$ and Nfkb1$^{hep-/-}$ mice experienced similar levels of liver damage caused by DEN (Figure 5.2).

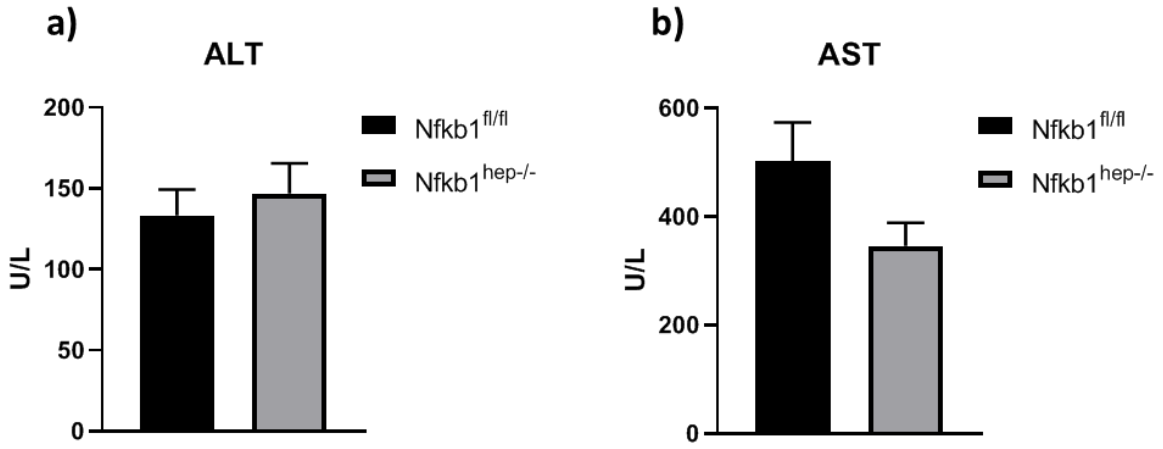

Figure 5.2 Serum ALT and AST levels in Nfkb1$^{fl/fl}$ and Nfkb1$^{hep-/-}$ mice. Graphs show serum ALT (a) and AST (b) levels in Nfkb1$^{fl/fl}$ and Nfkb1$^{hep-/-}$ mice 40 weeks after DEN injection.

5.4 Hepatocyte-specific Nfkb1 knock-out increases tumour incidence *in vivo*

Mice livers from Nfkb1$^{fl/fl}$ and Nfkb1$^{hep-/-}$ mice harvested at 40 weeks post-DEN injection were assessed for tumour number, proliferation and tumour grade to investigate the role of hepatocyte NF-κB1 in HCC outcome.

5.4.1 Hepatocyte Nfkb1 knock-out increases tumour incidence

Macroscopic liver tumours were counted at the time of harvest and large tumours (above 0.5 cm) were also counted. Nfkb1$^{hep-/-}$ mice displayed significantly more tumours compared to Nfkb1$^{fl/fl}$ mice (p=0.0397), and no significant difference in large tumour number was found, though this appeared slightly increased in Nfkb1$^{hep-/-}$ mice (p=0.0936) (Figure 5.3). This shows that hepatocyte NF-κB1 plays a role in limiting tumour development in HCC. Of note, while tumour numbers were significantly increased in Nfkb1$^{hep-/-}$ mice compared to Nfkb1$^{fl/fl}$ mice, the increase in tumour numbers previously observed in global Nfkb1$^{-/-}$ mice is much greater (~5 fold difference in Nfkb1$^{-/-}$ mice vs ~ 1.7 fold in Nfkb1$^{hep-/-}$ mice). Additionally, liver/body weight ratio

was measured, with no significant difference found between the two groups but a slight increase in Nfkb1$^{hep-/-}$ mice compared to Nfkb1$^{fl/fl}$ mice (p=0.1477).

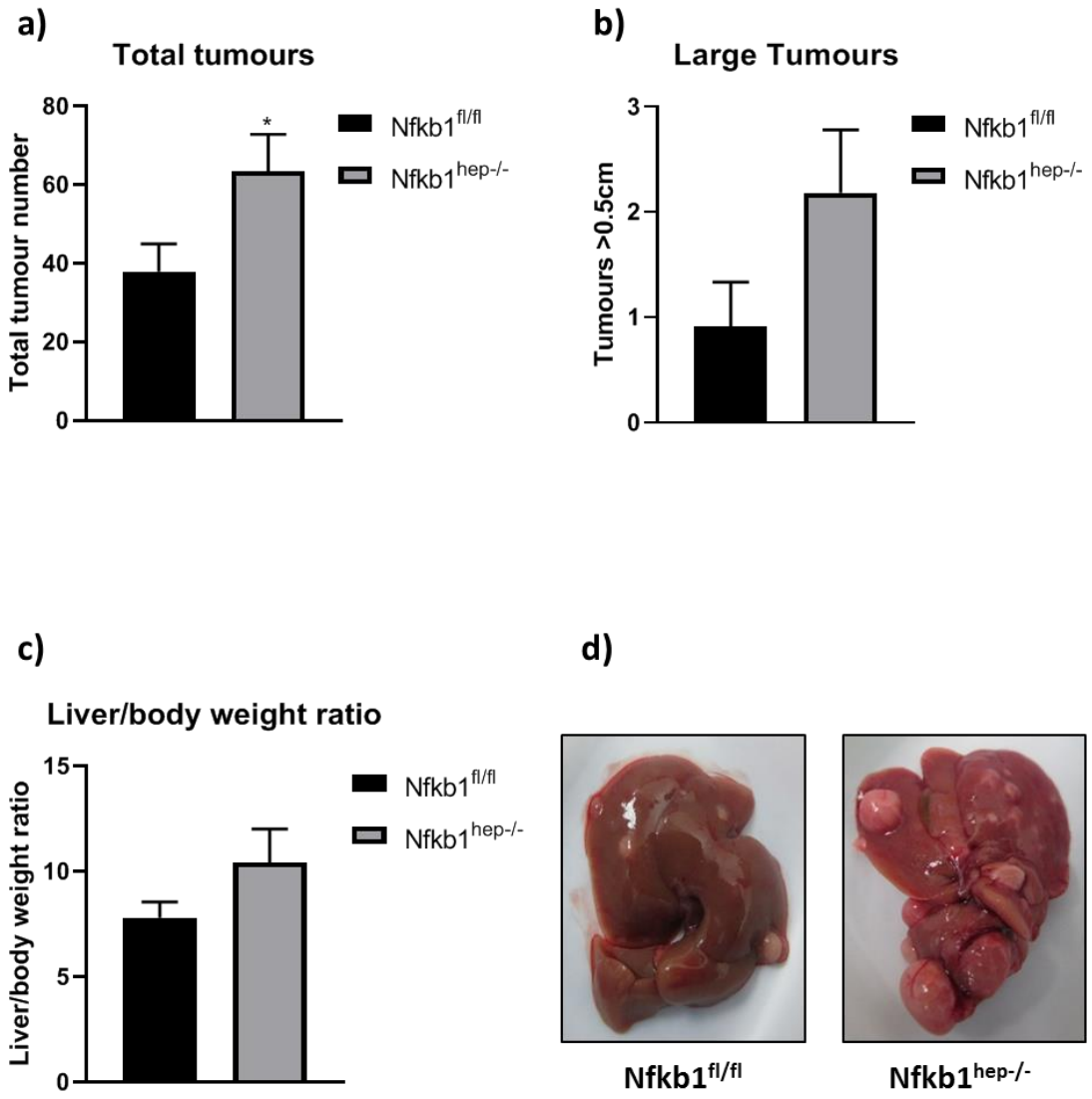

Figure 5.3 Liver tumours and liver/body weight ratio in Nfkb1$^{fl/fl}$ and Nfkb1$^{hep-/-}$ mice. Graphs show total number of liver tumours (a), the number of large tumours (b), and the liver/body weight ratio (c). Images show Nfkb1$^{fl/fl}$ and Nfkb1$^{hep-/-}$ tumorous livers (d).

5.4.2 Hepatocyte Nfkb1 knock-out increases hepatocyte proliferation

To further characterise the tumour phenotype, proliferation was assessed by PCNA immunohistochemistry in formalin-fixed paraffin-embedded liver tissues (PCNA stain was carried out as part of Sam Murray's undergraduate project under my supervision). There were significantly more PCNA positive hepatocytes in Nfkb1$^{hep-/-}$ mice livers compared to Nfkb1$^{fl/fl}$ mice livers (p<0.0001) (Figure 5.4). High proliferative PCNA

positive hepatocytes were also significantly increased in Nfkb1$^{hep-/-}$ mice ($p<0.0001$), as well as PCNA positive tumour hepatocytes ($p=0.001$).

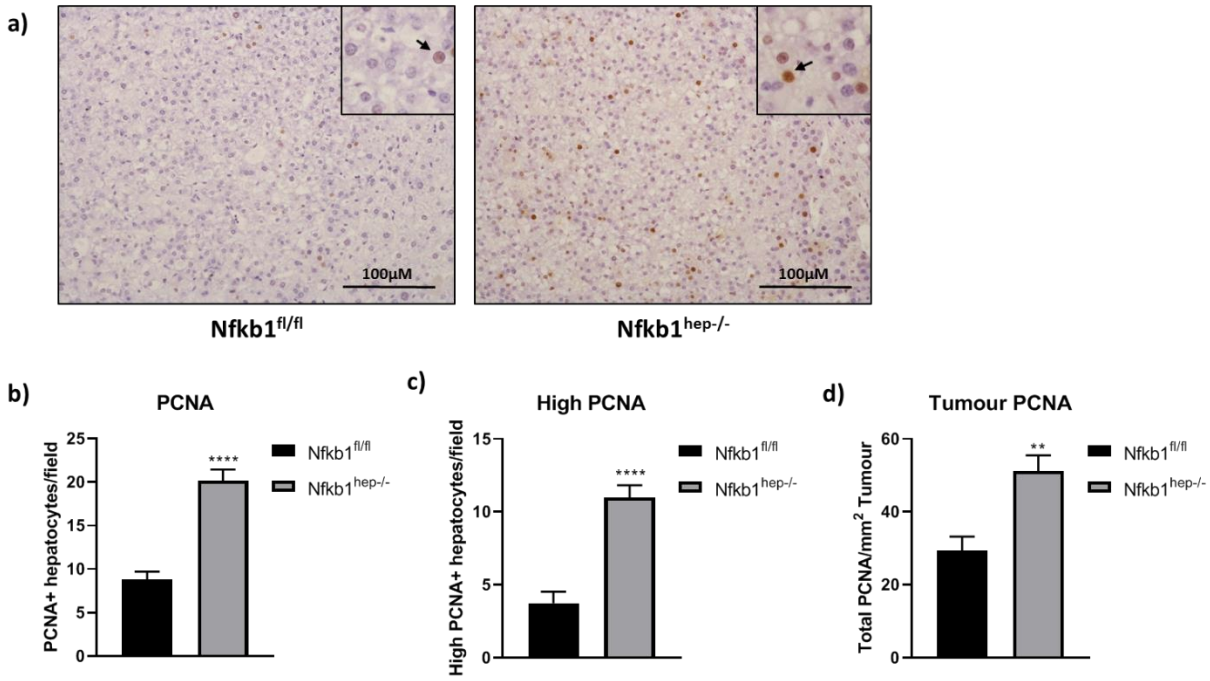

Figure 5.4 PCNA immunostain of Nfkb1$^{fl/fl}$ and Nfkb1$^{hep-/-}$ mice livers after 40 weeks DEN. Images show X20 PCNA immunostaining of formalin-fixed paraffin-embedded liver tissue in Nfkb1$^{fl/fl}$ and Nfkb1$^{hep-/-}$ mice (a). Graphs show average PCNA+ hepatocytes per field (b), average highly proliferative PCNA+ hepatocytes per field (c), and total PCNA staining per mm^2 tumour (d).

5.4.3 Higher HCC tumour grade in Nfkb1$^{hep-/-}$ mice

To characterise tumour burden, tumour grade was determined in Nfkb1$^{fl/fl}$ and Nfkb1$^{hep-/-}$ liver tumours using a grading system taking into account the presence of mitotic figures, proteoglycan globules, irregular nuclear contours, nuclear hyperchromasia and increased nuclear to cytoplasmic ratio, with grade 2 HCC being the most severe phenotype and HCA being the least severe (tumour grade was determined as part of Sam Murray's undergraduate project under my supervision). Nfkb1$^{hep-/-}$ mice liver tumours had overall higher tumour grades compared to Nfkb1$^{fl/fl}$ mice, with more HCC2 and HCC1 tumours (Figure 5.5). In Nfkb1$^{fl/fl}$ mice, 34.78% of tumours were HCC2, 30.43% were HCC1 and 34.78% were HCA. In Nfkb1$^{hep-/-}$ mice, 50.65% of tumours were HCC2, 29.87% were HCC1 and 19.48% were HCA.

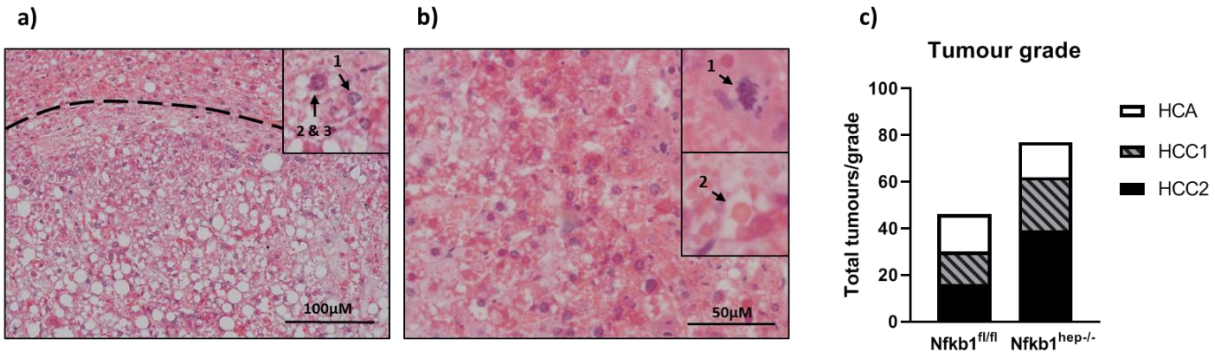

Figure 5.5 Liver tumour grade in Nfkb1$^{fl/fl}$ and Nfkb1$^{hep-/-}$ mice. Images show X10 H&E liver staining with irregular nuclear contour (1) and nuclear hyperchromasia and increased nuclear to cytoplasmic ratio (2&3) (a), and mitotic figures (1) and proteoglycan globules (2) (b). Graph shows tumour grade in Nfkb1$^{fl/fl}$ and Nfkb1$^{hep-/-}$ liver tumours.

5.5 Hepatocyte-specific Nfkb1 knock-out increases liver immune cell infiltration

HCC is accompanied by inflammation and immune cell infiltration (Rohr-Udilova et al., 2018), and Nfkb1 being an important regulator of immune responses, immune cell infiltration in the liver was characterised to determine the role of hepatocyte NF-κB1 as an immune effector in HCC.

5.5.1 Increased immune cell infiltration in hepatocyte Nfkb1 knock-out mice

H&E staining was carried out on Nfkb1$^{fl/fl}$ and Nfkb1$^{hep-/-}$ mice liver tissue to assess immune cell infiltration in the liver. Increased immune cell infiltration was observed in Nfkb1$^{hep-/-}$ mice compared to Nfkb1$^{fl/fl}$ mice (Figure 5.6). Total tumour area was also measured by H&E staining and was significantly increased in Nfkb1$^{hep-/-}$ mice compared to Nfkb1$^{fl/fl}$ mice (p=0.0005). Additionally, tumour and liver TNFα gene expression was determined by RT-qPCR, and appeared increased in Nfkb1$^{hep-/-}$ mice though this did not reach significance (p=0.0952).

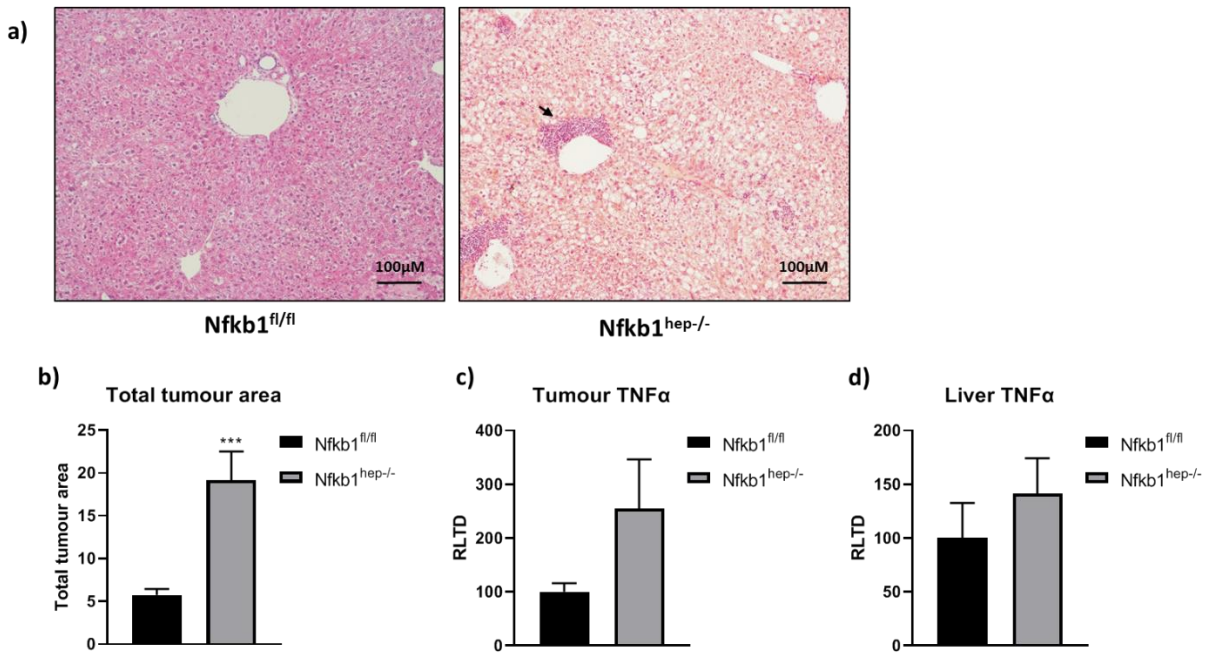

Figure 5.6 H&E stain and TNFα gene expression of Nfkb1$^{fl/fl}$ and Nfkb1$^{hep-/-}$ liver tissue. Images show X10 H&E staining of Nfkb1$^{fl/fl}$ and Nfkb1$^{hep-/-}$ liver tissue with immune cell infiltration (a). Graphs show total tumour area (b), tumour TNFα gene expression (c) and liver TNFα expression (d).

5.5.2 Increased neutrophil infiltration in hepatocyte Nfkb1 knock-out mice

To determine which immune cells were significantly increased in the livers of Nfkb1$^{hep-/-}$ mice compared to Nfkb1$^{fl/fl}$, immunostaining of several different immune cells was carried out on formalin-fixed paraffin-embedded liver tissues. NIMP immunohistochemistry was carried out to assess neutrophil infiltration in the liver. NIMP positive staining was significantly increased in Nfkb1$^{hep-/-}$ mice compared to Nfkb1$^{fl/fl}$ mice ($p=0.048$), indicating increased migration of neutrophils to the liver in Nfkb1$^{hep-/-}$ mice (Figure 5.7). Staining was visible in the tumours and the surrounding tissue. This demonstrates a role for NF-κB1 p50 in limiting neutrophil migration to the liver, which is associated with a worse outcome. This result mirrors what has previously been observed in Nfkb1$^{-/-}$ mice, whereby a significant increase in neutrophil infiltration in the liver was seen compared to WT mice. It is important to note however that some monocytes can also be NIMP positive, therefore not all the NIMP positive cells counted can be attributed to neutrophils.

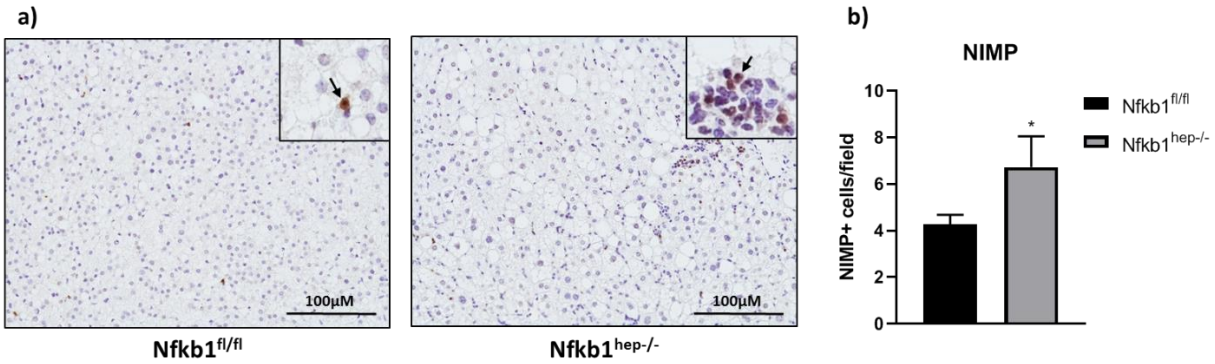

Figure 5.7 NIMP liver immunostaining in Nfkb1$^{fl/fl}$ and Nfkb1$^{hep-/-}$ mice. Images show X20 NIMP immunostaining in formalin-fixed paraffin-embedded liver tissue from Nfkb1$^{fl/fl}$ and Nfkb1$^{hep-/-}$ mice (a). Graph shows average NIMP+ staining per high-powered field in Nfkb1$^{fl/fl}$ and Nfkb1$^{hep-/-}$ mice livers (x20 magnification) (b).

5.5.3 Neutrophil chemokine S100A9, CXCL1 and CXCL2 expression unaltered in hepatocyte Nfkb1 knock-out mice

In order to understand how more neutrophils were recruited to Nfkb1$^{hep-/-}$ livers, the gene expression of neutrophil chemoattractant chemokines S100A9, CXCL1 and CXCL2 was determined in the tumour and in the liver by RT-qPCR. Surprisingly, no significant difference was found between Nfkb1$^{fl/fl}$ and Nfkb1$^{hep-/-}$ mice in the expression of these genes in the tumour and in the liver (Figure 5.8). This suggests that hepatocyte Nfkb1 p50 does not regulate the expression of the S100A9, CXCL1 and CXCL2 chemokines. Since Nfkb1$^{-/-}$ mice exhibited increased S100A9, CXCL1 and CXCL2 expression, hepatocyte NF-κB1 p50 must be regulating the expression of these genes in other liver cell types, such as immune cells. Other chemokines may be responsible for attracting more neutrophils to Nfkb1$^{hep-/-}$ mice livers, such as CXCL8. Also, since NIMP can also stain for monocytes, the increase in NIMP positive cells observed in Nfkb1$^{hep-/-}$ may be attributed to monocytes rather than neutrophils.

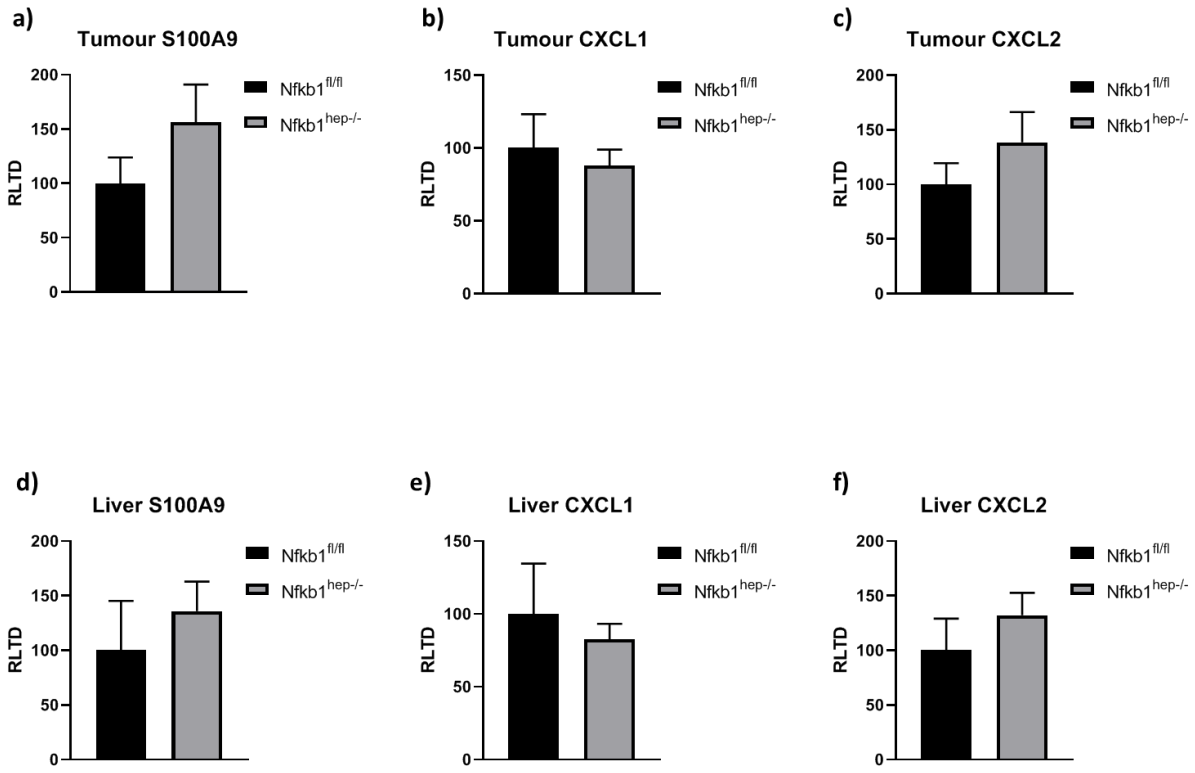

Figure 5.8 Gene expression of neutrophil chemoattractant chemokines S100A9, CXCL1 and CXCL2 in tumour and liver tissue. Graphs show gene expression determined by RT-qPCR of tumour S100A9 (a), CXCL1 (b) and CXCL2 (c) and of liver S100A9 (d), CXCL1 (e) and CXCL2 (f) in $Nfkb1^{fl/fl}$ and $Nfkb1^{hep-/-}$ mice.

5.5.4 Increased monocyte and macrophage infiltration in hepatocyte Nfkb1 knock-out mice

To assess the role of hepatocyte p50 in modulating the recruitment of monocytes/macrophages to the liver in DEN-induced HCC, CD68 immunohistochemistry was carried out on formalin-fixed paraffin-embedded liver tissue from $Nfkb1^{fl/fl}$ and $Nfkb1^{hep-/-}$ mice. Interestingly, significantly more CD68 positively stained cells were found in $Nfkb1^{hep-/-}$ mice compared to $Nfkb1^{fl/fl}$ mice ($p=0.0009$) (Figure 5.9). This reflects what was observed in the acute CCl_4 liver injury model where more F4/80 positive cells were found in $Nfkb1^{hep-/-}$ mice. It can thus be concluded that hepatocyte NF-κB1 p50 modulates monocyte chemotaxis to the liver or monocyte differentiation into macrophages in DEN-induced HCC.

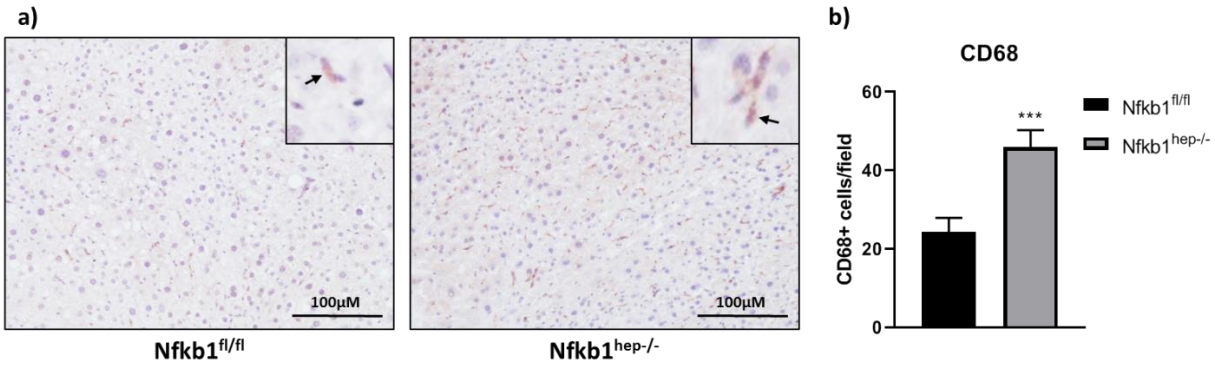

Figure 5.9 CD68 liver immunostain in Nfkb1$^{fl/fl}$ and Nfkb1$^{hep-/-}$ mice. Images show X20 CD68 immunostaining in formalin-fixed paraffin-embedded liver tissue from Nfkb1$^{fl/fl}$ and Nfkb1$^{hep-/-}$ mice (a). Graph shows average CD68+ cell count per field in Nfkb1$^{fl/fl}$ and Nfkb1$^{hep-/-}$ mice (b).

5.5.5 Monocyte chemoattractant chemokine CCL2 and CCL5 expression unaltered in hepatocyte Nfkb1 knock-out mice

To understand what drives the increased influx of monocytes and macrophages in Nfkb1$^{hep-/-}$ mice livers, gene expression of monocyte chemoattractant chemokines CCL2 and CCL5 was determined by RT-qPCR in the tumour and in the liver. Surprisingly, no significant difference in CCL2 or CCL5 expression was observed between Nfkb1$^{fl/fl}$ and Nfkb1$^{hep-/-}$ mice in the tumour and in the liver. This suggests that other chemokines are responsible for attracting monocytes to the liver and/or differentiating them into macrophages, such as CCL7 for example.

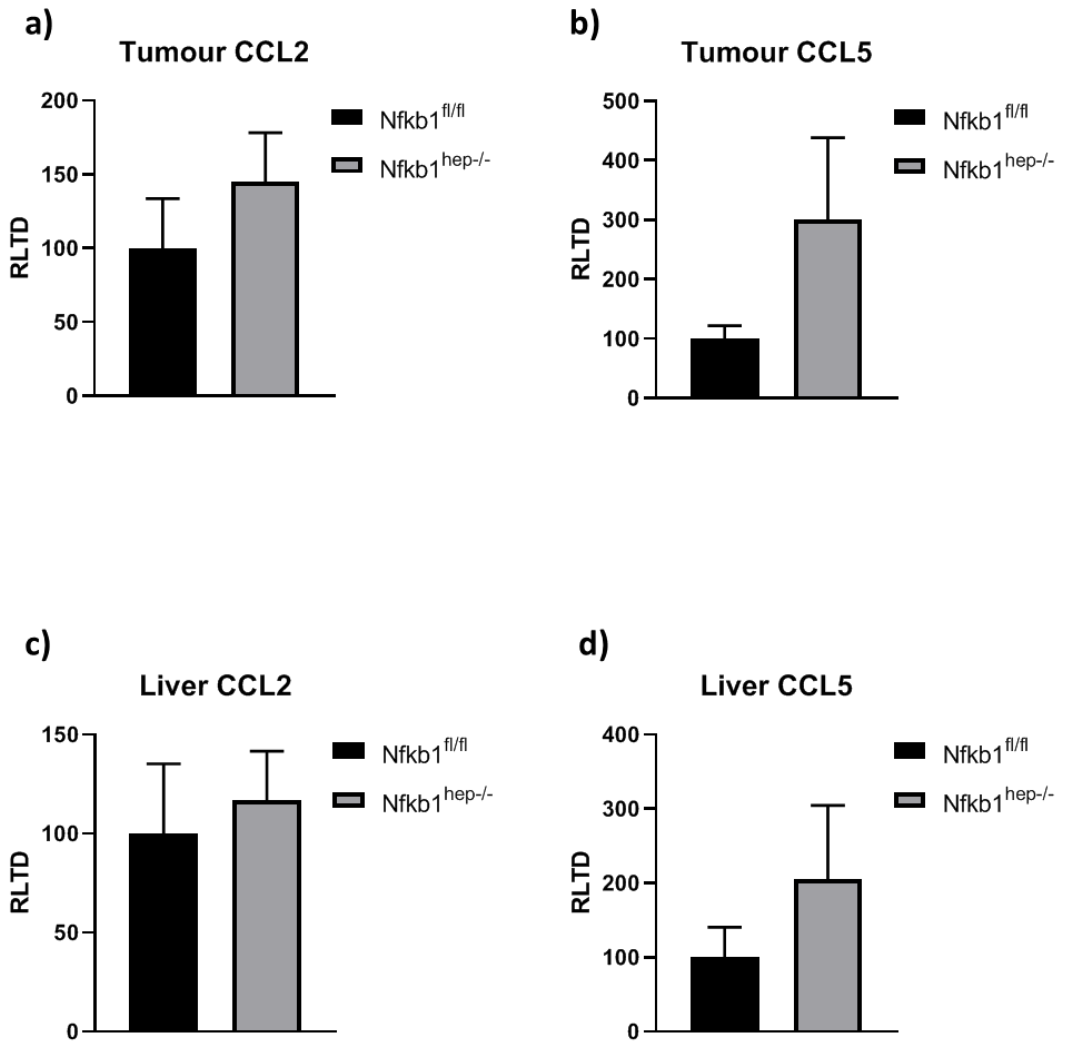

Figure 5.10 Tumour and liver gene expression of CCL2 and CCL5 in Nfkb1$^{fl/fl}$ and Nfkb1$^{hep-/-}$ mice. Graphs show tumour expression of CCL2 (a) and CCL5 (b) and liver expression of CCL2 (c) and CCL5 (d) in Nfkb1$^{fl/fl}$ and Nfkb1$^{hep-/-}$ mice, determined by RT-qPCR.

5.5.6 Lack of hepatocyte NF-κB1 does not affect T cell liver infiltration or T cell subsets

To further investigate the role of hepatocyte NF-κB1 p50 in the recruitment of immune cells to the liver in DEN-induced HCC, liver T cell infiltration and T cell subsets was assessed by immunohistochemistry of formalin-fixed paraffin-embedded liver tissue from Nfkb1$^{fl/fl}$ and Nfkb1$^{hep-/-}$ mice.

CD3 immunostaining was carried out to determine overall T cell recruitment to the liver. No significant difference in CD3 positive cells was found between Nfkb1$^{fl/fl}$ and Nfkb1$^{hep-/-}$ mice, though there appeared to be slightly more CD3 positive cells in

Nfkb1$^{hep-/-}$ mice (p=0.0959). This suggests that hepatocyte NF-κB1 p50 does not significantly modulate T cell infiltration in the liver in DEN-induced HCC.

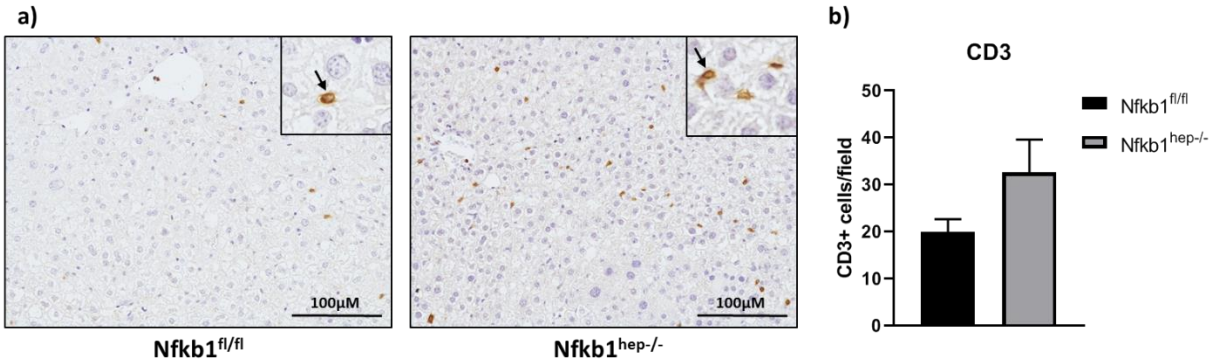

Figure 5.11 CD3 liver immunostain in Nfkb1$^{fl/fl}$ and Nfkb1$^{hep-/-}$ mice. Images show X20 CD3 immunostaining of formalin-fixed paraffin-embedded liver tissue from Nfkb1$^{fl/fl}$ and Nfkb1$^{hep-/-}$ mice (a). Graph shows average CD3 positive cell count per field in Nfkb1$^{fl/fl}$ and Nfkb1$^{hep-/-}$ mice (b).

While no significant difference was observed in overall T cell infiltration in the liver between Nfkb1$^{fl/fl}$ and Nfkb1$^{hep-/-}$ mice, it was hypothesized that hepatocyte NF-κB1 p50 may modulate the type of T cell that is recruited to the liver. T helper cells (CD4+), cytotoxic T cells (CD8+) and regulatory T cells (FOXP3+) recruitment to the liver was therefore assessed by immunohistochemistry in Nfkb1$^{fl/fl}$ and Nfkb1$^{hep-/-}$ liver tissue. No significant difference in CD4 positive cells (Figure 5.12), CD8 positive cells (Figure 5.13) or FOXP3 positive cells (Figure 5.14) was observed between Nfkb1$^{fl/fl}$ and Nfkb1$^{hep-/-}$ mice. However, CD8 positive cells appeared slightly increased in Nfkb1$^{hep-/-}$ mice (p=0.1523), as observed with CD3 positive cells, with infiltration in tumour and surrounding tissue, suggesting that NF-κB1 p50 may limit cytotoxic CD8+ T cell recruitment to the liver.

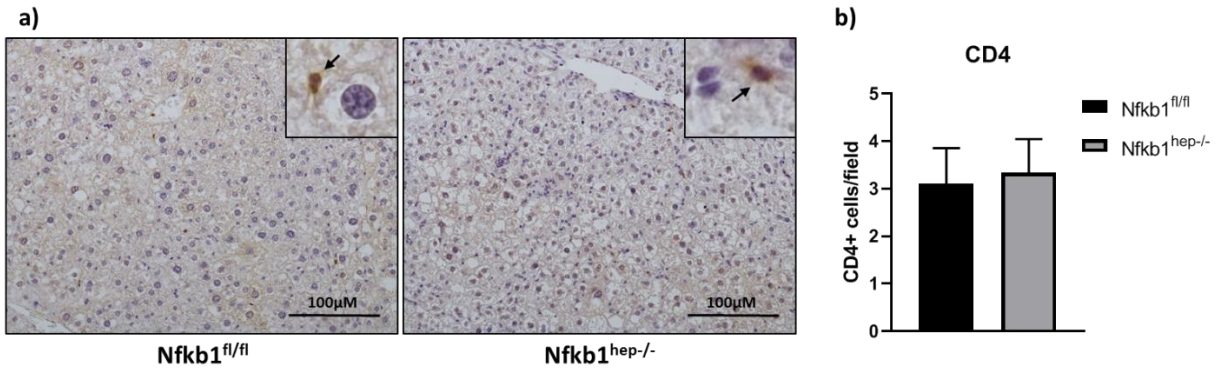

Figure 5.12 CD4 liver immunostaining in Nfkb1$^{fl/fl}$ and Nfkb1$^{hep-/-}$ mice. Images show X20 CD4 liver immunostaining in Nkb1$^{fl/fl}$ and Nfkb1$^{hep-/-}$ mice (a). Graph shows average CD4 positive cells per field in Nfkb1$^{fl/fl}$ and Nfkb1$^{hep-/-}$ mice (b).

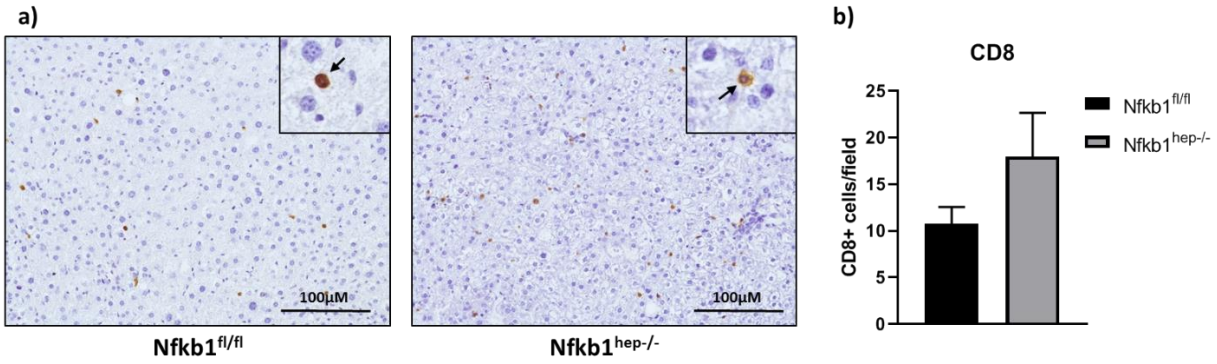

Figure 5.13 CD8 liver immunostaining in Nfkb1$^{fl/fl}$ and Nfkb1$^{hep-/-}$ mice. Images show X20 CD8 liver immunostaining in Nkb1$^{fl/fl}$ and Nfkb1$^{hep-/-}$ mice (a). Graph shows average CD8 positive cells per field in Nfkb1$^{fl/fl}$ and Nfkb1$^{hep-/-}$ mice (b).

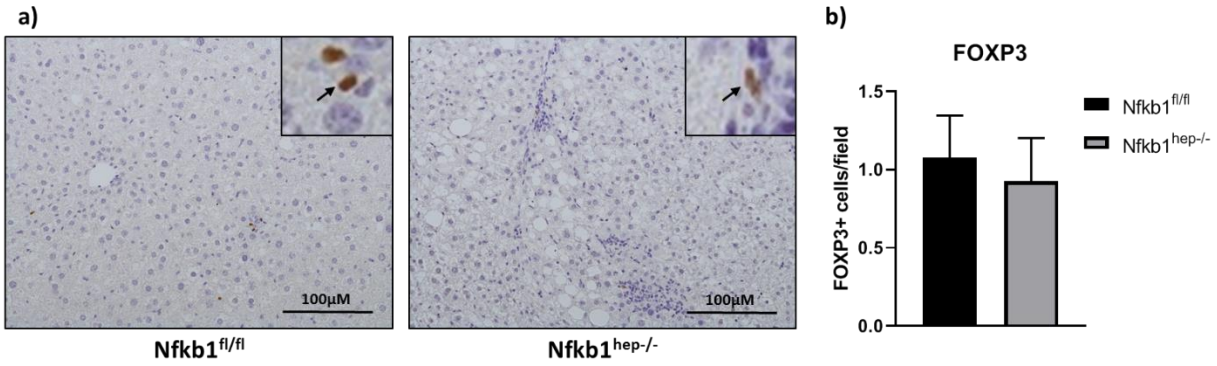

Figure 5.14 FOXP3 liver immunostaining in Nfkb1$^{fl/fl}$ and Nfkb1$^{hep-/-}$ mice. Images show X20 FOXP3 liver immunostaining in Nkb1$^{fl/fl}$ and Nfkb1$^{hep-/-}$ mice (a). Graph shows average FOXP3 positive cells per field in Nfkb1$^{fl/fl}$ and Nfkb1$^{hep-/-}$ mice (b).

5.5.7 Lack of hepatocyte NF-κB1 does not affect B cell liver infiltration

Nfkb1$^{-/-}$ mice are known to have B cell defects. It was therefore hypothesized that hepatocyte Nfkb1 p50 may play a role in this. B220 immunohistochemistry, which is specific for B cells, was thus carried out on formalin-fixed paraffin-embedded liver tissue in Nfkb1$^{fl/fl}$ and Nfkb1$^{hep-/-}$ mice. However no significant difference in B220 positive cells was found between Nfkb1$^{fl/fl}$ and Nfkb1$^{hep-/-}$ mice. This shows that hepatocyte NF-κB1 p50 does not modulate B cell recruitment to the liver in DEN-induced HCC.

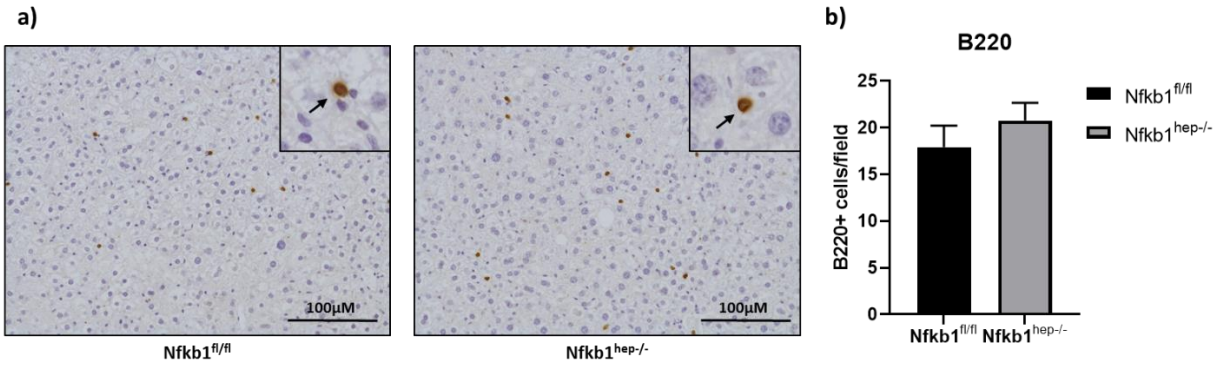

Figure 5.15 B220 liver immunostain in Nfkb1$^{fl/fl}$ and Nfkb1$^{hep-/-}$ mice. Images show X20 B220 liver immunostaining in Nkb1$^{fl/fl}$ and Nfkb1$^{hep-/-}$ mice (a). Graph shows average B220 positive cells per field in Nfkb1$^{fl/fl}$ and Nfkb1$^{hep-/-}$ mice (b).

5.6 Hepatocyte NF-κB1 regulation of apoptosis and oncogene expression

Dysregulation of cell survival and apoptosis, as well as oncogene overexpression is widely associated with carcinogenesis (Plati et al., 2008). NF-κB1 p50 is known to regulate the expression of genes that modulate cell survival and apoptosis, notably Gadd45β, Bcl-xL and Bcl-2. The expression of these genes was therefore determined by RT-qPCR in Nfkb1$^{fl/fl}$ and Nfkb1$^{hep-/-}$ tumour and liver tissue. Apoptotic signalling was also evaluated through protein expression of phosphorylated JNK and phosphorylated ERK, both marks of apoptotic signalling activation, as well as through protein expression of cleaved caspase 3, activated in anti-apoptotic signalling, cyclin D1, a cell cycle control protein found overexpressed in certain cancers, and γH2AX, a marker for DNA damage which is also overexpressed in certain cancers.

5.6.1 Anti-apoptotic genes and oncogenes expression upregulated in the absence of hepatocyte NF-κB1 in liver tumours but not in adjacent liver tissue

Gadd45β, Bcl-xL and Bcl-2 tumour and liver gene expression was determined by RT-qPCR. These genes were all significantly upregulated in Nfkb1$^{hep-/-}$ tumours compared to Nfkb1$^{fl/fl}$ control tumours (p=0.0019 for Gadd45β, p=0.049 for Bcl-xL and p=0.0261 for Bcl-2), but not in non-tumorous adjacent liver tissue (Figure 5.16). These results show that hepatocyte NF-κB1 p50 controls the expression of oncogenic and anti-apoptotic genes Gadd45β, Bcl-xL and Bcl-2 in DEN-induced HCC tumours. This suggests that hepatocyte NF-κB1 p50 limits anti-apoptotic signalling, and therefore that mice lacking hepatocyte NF-κB1 p50 have less cells undergoing apoptosis.

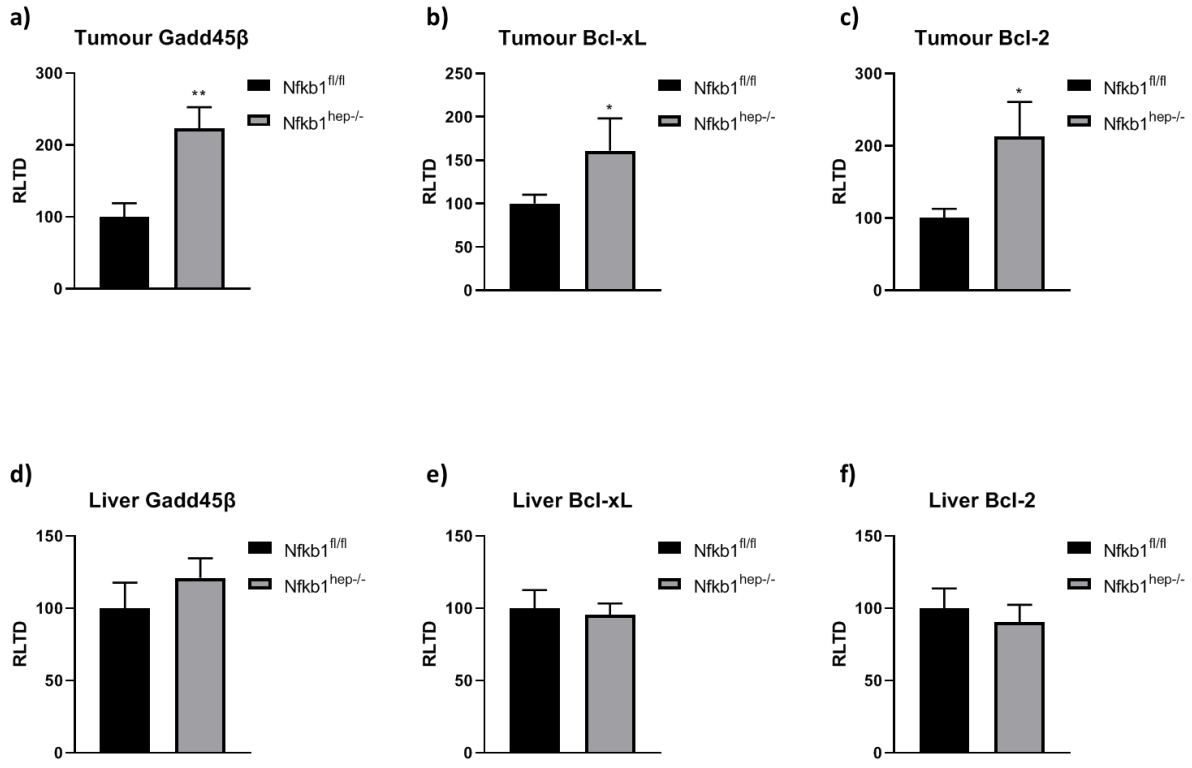

Figure 5.16 Tumour and liver gene expression of Gadd45β, Bcl-xL and Bcl-2. Graphs show gene expression of tumour Gadd45β (a), Bcl-xL (b) and Bcl-2 (c), and of liver Gadd45β (d), Bcl-xL (e) and Bcl-2 (f), determined by RT-qPCR.

5.6.2 Hepatocyte NF-κB1 does not modulate anti-apoptotic gene and oncogene expression at the protein level

To confirm the increased tumour expression of Bcl-xL and Bcl-2 in Nfkb1$^{hep-/-}$ mice compared to Nfkb1$^{fl/fl}$ mice at the protein level, western blot analysis was carried out in tumour and non-tumorous liver tissue from Nfkb1$^{fl/fl}$ and Nfkb1$^{hep-/-}$ mice. Surprisingly, Bcl-2 and Bcl-xL tumour protein expression showed little difference between Nfkb1$^{fl/fl}$ and Nfkb1$^{hep-/-}$ mice (Figure 5.17). Interestingly, Bcl-2 and Bcl-xL liver protein expression appeared slightly increased in Nfkb1$^{hep-/-}$ mice compared to control Nfkb1$^{fl/fl}$ mice. This shows that the increased gene expression of Bcl-2 and Bcl-xL in Nfkb1$^{hep-/-}$ mice tumours is not reflected at the protein level, therefore while hepatocyte p50 affects the gene expression level of Bcl-2 and Bcl-xL in DEN-induced HCC tumours, it does not affect the anti-apoptotic signalling function of the translated proteins. Additionally, western blot analysis was carried out on Nfkb1$^{fl/fl}$ and Nfkb1$^{hep-/-}$ tumours samples for γH2AX expression to assess the role of hepatocyte Nfkb1 in DNA damage, for cyclin D1 to assess the role of hepatocyte Nfkb1 p50 in cell cycle control, and for cleaved caspase 3 to further assess the role of hepatocyte NF-κB1 p50 in the modulation of apoptosis. No clear difference was observed in the tumour expression of these proteins between Nfkb1$^{fl/fl}$ and Nfkb1$^{hep-/-}$ mice. β-actin expression was used as a loading control.

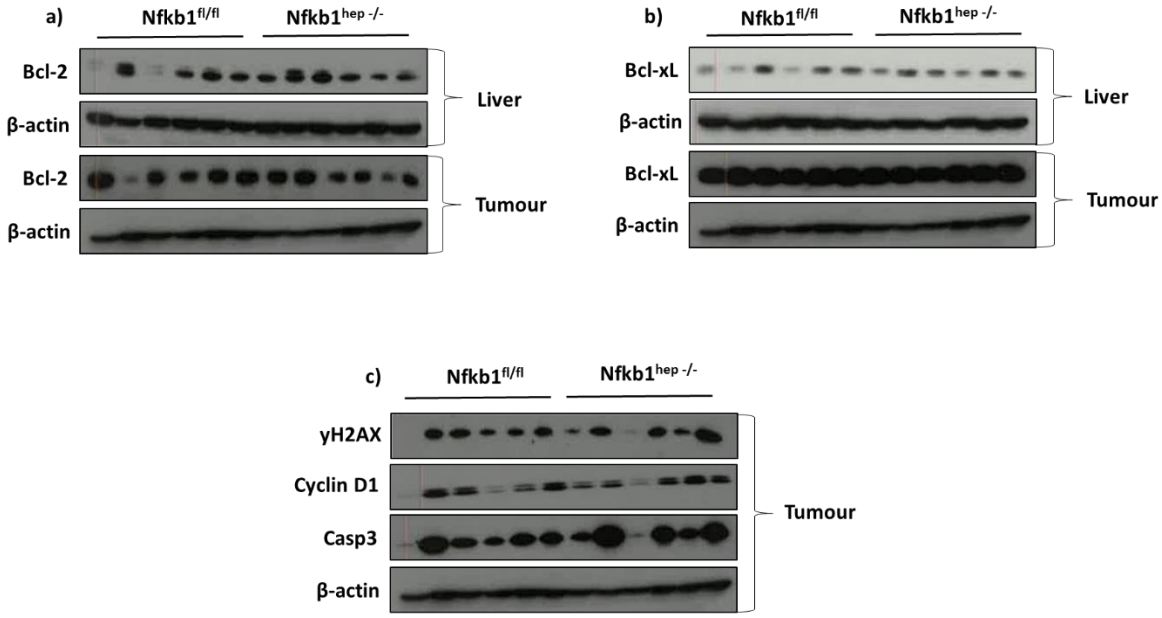

Figure 5.17 Liver and tumour expression of apoptotic signalling proteins. Western blots show Bcl-2 liver and tumour expression (a), Bcl-xL liver and tumour expression (b), and γH2AX, cyclin D1 and cleaved caspase 3 tumour expression (c) in Nfkb1$^{fl/fl}$ and Nfkb1$^{hep-/-}$ mice.

To further assess the role of hepatocyte NF-κB1 p50 in apoptotic signalling, western blot analysis was carried out to compare phosphorylated ERK (p-ERK) and phosphorylated JNK (p-JNK) expression between Nfkb1$^{fl/fl}$ and Nfkb1$^{hep-/-}$ mice, ERK and JNK being phosphorylated when activated, leading to apoptotic signalling. No difference in p-ERK expression was apparent between Nfkb1$^{fl/fl}$ and Nfkb1$^{hep-/-}$ mice tumour and liver tissue (Figure 5.18). Total ERK was also expressed at comparable levels in Nfkb1$^{fl/fl}$ and Nfkb1$^{hep-/-}$ tumours and livers. p-JNK protein expression levels in the tumour appeared to be slightly increased in some Nfkb1$^{hep-/-}$ mice compared to control Nfkb1$^{fl/fl}$ mice, while total JNK tumour expression levels were similar. No difference in p-JNK protein expression was observed in the liver however.

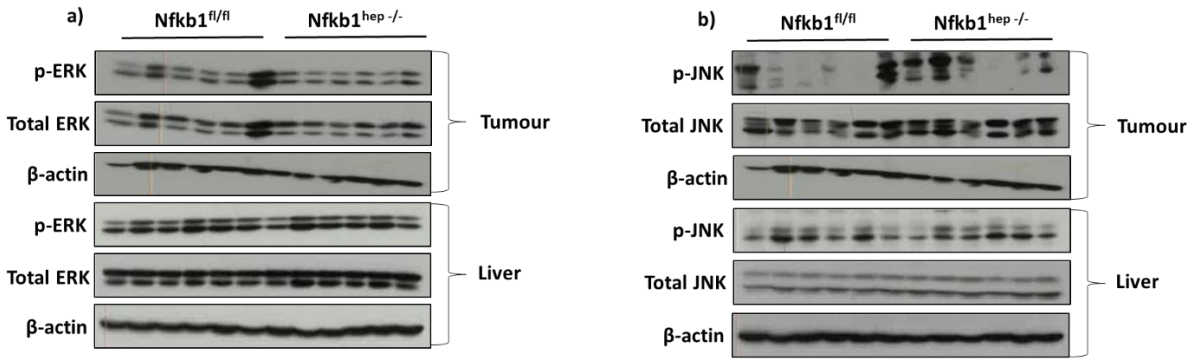

Figure 5.18 Tumour and liver expression of ERK and JNK signalling proteins. Western blots show p-ERK and total ERK tumour and liver protein expression (a), and p-JNK and total JNK tumour and liver protein expression (b) in Nfkb1$^{fl/fl}$ and Nfkb1$^{hep-/-}$ mice.

5.6.3 Lack of NF-κB1 does not alter cleaved caspase 3 protein expression

To further confirm the similarity in cleaved caspase 3 protein expression between Nfkb1$^{fl/fl}$ and Nfkb1$^{hep-/-}$ mice, cleaved caspase 3 immunohistochemistry was carried out on formalin-fixed paraffin-embedded liver tissue from Nfkb1$^{fl/fl}$ and Nfkb1$^{hep-/-}$ mice. Unsurprisingly, no significant difference in average cleaved caspase 3 positive hepatocytes per field was observed between Nfkb1$^{fl/fl}$ and Nfkb1$^{hep-/-}$ mice. This indicated that hepatocyte NF-κB1 p50 does indeed not modulate apoptotic signalling in DEN-induced HCC.

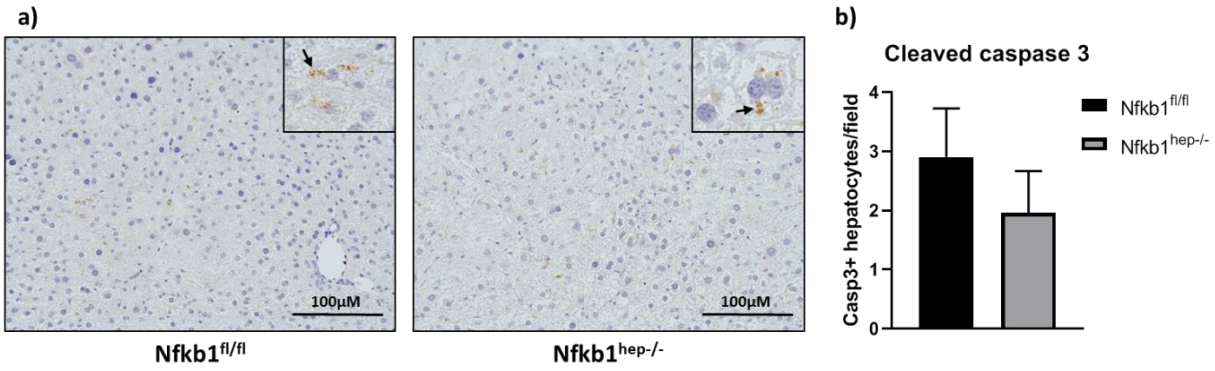

Figure 5.19 Cleaved caspase 3 liver immunostain in Nfkb1$^{fl/fl}$ and Nfkb1$^{hep-/-}$ mice. Images show X20 cleaved caspase 3 immunostaining of formalin-fixed paraffin-embedded liver tissue from Nfkb1$^{fl/fl}$ and Nfkb1$^{hep-/-}$ mice (a). Graph shows average cleaved caspase 3 positive hepatocyte cell count per field in Nfkb1$^{fl/fl}$ and Nfkb1$^{hep-/-}$ mice (b).

To further confirm the similarity in γH2AX protein expression and thus DNA damage between Nfkb1$^{fl/fl}$ and Nfkb1$^{hep-/-}$ mice, γH2AX immunohistochemistry was carried out on formalin-fixed paraffin-embedded liver tissue from Nfkb1$^{fl/fl}$ and Nfkb1$^{hep-/-}$ mice. No significant difference in average γH2AX positive hepatocytes per field was found between Nfkb1$^{fl/fl}$ and Nfkb1$^{hep-/-}$ mice, suggesting that lack of hepatocyte NF-κB1 does not affect DNA damage.

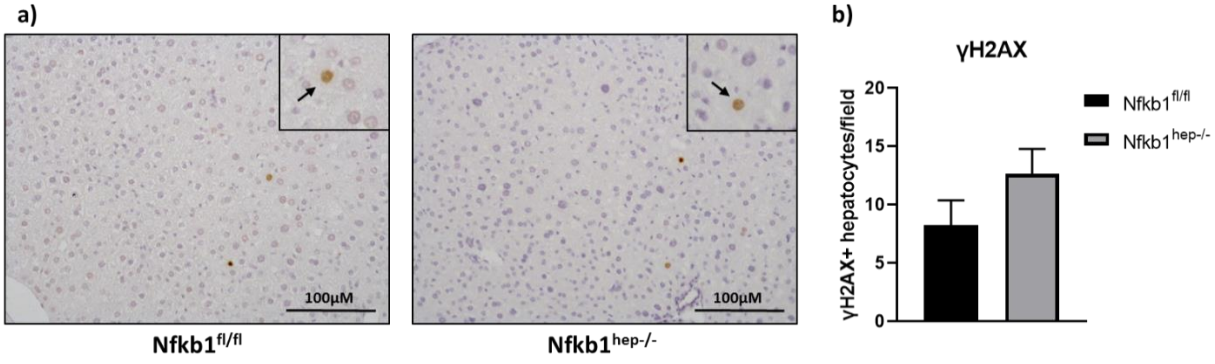

Figure 5.20 γH2AX liver immunostain in Nfkb1$^{fl/fl}$ and Nfkb1$^{hep-/-}$ mice. Images show X20 γH2AX immunostaining of formalin-fixed paraffin-embedded liver tissue from Nfkb1$^{fl/fl}$ and Nfkb1$^{hep-/-}$ mice (a). Graph shows average γH2AX positive hepatocyte cell count per field in Nfkb1$^{fl/fl}$ and Nfkb1$^{hep-/-}$ mice (b).

5.7 NF-κB subunit expression comparison in Nfkb1 floxed and Nfkb1 hepatocyte knock-out mice

In order to determine whether any compensatory NF-κB subunit expression was occurring in the absence of NF-κB1 p50, western blot analysis was performed to evaluate cRel, p65 and p52 protein expression in the liver in Nfkb1$^{fl/fl}$ and Nfkb1$^{hep-/-}$ mice. These subunits showed similar expression levels in Nfkb1$^{fl/fl}$ and Nfkb1$^{hep-/-}$ mice, indicating that no compensatory NF-κB subunit expression took place in Nfkb1$^{hep-/-}$ mice (Figure 5.21). p52 protein expression appeared slightly decreased in 2 Nfkb1$^{hep-/-}$ mice compared to Nfkb1$^{fl/fl}$ control mice.

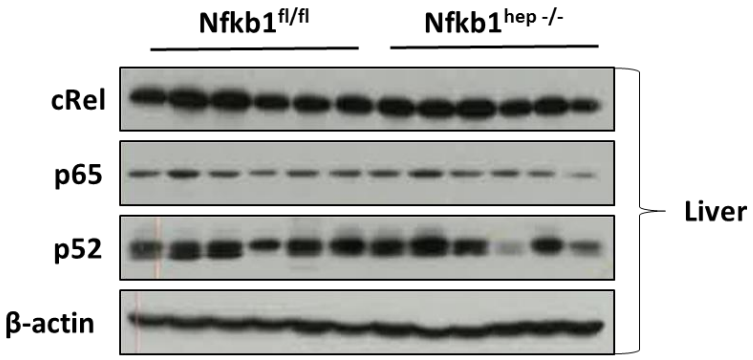

Figure 5.21 NF-κB subunit protein expression in Nfkb1$^{fl/fl}$ and Nfkb1$^{hep-/-}$ mice. Western blots show protein expression of NF-κB subunits cRel, p65 and p52 in Nfkb1$^{fl/fl}$ and Nfkb1$^{hep-/-}$ mice livers. β-actin protein expression was used as a loading control.

5.8 Differential mRNA expression profile in Nfkb1 hepatocyte knock-out mice tumours

15 liver tumour RNA samples (5 Nfkb1$^{fl/fl}$, 5 Nfkb1$^{hep-/-}$ and 5 Nfkb1$^{-/-}$) were sequenced on an Illumina NextSeq (high output), 75bp single end reads (Centre for LIFE, Newcastle University), in order to compare liver tumour mRNA expression profiles in Nfkb1$^{fl/fl}$, Nfkb1$^{hep-/-}$ and Nfkb1$^{-/-}$ mice, in a 40-week DEN-induced HCC model. RNA-Seq analysis was carried out by Simon Cockell, Newcastle University.

PCA (Principal Component Analysis) was performed to project the multivariate data vector of each RNA-Seq sample into a two-dimensional plot, such that the spatial

arrangement of the points in the plot reflects the overall data (dis)similarity between the samples.

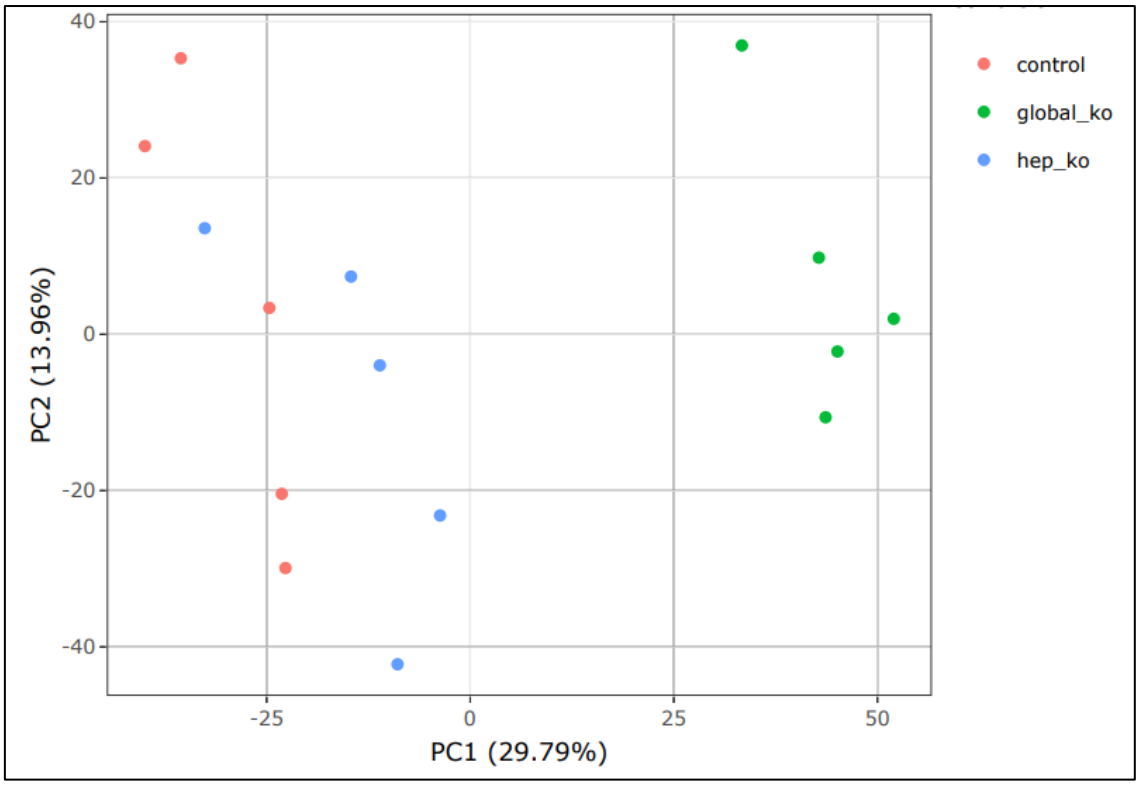

Figure 5.22 PCA plot comparing Nfkb1$^{-/-}$, Nfkb1$^{hep-/-}$ and Nfkb1$^{fl/fl}$ samples. Nfkb1$^{-/-}$ samples are represented by green dots, Nfkb1$^{hep-/-}$ samples are represented by blue dots and Nfkb1$^{fl/fl}$ samples are represented by red dots.

A sample distance heatmap was also generated, which shows the Euclidian distance between the samples; the lower this distance, the more closely related 2 samples are. Clustering is then applied over this distance, to give an idea of the relatedness of the samples.

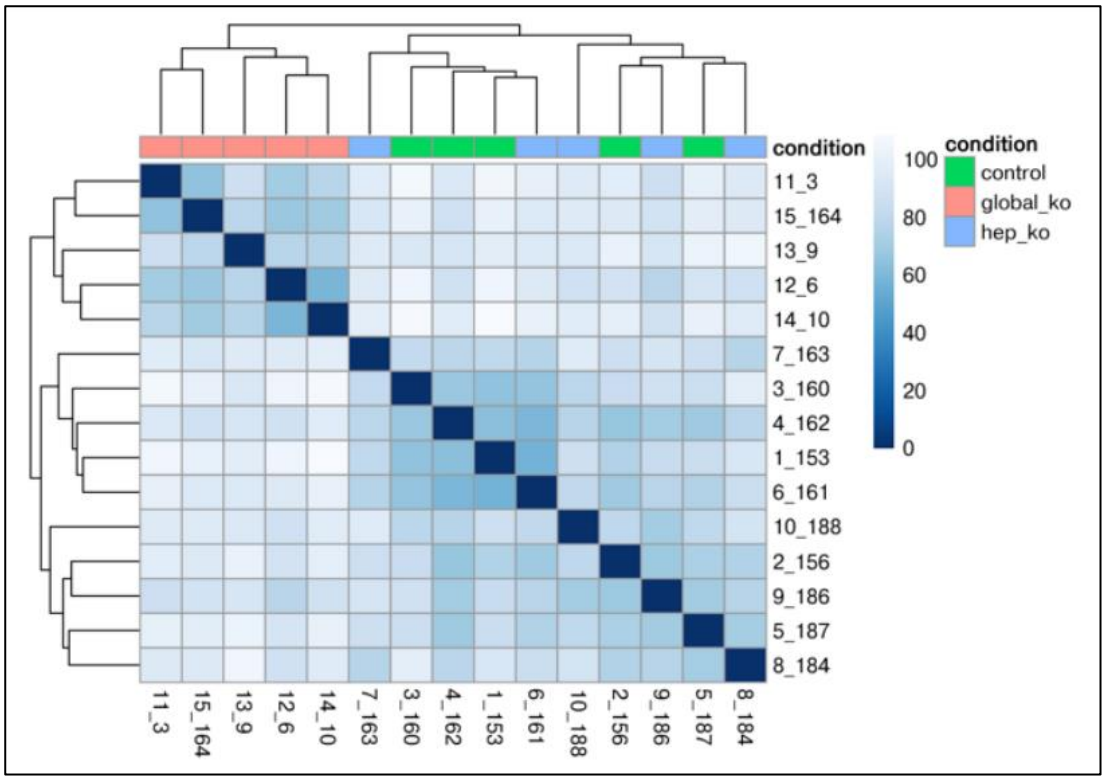

Figure 5.23 Sample distance heatmap comparing Nfkb1$^{-/-}$, Nfkb1$^{hep-/-}$ and Nfkb1$^{fl/fl}$ samples. Nfkb1$^{-/-}$ samples are represented in red, Nfkb1$^{hep-/-}$ samples are represented in blue and Nfkb1$^{fl/fl}$ samples are represented in green.

From these two plots, it can be seen that the 'Global KO' samples form a group, separated from the other samples. The 'Hep KO' samples overlap with the controls somewhat, but there may be sufficient difference between the samples as groups for subsequent analysis to be informative.

Comparing the Global KO samples to the controls gives 2,919 genes with a fold-change > 2 in either direction and an adjusted p-value < 0.05. Here is a volcano plot showing the DEGs (Differential Expression of Genes) for this comparison (FC>2, p<0.05):

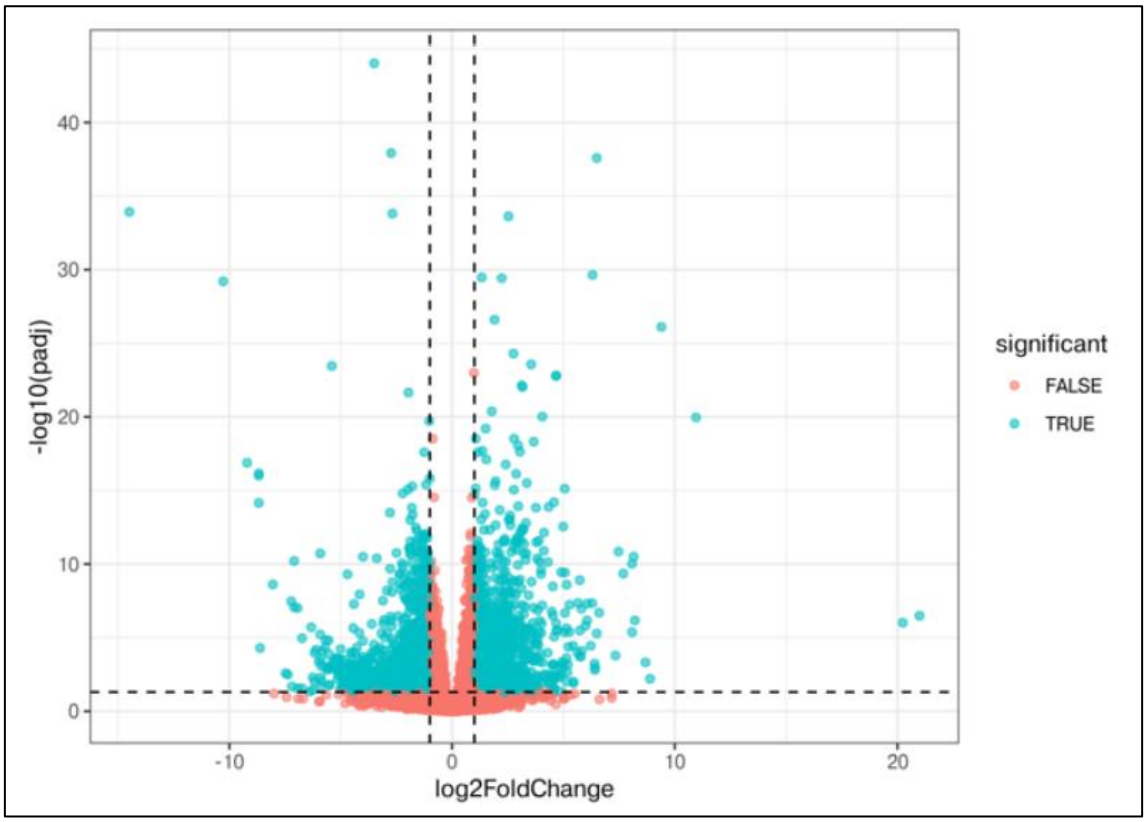

Figure 5.24 Volcano plot comparing Nfkb1$^{-/-}$ and Nfkb1$^{fl/fl}$ samples. Differentially expressed genes are represented by blue dots. Upregulated genes are shown in positive log2FoldChange and downregulated genes are shown in negative log2FoldChange.

Comparing the Hep KO samples to the controls gives 96 genes with a fold-change > 2 in either direction and an adjusted p-value < 0.05. Here is a volcano plot showing the DEGs for this comparison (FC>2, p<0.05):

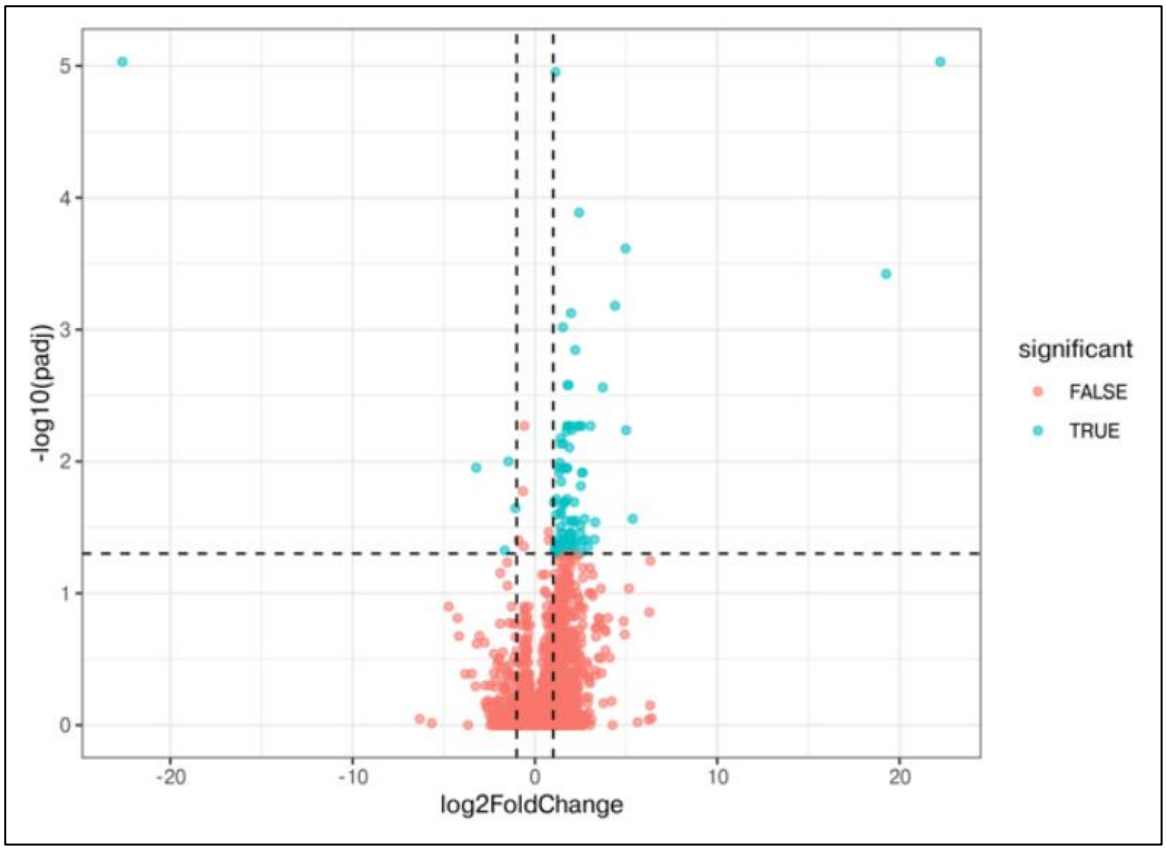

Figure 5.25 Volcano plot comparing Nfkb1$^{hep-/-}$ and Nfkb1$^{fl/fl}$ samples. Differentially expressed genes are represented by blue dots. Upregulated genes are shown in positive log2FoldChange and downregulated genes are shown in negative log2FoldChange.

Comparing the Global KO samples to the Hep KO samples gives 1,841 genes with a fold-change > 2 in either direction and an adjusted p-value < 0.05. Here is a volcano plot showing the DEGs for this comparison (FC>2, p<0.05):

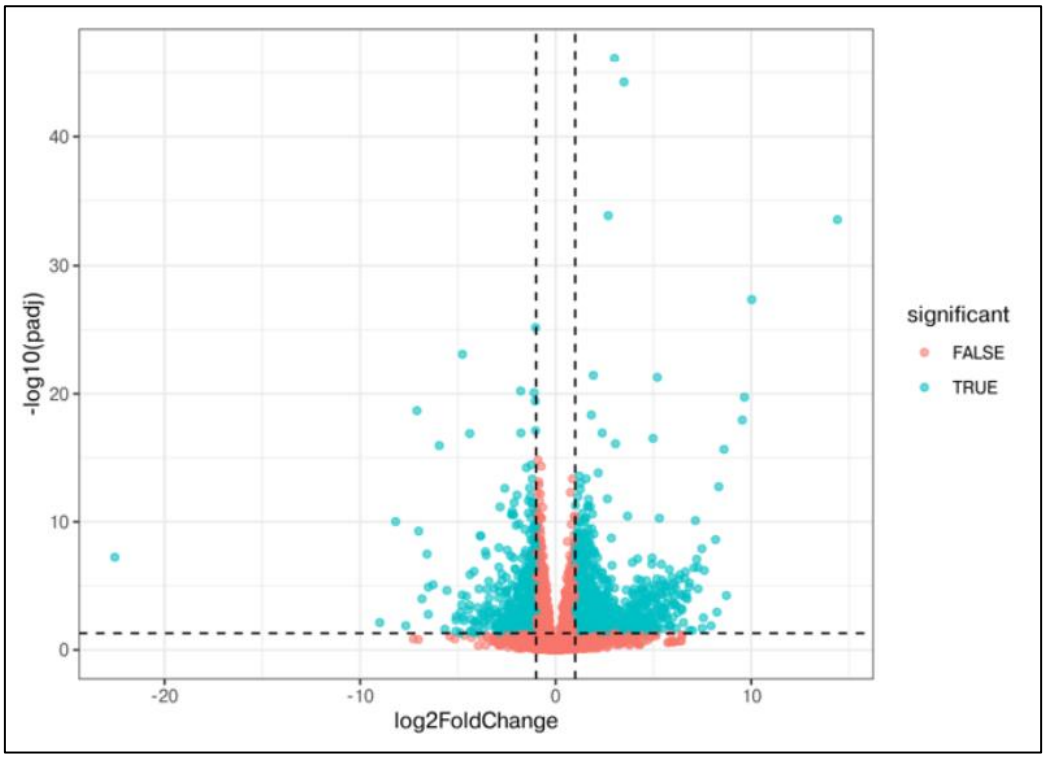

Figure 5.26 Volcano plot comparing Nfkb1$^{-/-}$ and Nfkb1$^{hep-/-}$ samples. Differentially expressed genes are represented by blue dots. Upregulated genes are shown in positive log2FoldChange and downregulated genes are shown in negative log2FoldChange.

Gene ontology and pathway analysis was also performed, filtered at FC>2, p<0.05 and removing genes with no annotation.

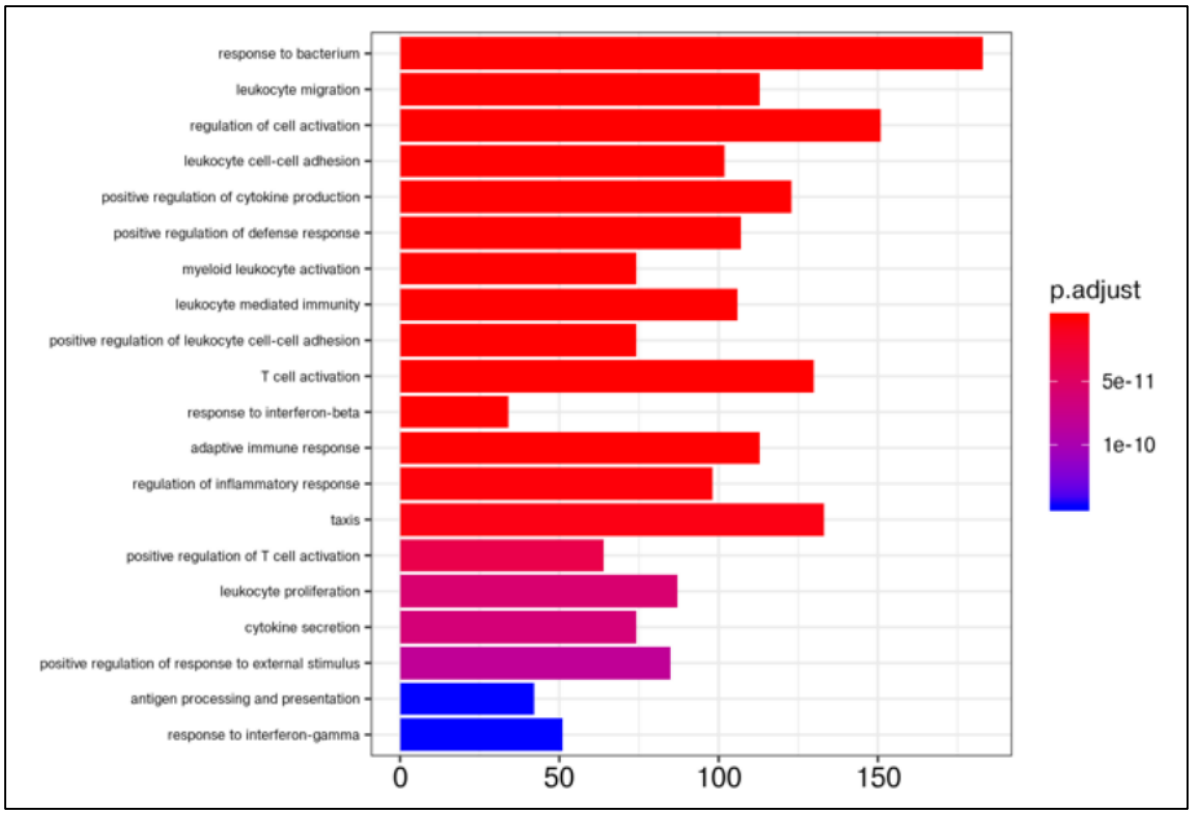

Figure 5.27 Gene ontology and pathway analysis plot comparing Nfkb1$^{-/-}$ and Nfkb1$^{fl/fl}$ samples. Differentially expressed genes include genes involved in responses to bacteria, leukocyte migration, regulation of cell activation and leukocyte cell-cell adhesion.

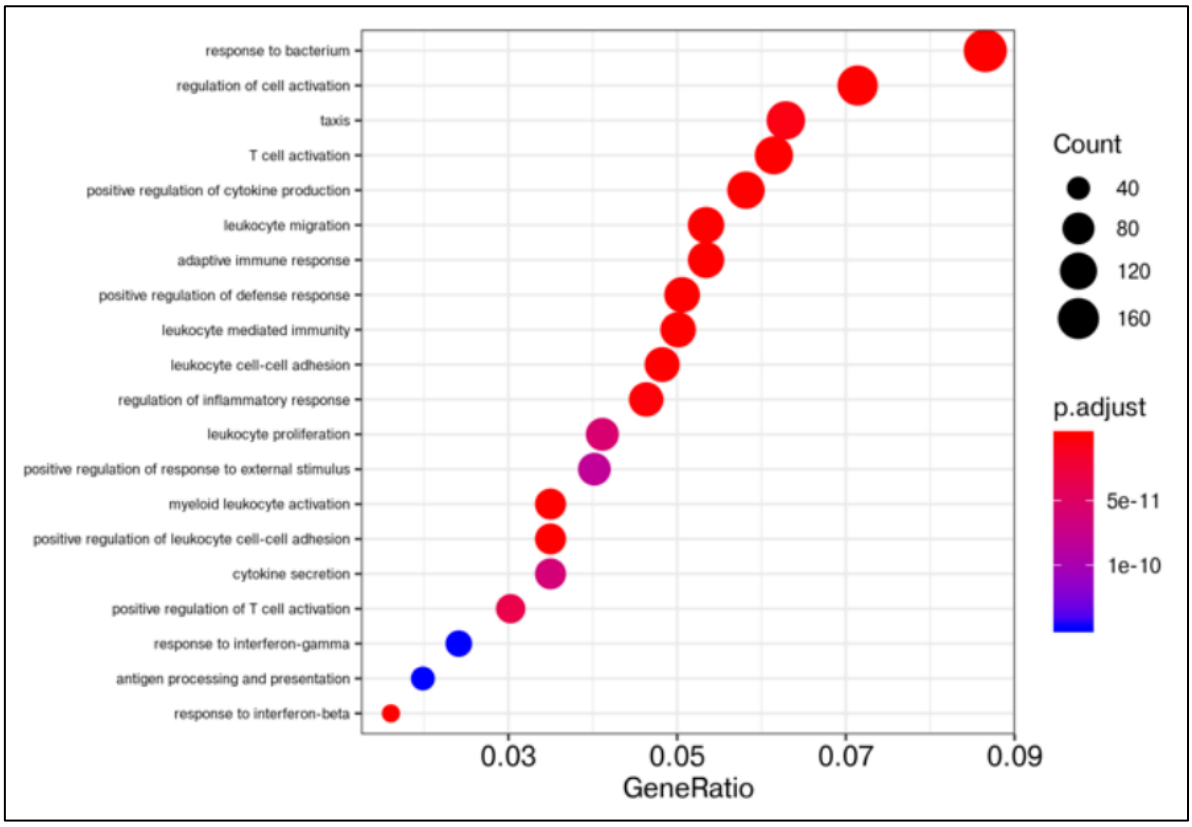

Figure 5.28 Gene ontology and pathway analysis plot comparing Nfkb1$^{-/-}$ and Nfkb1$^{fl/fl}$ samples. Differentially expressed genes include genes involved in responses to bacteria, regulation of cell activation, taxis, and T cell activation.

Among differentially expressed genes were genes involved in responses to bacteria, leukocyte migration, regulation of cell activation, leukocyte cell-cell adhesion, positive regulation of cytokine production, taxis and T cell activation.

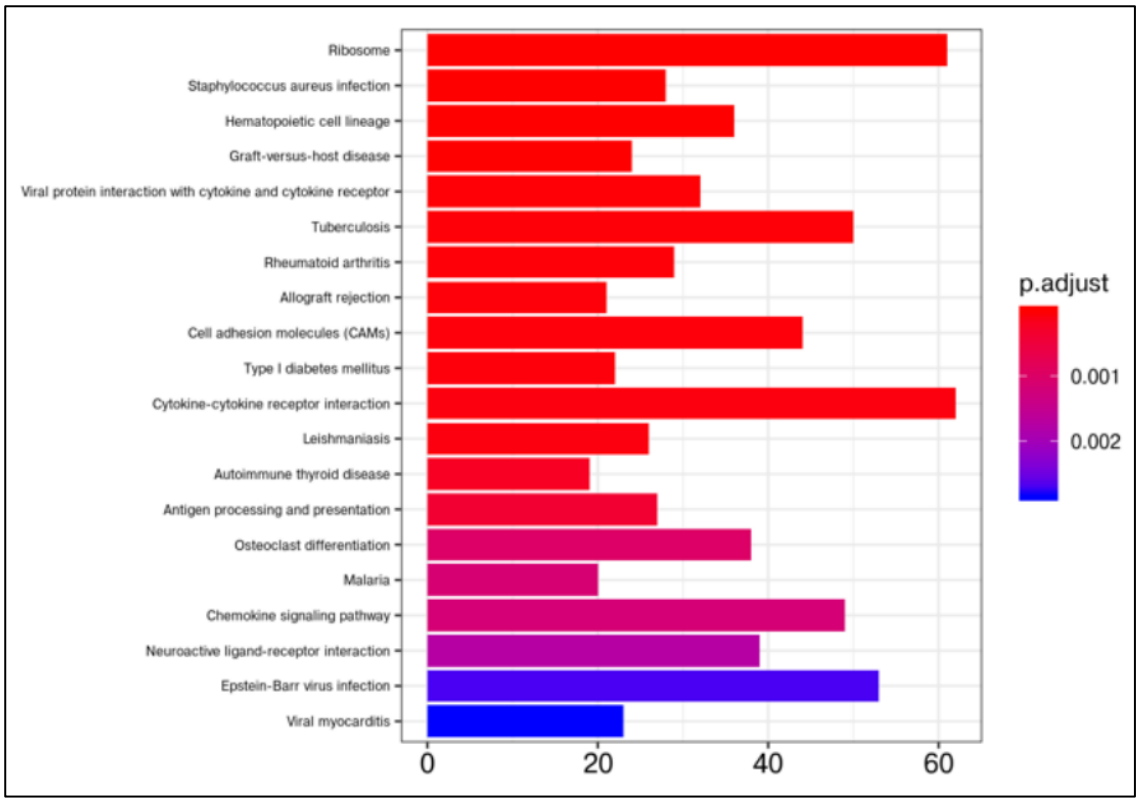

Figure 5.29 KEGG analysis plot comparing Nfkb1$^{-/-}$ and Nfkb1$^{fl/fl}$ samples. Differentially expressed genes include genes relating to the ribosome, Staphylococcus aureus infection, hematopoietic cell lineage, and genes involved in graft-versus-host disease.

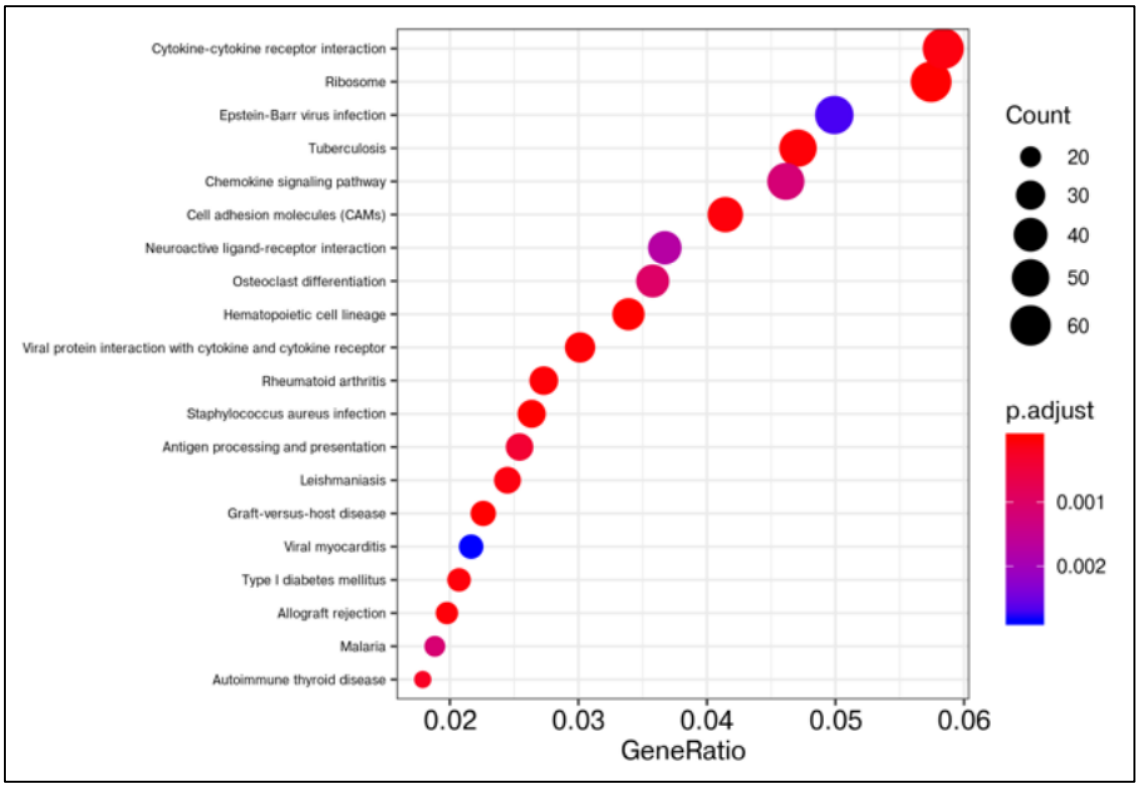

Figure 5.30 KEGG analysis plot comparing Nfkb1$^{-/-}$ and Nfkb1$^{fl/fl}$ samples. Differentially expressed genes include genes involved in cytokine-cytokine receptor interaction, genes relating to the ribosome, Epstein-Barr virus infection and Tuberculosis.

Among differentially expressed genes were genes relating to the ribosome, hematopoietic cell lineage, cell adhesion molecules (CAMs), cytokine-cytokine receptor interaction and chemokine signalling pathway genes.

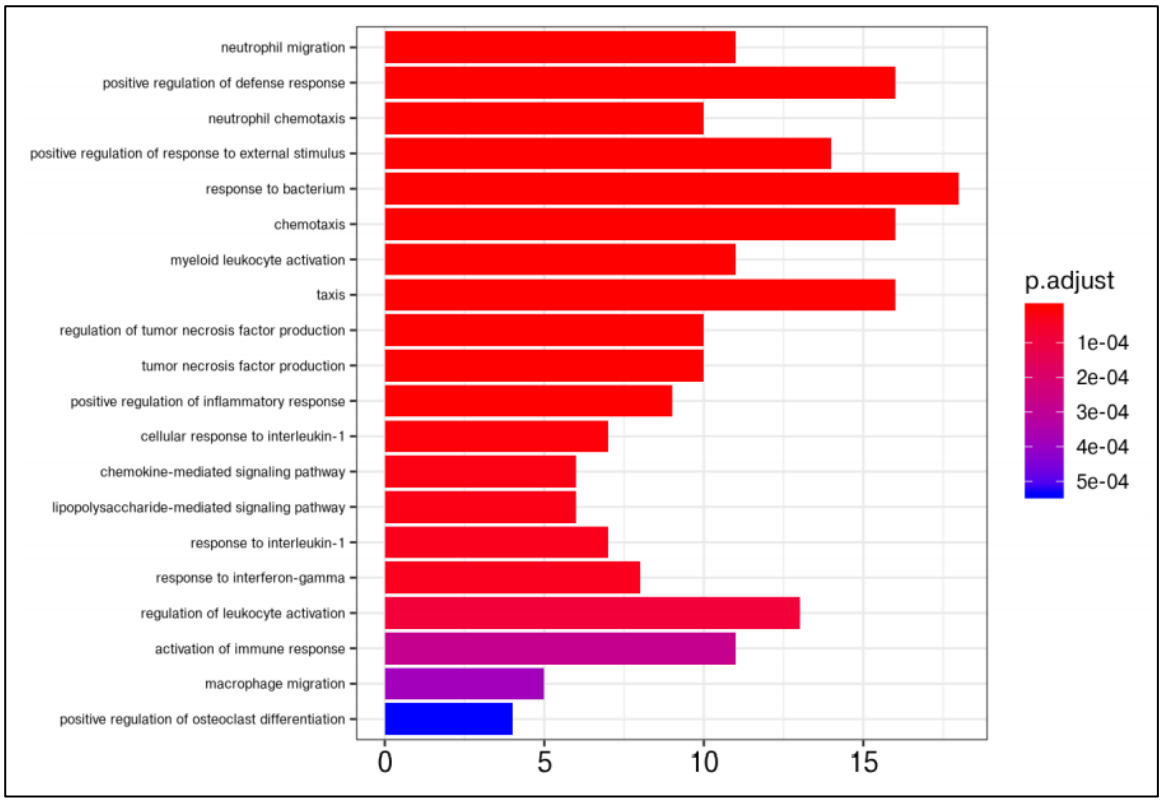

Figure 5.31 Gene ontology and pathway analysis plot comparing Nfkb1$^{hep-/-}$ and Nfkb1$^{fl/fl}$ samples. Differentially expressed genes include genes involved in neutrophil migration, positive regulation of defense responses, neutrophil chemotaxis, and positive regulation of responses to external stimuli.

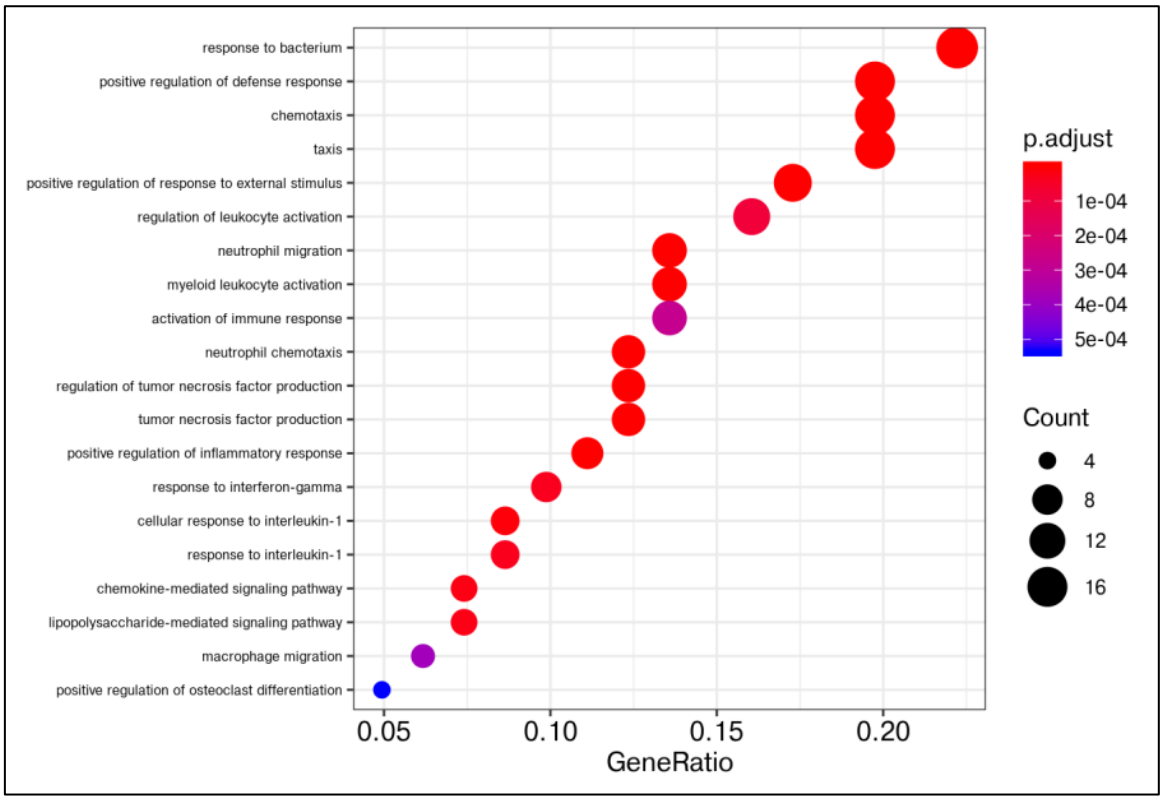

Figure 5.32 Gene ontology and pathway analysis plot comparing Nfkb1$^{hep-/-}$ and Nfkb1$^{fl/fl}$ samples. Differentially expressed genes include genes involved in responses to bacteria, positive regulation of defense responses, chemotaxis and taxis.

Among differentially expressed genes were genes involved in neutrophil migration and chemotaxis, myeloid leukocyte activation, chemotaxis and taxis, tumour necrosis factor production, responses to bacteria, positive regulation of defence responses, and regulation of leukocyte activation.

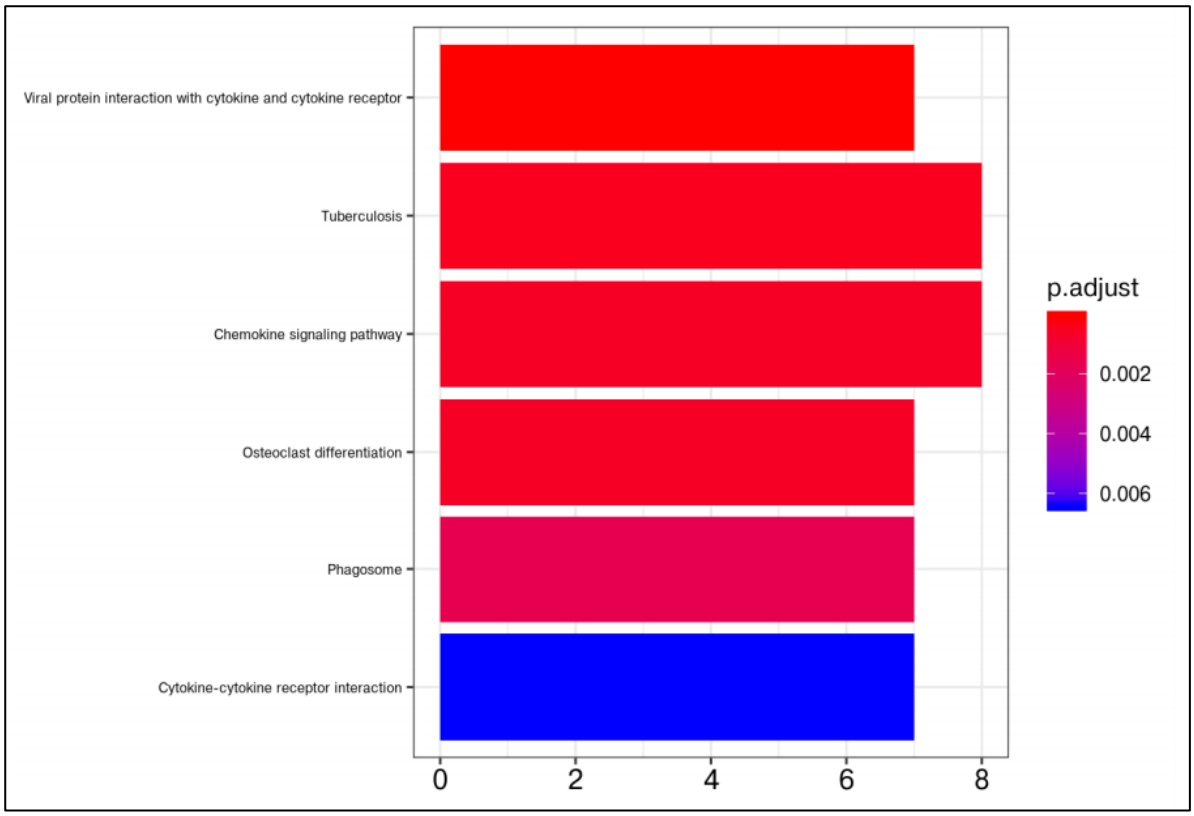

Figure 5.33 KEGG pathway analysis plot comparing Nfkb1$^{hep-/-}$ and Nfkb1$^{fl/fl}$ samples. Differentially expressed genes include genes involved in viral protein interaction with cytokines and cytokine receptors, Tuberculosis, chemokine signalling pathways and osteoclast differentiation.

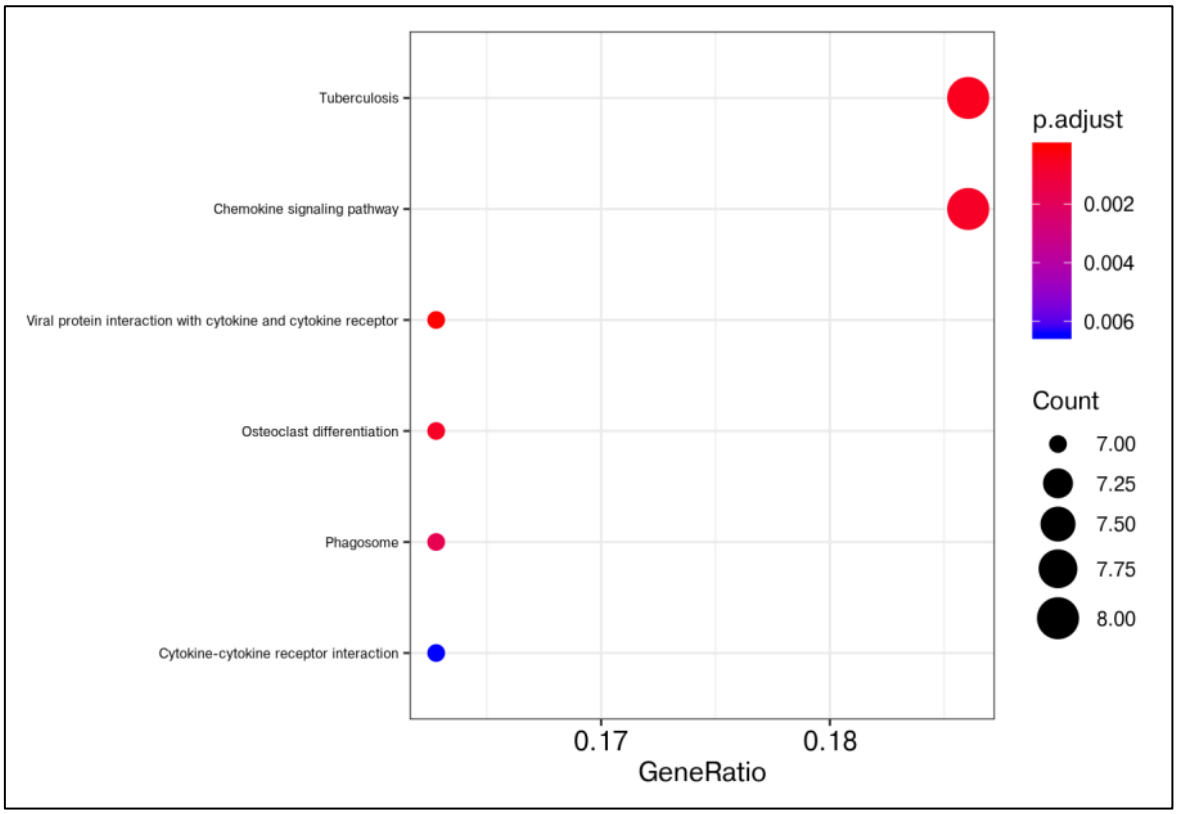

Figure 5.34 KEGG pathway analysis plot comparing Nfkb1$^{hep-/-}$ and Nfkb1$^{fl/fl}$ samples. Differentially expressed genes include genes involved in Tuberculosis, chemokine signalling pathways, viral protein interaction with cytokines and cytokine receptors and osteoclast differentiation.

Among differentially expressed genes were genes involved in chemokine signalling pathways, viral protein interaction with cytokines and cytokine receptors, and genes related to the phagosome.

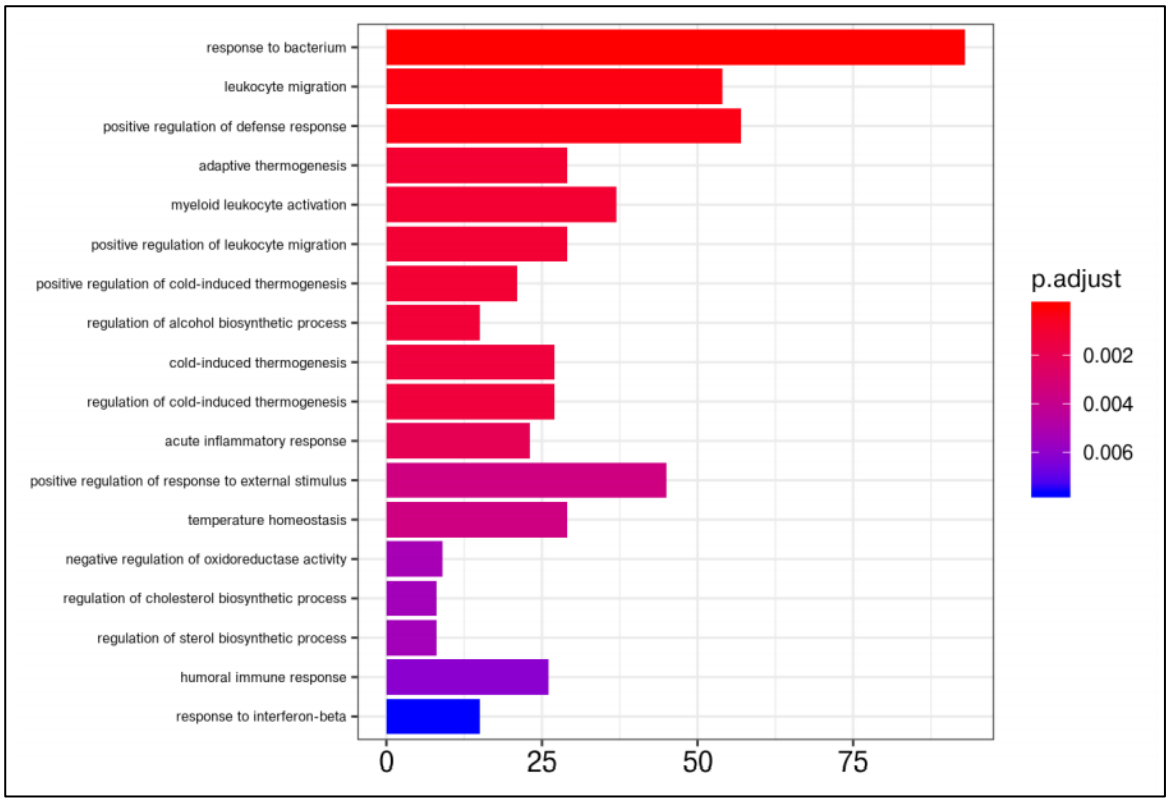

Figure 5.35 Gene ontology and pathway analysis plot comparing Nfkb1$^{-/-}$ and Nfkb1$^{hep-/-}$ samples. Differentially expressed genes include genes involved in responses to bacteria, leukocyte migration, positive regulation of defense responses, and adaptive thermogenesis.

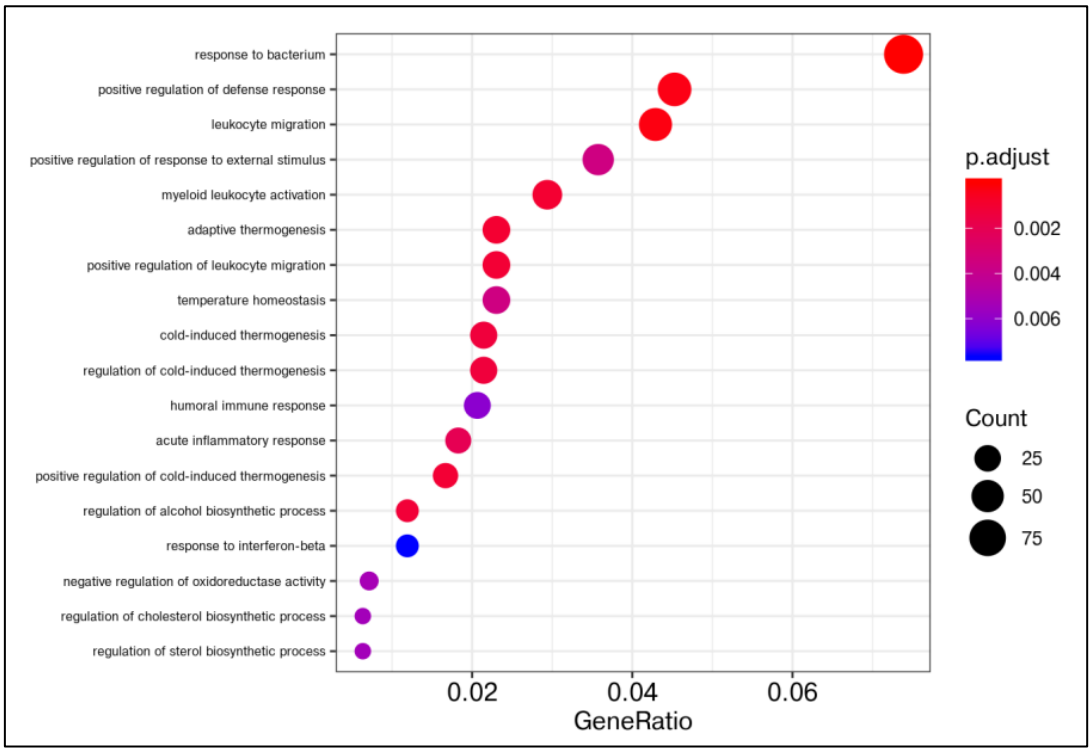

Figure 5.36 Gene ontology and pathway analysis plot comparing Nfkb1$^{-/-}$ and Nfkb1$^{hep-/-}$ samples. Differentially expressed genes include genes involved in responses to bacteria, positive regulation of defense responses, leukocyte migration, and positive regulation of responses to external stimuli.

Among differentially expressed genes were genes relating to responses to bacteria, leukocyte migration, myeloid leukocyte activation, positive regulation of defence responses, positive regulation of responses to external stimuli, adaptive thermogenesis and temperature homeostasis.

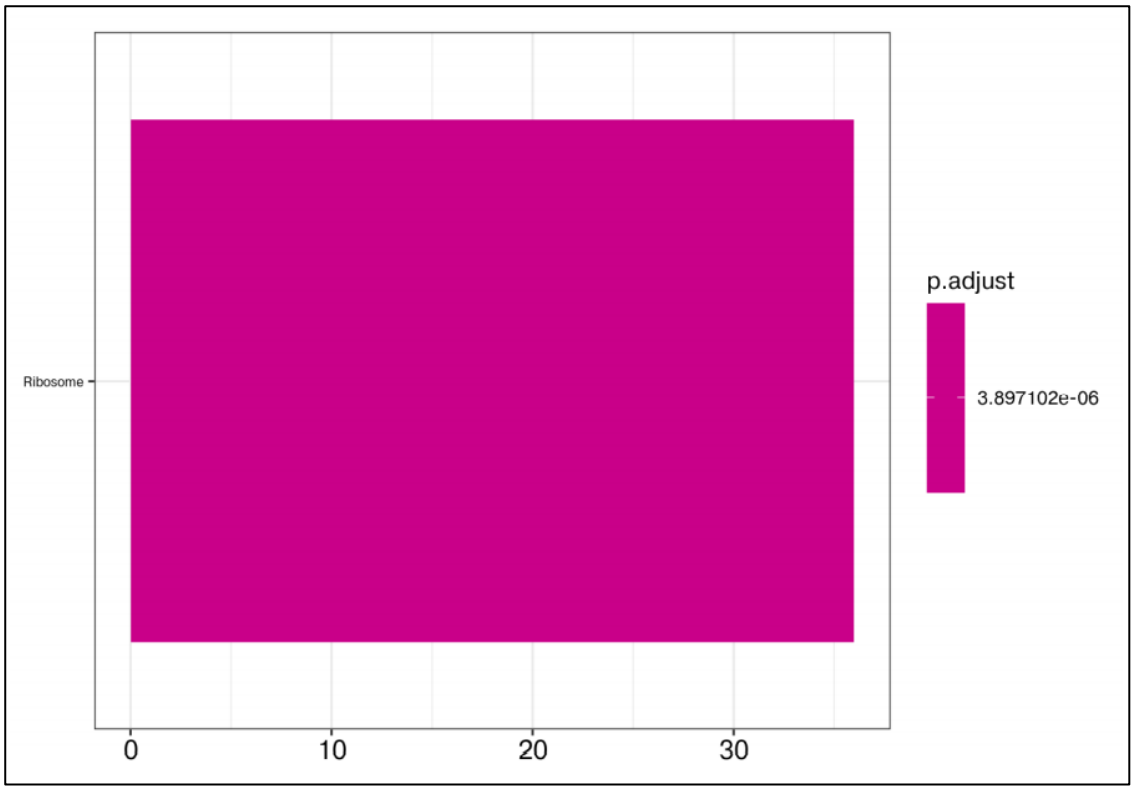

Figure 5.37 KEGG pathway analysis plot comparing Nfkb1$^{-/-}$ and Nfkb1$^{hep-/-}$ samples. Differentially expressed genes include genes relating to the ribosome.

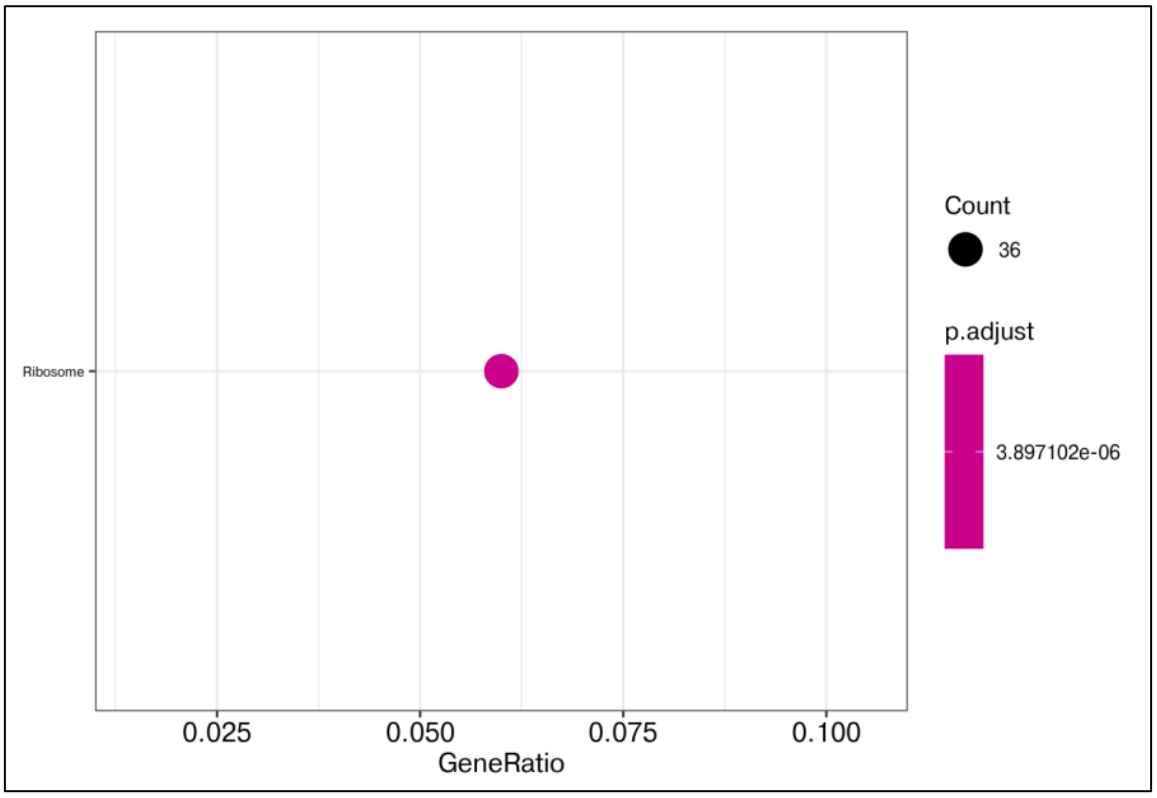

Figure 5.38 KEGG pathway analysis plot comparing Nfkb1$^{-/-}$ and Nfkb1$^{hep-/-}$ samples. Differentially expressed genes include genes relating to the ribosome.

Differentially expressed genes shown form the KEGG pathway analysis comparing Nfkb1$^{-/-}$ and Nfkb1$^{hep-/-}$ liver tumour samples included genes relating to the ribosome.

34 genes were found to be upregulated in Nfkb1$^{hep-/-}$ liver tumours compared to Nfkb1$^{fl/fl}$ liver tumours, shown in Table 5.1. Among these, genes linked to cancer were upregulated in Nfkb1$^{hep-/-}$ mice, including S100A6, GPNMB, Arl4c, Lgals3, Ear2 and bcl2a1a. Of these, the anti-apoptotic gene bcl2a1 and S100A6, involved in cell cycle progression and differentiation and known to promote proliferation in gastric cancer cells for example, could explain the increased proliferation observed in Nfkb1$^{hep-/-}$ tumours compared to Nfkb1$^{fl/fl}$ tumours.

Gene	log2FoldChange	p value	p adj
S100a6	1.52537	4.65E-07	0.000876
Crip1	1.113166	3.34E-09	2.53E-05
Acod1	4.964179	7.88E-08	0.000239
Ms4a7	1.708827	5.82E-06	0.004785
Gpnmb	2.991602	9.11E-06	0.005753
Hpgds	1.917221	7.87E-07	0.001192
Clec4e	4.232158	5.20E-07	0.000876

Rgs10	1.902592	6.87E-06	0.004785
Tlr13	1.586137	1.81E-05	0.009467
Gpsm3	1.482099	1.98E-05	0.009951
Saa3	2.402127	3.85E-08	0.000194
Atp1a3	2.440687	1.24E-05	0.006944
Gng2	2.441919	1.01E-05	0.005955
Gvin1	2.038723	5.28E-06	0.004785
Atg16l2	-1.46795	1.06E-06	0.001457
Arl4c	1.337008	2.17E-05	0.009951
Lgals3	2.027498	6.95E-06	0.004785
Rab7b	1.795152	6.43E-06	0.004785
Pla2g4a	3.620063	2.88E-06	0.002909
AB124611	1.422205	1.73E-05	0.009356
NA	4.943784	1.02E-05	0.005955
NA	22.05414	1.53E-09	2.31E-05
Lyz2	1.781101	6.37E-06	0.004785
Ear2	1.327194	2.14E-05	0.009951
Fign	-0.995062	2.76E-06	0.002909
Cyp3a41b	19.32369	1.24E-07	0.000313
Gm4070	2.420106	6.38E-06	0.004785
Evi2a	1.820405	4.29E-07	0.000876
Bcl2a1b	1.917961	1.45E-06	0.001686
Gm21188	2.262038	1.23E-06	0.001556
Bcl2a1a	2.646425	2.14E-05	0.009951
Lilr4b	1.414487	7.73E-06	0.005089
NA	19.70366	6.93E-08	0.000239

Table 5.1 Differentially expressed genes in Nfkb1$^{hep-/-}$ tumours compared to Nfkb1$^{fl/fl}$ liver tumours in DEN-induced HCC.

Together, these results demonstrate a significant difference in mRNA expression profile between Nfkb1$^{-/-}$ liver tumours and control Nfkb1$^{fl/fl}$ tumours, while the mRNA expression profile in Nfkb1$^{hep-/-}$ samples differs from that of the control tumours but has fewer genes differentially expressed. It can be concluded from this that hepatocyte NF-κB1 plays an important role in liver tumorigenesis, but that NF-κB1 present in other cell types (likely immune cells) plays a more substantial role in liver tumorigenesis given the increased difference in gene expression observed.

Moreover, most differentially expressed genes found relate to immune responses, notably chemotaxis and leukocyte activation, demonstrating an important role for NF-κB1 in immune function.

Nfkb1$^{-/-}$ and Nfkb1$^{hep-/-}$ mRNA expression profiles also differed, confirming the differential role of NF-κB1 in different cell types. It is important to note that the mRNA expression profiles reflect different cell types, given that tumours are heterogeneous in cell types, and therefore while most tumour cells are hepatocytes, other cells such as immune cells are likely contributing to the expression profiles observed.

5.9 The role of hepatocyte NF-κB1 in tumour progression in an adeno-associated viral NF-κB1 knock-out

After establishing that hepatocyte NF-κB1 p50 plays a role in tumour initiation in DEN-induced HCC when hepatocyte NF-κB1 is knocked out from an early age, limiting tumorigenesis, proliferation and monocyte/macrophage liver infiltration, it was hypothesized that hepatocyte NF-κB1 p50 could also play a role in tumour progression. AAV-TBG-Cre-mediated knock-out of hepatocyte NF-κB1 was therefore carried out at 32 weeks, in a 40 week DEN-induced HCC model where mice were injected IP with a single dose of DEN at 14 days of age. Nfkb1$^{fl/fl}$ mice were injected with either AAV-TBG-Cre or AAV-TBG-Null virus to knock out hepatocyte Nfkb1 or as a control, respectively, 32 weeks post-DEN injection. Previous research has shown that at 32 weeks, liver tumours have started to develop and become macroscopically visible in Nfkb1$^{-/-}$ mice, therefore this represents a good time-point to assess the role of hepatocyte NF-κB1 in tumour progression.

5.9.1. p50 expression in AAV-TBG-Null and AAV-TBG-Cre mice

Western blot analysis was carried out to assess NF-κB1 p50 expression in AAV-TBG-Null and AAV-TBG-Cre injected Nfkb1$^{fl/fl}$ mice livers and liver tumours. Results show abundant p50 expression in AAV-TBG-Null mice, and little or no expression of p50 in AAV-TBG-Cre mice (Figure 5.39). Where p50 is expressed in AAV-TBG-Cre mice, this can be attributed to non-parenchymal liver cells, such as immune cells. These results confirm the successful hepatocyte knock-out of Nfkb1 p50 in mice injected with AAV-TBG-Cre virus.

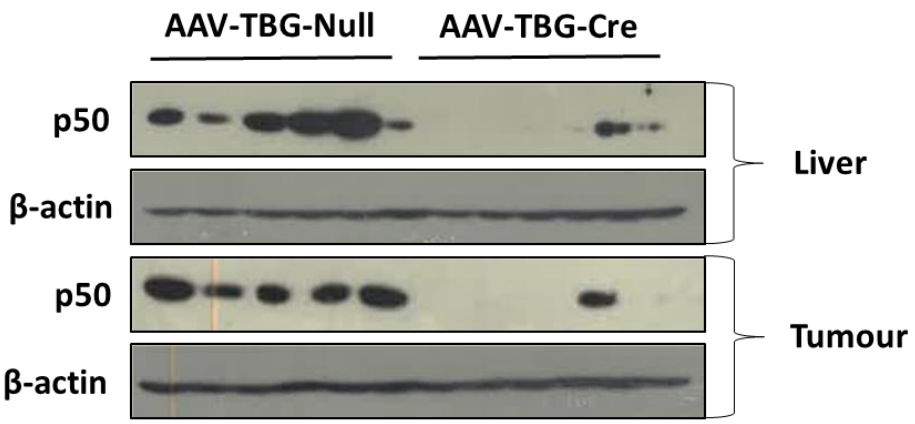

Figure 5.39 p50 expression in Nfkb1$^{fl/fl}$ and Nfkb1$^{hep-/-}$ livers and tumours. Western blots show Nfkb1 p50 expression in AAV-TBG-Null and AAV-TBG-Cre mice livers and tumours. β-actin protein expression was used as a loading control.

5.9.2 Liver damage ALT and AST serum enzymes unaltered by hepatocyte Nfkb1 knock-out in chronic DEN liver injury

To assess liver damage in AAV-TBG-Null and AAV-TBG-Cre mice, serum ALT and AST levels were measured. No significant difference was found between the two mice groups, however both ALT (p=0.1379) and AST (p=0.1101) appeared slightly increased in AAV-TBG-Cre mice, suggesting that hepatocyte NF-κB1 p50 may limit liver damage in liver tumour progression (Figure 5.40).

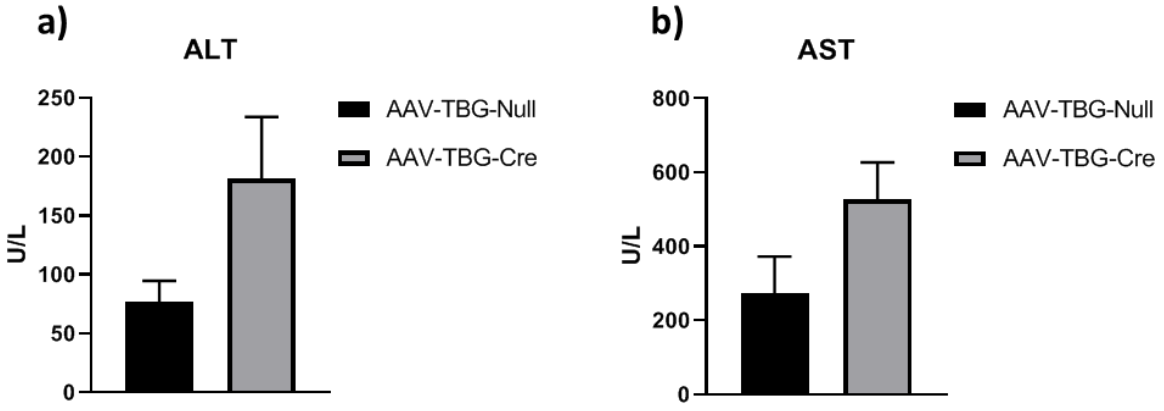

Figure 5.40 Serum ALT and AST levels in AAV-TBG-Null and AAV-TBG-Cre mice. Graphs show serum ALT (a) and AST (b) levels in AAV-TBG-Null control mice and AAV-TBG-Cre mice lacking hepatocyte NF-κB1 in 40 week DEN-induced HCC.

5.9.3 Tumour number and grade

Total macroscopic liver tumour number was counted at the time of harvest in AAV-TBG-Null and AAV-TBG-Cre mice livers. Significantly more liver tumours were found in AAV-TBG-Cre mice compared to AAV-TBG-Null control mice (p=0.0099) (Figure 5.41a). No significant difference in the number of large tumours above 0.5cm was found however (Figure 5.41b). Tumour grade was evaluated histologically in the same way as the previous 40 week DEN study, using formalin-fixed paraffin-embedded H&E stained liver tissue, with the grade HCC2 representing the most severe cancer phenotype (tumour grade was determined as part of Sam Murray's undergraduate project under my supervision). AAV-TBG-Cre mice had notably more HCC1 and HCC2 grade tumours compared to AAV-TBG-Null mice, indicating a more aggressive phenotype in AAV-TBG-Cre mice (Figure 5.41c). In AAV-TBG-Null, 34.78% of tumours were HCC2, 30.43% were HCC1 and 34.78% were HCA. In AAV-TBG-Cre, 50.65% of tumours were HCC2, 29.87% were HCC1 and 19.48% were HCA. This shows that the lack of hepatocyte NF-κB1 in HCC tumour progression leads to increased tumour burden, demonstrating that hepatocyte NF-κB1 plays a protective role in HCC development. Additionally, the liver/body weight ratio was significantly increased in AAV-TBG-Cre mice compared to AAV-TBG-Null mice (p=0.0403), in line with the increased tumour number observed in AAV-TBG-Cre mice (Figure 5.41d). Images of AAV-TBG-Cre mice livers also show more tumorous and diseased livers (Figure 5.41e). These results confirm the tumour-protective role of hepatocyte NF-κB1 in HCC, shown in $Nfkb1^{hep-/-}$ mice. Hepatocyte NF-κB1 therefore plays an important tumour-suppressive role in DEN-induced HCC at the tumour initiation and progression stages.

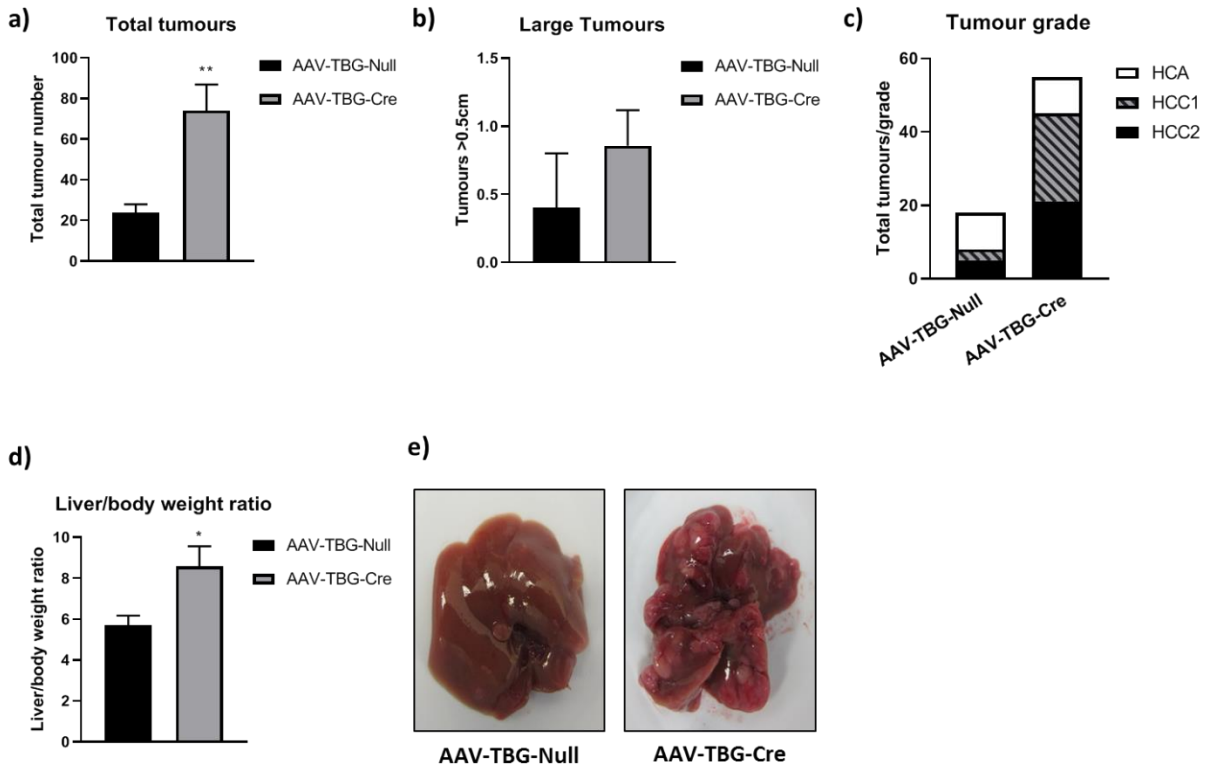

Figure 5.41 HCC liver tumour number and grade in AAV-TBG-Null and AAV-TBG-Cre mice. Graphs show total tumour number (a), large tumour number (b), tumour grade (c) and liver/body weight ratio (d) in AAV-TBG-Null and AAV-TBG-Cre mice. Images show tumorous livers of AAV-TBG-Null and AAV-TBG-Cre mice in DEN-induced HCC (e).

5.9.4 Proliferation

As Nfkb1$^{hep-/-}$ mice livers were found to be significantly more proliferative compared to control mice in DEN-induced HCC, proliferation was assessed in AAV-TBG-Null and AAV-TBG-Cre mice by PCNA immunohistochemistry of formalin-fixed paraffin-embedded liver tissue. The average number of PCNA positive hepatocytes per field ($p=0.0001$), as well as the average number of highly proliferative PCNA positive hepatocytes per field ($p=0.0090$), was significantly increased in AAV-TBG-Cre mice compared to AAV-TBG-Null mice. This shows that AAV-TBG-Cre mice have more hepatocytes undergoing proliferation and that the hepatocytes undergoing proliferation are more highly proliferative. This mirrors what was observed in Nfkb1$^{hep-/-}$ mice with DEN-induced HCC. These results confirm that hepatocyte NF-κB1 plays an important role in limiting hepatocyte proliferation, associated with carcinogenesis. Therefore, in the absence of hepatocyte NF-κB1, hepatocytes become more proliferative and they develop into more tumour cells in DEN-induced HCC.

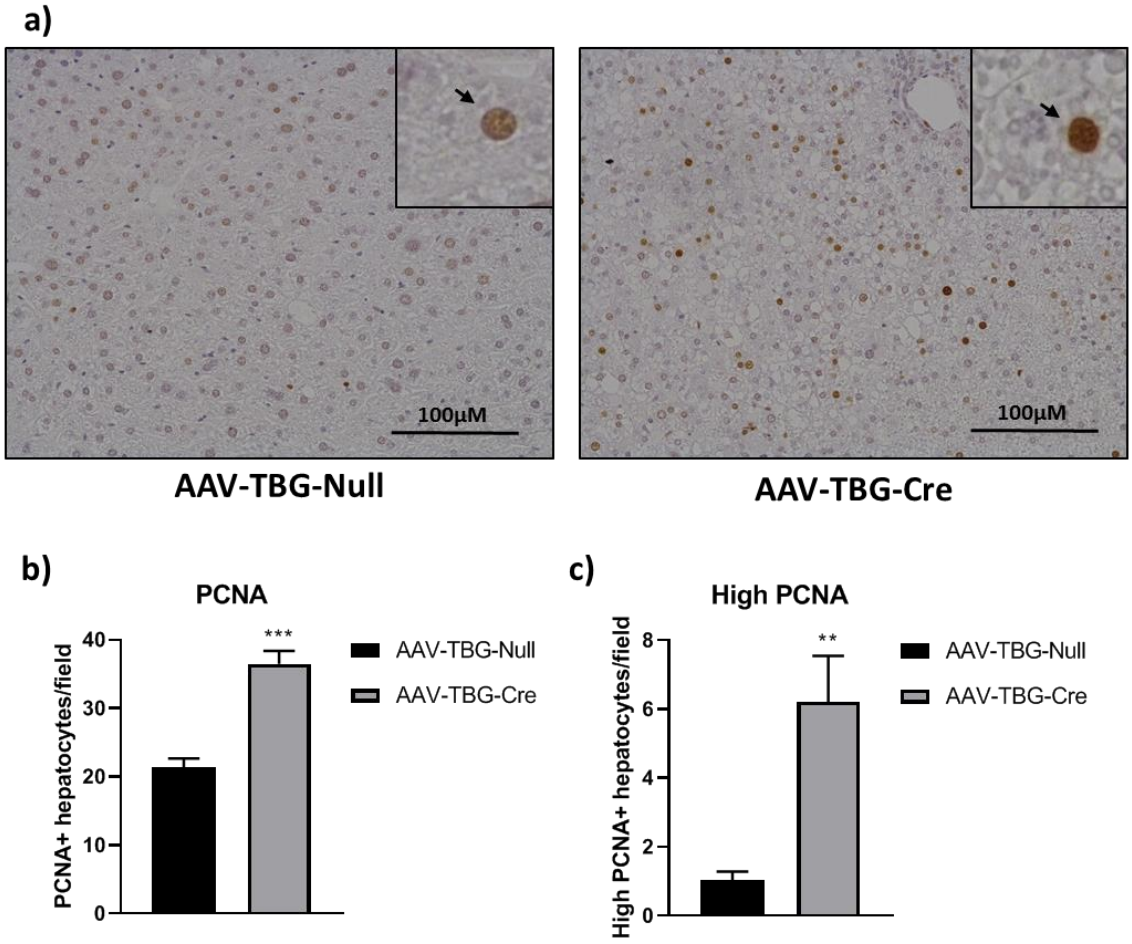

Figure 5.42 PCNA liver immunostain in AAV-TBG-Null and AAV-TBG-Cre mice. Images show X20 PCNA immunostaining of formalin-fixed paraffin-embedded liver tissue from AAV-TBG-Null and AAV-TBG-Cre mice (a). Graphs show average PCNA+ hepatocytes per field (b) and average highly proliferative PCNA+ hepatocytes per field (c).

5.9.5 Immune cell infiltration

DEN-induced HCC is accompanied by an inflammatory phenotype, notably immune cell infiltration and inflammatory chemokine expression (Wilson et al., 2015). Therefore inflammatory chemokine expression and the recruitment of different immune cell types to the liver was assessed in AAV-TBG-Null and AAV-TBG-Cre mice. Tumour and liver TNFα gene expression was determined by RT-qPCR, however no difference was observed between AAV-TBG-Null and AAV-TBG-Cre mice, though TNFα expression appeared slightly increased in AAV-TBG-Cre tumours compared to AAV-TBG-Null tumours (p=0.2466), and in AAV-TBG-Cre livers compared to AAV-TBG-Null livers

(p=0.0654) (Figure 5.43). This result is comparable to what was observed in Nfkb1$^{hep-/-}$ mice.

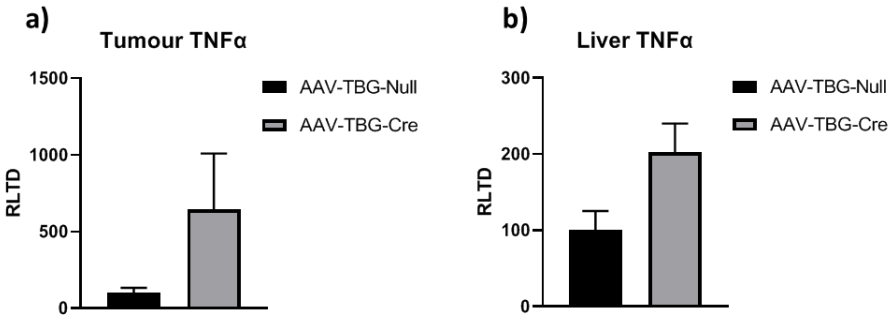

Figure 5.43 Tumour and liver TNFα gene expression in AAV-TBG-Null and AAV-TBG-Cre mice. Graphs show gene expression of tumour TNFα (a) and liver TNFα (b) in AAV-TBG-Null and AAV-TBG-Cre mice, determined by RT-qPCR.

5.9.6 Neutrophil recruitment to the liver in AAV-TBG-Null and AAV-TBG-Cre mice

Neutrophil recruitment to the liver was assessed by NIMP immunohistochemistry of formalin-fixed paraffin-embedded liver tissue from AAV-TBG-Null and AAV-TBG-Cre mice. As observed in Nfkb1$^{hep-/-}$ mice, AAV-TBG-Cre mice displayed significantly higher NIMP positive cells compared to AAV-TBG-Null mice (p=0.0189), indicating increased neutrophil infiltration in the livers of AAV-TBG-Cre mice, in the tumour and surrounding tissues. This shows that the lack of hepatocyte NF-κB1 p50 leads to increased neutrophil infiltration in the liver in DEN-induced HCC, therefore hepatocyte NF-κB1 p50 plays a role in limiting neutrophil recruitment to the liver in DEN-induced HCC. Although NIMP predominantly stains for neutrophils, some monocytes may stain positive for NIMP (Rehg et al., 2012), therefore the observed increase in NIMP+ cell staining could also be attributed to monocytes.

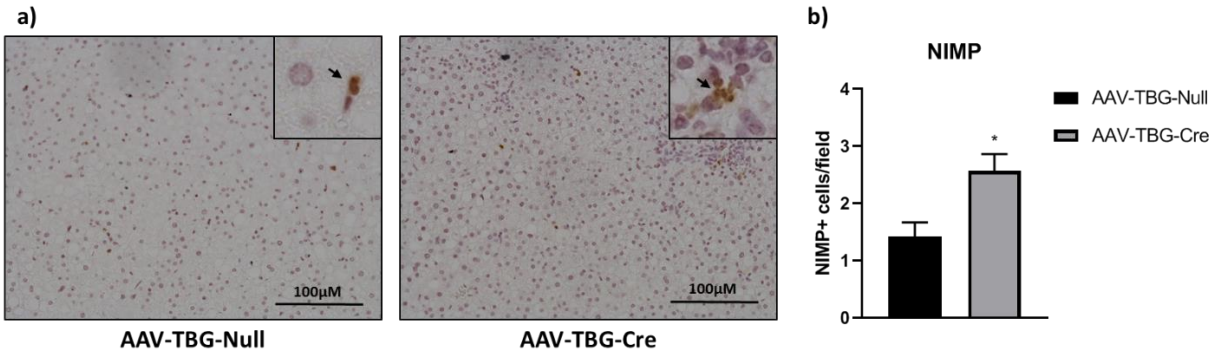

Figure 5.44 NIMP liver immunostain in AAV-TBG-Null and AAV-TBG-Cre mice. Images show X20 NIMP immunostaining of formalin-fixed paraffin-embedded liver tissue from AAV-TBG-Null and AAV-TBG-Cre mice (a). Graph shows average NIMP+ cells per field in AAV-TBG-Null and AAV-TBG-Cre mice (b).

5.9.7 Neutrophil chemokines

To elucidate the mechanism behind the increased neutrophil infiltration in AAV-TBG-Cre mice livers, the gene expression of neutrophil chemoattractant chemokines S100A9, CXCL1 and CXCL2 in AAV-TBG-Null and AAV-TBG-Cre mice tumours and livers was determined by RT-qPCR. Surprisingly, no significant difference was found in the expression of these genes in either tumour or liver tissue between AAV-TBG-Null and AAV-TBG-Cre mice (Figure 5.45). However, this is similar to what was observed in Nfkb1$^{hep-/-}$ mice, which exhibited increased liver neutrophil recruitment compared to control mice, but no difference in S100A9, CXCL1 and CXCL2 neutrophil chemoattractant chemokine gene expression. Therefore, hepatocyte NF-κB1 p50 must be regulating the expression of other neutrophil chemoattractant chemokines, such as CXCL5.

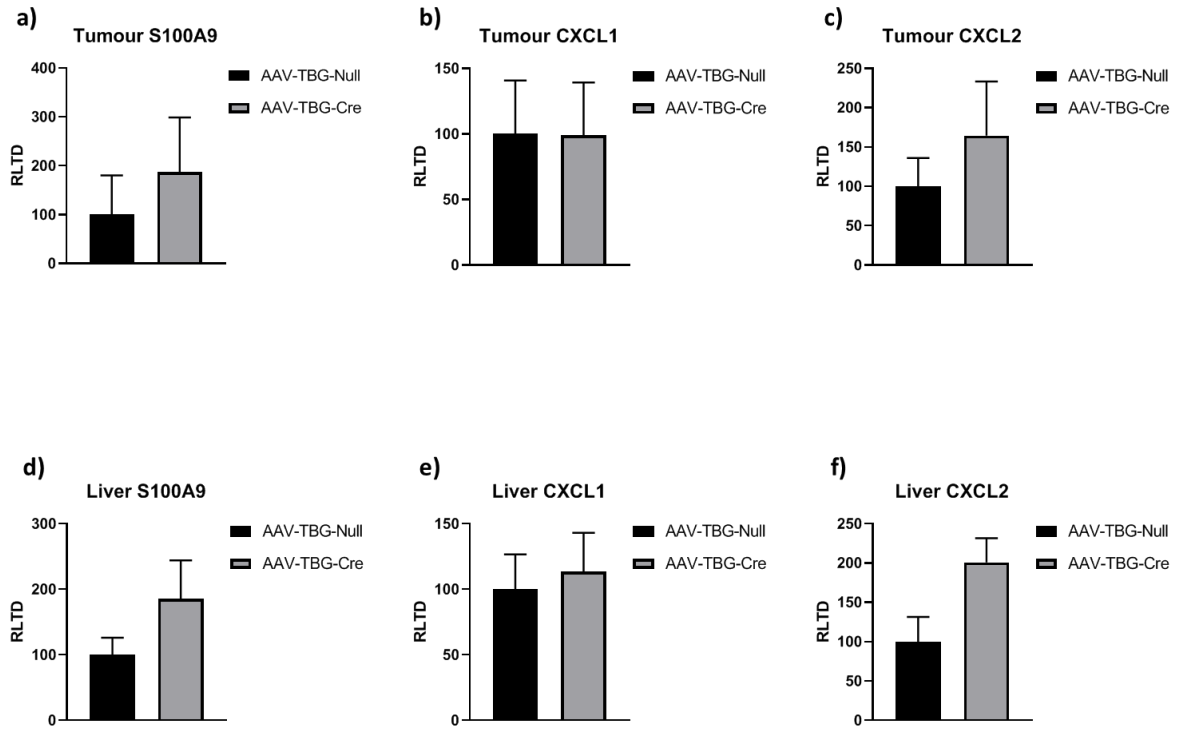

Figure 5.45 Tumour and liver gene expression of neutrophil chemoattractant chemokines. Graphs show gene expression of tumour S100A9 (a), CXCL1 (b) and CXCL2 (c), and of liver S100A9 (d), CXCL1 (e) and CXCL2 (f) in AAV-TBG-Null and AAV-TBG-Cre mice.

5.9.8 Monocytes/macrophages recruitment to the liver in AAV-TBG-Null and AAV-TBG-Cre mice

To further assess the role of hepatocyte NF-κB1 p50 in the recruitment of immune cells to the liver in DEN-induced HCC, CD68 immunohistochemistry was carried out on formalin-fixed paraffin-embedded liver tissue from AAV-TBG-Null and AAV-TBG-Cre mice to determine the role of hepatocyte NF-κB1 p50 in monocyte and macrophage recruitment to the liver. Interestingly, significantly more CD68 positive cells were found in AAV-TBG-Cre mice livers compared to AAV-TBG-Null control mice ($p=0.0083$), indicating that in the absence of hepatocyte NF-κB1 p50, significantly more monocytes and macrophages are recruited to the liver in DEN-induced HCC (Figure 5.46).

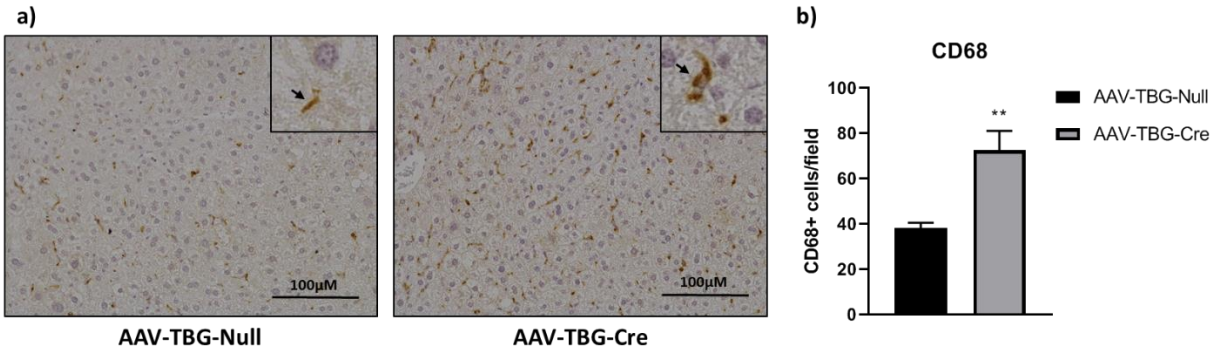

Figure 5.46 CD68 liver immunostain from AAV-TBG-Null and AAV-TBG-Cre mice. Images show X20 CD68 immunostaining of formalin-fixed paraffin-embedded liver tissue from AAV-TBG-Null and AAV-TBG-Cre mice (a). Graph shows average CD68+ cell count per field in AAV-TBG-Null and AAV-TBG-Cre mice (b).

5.9.9 Monocyte chemoattractant chemokines

To elucidate the mechanism behind the increased liver monocyte infiltration in AAV-TBG-Cre mice, the gene expression of monocyte chemoattractant chemokines CCL2 and CCL5 was determined in AAV-TBG-Null and AAV-TBG-Cre mice tumours and livers by RT-qPCR. No significant difference in tumour or liver CCL2 and CCL5 expression was found between AAV-TBG-Null and AAV-TBG-Cre mice (Figure 5.47). These results confirm what was observed in $Nfkb1^{hep-/-}$ mice in DEN-induced HCC, whereby the lack of hepatocyte NF-κB1 lead to increased recruitment of monocytes and macrophages to the liver, but no increase in CCL2 and CCL5 tumour and liver gene expression, compared to control $Nfkb1^{fl/fl}$ mice. Therefore, other monocyte chemoattractant chemokines, such as CCL7, are responsible for recruiting an increased number of monocytes to the liver. More monocytes may also be differentiated into macrophages in the absence of hepatocyte NF-κB1. It can thus be concluded from these results that hepatocyte NF-κB1 limits monocyte and macrophage infiltration into the liver and may limit monocyte differentiation to macrophages in DEN-induced HCC.

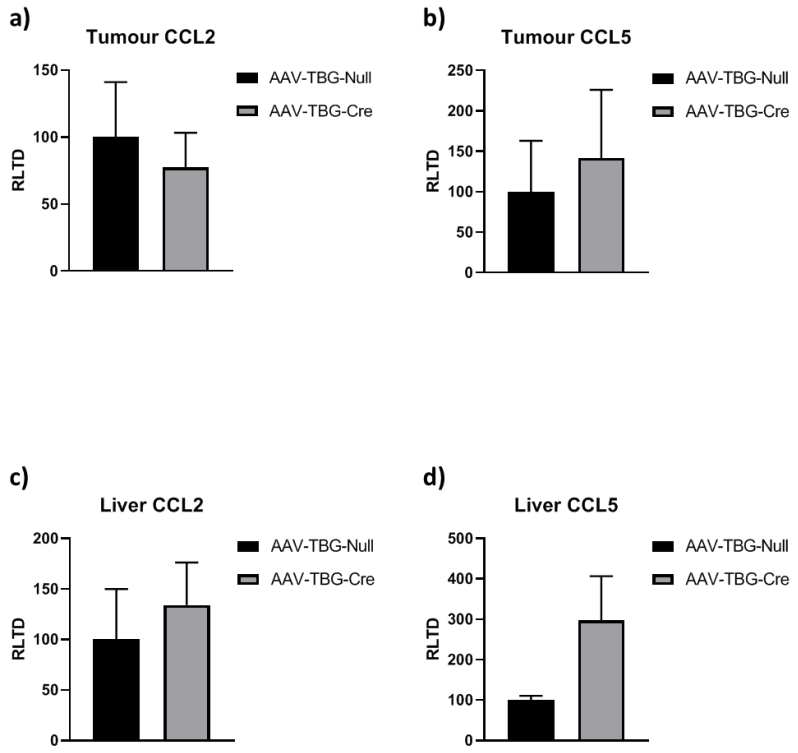

Figure 5.47 Tumour and liver gene expression of monocyte chemoattractant chemokines in AAV-TBG-Null and AAV-TBG-Cre mice. Graphs show gene expression of tumour CCL2 (a) and CCL5 (b), and of liver CCL2 (c) and CCL5 (d) in AAV-TBG-Null and AAV-TBG-Cre mice, determined by RT-qPCR.

5.9.10 Tumour and liver anti-apoptotic/oncogene expression in AAV-TBG-Null and AAV-TBG-Cre mice

Subsequently, the gene expression of anti-apoptotic oncogenes Gadd45β, Bcl-xL and Bcl-2 was determined in AAV-TBG-Null and AAV-TBG-Cre mice tumours and livers by RT-qPCR. Surprisingly, no significant difference was found in the tumour or liver expression of these genes between AAV-TBG-Null and AAV-TBG-Cre mice (Figure 5.48). These results show that hepatocyte NF-κB1 p50 may not play as important a role in the regulation of these genes in tumour progression compared to tumour initiation, though it may limit their expression slightly.

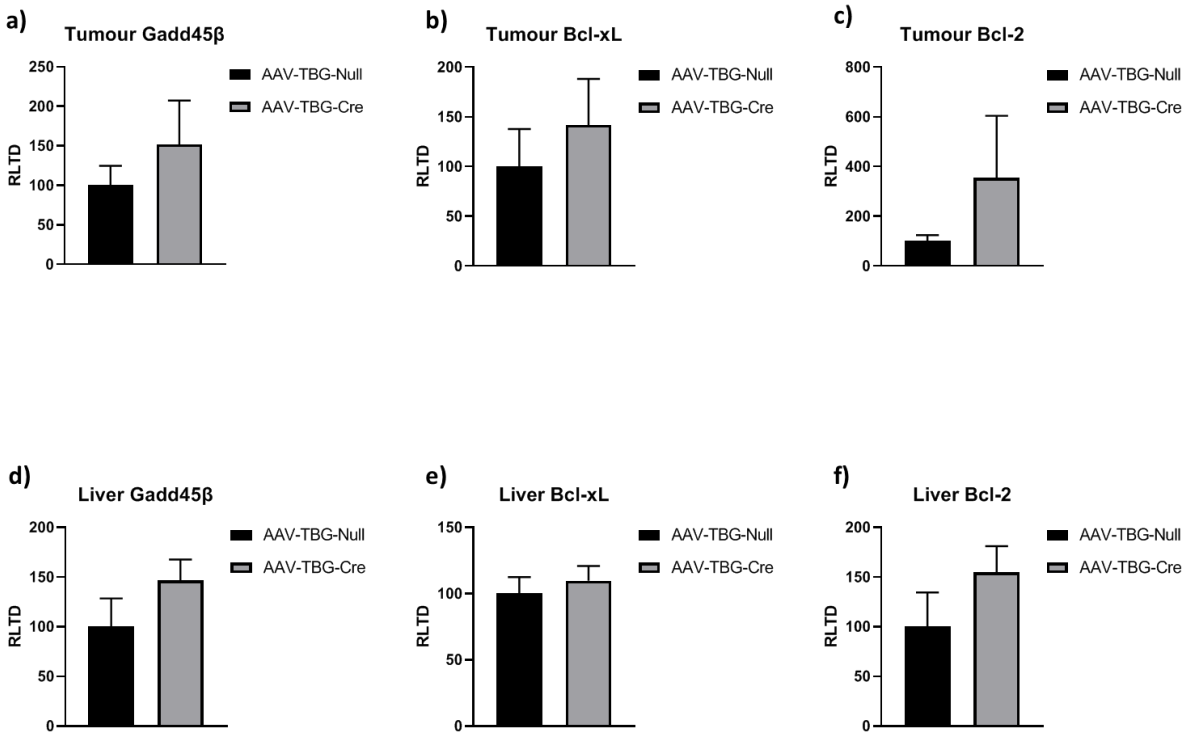

Figure 5.48 Tumour and liver apoptotic signalling gene and oncogene expression in AAV-TBG-Null and AAV-TBG-Cre mice. Graphs show gene expression of tumour Gadd45β (a), Bcl-xL (b) and Bcl-2 (c), and of liver Gadd45β (d), Bcl-xL (e) and Bcl-2 (f) in AAV-TBG-Null and AAV-TBG-Cre mice.

5.10 The role of hepatocyte NF-κB1 in aged 19 month mice

Nfkb1$^{-/-}$ mice have been shown to experience accelerated ageing and a worsened ageing phenotype, as well as the spontaneous development of tumours by around 15 months (Jurk et al., 2014). A pilot study was therefore carried out in Nfkb1$^{hep-/-}$ mice to see whether hepatocyte NF-κB1 plays a role on liver phenotype in ageing. WT and Nfkb1$^{hep-/-}$ mice were aged for 19 months and their livers harvested. Initial H&E staining analysis showed a remarkable difference, with Nfkb1$^{hep-/-}$ mice exhibiting increased steatosis. This can be seen in Figure 5.49a and Figure 5.49b, with a notable increase in white lipid droplets in the liver compared to WT mice. Liver steatosis was also visible macroscopically at the time of harvest, as shown in Figure 5.49c. Additionally, small macroscopic nodules were visible on Nfkb1$^{hep-/-}$ mice livers, indicating that aged Nfkb1$^{hep-/-}$ mice may be more prone to carcinogenesis. These initial results show an important role for hepatocyte NF-κB1 in lipid metabolism in aged mice, with further

investigation required to elucidate the mechanism behind this, and they additionally support the tumour-suppressive function of hepatocyte NF-κB1.

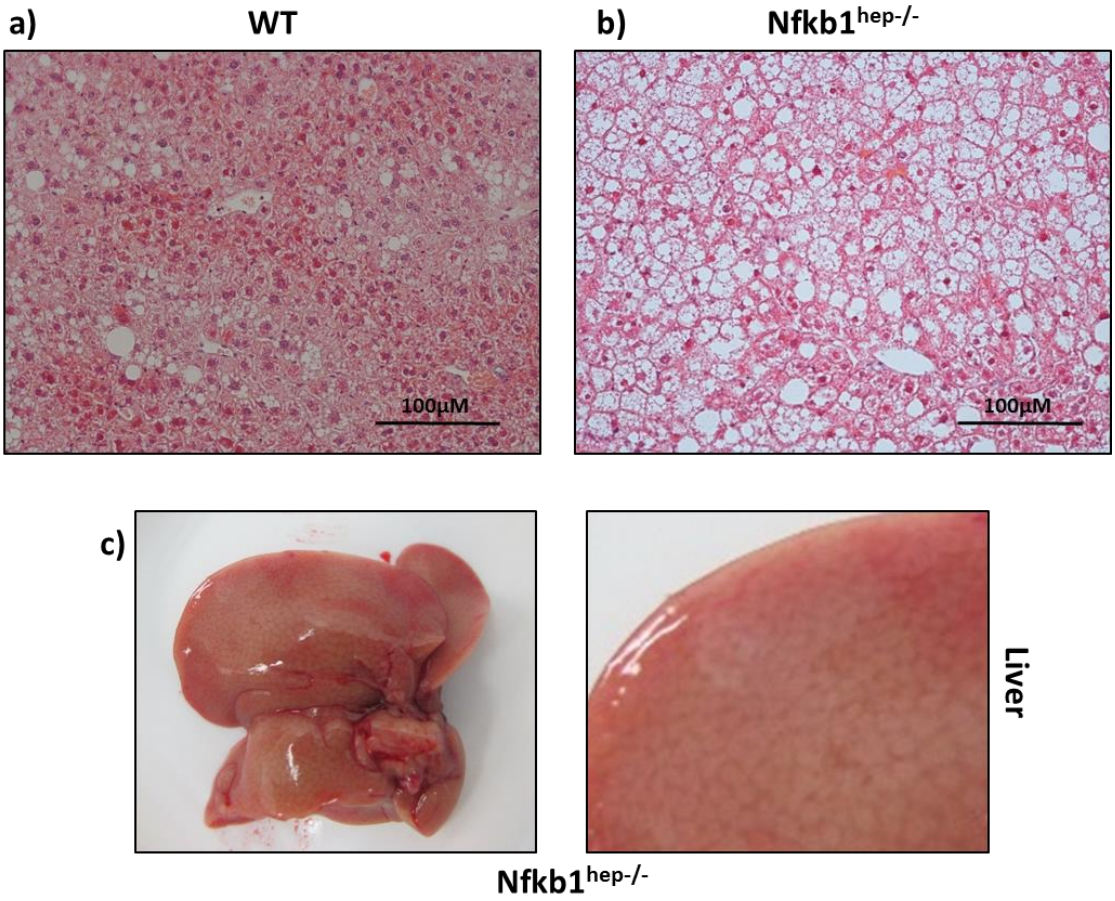

Figure 5.49 Liver steatosis in Nfkb1$^{hep-/-}$ 19 month old aged mice. Images show X20 H&E staining of WT (a) and X10 H&E staining of Nfkb1$^{hep-/-}$ (b) liver tissue from 19 month old aged mice, and liver harvest images from 19 month old aged Nfkb1$^{hep-/-}$ mice (c).

5.11 Chapter Discussion

The role of hepatocyte NF-κB1 p50 in immune cell recruitment to the liver, proliferation, apoptosis and carcinogenesis has been assessed here in a 40 week DEN-induced HCC model. The role of hepatocyte NF-κB1 p50 was assessed in tumour initiation, with Nfkb1$^{fl/fl}$ control and Nfkb1$^{hep-/-}$ mice, where hepatocyte Nfkb1 is knocked out from an early age, and in tumour progression, with AAV-TBG-Null control and AAV-TBG-Cre mice, where hepatocyte Nfkb1 was knocked out at a stage where macroscopic tumours have already started to develop: 32 weeks post DEN-injection.

Both models showed a significant increase in tumour number in the absence of hepatocyte Nfkb1, and an increased liver/body weight ratio, indicative of more tumours. This was accompanied by an increased tumour burden, with an increased number of higher grade HCC tumours (HCC1 and HCC2). Hepatocytes were also significantly more proliferative in the absence of NF-κB1 in both models. This greater proliferative capacity leads to the development of more HCC tumours in the absence of hepatocyte NF-κB1. Hepatocyte NF-κB1 p50 therefore plays a role in limiting tumour development and tumour proliferation in DEN-induced HCC, at the cancer initiation and progression stages.

Interestingly, mice lacking hepatocyte NF-κB1 displayed increased neutrophil, monocyte and macrophage recruitment to the liver in both models. This shows that hepatocyte NF-κB1 plays an important role in limiting neutrophil, monocyte and macrophage to the liver in the initiation and progression of DEN-induced HCC, and thus acts as a repressor of immune responses. The chemokines responsible for recruiting an increased number of neutrophils, monocytes and macrophages were not identified here, as no difference in S100A9, CXCL1, CXCL2, CCL2 and CCL5 gene expression was found between mice lacking hepatocyte NF-κB1 and control mice. However, their protein expression levels were not assessed, and therefore these chemokines may have increased protein expression despite not showing a difference at the gene expression level. Recruitment of cells of the adaptive immune system to the liver was also assessed in $Nfkb1^{fl/fl}$ and $Nfkb1^{hep-/-}$ mice, but no significant difference was found in the number of B cells, T cells, and T cell subsets, though there appeared to be a slight increase in overall T cells and in CD8+ cytotoxic T cells in $Nfkb1^{hep-/-}$ mice. This could indicate that mice lacking hepatocyte NF-κB1 may require more cytotoxic T cells to kill their liver cancer cells, since they have more tumours. Overall these results show that hepatocyte NF-κB1 predominantly plays a role in innate immune responses, with little modulation of adaptive immune responses.

The role of hepatocyte NF-κB1 in cell survival and apoptosis was also assessed. Overall, the results showed some evidence for hepatocyte NF-κB1 modulation of apoptotic signalling, with tumour Gadd45, Bcl-xL and Bcl-2 being significantly more expressed at the gene level in $Nfkb1^{hep-/-}$ mice compared to $Nfkb1^{fl/fl}$ control mice, however this was not mirrored at the protein level, and no significant difference in the expression of these genes was found in AAV-TBG-Cre mice compared to AAV-TBG-Null mice. Additionally, cleaved caspase 3 immunostaining, which marks apoptotic

signalling activation, showed no difference in Nfkb1$^{hep-/-}$ mice compared to Nfkb1$^{fl/fl}$ mice. While p-JNK western blots showed some evidence for increased anti-apoptotic signalling in Nfkb1$^{hep-/-}$ mice, this was not striking. Together these results show that hepatocyte NF-κB1 is not a key modulator of apoptotic signalling in DEN-induced HCC.

RNA-Seq analysis comparison between Nfkb1$^{fl/fl}$, Nfkb1$^{-/-}$ and Nfkb1$^{hep-/-}$ mice liver tumours resulting from the DEN-induced HCC model showed differential gene expression in the three groups. While more differentially expressed genes were found between Nfkb1$^{fl/fl}$ and Nfkb1$^{-/-}$ mice, Nfkb1$^{fl/fl}$ and Nfkb1$^{hep-/-}$ mice displayed important differences in gene expression. Notably, genes involved in neutrophil migration and chemotaxis, positive regulation of defence responses and responses to external stimuli, chemotaxis, myeloid leukocyte activation, regulation of TNF production and positive regulation of inflammatory responses were upregulated in Nfkb1$^{hep-/-}$ mice, supporting the increased immune cell infiltration observed in these mice. The differences in mRNA expression observed between Nfkb1$^{-/-}$ and Nfkb1$^{hep-/-}$ mice highlight the different roles played by NF-κB1 in different cell types; while hepatocyte NF-κB1 plays an important tumour-suppressive role, dampening inflammation, NF-κB1 also has important functions in other cell types, such as immune cells.

Importantly, the protein expression levels of NF-κB subunits cRel, p65 and p52 were similar between Nfkb1$^{fl/fl}$ and Nfkb1$^{hep-/-}$ mice livers, eliminating the possibility of NF-κB subunit compensation for the loss of NF-κB1.

19 month old aged Nfkb1$^{hep-/-}$ mice displayed a high amount of liver steatosis, characterised by the accumulation of fat lipid droplets in the liver, compared to WT 19 month old aged mice. Additionally, aged Nfkb1$^{hep-/-}$ mice displayed small macroscopically visible nodules in the liver, indicative of carcinogenesis. These results provide an additional insight into the role of hepatocyte NF-κB1 in cancer and ageing. Further investigation is required to understand the mechanisms behind the increased steatosis observed in Nfkb1$^{hep-/-}$ mice, and to deepen the understanding of how hepatocyte NF-κB1 limits liver cancer development.

Chapter 6. Discussion

The NF-κB1 transcription factor plays a central role in a number of key cellular functions, including immune responses, cell cycle regulation, cell survival and carcinogenesis (Best et al., 2019). Previously, NF-κB1 has been shown to act in a protective manner in cells, dampening the expression of pro-inflammatory and pro-tumorigenic genes (Wilson et al., 2015). NF-κB1 can exert several different functions depending on the cell type it is expressed in, regulating the expression of different genes. Here, the role of hepatocyte NF-κB1 in liver response to injury, inflammation, fibrosis and hepatocellular carcinoma was assessed through different *in vivo* mouse models.

Initial experiments involving acute liver injury in mice revealed a limited protective role for hepatocyte NF-κB1 in response to acute liver injury, comparing $Nfkb1^{fl/fl}$ and $Nfkb1^{hep-/-}$ mice livers. Acute CCl_4 injury experiments where mice were injected with the hepatotoxin CCl_4 and the livers harvested 24h and 48h post-injection were conducted in conditional knock-out mice, whereby the hepatocyte Nfkb1 gene was deleted through albumin cre recombinase LoxP site recombination. Hepatocyte Nfkb1 knockout was also triggered 2 weeks prior to acute liver injury in a TBG-AAV virus-induced knockout model.

Following acute CCl_4 liver injury, the liver inflammatory profile from $Nfkb1^{hep-/-}$ mice did not differ from that of $Nfkb1^{fl/fl}$ control mice. More specifically, the mRNA expression of neutrophil chemoattractant chemokines S100A9, CXCL1 and CXCL2 was comparable in both genotype groups, as well as monocyte chemoattractant chemokines CCL2 and CCL5. In support of this, no difference in neutrophil recruitment to the liver was seen in the absence of hepatocyte NF-κB1. Interestingly, macrophage liver infiltration was increased in $Nfkb1^{hep-/-}$ mice, indicating that hepatocyte NF-κB1 plays a role in limiting macrophage recruitment to the liver in response to injury. Previous studies have demonstrated a similar role for NF-κB1 in macrophage recruitment (Ward et al., 2008). While the monocyte chemoattractant chemokines responsible for the observed increase in macrophage numbers were not identified, RNA-Seq analysis would likely reveal differential expression of monocyte chemoattractant chemokines between $Nfkb1^{fl/fl}$ and $Nfkb1^{hep-/-}$ mice, providing interesting insights into the role of hepatocyte NF-κB1 relating to immune cell recruitment.

Similarly, following acute liver injury with the carcinogen DEN, Nfkb1$^{fl/fl}$ and Nfkb1$^{hep-/-}$ mice livers displayed no difference in their inflammatory gene expression profile, while previous studies have shown that Nfkb1$^{-/-}$ mice exhibit a higher inflammatory profile following acute DEN injury (Wilson et al., 2015). In support of this, liver infiltration of neutrophils was not affected by the lack of hepatocyte NF-κB1. Interestingly, while acute CCl_4 injury led to increased macrophage liver infiltration in Nfkb1$^{hep-/-}$ mice, acute DEN injury did not have this effect and no difference in macrophage liver infiltration was seen between Nfkb1$^{fl/fl}$ and Nfkb1$^{hep-/-}$ mice. The type of injury inflicted on the liver therefore affects which genes are modulated by hepatocyte NF-κB1, notably genes involved in immune responses, and therefore dictates immune cell recruitment to the liver. While CCl_4 liver hepatotoxicity leads to massive cell death, which may be triggering the observed increase in monocyte and macrophage infiltration in the liver in the absence of hepatocyte NF-κB1, DEN liver injury is mainly characterised by DNA damage, cell death and compensatory proliferation. Hepatocyte NF-κB1 may therefore play a more important role in monocyte/macrophage recruitment to the liver during hepatic cell death, while being less implicated in the regulation of genes in response to DNA damage and proliferation in acute liver injury.

No difference in liver apoptosis or necrosis was observed between Nfkb1$^{fl/fl}$ and Nfkb1$^{hep-/-}$ mice, suggesting that hepatocyte Nfkb1 does not modulate cell death in response to both CCl_4 and DEN acute liver injury. However, investigating the gene expression of different biomarkers, such as activated caspases (2, 3, 7, 8 and 9), cytochrome c, Apo-1, and p53 (Elsharkawy et al., 2010), could reveal differences in anti-apoptotic signalling for example. Experiments additionally showed no difference in proliferation and DNA damage between Nfkb1$^{fl/fl}$ and Nfkb1$^{hep-/-}$ mice, indicating that hepatocyte NF-κB1 does not play a protective role in DNA damage and does not modulate hepatocyte proliferation following CCl_4 or DEN induced acute liver injury.

Similar observations were made in AAV-TBG-Cre and AAV-TBG-Null mice, whereby no significant differences between the two genotypes were found in inflammatory cell recruitment to the liver, hepatocyte cell death and proliferation, following acute CCl_4-induced liver injury. Therefore, it can be concluded that hepatocyte NF-κB1 does not play a protective role in acute liver injury triggered by CCl_4 or DEN, and, more specifically, hepatocyte NF-κB1 does not modulate neutrophil inflammatory gene expression and recruitment to the liver, apoptosis, necrosis and DNA damage in this context. Additional experiments would be required to validate this further.

Previous work has shown that NF-κB1 protects against CCl_4-induced liver fibrosis *in vivo,* however cell-specific roles were not defined (Elsharkawy et al., 2010). Here, the role of hepatocyte NF-κB1 in liver fibrosis was investigated. Fibrosis was induced *in vivo* following biweekly CCl_4 IP injections carried out for 6 weeks in $Nfkb1^{-/-}$, $Nfkb1^{hep-/-}$ and control $Nfkb1^{fl/fl}$ mice, after which mice livers were harvested for analysis.

Interestingly, while a more severe liver fibrotic phenotype was found in $Nfkb1^{-/-}$ mice compared to $Nfkb1^{fl/fl}$ mice, in line with previous studies and further demonstrating a protective role for Nfkb1 in liver fibrosis, $Nfkb1^{fl/fl}$ mice were not protected against fibrosis compared to $Nfkb1^{hep-/-}$ mice. More specifically, increased neutrophil chemoattractant chemokine expression, neutrophil liver infiltration, fibrogenic gene expression and collagen deposition was observed in $Nfkb1^{-/-}$ mice, but not in $Nfkb1^{hep-/-}$ mice compared to control $Nfkb1^{fl/fl}$ mice. This is consistent with previous findings in a 12 week CCl_4-induced fibrosis *in vivo* model (Oakley, Mann, et al., 2005).

These results strongly suggest that, while NF-κB1 exerts an important protective role in liver fibrosis, when looking into cell-specific roles, hepatocyte NF-κB1 offers no protection against liver fibrosis. It can be concluded from this that NF-κB1 exerts an important anti-fibrotic and anti-inflammatory function in cells other than hepatocytes, with further experiments required to determine which cell types specifically. These could be hepatic stellate cells, which play a key role in liver fibrosis initiation, progression and regression (Zhang et al., 2016), or immune cells residing in the liver such as Kupffer cells. Cell-specific conditional knockout mice models could be used to test the involvement of these cell types in modulating responses to pro-fibrotic and pro-inflammatory stimuli, notably through the hepatotoxin CCl_4. Notably, similar PDGF Cre experiments are underway, whereby a mouse model of hepatic stellate cell knockout of nfkb1 has been generated through $Nfkb1^{fl/fl}$ mice and PDGF-$Cre^{+/-}$ mice recombination.

While no immune-modulatory role was revealed for hepatocyte NF-κB1 in the context of acute CCl_4, acute DEN or Chronic CCl_4 liver injury, hepatocyte NF-κB1 showed an important protective anti-tumorigenic role in DEN-induced hepatocellular carcinoma. Mice were injected IP with DEN at 2 weeks of age and sacrificed at 40 weeks, at which point macroscopic tumours had developed. Interestingly, $Nfkb1^{hep-/-}$ mice exhibited a significantly higher tumour incidence compared to $Nfkb1^{fl/fl}$ mice, demonstrating a tumour-protective role for hepatocyte NF-κB1. This was further reinforced by the increased prevalence of higher tumour grade tumours (HCC1 and HCC2) as well as

increased expression of the proliferation marker PCNA in Nfkb1$^{hep-/-}$ mice, in line with previous studies in Nfkb1$^{-/-}$ mice (Wilson et al., 2015). This demonstrates that sustained knockout of hepatocyte Nfkb1 has a profound effect on cellular function and homeostasis over time, leading to chronic inflammation and carcinogenesis. In contrast, knockout of hepatocyte Nfkb1 leads to little effect in the short term and in acute liver injury. Therefore mice must reach a certain age before pathological differences become significant between Nfkb1$^{fl/fl}$ and Nfkb1$^{hep-/-}$ mice. Also, the type of liver injury mice are subjected to lead to the generation of different metabolites which can act on different pathways leading to different phenotypes. While chronic DEN injury in Nfkb1$^{hep-/-}$ mice leads to a significantly more severe phenotype compared to Nfkb1$^{fl/fl}$ mice, no such effect is observed in a chronic CCl_4 model.

In addition, neutrophil recruitment to the liver was significantly increased in Nfkb1$^{hep-/-}$ mice compared to Nfkb1$^{fl/fl}$ mice, demonstrating that hepatocyte NF-κB1 restricts neutrophil liver chemotaxis in chronic DEN liver injury. Surprisingly, neutrophil chemoattractant chemokines S100A9, CXCL1 and CXCL2, previously shown to be significantly more expressed in the same DEN model in Nfkb1$^{-/-}$ mice compared to control mice, showed no differential expression between the two phenotypes. However, other chemokines involved in neutrophil migration and chemotaxis were found to be expressed at higher levels in Nfkb1$^{hep-/-}$ mice, as shown through RNA seq analysis. Additionally, monocyte and macrophage liver infiltration was significantly increased in Nfkb1$^{hep-/-}$ mice compared to Nfkb1$^{fl/fl}$ mice, however the chemokines responsible for this were not identified. However, genes involved in positive regulation of defence responses and responses to external stimuli, chemotaxis, myeloid leukocyte activation, regulation of TNF production and positive regulation of inflammatory responses were upregulated in Nfkb1$^{hep-/-}$ mice, shown by RNA seq analysis. These include Tlr13, MS4A7, ACOD1, CLEC4E, Lgals3, Rab7b, Lyz2 and Bcl2a1b. Overall these results demonstrate that hepatocyte NF-κB1 plays an anti-inflammatory role in DEN-induced hepatocellular carcinoma, restricting innate immune cell recruitment to the liver and thus dampening immune responses. T cell and B cell liver infiltration was unaffected by hepatocyte Nfkb1 knockout, demonstrating a specific role for hepatocyte NF-κB1 in the modulation of innate immune responses.

Interestingly, the increased inflammatory infiltrate observed in DEN-induced HCC Nfkb1$^{hep-/-}$ mice compared to Nfkb1$^{fl/fl}$ mice could be a consequence, rather than the cause, of the increased tumour burden. Since Nfkb1$^{hep-/-}$ mice exhibited more tumours,

this would likely lead to an increase in immune cells due to their known presence in tumour microenvironments. This could explain the lack of difference observed in neutrophil and macrophage chemoattractant chemokine expression; the total liver expression of these chemokines is therefore likely to be increased in $Nfkb1^{hep-/-}$ mice.

It was also shown that hepatocyte NF-κB1 plays a role in cell apoptosis modulation in DEN-induced hepatocellular carcinoma. The expression of anti-apoptotic genes Gadd45β, Bcl-2 and Bcl-xL was significantly increased in $Nfkb1^{hep-/-}$ mice compared to $Nfkb1^{fl/fl}$ mice, suggesting that hepatocyte NF-κB1 dampens anti-apoptotic signalling of tumorous cells, though this increase was not reflected at the protein level. Furthermore, genes linked to cancer were upregulated in $Nfkb1^{hep-/-}$ mice, including S100A6, GPNMB, Arl4c, Lgals3, Ear2 and bcl2a1a, further supporting the tumour suppressive function of hepatocyte NF-κB1.

Similar results were observed in AAV-TBG-Cre mice compared to AAV-TBG-Null mice, further supporting the anti-tumorigenic and anti-inflammatory function of hepatocyte Nfkb1.

Of note, while this was not performed here, controls for cre recombinase expression mediated toxicity would be valuable in demonstrating that the observed effects of Nfkb1 hepatocyte knockout are caused by the lack of hepatocyte Nfkb1 only rather than cre toxicity. Possible controls include performing similar experiments (e.g. acute or chronic CCl_4 or DEN) comparing WT mice and WT mice crossed with Alb-Cre mice, therefore expressing the cre recombinase enzyme. This would allow for the determination of any cre-specific mediated effects, particularly with regards to immune cell recruitment, apoptosis and tumorigenesis. Additionally, similar experiments could be conducted to as AAV control to account for any AAV-mediated effect; here, experiments should be carried out in WT mice injected with AAV8-TBG-Cre, WT mice injected with AAV8-TBG-Null, and Nfkb1fl/fl mice injected with AAV8-TBG-Cre.

In conclusion, while hepatocyte NF-κB1 demonstrated little protective and anti-inflammatory role in acute liver injury as well as in a CCl_4-induced fibrosis model, its anti-tumorigenic role was apparent in a DEN-induced hepatocellular carcinoma model. Future studies may further elucidate the cell-specific roles of NF-κB1, which is important in order to understand the full landscape of Nfkb1 gene expression modulation.

Serum	24h CCl_4	48h CCl_4	24h DEN	48h DEN	6 wks CCl_4	40 wks DEN
ALT	ns	ns	ns	ns	ns	ns
AST	ns	ns Nfkb1fl/fl vs Nfkb1hep-/- Sig decrease in AAV-TBG-Cre	ns	Sig decrease in Nfkb1hep-/-	ns	ns
Immunohistochemistry	**24h CCl_4**	**48h CCl_4**	**24h DEN**	**48h DEN**	**6 wks CCl_4**	**40 wks DEN**
F4/80	Sig increase in $Nfkb1^{hep-/-}$ ns AAV-TBG-Null vs AAV-TBG-Cre	ns $Nfkb1^{fl/fl}$ vs $Nfkb1^{hep-/-}$ Sig increase in AAV-TBG-Cre	-	-	-	-
CD68	-	-	ns	ns	ns	Sig increase in $Nfkb1^{hep-/-}$ and AAV-TBG-Cre
Ly6G	ns	ns	-	-	ns	-
NIMP	-	-	ns	ns		Sig increase in $Nfkb1^{hep-/-}$ and AAV-TBG-Cre
Cleaved caspase-3	ns	ns	-	-	-	ns
PCNA	-	-	ns	ns	-	Sig increase in $Nfkb1^{hep-/-}$ and AAV-TBG-Cre
High PCNA	-	-	-	-	-	Sig increase in $Nfkb1^{hep-/-}$ and AAV-TBG-Cre
Tumour PCNA	-	-	-	-	-	Sig increase in $Nfkb1^{hep-/-}$
γH2AX	-	-	ns	ns	-	ns
Sirius Red	-	-	-	-	ns	-
α-SMA	-	-	-	-	ns	-
CD3	-	-	-	-	-	ns
CD4	-	-	-	-	-	ns
CD8	-	-	-	-	-	ns
FOXP3	-	-	-	-	-	ns
B220	-	-	-	-	-	ns
Liver mRNA expression	**24h CCl_4**	**48h CCl_4**	**24h DEN**	**48h DEN**	**6 wks CCl_4**	**40 wks DEN**
S100A9	ns	ns	ns	ns	ns	ns
CXCL1	ns	ns	ns	ns	ns	ns
CXCL2	ns	ns	ns	ns	ns	ns
CCL2	ns	ns	ns	ns	ns	ns
CCL5	ns	ns	ns	ns	ns	ns
TNFα	ns	ns	ns	ns	ns	ns
IL-6	ns	ns	-	-	ns	-
CXCL10	-	-	-	-	ns	-
Gadd45β	ns	ns	ns	ns	-	ns
Bcl-2	ns	ns	ns	ns	-	ns
Bcl-xL	ns	ns	ns	ns	-	ns
XIAP	ns	ns	-	-	-	-
BAX	ns	ns	-	-	-	-
ARG1	-	-	-	-	ns	-
ARG2	-	-	-	-	ns	-
α-SMA	-	-	-	-	ns	-
COL1A1	-	-	-	-	ns	-
TIMP1	-	-	-	-	ns	-
TGF-β	-	-	-	-	ns	-
Tumour mRNA expression	**24h CCl_4**	**48h CCl_4**	**24h DEN**	**48h DEN**	**6 wks CCl_4**	**40 wks DEN**
TNFα	-	-	-	-	-	ns
S100A9	-	-	-	-	-	ns
CXCL1	-	-	-	-	-	ns
CXCL2	-	-	-	-	-	ns
CCL2	-	-	-	-	-	ns
CCL5	-	-	-	-	-	ns
Gadd45β	-	-	-	-	-	Sig increase in $Nfkb1^{hep-/-}$ ns in AAV-TBG-Cre
Bcl-xL	-	-	-	-	-	Sig increase in $Nfkb1^{hep-/-}$ ns in AAV-TBG-Cre
Bcl-2	-	-	-	-	-	Sig increase in $Nfkb1^{hep-/-}$ ns in AAV-TBG-Cre
Liver protein expression	**24h CCl_4**	**48h CCl_4**	**24h DEN**	**48h DEN**	**6 wks CCl_4**	**40 wks DEN**
p-ERK	-	-	-	-	-	ns
p-JNK	-	-	-	-	-	ns
cREL	-	-	-	-	-	ns
p65	-	-	-	-	-	ns
p52	-	-	-	-	-	ns
Bcl-2	-	-	-	-	-	ns
Bcl-xL	-	-	-	-	-	ns
Tumour protein expression	**24h CCl_4**	**48h CCl_4**	**24h DEN**	**48h DEN**	**6 wks CCl_4**	**40 wks DEN**
p-ERK	-	-	-	-	-	ns
p-JNK	-	-	-	-	-	ns
Bcl-2	-	-	-	-	-	ns
Bcl-xL	-	-	-	-	-	ns
γH2AX	-	-	-	-	-	ns
Cyclin D1	-	-	-	-	-	ns
Cleaved caspase 3	-	-	-	-	-	ns
Weight	**24h CCl_4**	**48h CCl_4**	**24h DEN**	**48h DEN**	**6 wks CCl_4**	**40 wks DEN**
Liver weight	-	-	-	-	ns	-
Mouse weight	-	-	-	-	ns	-
Liver/Body weight ratio	-	-	-	-	ns	ns in $Nfkb1^{fl/fl}$ vs $Nfkb1^{hep-/-}$ Sig increase in AAV-TBG-Cre
HCC	**24h CCl_4**	**48h CCl_4**	**24h DEN**	**48h DEN**	**6 wks CCl_4**	**40 wks DEN**
Total tumours	-	-	-	-	-	Sig increase in $Nfkb1^{hep-/-}$ and AAV-TBG-Cre
Large tumours	-	-	-	-	-	ns
Tumour grade	-	-	-	-	-	Sig increase in HCC2/HCC1 tumours in $Nfkb1^{hep-/-}$ and AAV-TBG-Cre
Total tumour area	-	-	-	-	-	Sig increase in $Nfkb1^{hep-/-}$

Table 6.1 Summary table of data from all liver injury models

References

Abstract, G. (2018) Loss of NF-κB1 Causes Gastric Cancer with Aberrant Inflammation and Expression of Immune Checkpoint Regulators in a STAT-1-Dependent Manner. *Immunity*. 48570-583.e8.

Alexander, M., Loomis, A.K., van der Lei, J., Duarte-Salles, T., Prieto-Alhambra, D., Ansell, D., Pasqua, A., Lapi, F., Rijnbeek, P., Mosseveld, M., Waterworth, D.M., Kendrick, S., Sattar, N. & Alazawi, W. (2019) Risks and clinical predictors of cirrhosis and hepatocellular carcinoma diagnoses in adults with diagnosed NAFLD: Real-world study of 18 million patients in four European cohorts. *BMC Medicine*. 17 (1), 95.

Al-Saad, S., Al-Shibli, K., Donnem, T., Persson, M., Bremnes, R.M. & Busund, L.T. (2008) The prognostic impact of NF-κB p105, vimentin, E-cadherin and Par6 expression in epithelial and stromal compartment in non-small-cell lung cancer. *British Journal of Cancer*. 99 (9), 1476–1483.

Ambrosino, G., Varotto, S., Basso, S.M.M., Cecchetto, A., Carraro, P., Naso, A., de Silvestro, G., Plebani, M., Abatangelo, G., Donato, D., Cestrone, A., Giron, G. & D'Amico, D.F. (2003) Hepatocyte transplantation in the treatment of acute liver failure: Microencapsulated hepatocytes versus hepatocytes attached to an autologous biomatrix. *Cell Transplantation*. 12 (1), 43–49.

Anon (n.d.) *SCFβ-TrCP ubiquitin ligase-mediated processing of NF-κB p105 requires phosphorylation of its C-terminus by IκB kinase*. [Online] [online]. Available from: https://www.ncbi.nlm.nih.gov/pmc/articles/PMC212749/ (Accessed 1 March 2020).

Anstee, Q.M., Reeves, H.L., Kotsiliti, E., Govaere, O. & Heikenwalder, M. (2019) From NASH to HCC: current concepts and future challenges. Nature Reviews Gastroenterology and Hepatology 16 (7) p.411–428.

Arisawa, T., Tahara, T., Shiroeda, H., Yamada, K., Nomura, T., Yamada, H., Hayashi, R., Matsunaga, K., Otsuka, T., Nakamura, M., Shimasaki, T., Toshikuni, N., Kawada, N. & Shibata, T. (2013) Functional promoter polymorphisms of NFKB1 influence susceptibility to the diffuse type of gastric cancer. *Oncology Reports*. 30 (6), 3013–3019.

Babu, G.R., Jin, W., Norman, L., Waterfield, M., Chang, M., Wu, X., Zhang, M. & Sun, S.C. (2006) Phosphorylation of NF-κB1/p105 by oncoprotein kinase Tpl2: Implications for a novel mechanism of Tpl2 regulation. *Biochimica et Biophysica Acta - Molecular Cell Research*. 1763 (2), 174–181.

Bartfai, T., Mantovani, A., Martinez, F.O., Sironi, M., Sozzani, S., Locati, M., Deuschle, U. & Massardi, M.L. (2020) Human Monocytes 5/RANTES and by Lipopolysaccharide in Activated by the CC Chemokine Ligand Analysis of the Gene Expression Profile. *J Immunol References*. 1683557–3562.

Bataller, R. & Brenner, D.A. (2005) Liver fibrosis. Journal of Clinical Investigation 115 (2) p.209–218.

Beinke, S., Deka, J., Lang, V., Belich, M.P., Walker, P.A., Howell, S., Smerdon, S.J., Gamblin, S.J. & Ley, S.C. (2003) NF- B1 p105 Negatively Regulates TPL-2 MEK Kinase Activity. *Molecular and Cellular Biology*. 23 (14), 4739–4752.

Beinke, S., Robinson, M.J., Hugunin, M. & Ley, S.C. (2004) Lipopolysaccharide activation of the TPL-2/MEK/extracellular signal-regulated kinase mitogen-activated protein kinase cascade is

regulated by IkappaB kinase-induced proteolysis of NF-kappaB1 p105. *Molecular and cellular biology*. 24 (21), 9658–67.

Benedict, M. & Zhang, X. (2017) Non-alcoholic fatty liver disease: An expanded review. World Journal of Hepatology 9 (16) p.715–732.

Bernal, G.M., Wahlstrom, J.S., Crawley, C.D., Cahill, K.E., Pytel, P., Liang, H., Kang, S., Weichselbaum, R.R. & Yamini, B. (2014) Loss of Nfkb1 leads to early onset aging. *Aging*. 6 (11), 931–943.

Best, K.T., Lee, F.K., Knapp, E., Awad, H.A. & Loiselle, A.E. (2019) Deletion of NFKB1 enhances canonical NF-κB signaling and increases macrophage and myofibroblast content during tendon healing. *Scientific Reports*. 9 (1), 1–11.

Bishayee, A. (2014) The role of inflammation in liver cancer. *Advances in Experimental Medicine and Biology*. 816401–435.

de Boer, Y.S., Kosinski, A.S., Urban, T.J., Zhao, Z., Long, N., Chalasani, N., Kleiner, D.E. & Hoofnagle, J.H. (2017) Features of Autoimmune Hepatitis in Patients With Drug-induced Liver Injury. *Clinical Gastroenterology and Hepatology*. 15 (1), 103-112.e2.

Bohuslav, J., Kravchenko, V. v., Parry, G.C.N., Erlich, J.H., Gerondakis, S., Mackman, N. & Ulevitch, R.J. (1998) Regulation of an essential innate immune response by the p50 subunit of NF-κB. *Journal of Clinical Investigation*. 102 (9), 1645–1652.

Bonizzi, G. & Karin, M. (2004) The two NF-κB activation pathways and their role in innate and adaptive immunity. Trends in Immunology 25 (6) p.280–288.

Bonkovsky, H.L. (1991) Iron and the liver. *American Journal of the Medical Sciences*. 301 (1), 32–43.

Bouwens, L., de Bleser, P., Vanderkerken, K., Geerts, B. & Wisse, E. (1992) Liver cell heterogeneity: Functions of non-parenchymal cells. Enzyme 46 (1–3) p.155–168.

Brenner, C., Rosenthal, D., Perec, L. & Merajver, S. (2008) Down regulation of NfkB1 expression blocks cell motility in a cell line model of inflammatory breast cancer. *Cancer Research*. 68 (9 Supplement), .

Brenner, D.A. (2009) Molecular pathogenesis of liver fibrosis. Transactions of the American Clinical and Climatological Association 120 p.361–368.

Brücher, B.L.D.M. & Jamall, I.S. (2019) Transition from normal to cancerous cell by precancerous niche (PCN) induced chronic cell-matrix stress. *4open*. 214.

Bruha, R., Dvorak, K. & Petrtyl, J. (2012) Alcoholic liver disease. *World Journal of Hepatology*. 4 (3), 81–90.

Budunova, I. v., Perez, P., Vaden, V.R., Spiegelman, V.S., Slaga, T.J. & Jorcano, J.L. (1999) Increased expression of p50-NF-κB and constitutive activation of NF-κB transcription factors during mouse skin carcinogenesis. *Oncogene*. 18 (52), 7423–7431.

Cai, Q., Tu, M., Xu-Monette, Z.Y., Sun, R., Manyam, G.C., Xu, X., Tzankov, A., Hsi, E.D., Møller, M.B., Medeiros, L.J., Ok, C.Y. & Young, K.H. (2017) NF-κ B p50 activation associated with immune dysregulation confers poorer survival for diffuse large B-cell lymphoma patients with wild-type p53. *Modern Pathology*. 30 (6), 854–876.

Canbay, A., Tacke, F., Hadem, J., Trautwein, C., Gerken, G. & Manns, M.P. (2011) Übersichtsarbeit - Akutes leberversagen. Deutsches Arzteblatt 108 (42) p.714–720.

Cao, L., Quan, X.B., Zeng, W.J., Yang, X.O. & Wang, M.J. (2016) Mechanism of hepatocyte apoptosis. *Journal of Cell Death*. 919–29.

Cao, S., Zhang, X., Edwards, J.P. & Mosser, D.M. (2006) NF-κB1 (p50) homodimers differentially regulate pro- and anti-inflammatory cytokines in macrophages. *Journal of Biological Chemistry*. 281 (36), 26041–26050.

Carrillo-Carrasco, N., Chandler, R.J., Chandrasekaran, S. & Venditti, C.P. (2010) Liver-directed recombinant adeno-associated viral gene delivery rescues a lethal mouse model of methylmalonic acidemia and provides long-term phenotypic correction. *Human Gene Therapy*. 21 (9), 1147–1154.

Cartwright, T., Perkins, N.D. & L Wilson, C. (2016) NFKB1: a suppressor of inflammation, ageing and cancer. The FEBS journal 283 (10) p.1812–1822.

Cartwright, T.N., Worrell, J.C., Marchetti, L., Dowling, C.M., Knox, A., Kiely, P., Mann, J., Mann, D.A. & Wilson, C.L. (2018) HDAC1 interacts with the p50 NF-κB subunit via its nuclear localization sequence to constrain inflammatory gene expression. *Biochimica et Biophysica Acta - Gene Regulatory Mechanisms*. 1861 (10), 962–970.

Chang, T.P. & Vancurova, I. (2014) Bcl3 regulates pro-survival and pro-inflammatory gene expression in cutaneous T-cell lymphoma. *Biochimica et Biophysica Acta - Molecular Cell Research*. 1843 (11), 2620–2630.

Chen, T.L., Tran, M., Lakshmanan, A., Harrington, B.K., Gupta, N., Goettl, V.M., Lehman, A.M., Trudeau, S., Lucas, D.M., Johnson, A.J., Byrd, J.C. & Hertlein, E. (2017) NF-kB p50 (nfkb1) contributes to pathogenesis in the Eμ-TCL1 mouse model of chronic lymphocytic leukemia. Blood 130 (3) p.376–379.

Choudhary, C., Kumar, C., Gnad, F., Nielsen, M.L., Rehman, M., Walther, T.C., Olsen, J. v. & Mann, M. (2009) Lysine acetylation targets protein complexes and co-regulates major cellular functions. *Science*. 325 (5942), 834–840.

Chowdhury, G., Calcutt, M.W., Nagy, L.D. & Guengerich, F.P. (2012) Oxidation of methyl and ethyl nitrosamines by cytochrome P450 2E1 and 2B1. *Biochemistry*. 51 (50), 9995–10007.

Cogswell, P.C., Guttridge, D.C., Funkhouser, W.K. & Baldwin, A.S. (2000) Selective activation of NF-κB subunits in human breast cancer: Potential roles for NF-κB2/p52 and for Bcl-3. *Oncogene*. 19 (9), 1123–1131.

Collins, P., Mitxitorena, I. & Carmody, R. (2016) The Ubiquitination of NF-κB Subunits in the Control of Transcription. *Cells*. 5 (2), 23.

Collins, P.E., Kiely, P.A. & Carmody, R.J. (2014) Inhibition of transcription by B cell leukemia 3 (Bcl-3) protein requires interaction with nuclear factor κB (NF-κB) p50. *Journal of Biological Chemistry*. 289 (10), 7059–7067.

Concetti, J. & Wilson, C.L. (2018) NFKB1 and Cancer: Friend or Foe? *Cells*. 7 (9), 133.

Corless, J.K. (1983) Normal liver function. A basis for understanding hepatic disease. *Archives of Internal Medicine*. 143 (12), 2291–2294.

Crawley, C.D., Kang, S., Bernal, G.M., Wahlstrom, J.S., Voce, D.J., Cahill, K.E., Garofalo, A., Raleigh, D.R., Weichselbaum, R.R. & Yamini, B. (2015) S-phase-dependent p50/NF-κB1 phosphorylation in response to ATR and replication stress acts to maintain genomic stability. *Cell Cycle*. 14 (4), 566–576.

Crowley, L.C. & Waterhouse, N.J. (2016) Detecting cleaved caspase-3 in apoptotic cells by flow cytometry. *Cold Spring Harbor Protocols*. 2016 (11), 958–962.

Deshmane, S.L., Kremlev, S., Amini, S. & Sawaya, B.E. (2009) Monocyte chemoattractant protein-1 (MCP-1): An overview. Journal of Interferon and Cytokine Research 29 (6) p.313–325.

Dobrzanski, P., Ryseck, R.P. & Bravo, R. (1993) Both N- and C-terminal domains of RelB are required for full transactivation: role of the N-terminal leucine zipper-like motif. *Molecular and Cellular Biology*. 13 (3), 1572–1582.

Doi, T.S., Marino, M.W., Takahashi, T., Yoshida, T., Sakakura, T., Old, L.J. & Obata, Y. (1999a) Absence of tumor necrosis factor rescues RelA-deficient mice from embryonic lethality. *Proceedings of the National Academy of Sciences of the United States of America*. 96 (6), 2994–2999.

Doi, T.S., Marino, M.W., Takahashi, T., Yoshida, T., Sakakura, T., Old, L.J. & Obata, Y. (1999b) Absence of tumor necrosis factor rescues RelA-deficient mice from embryonic lethality. *Proceedings of the National Academy of Sciences of the United States of America*. 96 (6), 2994–2999.

Ea, C.K., Hao, S.L., Yeo, K.S. & Baltimore, D. (2012) EHMT1 protein binds to nuclear factor-κB p50 and represses gene expression. *Journal of Biological Chemistry*. 287 (37), 31207–31217.

Eck, S.L., Perkins, N.D., Carr, D.P. & Nabel, G.J. (1993) Inhibition of phorbol ester-induced cellular adhesion by competitive binding of NF-kappa B in vivo. *Molecular and Cellular Biology*. 13 (10), 6530–6536.

Elmore, S.A., Dixon, D., Hailey, J.R., Harada, T., Herbert, R.A., Maronpot, R.R., Nolte, T., Rehg, J.E., Rittinghausen, S., Rosol, T.J., Satoh, H., Vidal, J.D., Willard-Mack, C.L. & Creasy, D.M. (2016) Recommendations from the INHAND Apoptosis/Necrosis Working Group. *Toxicologic Pathology*. 44 (2), 173–188.

Elsharkawy, A.M., Oakley, F., Lin, F., Packham, G., Mann, D.A. & Mann, J. (2010) The NF-κB p50:p50:HDAC-1 repressor complex orchestrates transcriptional inhibition of multiple pro-inflammatory genes. *Journal of Hepatology*. 53 (3), 519–527.

Feitelson, M.A., Arzumanyan, A., Kulathinal, R.J., Blain, S.W., Holcombe, R.F., Mahajna, J., Marino, M., Martinez-Chantar, M.L., Nawroth, R., Sanchez-Garcia, I., Sharma, D., Saxena, N.K., Singh, N., Vlachostergios, P.J., Guo, S., Honoki, K., Fujii, H., Georgakilas, A.G., Bilsland, A., et al. (2015) Sustained proliferation in cancer: Mechanisms and novel therapeutic targets. Seminars in Cancer Biology 35 (Suppl) p.S25–S54.

de Feo, P. & Lucidi, P. (2002) Liver protein synthesis in physiology and in disease states. Current opinion in clinical nutrition and metabolic care 5 (1) p.47–50.

Ferrier, R., Nougarede, R., Doucet, S., Kahn-Perles, B., Imbert, J. & Mathieu-Mahul, D. (1999) Physical interaction of the bHLH LYL1 protein and NF-κB1 p105. *Oncogene*. 18 (4), 995–1005.

Fink, S.L. & Cookson, B.T. (2005) Apoptosis, pyroptosis, and necrosis: Mechanistic description of dead and dying eukaryotic cells. Infection and Immunity 73 (4) p.1907–1916.

Fujimoto, K., Yasuda, H., Sato, Y. & Yamamoto, K. ichi (1995) A role for phosphorylation in the proteolytic processing of the human NF-KB1 precursor. *Gene*. 165 (2), 183–189.

Gao, B. (2016) Basic liver immunology. Cellular and Molecular Immunology 13 (3) p.265–266.

Gerondakis, S. & Siebenlist, U. (2010) Roles of the NF-kappaB pathway in lymphocyte development and function. Cold Spring Harbor perspectives in biology 2 (5) p.a000182.

Ghouri, Y.A., Mian, I. & Rowe, J.H. (2017) Review of hepatocellular carcinoma: Epidemiology, etiology, and carcinogenesis. Journal of Carcinogenesis 16 (1) p.1–8.

Giannini, E.G., Testa, R. & Savarino, V. (2005) Liver enzyme alteration: A guide for clinicians. CMAJ 172 (3) p.367–379.

Giri, B., Garg, B., Modi, S., George, J., Sethi, V., Banerjee, S., Saluja, A. & Dudeja, V. (2016) NF-κB P50 Subunit in Stellate-Cells Actively Modulates Cancer Growth in Mouse Models of Pancreatic Cancer. *Journal of the American College of Surgeons*. 223 (4), S142.

Grundström, S., Anderson, P., Scheipers, P. & Sundstedt, A. (2004) Bcl-3 and NFκB p50-p50 Homodimers Act as Transcriptional Repressors in Tolerant CD4+ T Cells. *Journal of Biological Chemistry*. 279 (9), 8460–8468.

Guan, H., Hou, S. & Ricciardi, R.P. (2005) DNA binding of repressor nuclear factor-κB p50/p50 depends on phosphorylation of Ser337 by the protein kinase A catalytic subunit. *Journal of Biological Chemistry*. 280 (11), 9957–9962.

Guicciardi, M.E. & Gores, G.J. (2005) Apoptosis: A mechanism of acute and chronic liver injury. Gut 54 (7) p.1024–1033.

Guicciardi, M.E., Malhi, H., Mott, J.L. & Gores, G.J. (2013) Apoptosis and necrosis in the liver. *Comprehensive Physiology*. 3 (2), 977–1010.

Guo, X., Koff, J.L., Moffitt, A.B., Cinar, M., Ramachandiran, S., Chen, Z., Switchenko, J.M., Mosunjac, M., Neill, S.G., Mann, K.P., Bagirov, M., Du, Y., Natkunam, Y., Khoury, H.J., Rossi, M.R., Harris, W., Flowers, C.R., Lossos, I.S., Boise, L.H., et al. (2017) Molecular impact of selective NFKB1 and NFKB2 signaling on DLBCL phenotype. *Oncogene*. 36 (29), 4224–4232.

Hanahan, D. & Weinberg, R.A. (2011) Hallmarks of cancer: The next generation. Cell 144 (5) p.646–674.

Hassa, P.O., Buerki, C., Lombardi, C., Imhof, R. & Hottiger, M.O. (2003) Transcriptional Coactivation of Nuclear Factor-κB-dependent Gene Expression by p300 Is Regulated by Poly(ADP)-ribose Polymerase-1. *Journal of Biological Chemistry*. 278 (46), 45145–45153.

Havard, L., Rahmouni, S., Boniver, J. & Delvenne, P. (2005) High levels of p105 (NFKB1) and p100 (NFKB2) proteins in HPV16-transformed keratinocytes: Role of E6 and E7 oncoproteins. *Virology*. 331 (2), 357–366.

Hayato, N. & Shin, M. (2012) Inflammation- and stress-related signaling pathways in hepatocarcinogenesis. World Journal of Gastroenterology 18 (31) p.4071–4081.

Hayden, M.S. & Ghosh, S. (2004) Signaling to NF-κB. Genes and Development 18 (18) p.2195–2224.

Hayden, M.S., West, A.P. & Ghosh, S. (2006) NF-κB and the immune response. Oncogene 25 (51) p.6758–6780.

Heindryckx, F., Colle, I. & van Vlierberghe, H. (2009) Experimental mouse models for hepatocellular carcinoma research. International Journal of Experimental Pathology 90 (4) p.367–386.

Hinz, B., Phan, S.H., Thannickal, V.J., Galli, A., Bochaton-Piallat, M.L. & Gabbiani, G. (2007) The myofibroblast: One function, multiple origins. *American Journal of Pathology*. 170 (6), 1807–1816.

Hoebe, K., Janssen, E.M., Kim, S.O., Alexopoulou, L., Flavell, R.A., Han, J. & Beutler, B. (2003) Upregulation of costimulatory molecules induced by lipopolysaccharide and double-stranded

RNA occurs by Trif-dependent and Trif-independent pathways. *Nature Immunology*. 4 (12), 1223–1229.

Hoesel, B. & Schmid, J.A. (2013) The complexity of NF-κB signaling in inflammation and cancer. Molecular Cancer 12 (1).

Horiguchi, N., Lafdil, F., Miller, A.M., Park, O., Wang, H., Rajesh, M., Mukhopadhyay, P., Fu, X.Y., Pacher, P. & Gao, B. (2010) Dissociation between liver inflammation and hepatocellular damage induced by carbon tetrachloride in myeloid cell-specific signal transducer and activator of transcription 3 gene knockout mice. *Hepatology*. 51 (5), 1724–1734.

Hua, T., Qinsheng, W., Xuxia, W., Shuguang, Z., Ming, Q., Zhenxiong, L. & Jingjie, W. (2014) Nuclear factor-kappa b1 is associated with gastric cancer in a Chinese population. *Medicine (United States)*. 93 (28), e279.

Huang, T., Kang, W., Zhang, B., Wu, F., Dong, Y., Tong, J.H.M., Yang, W., Zhou, Y., Zhang, L., Cheng, A.S.L., Yu, J. & To, K.F. (2016) miR-508-3p concordantly silences NFKB1 and RELA to inactivate canonical NF-KB signaling in gastric carcinogenesis. *Molecular Cancer*. 15 (1), 9.

I, G., V, B., P, P., I, L., P, A., D, P., S, K. & H, P. (2014) Metadherin, p50, and p65 Expression in Epithelial Ovarian Neoplasms: An Immunohistochemical Study. *BioMed research international*. 2014.

Jacque, E., Schweighoffer, E., Visekruna, A., Papoutsopoulou, S., Janzen, J., Zillwood, R., Tarlinton, D.M., Tybulewicz, V.L.J. & Ley, S.C. (2014) IKK-induced NF-κB1 p105 proteolysis is critical for B cell antibody responses to T cell-dependent antigen. *Journal of Experimental Medicine*. 211 (10), 2085–2101.

Jung, H., Kim, J.S., Kim, W.K., Oh, K.J., Kim, J.M., Lee, H.J., Han, B.S., Kim, D.S., Seo, Y.S., Lee, S.C., Park, S.G. & Bae, K.H. (2015) Intracellular annexin A2 regulates Nf-kB signaling by binding to the p50 subunit: Implications for gemcitabine resistance in pancreatic cancer. *Cell Death and Disease*. 6 (1), .

Jurk, D., Wilson, C., Passos, J.F., Oakley, F., Correia-Melo, C., Greaves, L., Saretzki, G., Fox, C., Lawless, C., Anderson, R., Hewitt, G., Pender, S.L.F., Fullard, N., Nelson, G., Mann, J., van de Sluis, B., Mann, D.A. & von Zglinicki, T. (2014) Chronic inflammation induces telomere dysfunction and accelerates ageing in mice. *Nature Communications*. 2 (1), 1–14.

Kang, S.M., Tran, A.C., Grilli, M. & Lenardo, M.J. (1992) NF-κB subunit regulation in nontransformed CD4+ T lymphocytes. *Science*. 256 (5062), 1452–1456.

Karin, M. (2009) NF-kappaB as a critical link between inflammation and cancer. Cold Spring Harbor perspectives in biology 1 (5).

Karin, M. (2006) Nuclear factor-κB in cancer development and progression. Nature 441 (7092) p.431–436.

Keenan, B.P., Fong, L. & Kelley, R.K. (2019) Immunotherapy in hepatocellular carcinoma: The complex interface between inflammation, fibrosis, and the immune response. Journal for ImmunoTherapy of Cancer 7 (1) p.1–13.

Keepers, T.R., Gross, L.K. & Obrig, T.G. (2007) Monocyte chemoattractant protein 1, macrophage inflammatory protein 1α, and RANTES recruit macrophages to the kidney in a mouse model of hemolytic-uremic syndrome. *Infection and Immunity*. 75 (3), 1229–1236.

Kipps, T.J., Stevenson, F.K., Wu, C.J., Croce, C.M., Packham, G., Wierda, W.G., O'Brien, S., Gribben, J. & Rai, K. (2017) Chronic lymphocytic leukaemia. *Nature Reviews Disease Primers*. 3.

Kmiec, Z. (2001) Cooperation of liver cells in health and disease. Advances in anatomy, embryology, and cell biology 161.

Kravtsova-Ivantsiv, Y., Shomer, I., Cohen-Kaplan, V., Snijder, B., Superti-Furga, G., Gonen, H., Sommer, T., Ziv, T., Admon, A., Naroditsky, I., Jbara, M., Brik, A., Pikarsky, E., Kwon, Y.T., Doweck, I. & Ciechanover, A. (2015a) KPC1-mediated ubiquitination and proteasomal processing of nf-κb1 p105 to p50 restricts tumor growth. *Cell*. 161 (2), 333–347.

Kravtsova-Ivantsiv, Y., Shomer, I., Cohen-Kaplan, V., Snijder, B., Superti-Furga, G., Gonen, H., Sommer, T., Ziv, T., Admon, A., Naroditsky, I., Jbara, M., Brik, A., Pikarsky, E., Kwon, Y.T., Doweck, I. & Ciechanover, A. (2015b) KPC1-mediated ubiquitination and proteasomal processing of nf-κb1 p105 to p50 restricts tumor growth. *Cell*. 161 (2), 333–347.

Krenkel, O. & Tacke, F. (2017) Liver macrophages in tissue homeostasis and disease. Nature Reviews Immunology 17 (5) p.306–321.

Krishna, M. (2013) Microscopic anatomy of the liver. Clinical Liver Disease 2 (SUPPL. 1) p.S4.

Lawrence, T. (2009) The nuclear factor NF-kappaB pathway in inflammation. Cold Spring Harbor perspectives in biology 1 (6).

Lee, H.W., Choi, H.Y., Joo, K.M. & Nam, D.H. (2015) Tumor progression locus 2 (Tpl2) kinase as a novel therapeutic target for cancer: Double-sided effects of Tpl2 on cancer. International Journal of Molecular Sciences 16 (3) p.4471–4491.

Lee, J.S. (2015) The mutational landscape of hepatocellular carcinoma. Clinical and molecular hepatology 21 (3) p.220–229.

Li, C.W., Chang, P.Y. & Chen, B. sen (2016) Investigating the mechanism of hepatocellular carcinoma progression by constructing genetic and epigenetic networks using NGS data identification and big database mining method. *Oncotarget*. 7 (48), 79453–79473.

Li, J., Jia, H., Xie, L., Wang, Xuedong, Wang, Xia, He, H., Lin, Y. & Hu, L. (2009) Association of constitutive nuclear factor-JB activation with aggressive aspects and poor prognosis in cervical cancer. *International Journal of Gynecological Cancer*. 19 (8), 1421–1426.

Li, Q. & Verma, I.M. (2002) NF-κB regulation in the immune system. Nature Reviews Immunology 2 (10) p.725–734.

Li, Z., Zhang, J., Chen, D. & Shu, H.B. (2003) Casper/c-FLIP is physically and functionally associated with NF-κB1 p105. *Biochemical and Biophysical Research Communications*. 309 (4), 980–985.

Lin, G., Li, C., Huang, C., Zhuang, W., Huang, Y., Xu, H., Miao, Q. & Hu, D. (2018) Co-expression of NF-κB-p65 and phosphorylated NF-κB-p105 is associated with poor prognosis in surgically resectable non-small cell lung cancer. *Journal of Cellular and Molecular Medicine*. 22 (3), 1923–1930.

Lin, L., DeMartino, G.N. & Greene, W.C. (1998) Cotranslational biogenesis of NF-kappaB p50 by the 26S proteasome. *Cell*. 92 (6), 819–28.

Liu, T., Zhang, L., Joo, D. & Sun, S.C. (2017) NF-κB signaling in inflammation. Signal Transduction and Targeted Therapy 2 p.17023.

Luedde, T. & Schwabe, R.F. (2011a) NF-κB in the liver-linking injury, fibrosis and hepatocellular carcinoma. Nature Reviews Gastroenterology and Hepatology 8 (2) p.108–118.

Luedde, T. & Schwabe, R.F. (2011b) NF-κB in the liver-linking injury, fibrosis and hepatocellular carcinoma. Nature Reviews Gastroenterology and Hepatology 8 (2) p.108–118.

Maeda, S., Kamata, H., Luo, J.L., Leffert, H. & Karin, M. (2005) IKKβ couples hepatocyte death to cytokine-driven compensatory proliferation that promotes chemical hepatocarcinogenesis. *Cell*. 121 (7), 977–990.

Manco, R., Leclercq, I.A. & Clerbaux, L.A. (2018a) Liver regeneration: Different sub-populations of parenchymal cells at play choreographed by an injury-specific microenvironment. International Journal of Molecular Sciences 19 (12).

Manco, R., Leclercq, I.A. & Clerbaux, L.A. (2018b) Liver regeneration: Different sub-populations of parenchymal cells at play choreographed by an injury-specific microenvironment. International Journal of Molecular Sciences 19 (12).

Margetts, J., Ogle, L.F., Chan, S.L., Chan, A.W.H., Chan, K.C.A., Jamieson, D., Willoughby, C.E., Mann, D.A., Wilson, C.L., Manas, D.M., Yeo, W. & Reeves, H.L. (2018) Neutrophils: Driving progression and poor prognosis in hepatocellular carcinoma? *British Journal of Cancer*. 118 (2), 248–257.

Mathas, S., Jöhrens, K., Joos, S., Lietz, A., Hummel, F., Janz, M., Jundt, F., Anagnostopoulos, I., Bommert, K., Lichter, P., Stein, H., Scheidereit, C. & Dörken, B. (2005) Elevated NF-κB p50 complex formation and Bcl-3 expression in classical Hodgkin, anaplastic large-cell, and other peripheral T-cell lymphomas. *Blood*. 106 (13), 4287–4293.

McGlynn, K.A., Petrick, J.L. & London, W.T. (2015) Global Epidemiology of Hepatocellular Carcinoma: An Emphasis on Demographic and Regional Variability. Clinics in Liver Disease 19 (2) p.223–238.

McIlwain, D.R., Berger, T. & Mak, T.W. (2013) Caspase functions in cell death and disease. *Cold Spring Harbor Perspectives in Biology*. 5 (4), 1–28.

Meli, R., Raso, G.M. & Calignano, A. (2014) Role of innate immune response in non-alcoholic fatty liver disease: Metabolic complications and therapeutic tools. Frontiers in Immunology 5 (APR).

Mishra, A., Bharti, A.C., Varghese, P., Saluja, D. & Das, B.C. (2006) Differential expression and activation of NF-κB family proteins during oral carcinogenesis: Role of high risk human papillomavirus infection. *International Journal of Cancer*. 119 (12), 2840–2850.

Miyaoka, Y., Ebato, K., Kato, H., Arakawa, S., Shimizu, S. & Miyajima, A. (2012) Hypertrophy and unconventional cell division of hepatocytes underlie liver regeneration. *Current biology : CB*. 22 (13), 1166–1175.

Mizgerd, J.P., Lupa, M.M., Kogan, M.S., Warren, H.B., Kobzik, L. & Topulos, G.P. (2003) Nuclear factor-κB p50 limits inflammation and prevents lung injury during Escherichia coli pneumonia. *American Journal of Respiratory and Critical Care Medicine*. 168 (7), 810–817.

Mogensen, T.H. (2009) Pathogen recognition and inflammatory signaling in innate immune defenses. Clinical Microbiology Reviews 22 (2) p.240–273.

Mori, N., Fujii, M., Ikeda, S., Yamada, Y., Tomonaga, M., Ballard, D.W. & Yamamoto, N. (1999) Constitutive activation of NF-kappaB in primary adult T-cell leukemia cells. *Blood*. 93 (7), 2360–8.

Nagaraju, C.K., Robinson, E.L., Abdesselem, M., Trenson, S., Dries, E., Gilbert, G., Janssens, S., van Cleemput, J., Rega, F., Meyns, B., Roderick, H.L., Driesen, R.B. & Sipido, K.R. (2019) Myofibroblast Phenotype and Reversibility of Fibrosis in Patients With End-Stage Heart Failure. *Journal of the American College of Cardiology*. 73 (18), 2267–2282.

Oakley, F., Mann, J., Nailard, S., Smart, D.E., Mungalsingh, N., Constandinou, C., Ali, S., Wilson, S.J., Millward-Sadler, H., Iredale, J.P. & Mann, D.A. (2005) Nuclear factor-κB1 (p50) limits the inflammatory and fibrogenic responses to chronic injury. *American Journal of Pathology*. 166 (3), 695–708.

Oakley, F., Meso, M., Iredale, J.P., Green, K., Marek, C.J., Zhou, X., May, M.J., Millward-Sadler, H., Wright, M.C. & Mann, D.A. (2005) Inhibition of inhibitor of κb kinases stimulates hepatic stellate cell apoptosis and accelerated recovery from rat liver fibrosis. *Gastroenterology*. 128 (1), 108–120.

Oeckinghaus, A., Hayden, M.S. & Ghosh, S. (2011) Crosstalk in NF-κB signaling pathways. Nature Immunology 12 (8) p.695–708.

Okamoto, T., Sanda, T. & Asamitsu, K. (2007) NF-kappa B signaling and carcinogenesis. *Current pharmaceutical design*. 13 (5), 447–62.

O'Rourke, J.M., Sagar, V.M., Shah, T. & Shetty, S. (2018a) Carcinogenesis on the background of liver fibrosis: Implications for the management of hepatocellular cancer. World Journal of Gastroenterology 24 (39) p.4436–4447.

O'Rourke, J.M., Sagar, V.M., Shah, T. & Shetty, S. (2018b) Carcinogenesis on the background of liver fibrosis: Implications for the management of hepatocellular cancer. World Journal of Gastroenterology 24 (39) p.4436–4447.

O'Rourke, J.M., Sagar, V.M., Shah, T. & Shetty, S. (2018c) Carcinogenesis on the background of liver fibrosis: Implications for the management of hepatocellular cancer. World Journal of Gastroenterology 24 (39) p.4436–4447.

Paz-Priel, I., Houng, S., Dooher, J. & Friedman, A.D. (2011) C/EBPA and C/EBPA oncoproteins regulate nfkb1 and displace histone deacetylases from NF-κB p50 homodimers to induce NF-κB target genes. *Blood*. 117 (15), 4085–4094.

Perkins, N.D. (2007) Integrating cell-signalling pathways with NF-κB and IKK function. Nature Reviews Molecular Cell Biology 8 (1) p.49–62.

Plati, J., Bucur, O. & Khosravi-Far, R. (2008) Dysregulation of apoptotic signaling in cancer: Molecular mechanisms and therapeutic opportunities. Journal of Cellular Biochemistry 104 (4) p.1124–1149.

Pogribny, I.P. & Rusyn, I. (2014) Role of epigenetic aberrations in the development and progression of human hepatocellular carcinoma. Cancer Letters 342 (2) p.223–230.

Porta, C., Ippolito, A., Consonni, F.M., Carraro, L., Celesti, G., Correale, C., Grizzi, F., Pasqualini, F., Tartari, S., Rinaldi, M., Bianchi, P., Balzac, F., Vetrano, S., Turco, E., Hirsch, E., Laghi, L. & Sica, A. (2018) Protumor steering of cancer inflammation by p50 nf-kb enhances colorectal cancer progression. *Cancer Immunology Research*. 6 (5), 578–593.

Porter, A.G. & Jänicke, R.U. (1999) Emerging roles of caspase-3 in apoptosis. Cell Death and Differentiation 6 (2) p.99–104.

Prusty, B.K., Husain, S.A. & Das, B.C. (2005) Constitutive activation of nuclear factor -kB: Preferntial homodimerization of p50 subunits in cervical carcinoma. *Frontiers in Bioscience*. 10 (2), 1510–1519.

Ramakrishna, G., Rastogi, A., Trehanpati, N., Sen, B., Khosla, R. & Sarin, S.K. (2013) From Cirrhosis to Hepatocellular Carcinoma: New Molecular Insights on Inflammation and Cellular Senescence. *Liver Cancer*. 2 (3–4), 367–383.

Rehg, J.E., Bush, D. & Ward, J.M. (2012) The utility of immunohistochemistry for the identification of hematopoietic and lymphoid cells in normal tissues and interpretation of proliferative and inflammatory lesions of mice and rats. *Toxicologic pathology*. 40 (2), 345–74.

Robinson, M.W., Harmon, C. & O'Farrelly, C. (2016) Liver immunology and its role in inflammation and homeostasis. Cellular and Molecular Immunology 13 (3) p.267–276.

Rohr-Udilova, N., Klinglmüller, F., Schulte-Hermann, R., Stift, J., Herac, M., Salzmann, M., Finotello, F., Timelthaler, G., Oberhuber, G., Pinter, M., Reiberger, T., Jensen-Jarolim, E., Eferl, R. & Trauner, M. (2018) Deviations of the immune cell landscape between healthy liver and hepatocellular carcinoma. *Scientific Reports*. 8 (1), 1–11.

Ruland, J., Duncan, G.S., Elia, A., del Barco Barrantes, I., Nguyen, L., Plyte, S., Millar, D.G., Bouchard, D., Wakeham, A., Ohashi, P.S. & Mak, T.W. (2001) Bcl10 is a positive regulator of antigen receptor-induced activation of NF-κB and neural tube closure. *Cell*. 104 (1), 33–42.

Saccani, A., Schioppa, T., Porta, C., Biswas, S.K., Nebuloni, M., Vago, L., Bottazzi, B., Colombo, M.P., Mantovani, A. & Sica, A. (2006) p50 nuclear factor-κB overexpression in tumor-associated macrophages inhibits M1 inflammatory responses and antitumor resistance. *Cancer Research*. 66 (23), 11432–11440.

Savinova, O. v., Hoffmann, A. & Ghosh, G. (2009) The Nfkb1 and Nfkb2 Proteins p105 and p100 Function as the Core of High-Molecular-Weight Heterogeneous Complexes. *Molecular Cell*. 34 (5), 591–602.

Schmitt, A.M., Crawley, C.D., Kang, S., Raleigh, D.R., Yu, X., Wahlstrom, J.S., Voce, D.J., Darga, T.E., Weichselbaum, R.R. & Yamini, B. (2011) P50 (NF-κB1) is an effector protein in the cytotoxic response to DNA methylation damage. *Molecular Cell*. 44 (5), 785–796.

Scholten, D., Trebicka, J., Liedtke, C. & Weiskirchen, R. (2015) The carbon tetrachloride model in mice. *Laboratory Animals*. 49 (1 Suppl), 4–11.

Scholten, D., Trebicka, J., Liedtke, C. & Weiskirchen, R. (n.d.) *The carbon tetrachloride model in mice*.

Scholten, D, Trebicka, J., Liedtke, C. & Weiskirchen, R. (2015) The carbon tetrachloride model in mice. *Laboratory animals*. 49 (1 Suppl), 4–11.

Seo, W. & Jeong, W. il (2016) Hepatic non-parenchymal cells: Master regulators of alcoholic liver disease? World journal of gastroenterology 22 (4) p.1348–1356.

Sha, W.C., Liou, H.C., Tuomanen, E.I. & Baltimore, D. (1995a) Targeted disruption of the p50 subunit of NF-κB leads to multifocal defects in immune responses. *Cell*. 80 (2), 321–330.

Sha, W.C., Liou, H.C., Tuomanen, E.I. & Baltimore, D. (1995b) Targeted disruption of the p50 subunit of NF-κB leads to multifocal defects in immune responses. *Cell*. 80 (2), 321–330.

Shiani, A., Narayanan, S., Pena, L. & Friedman, M. (2017) The Role of Diagnosis and Treatment of Underlying Liver Disease for the Prognosis of Primary Liver Cancer. Cancer Control 24 (3).

Shibata, W., Takaishi, S., Muthupalani, S., Pritchard, D.M., Whary, M.T., Rogers, A.B., Fox, J.G., Betz, K.S., Kaestner, K.H., Karin, M. & Wang, T.C. (2010) Conditional Deletion of IκB-Kinase-β

Accelerates Helicobacter-Dependent Gastric Apoptosis, Proliferation, and Preneoplasia. *Gastroenterology*. 138 (3), 1022.

Sijamhodžić, R., Roža, N., Debelić, M.I. & Hrstić, I. (2019) Drug-induced liver injury. *Medicus*. 29 (1), 7–12.

Sokolova, O. & Naumann, M. (2017) NF-κB signaling in gastric cancer. Toxins 9 (4).

Southern, S.L., Collard, T.J., Urban, B.C., Skeen, V.R., Smartt, H.J., Hague, A., Oakley, F., Townsend, P.A., Perkins, N.D., Paraskeva, C. & Williams, A.C. (2012) BAG-1 interacts with the p50-p50 homodimeric NF-B complex: Implications for colorectal carcinogenesis. *Oncogene*. 31 (22), 2761–2772.

Sriskantharajah, S., Belich, M.P., Papoutsopoulou, S., Janzen, J., Tybulewicz, V., Seddon, B. & Ley, S.C. (2009) Proteolysis of NF-κB1 p105 is essential for T cell antigen receptor-induced proliferation. *Nature Immunology*. 10 (1), 38–47.

Stanger, B.Z. (2015) Probing hepatocyte heterogeneity. Cell Research 25 (11) p.1181–1182.

Stoyanovsky, D.A. & Cederbaum, A.I. (1996) Thiol oxidation and cytochrome P450-dependent metabolism of CCl4 triggers Ca2+ release from liver microsomes. *Biochemistry*. 35 (49), 15839–15845.

Sun, F., Qu, Z., Xiao, Y., Zhou, J., Burns, T.F., Stabile, L.P., Siegfried, J.M. & Xiao, G. (2016) NF-κB1 p105 suppresses lung tumorigenesis through the Tpl2 kinase but independently of its NF-κB function. *Oncogene*. 35 (18), 2299–2310.

Syntichaki, P. & Tavernarakis, N. (2002) Death by necrosis: Uncontrollable catastrophe, or is there order behind the chaos? *EMBO Reports*. 3 (7), 604.

Tanaka, M. & Miyajima, A. (2016) Liver regeneration and fibrosis after inflammation. *Inflammation and Regeneration*. 36 (1), 19.

Tang, Q., Wang, Q., Zhang, Q., Lin, S.-Y., Zhu, Y., Yang, X. & Guo, A.-Y. (2017) Gene expression, regulation of DEN and HBx induced HCC mice models and comparisons of tumor, para-tumor and normal tissues. *BMC Cancer*. 17 (1), 862.

Tanimizu, N., Nakamura, Y., Ichinohe, N., Mizuguchi, T., Hirata, K. & Mitaka, T. (n.d.) Hepatic biliary epithelial cells acquire epithelial integrity but lose plasticity to differentiate into hepatocytes in vitro during development. *Journal of Cell Science*. 1265239–5246.

Thornburg, N.J., Pathmanathan, R. & Raab-Traub, N. (2003) Activation of Nuclear Factor-κB p50 Homodimer/Bcl-3 Complexes in Nasopharyngeal Carcinoma. *Cancer Research*. 63 (23), 8293–8301.

Tolba, R., Kraus, T., Liedtke, C., Schwarz, M. & Weiskirchen, R. (2015) Diethylnitrosamine (DEN)-induced carcinogenic liver injury in mice. *Laboratory animals*. 49 (1 Suppl), 59–69.

Tolba, R., Kraus, T., Liedtke, C., Schwarz, M., Weiskirchen, R & Weiskirchen, Ralf (2015a) Diethylnitrosamine (DEN)-induced carcinogenic liver injury in mice Historic background of the model. *Laboratory Animals*. 49 (S1), 59–69.

Tolba, R., Kraus, T., Liedtke, C., Schwarz, M., Weiskirchen, R & Weiskirchen, Ralf (2015b) Diethylnitrosamine (DEN)-induced carcinogenic liver injury in mice Historic background of the model. *Laboratory Animals*. 49 (S1), 59–69.

Tsujimoto, Y. (1998) Role of Bcl-2 family proteins in apoptosis: Apoptosomes or mitochondria? Genes to Cells 3 (11) p.697–707.

Tzirogiannis, K.N., Panoutsopoulos, G.I., Demonakou, M.D., Hereti, R.I., Alexandropoulou, K.N., Basayannis, A.C. & Mykoniatis, M.G. (2003) Time-course of cadmium-induced acute hepatotoxicity in the rat liver: The role of apoptosis. *Archives of Toxicology*. 77 (12), 694–701.

Uehara, T., Pogribny, I.P. & Rusyn, I. (2014) The DEN and CCl4-induced mouse model of fibrosis and inflammation-associated hepatocellular carcinoma. *Current Protocols in Pharmacology*. 201414.30.1-14.30.10.

Vekemans, K. & Braet, F. (2005) Structural and functional aspects of the liver and liver sinusoidal cells in relation to colon carcinoma metastasis. World Journal of Gastroenterology 11 (33) p.5095–5102.

Viennois, E., Chen, F. & Merlin, D. (2013) NF-κB pathway in colitis-associated cancers. *Translational gastrointestinal cancer*. 2 (1), 21–29.

Vincenti, M.P., Coon, C.I. & Brinckerhoff, C.E. (1998) Nuclear factor kappaB/p50 activates an element in the distal matrix metalloproteinase 1 promoter in interleukin-1beta-stimulated synovial fibroblasts. *Arthritis and rheumatism*. 41 (11), 1987–94.

Voce, D.J., Schmitt, A.M., Uppal, A., McNerney, M.E., Bernal, G.M., Cahill, K.E., Wahlstrom, J.S., Nassiri, A., Yu, X., Crawley, C.D., White, K.P., Onel, K., Weichselbaum, R.R. & Yamini, B. (2015) Nfkb1 is a haploinsufficient DNA damage-specific tumor suppressor. *Oncogene*. 34 (21), 2807–2813.

Wang, J.X., Bair, A.M., King, S.L., Shnayder, R., Huang, Y.F., Shieh, C.C., Soberman, R.J., Fuhlbrigge, R.C. & Nigrovic, P.A. (2012) Ly6G ligation blocks recruitment of neutrophils via a β2-integrin-dependent mechanism. *Blood*. 120 (7), 1489–1498.

Ward, T.H., Cummings, J., Dean, E., Greystoke, A., Hou, J.M., Backen, A., Ranson, M. & Dive, C. (2008) Biomarkers of apoptosis. British Journal of Cancer 99 (6) p.841–846.

Watanabe, A., Watanabe, N., Wachi, S. & Fujita, T. (2003) *Identification and characterization of B3BP Identification and characterization of BCL-3 binding protein, B3BP: Implications for transcription and DNA repair or recombination* Downloaded from*.

Wessells, J., Baer, M., Young, H.A., Claudio, E., Brown, K., Siebenlist, U. & Johnson, P.F. (2004a) BCL-3 and NF-κB p50 attenuate lipopolysaccharide-induced inflammatory responses in macrophages. *Journal of Biological Chemistry*. 279 (48), 49995–50003.

Wessells, J., Baer, M., Young, H.A., Claudio, E., Brown, K., Siebenlist, U. & Johnson, P.F. (2004b) BCL-3 and NF-κB p50 attenuate lipopolysaccharide-induced inflammatory responses in macrophages. *Journal of Biological Chemistry*. 279 (48), 49995–50003.

Williams, S.A., Chen, L.F., Kwon, H., Ruiz-Jarabo, C.M., Verdin, E. & Greene, W.C. (2006) NF-κB p50 promotes HIV latency through HDAC recruitment and repression of transcriptional initiation. *EMBO Journal*. 25 (1), 139–149.

Wilson, C.L., Jurk, D., Fullard, N., Banks, P., Page, A., Luli, S., Elsharkawy, A.M., Gieling, R.G., Chakraborty, J.B., Fox, C., Richardson, C., Callaghan, K., Blair, G.E., Fox, N., Lagnado, A., Passos, J.F., Moore, A.J., Smith, G.R., Tiniakos, D.G., et al. (2015) NFκ B1 is a suppressor of neutrophil-driven hepatocellular carcinoma. *Nature Communications*. 66818.

Wynn, T.A. (2008) Cellular and molecular mechanisms of fibrosis. Journal of Pathology 214 (2) p.199–210.

Xiao, Y., Karnati, S., Qian, G., Nenicu, A., Fan, W., Tchatalbachev, S., Höland, A., Hossain, H., Guillou, F., Lüers, G.H. & Baumgart-Vogt, E. (2012) Cre-Mediated Stress Affects Sirtuin Expression Levels, Peroxisome Biogenesis and Metabolism, Antioxidant and Proinflammatory Signaling Pathways Marcelo G. Bonini (ed.). *PLoS ONE*. 7 (7), e41097.

Xie, Y. (2017) 'Hepatitis B virus-associated hepatocellular carcinoma', in *Advances in Experimental Medicine and Biology*. [Online]. Springer New York LLC. pp. 11–21.

Yamamoto, M., Yamazaki, S., Uematsu, S., Sato, S., Hemmmi, H., Hoshino, K., Kaisho, T., Kuwata, H., Takeuchi, O., Takeshige, K., Saitoh, T., Yamaoka, S., Yamamoto, N., Yamamoto, S., Muta, T., Takeda, K. & Akira, S. (2004) Regulation of Toll/IL-1-receptor-mediated gene expression by the inducible nuclear protein IκBζ. *Nature*. 430 (6996), 218–222.

Yan, Z., Yan, H. & Ou, H. (2012a) Human thyroxine binding globulin (TBG) promoter directs efficient and sustaining transgene expression in liver-specific pattern. *Gene*. 506 (2), 289–294.

Yan, Z., Yan, H. & Ou, H. (2012b) Human thyroxine binding globulin (TBG) promoter directs efficient and sustaining transgene expression in liver-specific pattern. *Gene*. 506 (2), 289–294.

Yang, Y., Jiang, G., Zhang, P. & Fan, J. (2015) Programmed cell death and its role in inflammation. Military Medical Research 2 (1).

Yokoo, H., Yasuda, J., Nakanishi, K., Chuma, M., Kamiyama, T., Todo, S., Hirohashi, S. & Sakamoto, M. (2011) Clinicopathological significance of nuclear factor-κB activation in hepatocellular carcinoma. *Hepatology Research*. 41 (3), 240–249.

Zhang, C.Y., Yuan, W.G., He, P., Lei, J.H. & Wang, C.X. (2016) Liver fibrosis and hepatic stellate cells: Etiology, pathological hallmarks and therapeutic targets. World Journal of Gastroenterology 22 (48) p.10512–10522.

Zhang, J., Xu, L.G., Han, K.J. & Shu, H.B. (2004) Identification of a ZU5 and Death Domain-containing Inhibitor of NF-κB. *Journal of Biological Chemistry*. 279 (17), 17819–17825.

Zhou, Y., Eppenberger-Castori, S., Eppenberger, U. & Benz, C.C. (2005) 'The NFκB pathway and endocrine-resistant breast cancer', in *Endocrine-Related Cancer*. [Online]. July 2005 Endocr Relat Cancer. p.

Zhou, Z., Xu, M.J. & Gao, B. (2016) Hepatocytes: A key cell type for innate immunity. Cellular and Molecular Immunology 13 (3) p.301–315.